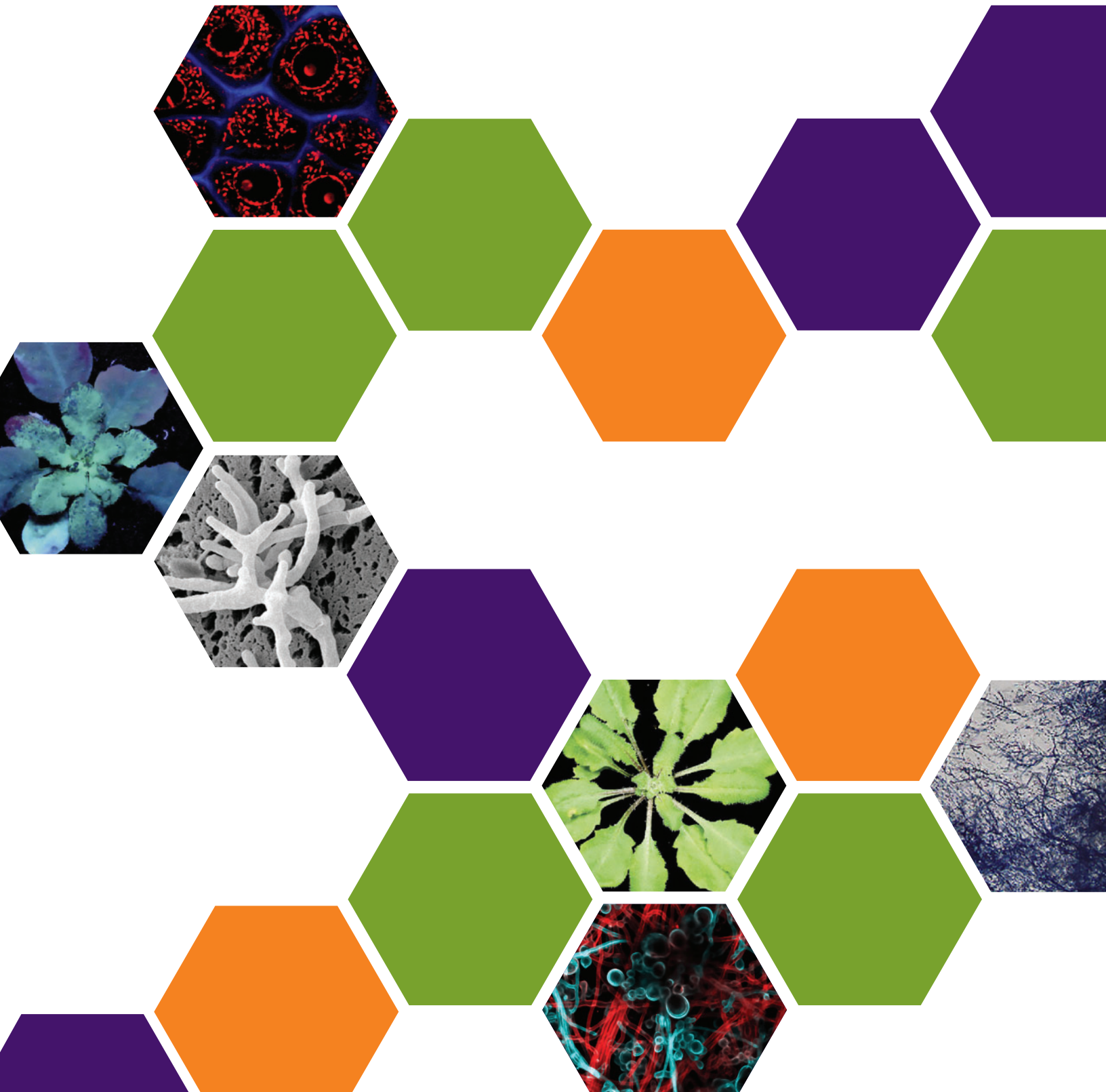


MPMI

Molecular Plant-Microbe Interactions®



Volume 36, Number 9 | September 2023





Volume 36, Number 9 | September 2023

COMMENTARY

- 534 **Unraveling the Molecular Arms Race: Grapevine Fanleaf Virus Proteins as Suppressors of Plant Antiviral Silencing Pathways**
Siva Sankari and Amelia Helen Lovelace

CURRENT REVIEW

- 536 **Molecular Mechanisms of *Pseudomonas*-Assisted Plant Nitrogen Uptake: Opportunities for Modern Agriculture**
Stefan Sanow, Weiqi Kuang, Gabriel Schaaf, Pitter Huesgen, Ulrich Schurr, Ute Roessner, Michelle Watt, and Borjana Arsova

MEETING REVIEW

- 549 **12th Japan-US Seminar in Plant Pathology Meeting Report**
Yumino Sasaki, Juliana González-Tobón, Yuta Hino, Chujia Jin, Tianrun Li, Tan Anh Nhi Nguyen, Blake Oakley, and Danielle Stevens

SHORT COMMUNICATION

- 554 **Targeting Disease Susceptibility Genes in Wheat Through Wide Hybridization with Maize Expressing Cas9 and Guide RNA**
Anil Karmacharya, Dandan Li, Yueqiang Leng, Gongjun Shi, Zhaohui Liu, Shengming Yang, Yang Du, Wenhao Dai, and Shaobin Zhong

RESEARCH

- 558 **Grapevine Fanleaf Virus RNA1-Encoded Proteins 1A and 1B^{Hel} Suppress RNA Silencing**
Jiyeong Choi, Samira Pakbaz, Luz Marcela Yepes, Elizabeth Jeannette Cieniewicz, Corinne Schmitt-Keichinger, Rossella Labarile, Serena Anna Minutillo, Michelle Heck, Jian Hua, and Marc Fuchs
- 572 **VdTps2 Modulates Plant Colonization and Symptom Development in *Verticillium dahliae***
Luyao Xiao, Chen Tang, Steven J. Klosterman, and Yonglin Wang
- 584 **Host Specificity Controlled by *PWL1* and *PWL2* Effector Genes in the Finger Millet Blast Pathogen *Magnaporthe oryzae* in Eastern Africa**
Hosea Isanda Masaki, Santie de Villiers, Peng Qi, Kathryn A. Prado, Davies Kiambi Kaimenyi, Kassahun Tesfaye, Tesfaye Alemu, John Takan, Mathews Dida, Justin Ringo, Wilton Mbinda, Chang Hyun Khang, and Katrien M. Devos
- 592 **Maize Phyto cytokines Modulate Pro-Survival Host Responses and Pathogen Resistance**
Maurice Koenig, Daniel Moser, Julian Leusner, Jasper R. L. Depotter, Gunther Doehlemann, and Johana Misas Villamil



Submit manuscripts electronically following the instructions provided on the [APS Information for Authors](#) page.
Article Publication Charges are mandatory to cover publication costs. Fees are set by the governing council of The American Phytopathological Society.
Submission requires the paper is not submitted elsewhere.



MPMI Editorial Board

Molecular Plant-Microbe Interactions® (e-ISSN: 1943-7706) is published monthly by The American Phytopathological Society,
3285 Northwood Circle, Suite 100, St. Paul, MN 55121, U.S.A. Telephone: +1.651.454.7250. E-mail: pubdept@scisoc.org; <https://apsjournals.apsnet.org/>



COMMENTARY

Unraveling the Molecular Arms Race: Grapevine Fanleaf Virus Proteins as Suppressors of Plant Antiviral Silencing Pathways

Siva Sankari^{1,†}  and Amelia Helen Lovelace² ¹ Stowers Institute for Medical Research, 1000 E. 50th St., Kansas City, MO 64110, U.S.A.² The Sainsbury Laboratory, Norwich Research Park, Norwich, NR4 7UH, U.K.

Accepted for publication 9 August 2023.

There exists a constant evolutionary combat between hosts and their invading pathogens. The plant-virus pathosystem is no exception. Plants have evolved multiple defense mechanisms to combat viral invasion. One of these mechanisms involves the viral RNA-induced silencing complex that targets and cleaves viral RNAs, thereby preventing viral RNA translation and replication. The RNA silencing pathway starts with the host RNA III-type Dicer-like (DCL) endoribonuclease cleavage of double-stranded RNA into virus-derived short interfering RNAs. This guide strand combines with Argonaute (AGO) protein to form the RNA-induced silencing complex used to cleave viral transcripts (Gaffar and Koch 2019; Jin et al. 2022). On the other hand, viruses have evolved counteracting strategies to overcome this antiviral mechanism by encoding viral suppressors of RNA silencing (VSR) proteins, which inhibit one or more steps of host RNA silencing pathways (Lopez-Gomollon and Baulcombe 2022). For instance, the poliovirus protein P0 destabilizes AGO, and the helper component protease of potyvirus sequester short interfering RNAs (Li and Wang 2019). Understanding this complex molecular arms race is important for gaining insights into the various strategies viruses deploy to overcome host defense and to develop effective tools to inhibit viral anti-silencing methods.

Grapevine fanleaf virus (GFLV) causes fanleaf degeneration that leads to economic losses in most viticultural regions of the world (Andret-Link et al. 2004). It is transmitted by the nematode *Xiphinema index*, a plant ectoparasite. GFLV belongs to the genus *Nepovirus* in the family *Secoviridae* and harbors a genome of two positive-sense RNAs (RNA1 and RNA2). The mechanisms of how GFLV evades host antiviral RNA silencing and causes devastating infections are poorly understood.

In this September 2023 issue of *Molecular Plant-Microbe Interactions*, Choi et al. (2023) report the first elucidation of the

GFLV RNA1-encoded proteins in suppressing plant antiviral RNA silencing. The authors employed an innovative approach of silencing the gene encoding enhanced green fluorescent protein (EGFP) in transgenic *Nicotiana benthamiana* expressing EGFP by *Agrobacterium tumefaciens*-mediated delivery of pHELLSGATE8-EGFP construct. This construct encodes an EGFP hairpin that induces systemic RNA silencing of EGFP to mimic the antiviral silencing without the involvement of the virus. Subsequently, they tested the capability of GFLV in reversal of this systemic silencing of EGFP by mechanical infiltration with constructs specifically encoding products of proteolytic cleavage of the polyproteins of GFLV. The authors discovered that proteins 1A and 1B^{Hel}, both encoded by GFLV RNA1, either individually, together (1A+1B^{Hel}), or in fused preproteolytic form (1A1B^{Hel}), successfully reversed the silencing effect. The function of protein 1A had yet to be characterized and protein 1B^{Hel} is a putative helicase. In addition, the transcription of a variety of host genes involved in antiviral silencing including DCL2, DCL4, AGO1, AGO2, and RDR6 were also differentially affected by these VSR proteins (Fig. 1).

This is the first report of VSRs encoded by RNA1 from a nepovirus. Moreover, this study provides evidence showing that two VSRs, either individually or in a fused preproteolytic form, can act on plant antiviral silencing pathways. These findings suggest that GFLV might have unique mechanisms of counteracting host defense strategies. Furthermore, this work represents the first study to assign a function to the GFLV protein 1A. The function of this protein, referred to as X1, in closely related nepoviruses remains elusive.

Crosstalk between the host and invading viral pathogens is multifaceted and complex. Every step towards untangling these complex mechanisms reveals new ways viruses evade host defense mechanisms and cause infection. This manuscript has not only significantly contributed to our knowledge of the existence of VSRs in GFLV but also to a distinct way GFLV VSRs could act on plants. This study raises some interesting questions. i) Do X1 proteins encoded by related nepoviruses act as VSRs in respective plants they infect? ii) What are the mechanisms of actions of the VSRs of GFLV? iii) Do other nepoviruses encode preproteolytic products that can act as VSRs? iv) How can we devise strategies to block the function of proteins 1A and 1B^{Hel} to prevent economic loss? Further studies are needed to address these questions.

†Corresponding author: S. Sankari; ssankari@stowers.org

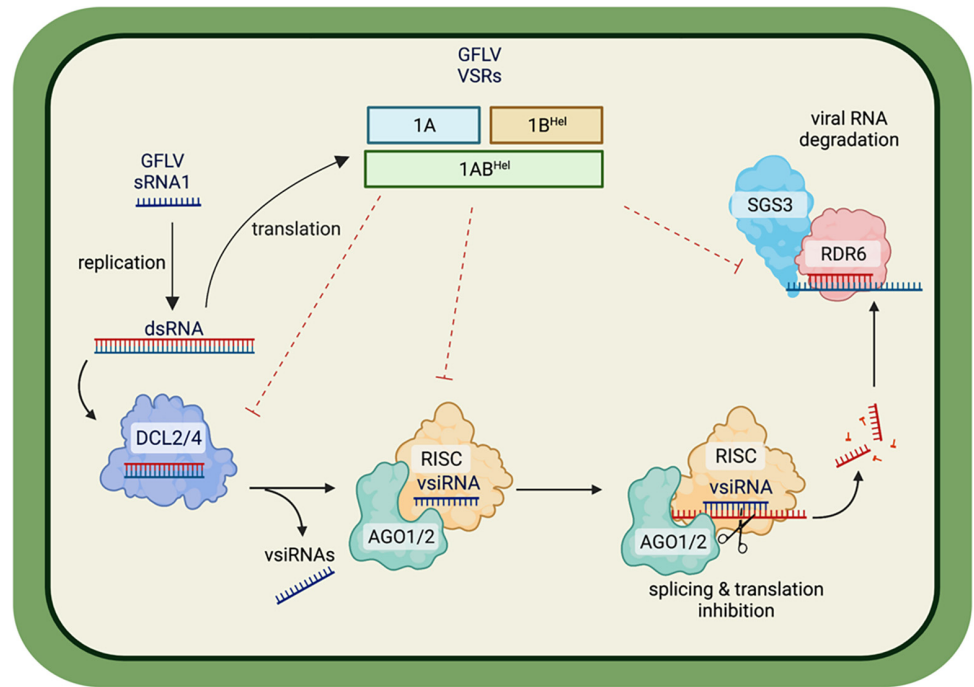
Linked article: This article refers to Choi et al. (2023). To view this article, please visit <https://doi.org/10.1094/MPMI-01-23-0008-R>.

The author(s) declare no conflict of interest.



Copyright © 2023 The Author(s). This is an open access article distributed under the CC BY-NC-ND 4.0 International license.

Fig. 1. Plant defense and counter defense of grapevine fanleaf virus (GFLV) via novel viral suppressor of RNA silencing (VSR) proteins. Plants use RNA silencing to defend against viral pathogens. This is initiated by the cleavage of double-stranded RNA (dsRNA) by the plant host RNA III-type Dicer-like (DCL) endoribonucleases 2 and 4 to produce virus-derived short interfering RNAs (vsiRNAs). These combine with Argonaute (AGO) proteins 1 and 2 to form the RNA-inducing silencing complex (RISC) used to cleave viral transcripts and inhibit translation. The byproducts of this cleavage, along with RNA-dependent RNA polymerase 6 (RDR6) and suppressor of gene silencing 3 (SGS3), generate secondary short interfering RNAs, leading to amplification of systemic RNA silencing in the plant host. GFLV produces VSR proteins 1A, 1B^{Het}, and 1AB^{Het}, which reverse this systemic RNA silencing. These VSRS alter the expression of the RNA-silencing machinery.



Literature Cited

Andret-Link, P., Schmitt-Keichinger, C., Demangeat, G., Komar, V., and Fuchs, M. 2004. The specific transmission of *Grapevine fanleaf virus* by its nematode vector *Xiphinema index* is solely determined by the viral coat protein. *Virology* 320:12-22.

Choi, J., Pakbaz, S., Yepes, L. M., Cieniewicz, E. J., Schmitt-Keichinger, C., Labarile, R., Minutillo, S. A., Heck, M., Hua, J., and Fuchs, M. 2023. Grapevine fanleaf virus RNA1-encoded proteins 1A and 1B^{Het} suppress RNA silencing. *Mol. Plant-Microbe Interact.* 36:558-571.

Gaffar, F. Y., and Koch, A. 2019. Catch me if you can! RNA silencing-based improvement of antiviral plant immunity. *Viruses* 11:673.









Jin, L., Chen, M., Xiang, M., and Guo, Z. 2022. RNAi-based antiviral innate immunity in plants. *Viruses* 14:432.

Li, F., and Wang, A. 2019. RNA-targeted antiviral immunity: More than just RNA silencing. *Trends Microbiol.* 27:792-805.

Lopez-Gomollon, S., and Baulcombe, D. C. 2022. Roles of RNA silencing in viral and non-viral plant immunity and in the crosstalk between disease resistance systems. *Nat. Rev. Mol. Cell Biol.* 23:645-662.

CURRENT REVIEW

Molecular Mechanisms of *Pseudomonas*-Assisted Plant Nitrogen Uptake: Opportunities for Modern Agriculture

Stefan Sanow,^{1,2}  Weiqi Kuang,³  Gabriel Schaaf,⁴  Pitter Huesgen,⁵  Ulrich Schurr,¹ 
 Ute Roessner,⁶  Michelle Watt,²  and Borjana Arsova^{1,†} 

¹ Institute for Bio- and Geosciences, Plant Sciences (IBG-2), Forschungszentrum Juelich GmbH, Germany

² School of BioSciences, Faculty of Science, The University of Melbourne, Parkville, 3010 Victoria, Australia

³ College of life and Environmental Sciences, Hunan University of Arts and Science, China

⁴ Institute of Crop Science and Resource Conservation, University of Bonn, 53115 Bonn, Germany

⁵ Central institute for Engineering, Electronics and Analytics (ZEA-3), Forschungszentrum Juelich GmbH, Germany

⁶ Research School of Biology, The Australian National University, Acton, 2601 Australian Capital Territory, Australia

Accepted for publication 27 March 2023.

***Pseudomonas* spp. make up 1.6% of the bacteria in the soil and are found throughout the world. More than 140 species of this genus have been identified, some beneficial to the plant. Several species in the family Pseudomonadaceae, including *Azotobacter vinelandii* AvOP, *Pseudomonas stutzeri* A1501, *Pseudomonas stutzeri* DSM4166, *Pseudomonas szotifigens* 6HT33bT, and *Pseudomonas* sp. strain K1 can fix nitrogen from the air. The genes required for these reactions are organized in a nitrogen fixation island, obtained via horizontal gene transfer from *Klebsiella pneumoniae*, *Pseudomonas stutzeri*, and *Azotobacter vinelandii*. Today, this island is conserved in *Pseudomonas* spp. from different geographical locations, which, in turn, have evolved to deal with different geo-climatic conditions. Here, we summarize the molecular mechanisms behind *Pseudomonas*-driven plant growth promotion, with particular focus on improving plant performance at limiting nitrogen (N) and improving plant N content. We describe *Pseudomonas*-plant interaction strategies in the soil, noting that the mechanisms of denitrification, ammonification, and secondary metabolite signaling are only marginally explored. Plant growth promotion is dependent on the abiotic conditions and differs at sufficient and deficient N. The molecular controls behind different plant responses are not fully elucidated. We suggest that superposition of transcriptome, proteome, and metabolome data and their integration with plant phenotype development through time will help fill these gaps. The aim of this review is to summarize the knowledge behind *Pseudomonas*-driven nitrogen fixation and to point to possible agricultural solutions.**

†Corresponding author: B. Arsova; b.arsova@fz-juelich.de

Funding: This work was funded by the Deutsche Forschungsgemeinschaft grants EXC 2048 (CEPLAS), EXC 2070–390732324 (PhenoRob), and grant 491111487 to fund open access publication. B. Arsova and U. Schurr were supported by the Helmholtz-Gemeinschaft “Changing Earth” Topic program. M. Watt was supported through University of Melbourne Botany Foundation by holding the Adrienne Clarke Chair of Botany. S. Sanow received support from the Forschungszentrum Jülich through the Jülich-University of Melbourne Post-Graduate Academy (JUMPA) program.

The author(s) declare no conflict of interest.



Copyright © 2023 The Author(s). This is an open access article distributed under the CC BY 4.0 International license.

Keywords: biological nitrogen fixation, molecular mechanism, N-fixation, plant growth-promoting bacteria, *Pseudomonas*

Synthesized fertilizers containing nitrogen (N) have become obligatory in today’s agriculture to meet global food demand (Erisman et al. 2008). N fertilizer production is one of the most important innovations for humanity, allowing us to feed an increasing world population. A conservative study estimates that a majority of today’s population (7.75 billion) relies on mineral fertilizer (Fig. 1) (Erisman et al. 2008).

However, mineral fertilizer is a double-edged sword creating a number of problems inherent to its production and use. First, N fertilizer production by the Haber-Bosch process is energy intensive and currently still driven by fossil fuels, resulting in greenhouse gas emissions (Smith et al. 2020). Second, in addition to the growing price of fertilizer, a looming problem is excessive nitrogen use that can lead to nitrate leaching into ground water or, depending on soil pH, redox potential, and microbial activity, to NH₃ or N₂O emissions causing N losses and environmental pollution (Hirel et al. 2011; Klimczyk et al. 2021; Padilla et al. 2018; Ravishankara et al. 2009). Thus, governments have started to restrict application of N fertilizers (<https://www.bmel.de/DE/themen/landwirtschaft/pflanzenbau/ackerbau/ernte2020.html>, accessed March 28, 2023). Recent global events like the pandemic, the Russian invasion of Ukraine, and the consequent rise of energy prices by 80% during 2021 not only increased fertilizer prices (Ben Hassen and El Bilali 2022), but, more importantly, affected the fertilizer export chains. This, in turn, threatens the productivity of agriculture in other parts of the world (Jagtap et al. 2022; Mustafa 2022). In the future, the invasion of Ukraine is expected to put further pressure on fertilizer availability (Jagtap et al. 2022).

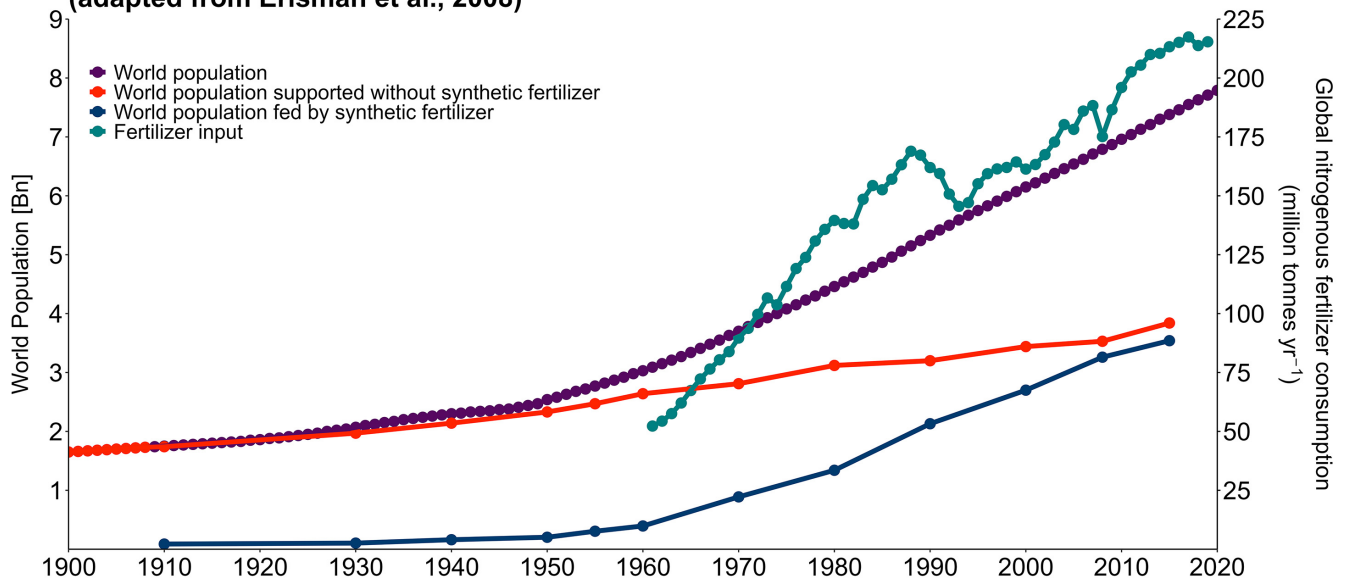
Restricted N fertilizer use may eventually result in lower yields in existing farming systems with today’s crop cultivars and soil management practices. An estimate from the European Union is that the caps led to a 10 to 15.9% yield reduction in wheat over the past six years (BMEL). This will cause less food production and increased prices unless new reliable solutions are found through more nutrient-efficient plant varieties, new farming practices, or new biological N-fixation associations that are reliable across a variety of field conditions.

N is a crucial nutrient for plants, incorporated as the main building block of amino acids, proteins, and many secondary

metabolites. In most agricultural systems, N deficiency plays a major role in plant growth limitation (Bakkou 2011). It is mainly available to the plant in two distinct forms, ammonium (NH_4^+) or nitrate (NO_3^-). Ammonium is taken up by plants via the AMT/MEP/Rh-type (ammonium transport system, methylammonium permeases, and Rhesus protein) ammonium transport system. Studies in *Arabidopsis* place most AMTs in the root, contributing to ammonium uptake. One has been found in pollen and one, AMT2.1, contributes to xylem loading and root to shoot ammonium transport (Bindel and Neuhäuser 2021; Giehl et al. 2017). In rice, AMT1.1 and AMT1.3 contribute to ammonium

uptake under limited nitrogen conditions and, in the case of AMT1.3, also under sufficient nitrogen conditions (Ranathunge et al. 2014). While ammonium can be directly assimilated to glutamine in the root, nitrate is first transported to the shoot and reduced to ammonium by nitrate- and nitrite- reductase. Nitrate can be taken up by plants via the nitrate transport system (Bock and Wagner 2001; Daims et al. 2015). Among the multiple nitrate transporters, we mention NRT2.1 as an important component of the inducible high-affinity transport system for NO_3^- in the root (Cerezo et al. 2001; Filleur et al. 2001; Li et al. 2007; Trinh et al. 2018). NRT2.1 is induced by NO_3^- , but strongly re-

A World population development with and without synthetic nitrogen fertilizers (adapted from Erisman et al., 2008)



B Nitrogen fixed by 'free-living' bacteria in non-legumes

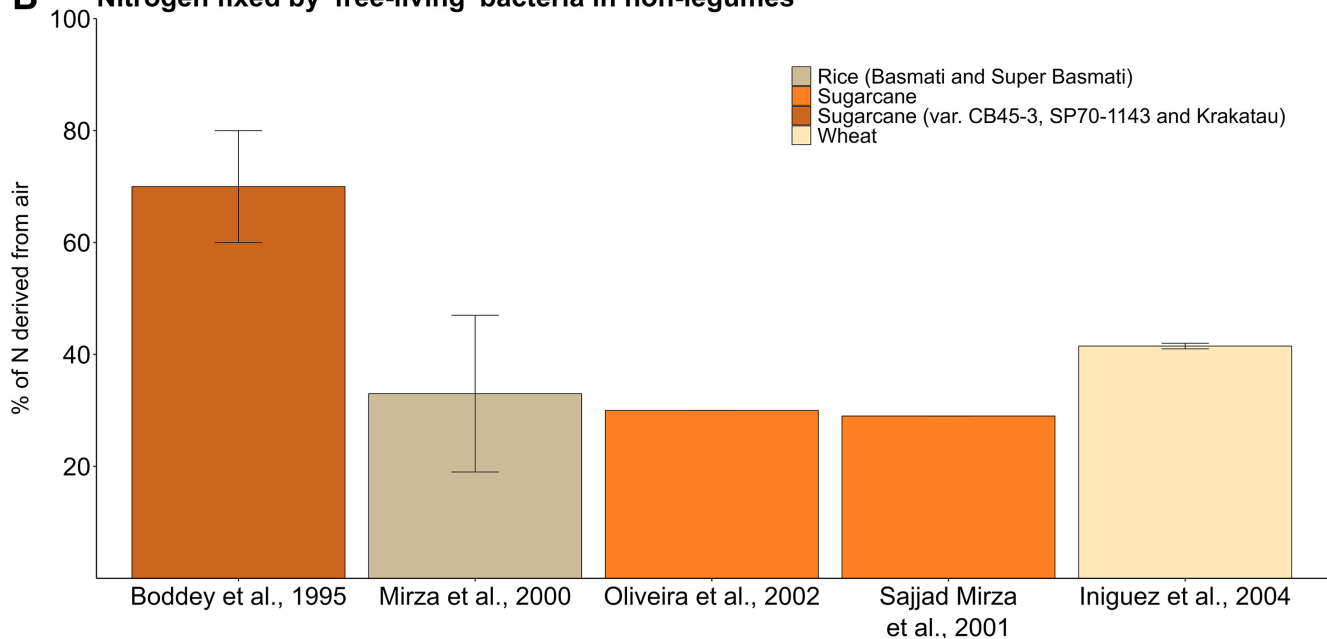


Fig. 1. A, World population development with and without the support of synthetic fertilizer during the 20th century, as calculated, simulated, and estimated by Erisman et al. 2008 and the United States Department of Agriculture. The purple line represents world population development, while the red line represents the estimated global population that could be fed without the invention of reactive nitrogen from the Haber-Bosch process. The blue line provides the estimated global population that is fed by synthesized nitrogen. The global consumption of nitrogenous fertilizer in million ton per year is represented in teal. **B**, Nitrogen fixed by 'free-living' bacteria in non-legumes, especially in rice, wheat, and sugarcane variants. Free-living bacteria used in the studies involve *Acetobacter* spp., *Azospirillum* spp., *Burkholderia* spp., *Enterobacter* sp., *Herbaspirillum* spp., and *Klebsiella* sp. Data shown are the average percentages of N content in plants derived from the air via biological nitrogen fixation (BNF) of the bacteria. Error bars are the standard error, representing the range of contribution to total N content via BNF data from Boddey et al. 1995, Mirza et al. 2000, Sajjad Mirza et al. 2001, Oliveira et al. 2002, and Iniguez et al. 2004.

pressed by high N supply to the plant (Filleur et al. 2001; Girin et al. 2007; Lejay et al. 1999; Zhuo et al. 1999), which leads to an altered root system based on nutrition. During N deficiency, the higher abundance of NRT2.1 leads to lateral root initiation, coordinating the development of lateral roots and, therefore, increases N uptake (Remans et al. 2006). An interaction with a partner protein, NAR2.1, is required for NRT2.1 to transport NO_3^- (Okamoto et al. 2006; Orsel et al. 2006). Plants are also able to take up certain organic N compounds such as urea, amino acids, nucleic acids, and small peptides that are naturally present in soils or are added as fertilizers, as is the case for urea (Beier et al. 2019; Girke et al. 2014; Liu et al. 2003; Mériçout et al. 2008; Owen and Jones 2001; Sopenan et al. 1977; Waterworth and Bray 2006).

Molecular nitrogen is abundant in the atmosphere (78.1%) and is accessible to certain bacterial strains, which can fix it for their own use. As such, it presents an untapped resource that can be used for agriculture. Symbiotic biological nitrogen fixation (BNF) in nodules converts atmospheric nitrogen (N_2) into ammonia (NH_3), which is subsequently protonated to ammonium (NH_4^+) upon export in the peribacteroid space, which is in an acidic pH range (Day et al. 2001; Franche et al. 2009; Lam et al. 1996; Raymond et al. 2004). Free-living bacterial nitrogen fixation results in ammonia (Smercina et al. 2019), which can either be protonated in the soil to ammonium (requires acidic environment) or converted to nitrate via nitrifiers. Subsequently, second reduction of nitrate to ammonium is performed by plant metabolism, as explained above. Ammonia-oxidizing bacteria, Archea, and nitrite-oxidizing bacteria, such as *Nitrospira* bacteria, can either convert i) ammonia to nitrite and in a consecutive step to nitrate or ii) ammonia directly to nitrate via the enzymes ammonia monooxygenase or nitrite oxidoreductase, respectively (Daims et al. 2015). The ammonia used during nitrification is not necessarily derived from BNF.

One of the best-studied groups of plants that form symbiotic relationships with rhizobacteria are legumes. Readers interested in nodule-related processes can consult Gautrat et al. (2020) and Etesami and Adl (2020). Here, we will focus on non-legumes and so called free-living plant-associated microorganisms from the genus *Pseudomonas*. Historically, there are numerous ex-

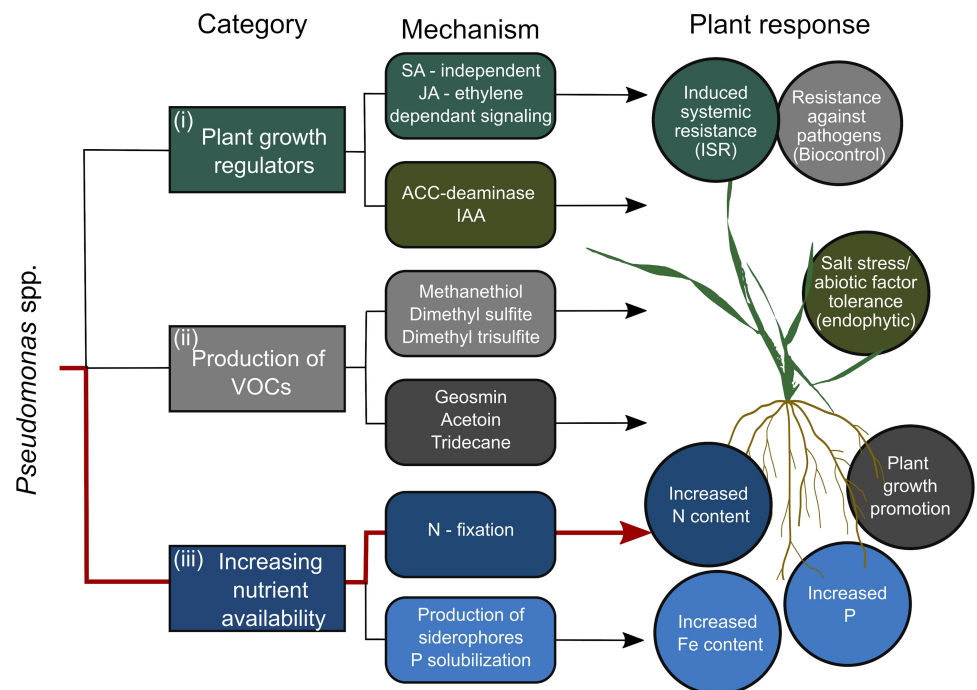
amples of transfer of N from bacteria to plants in non-legume systems (Fig. 1B), however, the potential is not fully exploited yet. We propose that a greater understanding of the molecular mechanisms in the interaction between N-fixing *Pseudomonas* spp. and the plant is crucial for further development of their application in agriculture.

Plant Growth Promotion by Bacteria of the Genus *Pseudomonas*

Pseudomonas spp. make up 1.6% of the bacteria in the soil and are found in all areas in the world (Trivedi et al. 2020). They attract major attention due to their various growth-promoting characteristics, good root colonization, and production of enzymes and metabolites that positively impact plant growth (Glick and Bashan 1997; Kloepper et al. 1989; Podile and Kishore 2007; Ramamoorthy et al. 2001; Saharan and Nehra 2011).

The means by which beneficial *Pseudomonas* spp. promote the growth of the host plants can be categorized into three areas (Fig. 2). The first is by producing plant growth regulators, such as gibberellin, auxins (indole acetic acid [IAA]), and cytokinin-zeatin. IAA increases seedling root growth and, thus, nutrient foraging. Often, the increase in IAA comes with a higher abundance of the enzyme l-aminocyclopropane-1-carboxylate (ACC) deaminase, which lowers the increased ethylene levels caused by stress, resulting in, e.g., an increased salt-stress tolerance (IAA, ACC-deaminase) (Egamberdieva 2009; Glick 2014; Nadeem et al. 2010). *Pseudomonas* spp. can alter salicylic acid and jasmonic acid pathways in the plant, leading to induced systemic resistance (ISR) (Glick 1995; Glick et al. 1999; Ryu et al. 2003). The second way by which *Pseudomonas* spp. can influence plants is through volatile organic compounds produced by *Pseudomonas* spp. These include geosmin, 2,3-butanediol, acetoin, and tridecane, which can promote plant growth (Panpatte et al. 2017). Other *Pseudomonas* spp. can produce compounds for biocontrol, including methanethiol, dimethyl sulfite, and dimethyl trisulfite (Panpatte et al. 2017). Finally, the third way is by *Pseudomonas* spp. increasing the availability of nutrients in the rhizosphere by nitrogen fixation, phosphate solubilization, or siderophore production, making more N, P,

Fig. 2. Overview of plant growth-promoting traits by *Pseudomonas* spp. Beneficial pseudomonads can interact with plants by i) regulating plant growth via the hormonal pathways, ii) producing volatile organic compounds (VOCs), and iii) increasing nutrient availability, resulting in various plant growth-promoting traits, increased resistance against diverse pathogens and abiotic factor tolerance. SA = salicylic acid, JA = jasmonic acid, ACC = l-aminocyclopropane-1-carboxylic acid, IAA = indole acetic acid.



and Fe, respectively, available to plants (Fig. 2) (Glick 1995; Glick et al. 1999; Kloepper et al. 1989; Liu et al. 2017; Nadeem et al. 2010; Richardson 2001; Vessey 2003; Walter et al. 1994).

***Pseudomonas*-Driven Soil Nitrogen Biochemistry, Relevant for Improvement of Plant N**

Pseudomonas spp. can improve the availability of inorganic N to roots by the three main strategies exemplified in Figure 3.

These are i) ammonification of organic N (e.g., by *P. psychrotolerans* [Kang et al. 2020]), ii) stimulation of adjacent bacterial strains to increase N fixation (e.g., between *P. fluorescens* and *Azospirillum brasilense* [Combes-Meynet et al. 2011]), and iii) production and release of NH_4^+ in the rhizosphere (e.g., by *P. stutzeri* [Zhang et al. 2012]).

Ammonification and denitrification.

The process of ammonification allows the conversion of organic nitrogen (amino acids, amino sugars, urea, nucleotides)

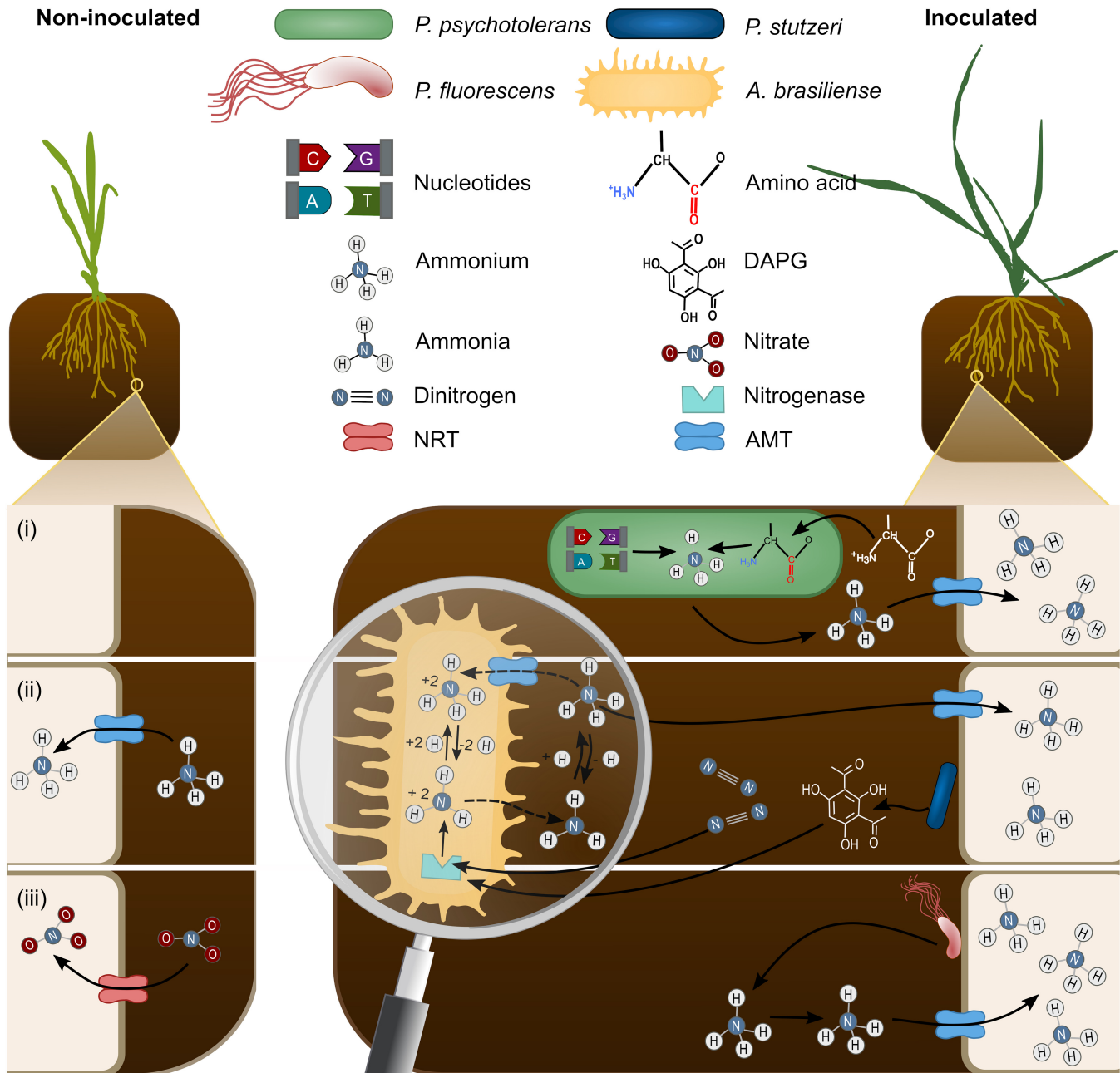


Fig. 3. Conceptual figure of shared nitrogen biochemistry and transport across root and bacterial cells in the rhizosphere. Bacterial processes that impact plant N content. The left side represents plants growing on limited N resulting in a decreased aerial biomass and increased root growth, whereas the right side represents potential plant growth-promoting mechanisms by *Pseudomonas* species increasing the aerial biomass under the same limited N conditions. Ammonium (NH_4^+) and nitrate (NO_3^-) are taken up by the plant via dedicated transporters of the AMT and NRT families, respectively (Bock and Wagner 2001; Daims et al. 2015). Plant growth-promoting bacteria increase availability of inorganic N to plants via following mechanisms: i) ammonification of organic N by *Pseudomonas psychrotolerans* (Kang et al. 2020), ii) *Pseudomonas stutzeri* upregulating *nif* genes in *Azospirillum brasilense* via 2,4-diacetylphloroglucinol (DAPG), resulting in the conversion of N_2 into NH_4^+ (biological nitrogen fixation) (Day et al. 2001; Combes-Meynet et al. 2011) and iii) production and release of NH_4^+ by *P. fluorescens* (Zhang et al. 2012). Dashed lines indicate reactions from or to the bacterium that occur based on the concentration of each reaction product in the respective space and pH of the environment.

into NH_4^+ (Song and Tobias 2011), which contributes to an increase of plant-available N in the soil (Figs. 3i and 4) (Kang et al. 2020). On the other hand, denitrification decreases the amount of NO_3^- in the soil by reducing NO_3^- to $\text{N}_2\text{O}_{(g)}$ and $\text{N}_{2(g)}$ (Fig. 4).

Until 2016, it was widely believed that denitrification and ammonification did not occur within the same bacterium. However, Torres et al. (2016) show that at least three bacteria (*Opitutus terrae* PB90-1, *Marivirga tractuosa* DSM 4126, and the gammaproteobacterium *Shewanella loihica* PV-4) contain the complete set of genes for denitrification and respiratory ammonification, based on genome analyses (Sanford et al. 2012; Torres et al. 2016). Interestingly *P. psychrotolerans* CS51 also contains genes for both processes; Kang et al. (2020) found that ammonification would be possible via the three nitrate ABC transporter genes and *NasT* (response regulator), while denitrification via the genes nitrite reductase (*nirB*), nitrate reductase (*napA*), and nitric oxide reductase (*norB*) (Kang et al. 2020). The enzymes *nirB*, *napA*, and *norB* convert nitrate to nitrite to nitric oxide and, finally, to nitrous oxide (N_2O), notably *nosZ* for the conversion to gaseous nitrogen was not found (Kang et al. 2020; Smith et al. 2007; Wang et al. 2017). Additionally, the genes involved in ammonia assimilation *GlxC* (glutamate synthase [NADPH] putative *GlxC* chain [EC 1.4.1.13]) and *GlxB* (glutamine amidotransferase protein *GlxB* [EC 2.4.2.-]) have been found in the genome of *P. psychrotolerans* (Kang et al. 2020). This leads to the hypothesis that *P. psychrotolerans* CS51 could also perform both ammonification and denitrification.

Production of secondary metabolites that stimulate N fixation in adjacent bacterial strains.

In the case of *Pseudomonas fluorescens* F113 and *Azospirillum brasilense* S245, Combes-Meynet et al. (2011) found an example of positive interaction, in which one strain stimulates N fixation in another. *Pseudomonas fluorescens* F113 produces a secondary metabolite, 2,4-diacetylphloroglucinol (DAPG), that acts as a signal for *Azospirillum brasilense* S245. When *Azospirillum brasilense* detects DAPG, it upregulates the *nirK* and *nifX-nifB* genes, which leads to increased nitro-

gen fixation. This was demonstrated by co-inoculating wheat with both strains (Combes-Meynet et al. 2011) (Figs. 3ii and 4; Table 1). Sequence analysis of DAPG-induced promoters, followed by functional prediction of the corresponding downstream open reading frame, revealed that their deduced protein sequences are homologous to the nitrogen-fixation gene *nifX-nifB* (Combes-Meynet et al. 2011; Rubio and Ludden 2008). This highlights the importance of using bacterial combinations (communities) in which the members function in an additive manner to unlock their full potential.

However, it needs to be kept in mind that using bacterial inoculants in the field will lead to interactions with the native microbiome. While the full extent of the interactions is not clear, we speculate that there might be events in which inoculants may become overrun by the native microbial varieties or, like in the case of *P. taiwanensis* used for maize inoculation and *P. fluorescens* LBUM677 and oilseed crops, there might be changes in the microbiome around the plant roots (Chaudhary et al. 2021; Jiménez et al. 2020). Further understanding of the suitability of inoculants to specific soil environments is needed to ensure reproductive results in the field.

Production and release of NH_4^+ via BNF in *Pseudomonas* spp.

Another step of enhancing the N available for plants is achieved by ammonium excretion of bacteria (Fig. 3iii). The step of ammonification, oxidation of organic N to ammonium, releases energy for metabolic processes. The excess ammonium will be excreted by the microorganism to avoid ammonium toxicity and can either be used for nitrification or taken up by the plant via dedicated AMT transporters (if excreted by root-associated bacteria). The *Pseudomonas* genes *amtB1* and *amtB2* have been demonstrated to regulate the internal ammonia pool and excretion of ammonium (Zhang et al. 2012) (Table 1). A *P. stutzeri* A1501 mutant expressing *nifA* constitutively showed an increased ammonia excretion. Coincidentally, no increase in nitrogenase activity was detected, leaving the role of constitutively expressed *nifA* unclear (Zhang et al. 2012).

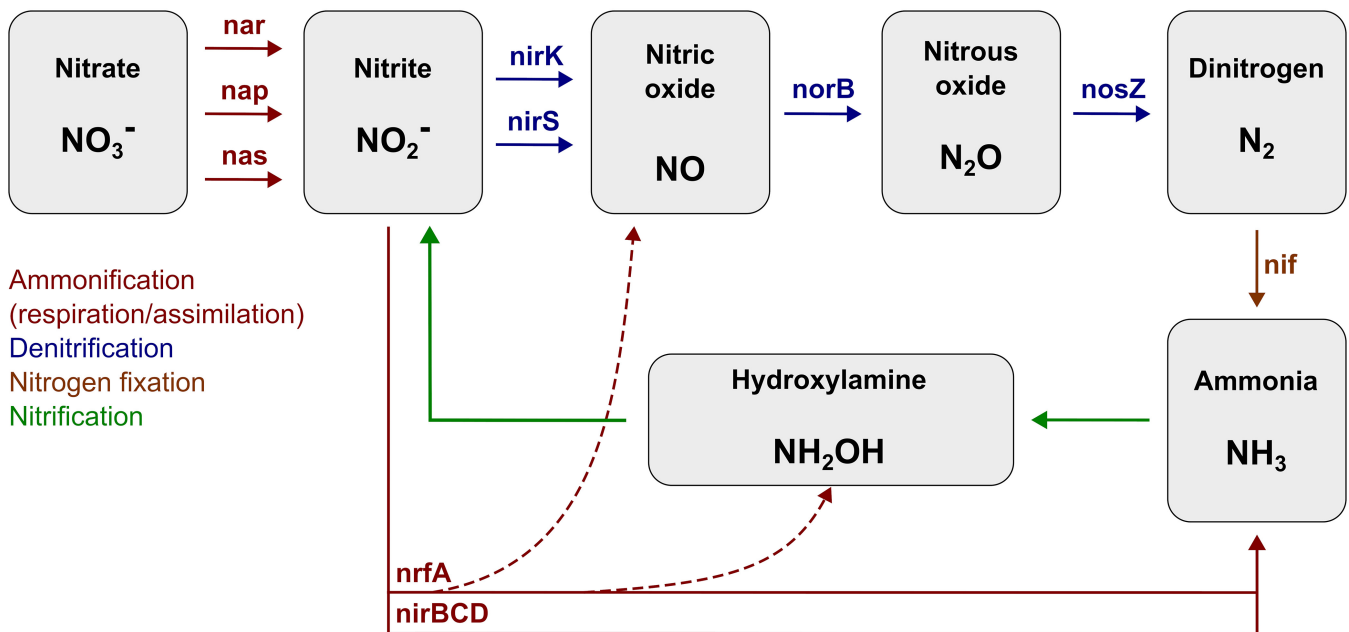


Fig. 4. Bacterial inorganic nitrogen cycle. Ammonification, denitrification, nitrogen fixation, and nitrification are displayed by colored solid lines, with genes involved in the pathway. Dotted lines show additional formation of nitric oxide and hydroxylamine during nitrite ammonification. Figure adapted from Rodionov et al. 2005.

Pseudomonas Genetic Machinery That Could Provide Alternative Nitrogen

Diazotrophic bacteria fix nitrogen via proteins encoded by the nitrogenase gene cluster, and the organisation, abundance and regulation of nitrogen-fixation related genes is different from species to species (Yan et al. 2008). Several species in the family of Pseudomonaceae, including *Azotobacter vinelandii* AvOP, *Pseudomonas stutzeri* A1501, *Pseudomonas stutzeri* DSM4166, *Pseudomonas szotifigens* 6HT33bT and *Pseudomonas* sp. strain K1 have been demonstrated to be capable of nitrogen fixation (Setten et al. 2013).

Specific to *Pseudomonas*, a nitrogen-fixation island (NFI) was discovered and found to be conserved in *P. stutzeri* strains from geographically close (<300 km within Greece) or distant (China, Germany, Greece) locations (Venieraki et al. 2014). The NFI was presumably acquired by lateral gene transfer of a common ancestor of *Klebsiella pneumoniae*, *Pseudomonas stutzeri* and *Azotobacter vinelandii* and inserted between cobalamin synthase (*cobS*) and glutathione peroxidase (*gspH*) (Yan et al. 2008, Setten et al. 2013).

The size of the NFI in *P. stutzeri* is about 49 kb and contains 52 *nif*-related genes, which are organized into 11 putative *NifA*- σ 54-dependent operons (Table 1, Yan et al. 2010; Yang et al. 2018). The σ 54 transcription factor (or RpoN) is a well-known alternative factor for RNA polymerase that enables the transcription of *nif* genes in conjunction with the transcriptional activator *NifA* or activates other genes involved in nitrogen metabolism and functions with the nitrogen regulatory protein C (*NtrC*), the *psp* operon transcriptional activator (*pspF*), and C4-dicarboxylate transport transcriptional regulatory protein DctD (Yan et al. 2010).

Pseudomonas protegens Pf-5 was genetically modified to contain the X940 cosmid, which includes all genes (numbered

from PST1302 to PST1359) from the nitrogen fixation island of *P. stutzeri* A1501. X490 with nitrogenase activity was transferred to various other *Pseudomonas* spp., including *P. putida*, *P. veronii*, *P. taetrolens*, *P. balearica*, and *P. stutzeri* (Setten et al. 2013). A constitutive nitrogenase activity and high ammonium production was observed in all mentioned strains except *P. balearica* and *P. stutzeri*, indicating that a genome context is required for the activity of the X940 cosmid (Setten et al. 2013).

Nitrogen fixation and assimilation are intrinsically coupled and controlled by complex regulatory circuits, favoring the assimilation of fixed nitrogen into biomass instead of excreting it. The processes are controlled by the PII complex, which includes signal transduction proteins such as GlnB and GlnK, enzymes responding to metabolite control via reversible post-translational modifications of proteins (GlnD and GlnE), and a two-component regulatory system (*NtrB* or *NRII* and *NtrC* or *NRI*) controlling many nitrogen metabolism genes. PII tightly regulates *NifA*, a positive regulatory element (Table 1) to fix nitrogen by demand. Readers wanting a comprehensive review can refer to Bueno Batista and Dixon (2019).

To unravel the underlying genetic mechanism of the *P. stutzeri* NFI genes, the complete NFI was transferred into the recombinant *Escherichia coli* EN-01 and was investigated by transcriptomics and proteomics for functional investigation (Yang et al. 2018). In the genetically engineered *E. coli* EN-01 harboring the heterologous NFI island from *P. stutzeri*, primary nitrogen assimilation is achieved by synthesis of glutamate from ammonium and 2-oxoglutarate, catalyzed by two alternative pathways (Yang et al. 2018). In an N-rich environment, the pathway involving the enzyme glutamate dehydrogenase was active. Alternatively, in an N-limited environment, the enzymes glutamate synthetase (GS [gene *glnA*]) and glutamine oxoglutarate aminotransferase (GOGAT [gene *gltBD*]) were predominantly active (Yang et al. 2018). This is in agreement with data showing that bacterial cel-

Table 1. The *nif* genes and their known or proposed roles during nitrogen fixation in all species^a

Cluster/gene	Function
<i>nifQ</i>	Involved in FeMo-co synthesis; proposed to function in early MoO ₄ ²⁻ processing
<i>nifB</i>	Required for FeMo-co synthesis; its metabolic product, <i>nifB</i> -co, is a specific Fe and S donor to FeMo-co
<i>nifA</i>	Positive regulatory element
<i>nifL</i>	Negative regulatory element
mfABCDGEH	Involved in electron transport to nitrogenase, possibly functioning to drive the thermodynamically unfavorable reverse electron transfer from NADH to ferredoxin
nifHDKTY	
<i>nifH</i>	Fe protein; required for FeMo-co biosynthesis and apo-MoFe protein maturation; electron donor to MoFe protein during nitrogenase
<i>nifD</i>	Alpha subunit of MoFe protein; forms an $\alpha_2\beta_2$ tetramer with the β subunit; the site of substrate reduction, FeMo-co, is within the α subunit of MoFe protein
<i>nifK</i>	Beta subunits of MoFe protein P clusters are present at each $\alpha\beta$ subunit interface
<i>nifT</i>	Unknown
<i>nifY/nafY</i>	Chaperone for the apo-MoFe protein <i>NafY</i> is also a FeMo-co carrier and is proposed to aid in the insertion of FeMo-co into apo-MoFe protein
nifENX	
<i>nifE</i>	Forms $\alpha_2\beta_2$ tetramer with <i>NifN</i> ; required for FeMo-co synthesis; proposed to function as a scaffold on which FeMo-co is synthesized
<i>nifN</i>	Required for FeMo-co synthesis; tetramer with <i>NifE</i>
<i>nifX</i>	Involved in FeMo-co synthesis; accumulates a FeSMo-containing precursor
nifUSV	
<i>nifU</i>	Molecular scaffold for the formation of Fe-S cluster for nitrogenase components
<i>nifS</i>	Involved in mobilization of S for Fe-S cluster synthesis and repair
<i>nifV</i>	Homocitrate synthase, involved in FeMo-co synthesis
nifWZM	
<i>nifW</i>	Involved in stability of MoFe protein
<i>nifZ</i>	Unknown
<i>nifM</i>	Required for the maturation of <i>NifH</i>
<i>nifF</i>	Flavodoxin; physiological electron donor to <i>NifH</i> in <i>Klebsiella pneumoniae</i>
modABC	Encodes an ABC-type, high-affinity, molybdate transporter
<i>hesB</i>	Binding to a 2 iron, 2 sulfur (2Fe-2S) cluster; this cluster consists of two iron atoms, with two inorganic sulfur atoms found between the irons and acting as bridging ligands
<i>cysE</i>	Biosynthesis of cysteine

^a As reported by Rubio and Ludden 2005; Yan et al. 2008.

lular nitrogen is composed of 75 to 88% of glutamate and 12 to 25% glutamine, which act as main nitrogen donors (Prusiner and Stadtman 1973; Yang et al. 2018).

In *P. stutzeri* A1501, the expression of the nitrogen fixation-specific regulatory protein NifLA is controlled by the nitrogen regulatory cascade AmtB-GlnK-NtrBC (Yang et al. 2018). During N-fixing conditions, genes of the NFI had a more than tenfold higher transcript level and were downregulated after ammonium shock (Yan et al. 2010; Yang et al. 2018). *NtrC* and *glnK* are necessary for the expression of NifA, and in turn NifA is expected to play a major role in the expression of *Ntr* (nitroreductase) genes. Under constitutive expression of NifA in a *P. stutzeri* A1501 *glnK*⁻ mutant, nitrogenase activity and nitrogen fixation have been restored and observed under presence of ammonia (He et al. 2008). Thus, it was proposed that GlnK acts as a key regulatory element in control of ammonia assimilation, *nifA* expression, and in modulation of NifA activity by NifL (He et al. 2008).

The study by Yang et al. 2018 showed that other microbes can be genetically engineered to acquire the ability to fix nitrogen via the NFI. Furthermore, it successfully combines multi-omics approaches in the study of microbes and their metabolic processes.

Understanding the microbial process of N fixation is fundamental to shed light on the molecular mechanism of plant-microbe interactions (PMI). However, this knowledge must be put into context with plant responses also, to fully understand the interaction between plants and *Pseudomonas* spp. during N fixation.

Plant Molecular Components Involved in Uptake of *Pseudomonas*-Derived N

Root nitrogen transporters and central N metabolism.

It has been shown that, in cases of excess or deficient N supply, the plant transporters of the AMT and the nitrate transport system (NRT) will be adjusted accordingly, together with other crucial enzymes of central N metabolism, such as nitrate reductase, nitrite reductase, GS, and GOGAT (Muratore et al. 2021).

To check if this is true under bacterial inoculation, Trinh et al. (2018) investigated the expression of N-related genes during *A. thaliana* and *Lactuca sativa* (lettuce) interaction with *P. nitroreducens* IHB B 13561. They focused on the nitrate transporter genes *NRT1.1*, *NRT1.2*, *NRT2.1*, *NRT2.2*, *NRT2.5*, and *NRT2.6* (Mantelin et al. 2006); *NIR1*, *NLP6*, and *NLP7*, which are involved in nitrate response; *EIN1* and *ERF1*, which play roles in the ethylene response pathway; *ARF19*, *ARF7*, and *AXR4*, which are involved in the auxin signaling pathways; and the ammonium transporters *AMT1.1*, *AMT1.2*, and *AMT2* (Trinh et al. 2018).

Out of these genes in *A. thaliana*, higher expression levels were found for *NRT2.1*, *NRT2.2*, and *NRT2.6*.

However, a lower N content was measured in the seedlings during inoculation with *P. nitroreducens* IHB, which the authors assumed to be based on a higher rate of cell division requiring a more rapid nitrate metabolism. In return, a lower inner nitrate content induced NRT2 genes, increasing nitrate uptake (Trinh et al. 2018). Thus, in *Arabidopsis*, *P. nitroreducens* IHB influenced root physiology (Fig. 5).

Similarly, in lettuce, three nitrate transporter genes (*LsNRT1*, *LsNRT2*, *LsNRT2.5*) were examined after inoculation with *P. nitroreducens* IHB. *LsNRT1* and *LsNRT2* showed higher levels of expression. *LsNRT2* and *AtNRT2.1* are highly similar in their sequence alignments, suggesting similar responses in these two different species. Consequently, *P. nitroreducens* IHB inoculation increased the nitrate uptake and promoted growth by increasing the levels of transcripts of *NRT2.1* in both *A. thaliana*

and *L. sativa* (Fig. 5) (Poitout et al. 2017; Trinh et al. 2018). In addition, metabolic stimulation and induction of cell development is proposed to be a driving force for the growth promotion in both *A. thaliana* and *L. sativa* by *P. nitroreducens* IHB (Trinh et al. 2018). It is speculated that ammonium is primarily used for the elevated cell division to synthesize essential proteins and other compounds (Howitt and Udvardi 2000; Pratelli and Pilot 2014). Interestingly, increased transcripts of transporters of the NRT2 family were observed in both *L. sativa* and *A. thaliana* during this study, while the nitrate levels in the plant declined (Trinh et al. 2018), indicating that the assimilation of nitrate is preferred over storage in the vacuole. *P. nitroreducens* IHB seems to be a promising candidate for improved plant performance by increasing plant growth in *A. thaliana* and *L. sativa* and improving soil nitrate utilization (Fig. 5, top) (Trinh et al. 2018).

Solanum lycopersicum (tomato) inoculated with *P. fluorescens* Pf-16 showed a molecular reprogramming during the early stages of inoculation (Fig. 5, middle) (Scotti et al. 2019). The stages can be distinguished into <48 h and >48 h. During the earlier stage, Pf-16 inoculation led to increased gene expression of *AMT1.3* (Solyc03g045070.1.1) while decreasing gene expression of *NRT2.1* (Solyc00g090860.1.1) and *NRT2.4* (Solyc11g069760.1.1) (Fig. 6). In the later stage, almost no changes in the expression of *AMT1.3*, *NRT2.1*, and *NRT2.4* were detectable, while cell-wall modifications and upregulations of plant growth-promotion genes were observed (Scotti et al. 2019). The main finding of the study by Scotti et al. (2019) was that Pf-16 inoculation can both increase the tolerance against biotic and abiotic stresses and promote plant growth simultaneously. However, the authors have also shown that nitrogen-related transcript dynamics during the early stage of PMI, measuring the plant response over a longer period, might give further insight in the molecular mechanism. Those dynamics could be used to identify the timepoint of growth promotion during PMI and would clarify whether the plant responds only for a short period after inoculation, requiring more frequent inoculations to improve plant growth, or if a single inoculation is sufficient.

Amino acid metabolism.

Besides changes on N-related transporters or enzymes, other pathways are involved in promoting plant growth during PMI. Transcription analyses discovered the upregulation of two genes in *Arabidopsis* inoculated with *P. putida* MTCC5279, namely, At3g47340, a glutamine-dependent asparagine synthase 1, and At3g10340, an ammonia lyase (Fig. 5, bottom) (Srivastava et al. 2012). Asparagine, due to its high N:C ratio and stability, is the preferred form for long-distance transport and storage of N in most higher plants and can account for 86% of transported N (Mifflin and Lea 1980; Urquhart and Joy 1981; Sieciechowicz et al. 1988). The higher abundance of transcripts of the glutamine-dependent asparagine synthase 1 (At3g47340) indicate that assimilated nitrogen might be converted into glutamine and, further, into asparagine for potential transport within the plant during PMI. Thus, it might be interesting to analyze the amino acid profile of plants during PMI to investigate this hypothesis. At3g10340 encodes phenylalanine ammonia lyase 4 (PAL4), which is involved in the phenylpropanoid pathway, catalyzing the first step of non-oxidative deamination of L-phenylalanine to 7,8-unsaturated *trans*-cinnamic acid and an ammonium ion. Ammonium is directly recycled via the GS/GOGAT pathway to regenerate arogenate, which is required for further metabolism of cinnamic acid to various phenylpropanoids and their derivatives. The phenylpropanoid pathway is responsible for the synthesis of a large range of natural products in plants, including flavonoids (pigments and UV protectants), the structural polymer lignin, and antimicrobial furanocoumarin and isoflavonoid phytoalexins (Hahlbrock and

Scheel 1989; Dixon and Paiva 1995). Salicylic acid, which is involved in the establishment of both local and systemic plant defense responses, is also a product of this pathway (Klessig and Malamy 1994).

Open questions.

Despite several approaches to study molecular mechanisms, a big challenge is missing characterizations of proteins involved in PMI, showing the importance of functional characterization approaches to update databases and allow further research in this area. One example is a study about the interaction of *P. fluorescens* PICF7 with wheat and barley on a molecular basis by performing a proteomics approach (Fröhlich et al. 2012). The root proteome of inoculated seedlings of wheat and barley re-

vealed 14 and 24 proteins exclusively abundant during PICF7 inoculation, respectively. However, only three of the 14 proteins in wheat have shown similarities to databases, namely a putative Nodal modulator 3, a phosphoenolpyruvate carboxylase, and an *S*-formylglutathione hydrolase-like protein, whereas the proteins of barley are predicted or uncharacterized proteins (0 of 6 known proteins in barley).

BNF in *Pseudomonas* spp. and the Influence of the Abiotic Environment to Plant Growth Promotion

To test the contribution of BNF to total plant N content, maize and wheat were grown in ¹⁵N-supplemented soil, with *P. prote-*

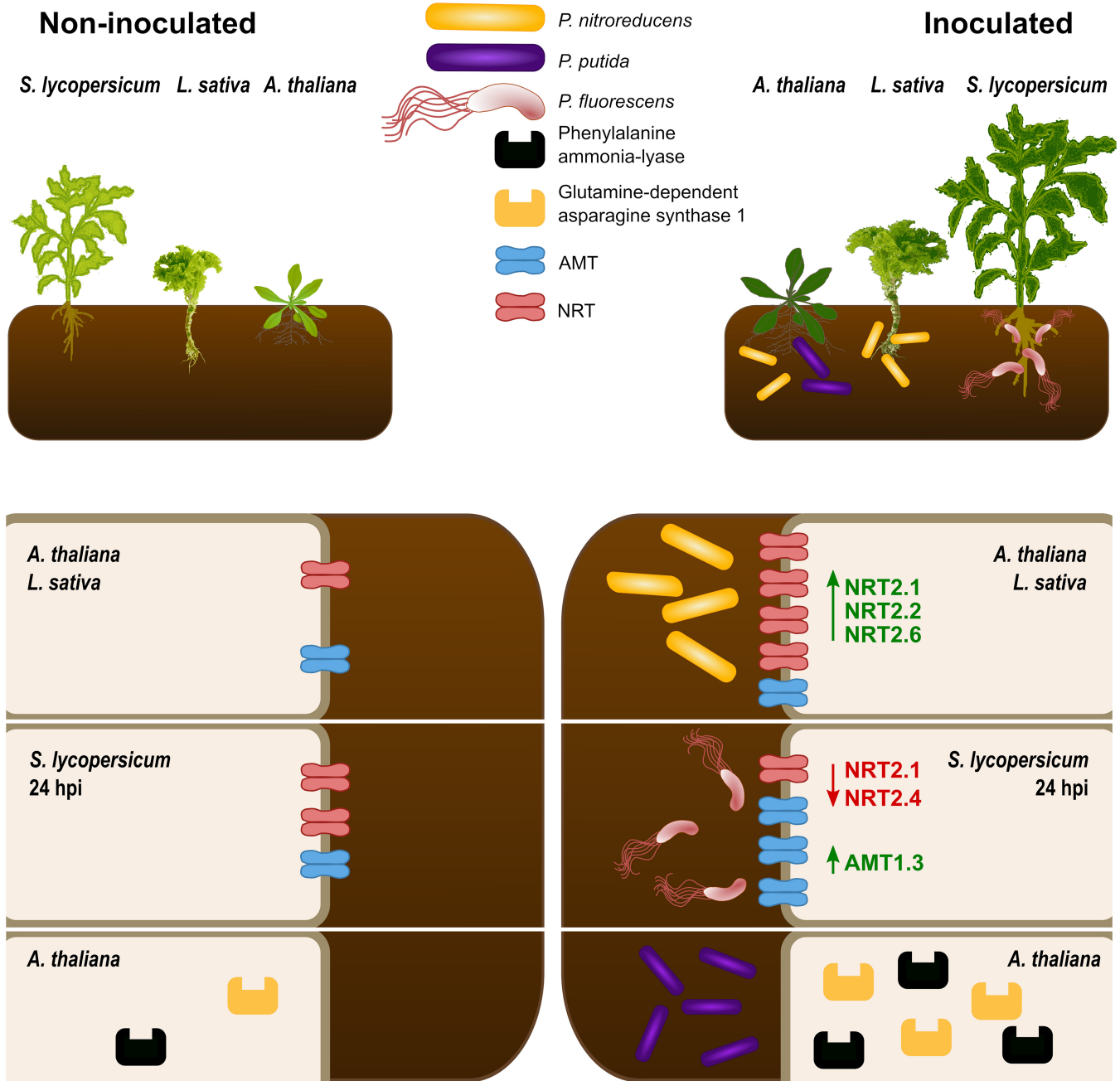


Fig. 5. Molecular mechanisms of plant-microbe interactions. Colonization with beneficial bacteria alters the expression of genes, transcripts, and proteins. Inoculation with *Pseudomonas nitroreducens* increases the abundance of N-related transporters NRT2.1, NRT2.2, NRT2.6, while inoculation with *Pseudomonas fluorescens* increases abundance of AMT1.3 but decreases NRT2.1 and NRT2.4. Genes encoding glutamine-dependent asparagine synthase 1 and phenylalanine ammonia lyase are upregulated in response to inoculation with *Pseudomonas putida*.

gens Pf-5 with and without the X940 cosmid in the greenhouse (Table 2) (Fox et al. 2016). ^{15}N was used to increase the $^{15}\text{N}/^{14}\text{N}$ ratio in the soil. Thus, nitrogen originating from the air would have a comparatively higher ^{14}N fraction than that from soil and would be indicative of N fixation. BNF was proposed to be active from the early stages of plant growth, since measurements of the $\delta^{15}\text{N}$ value 1 month after inoculation showed significantly lower ^{15}N in root, leaf, and stem tissues of Pf-5 X940-treated maize and wheat plants than in those of Pf-5-treated plants (Fox et al. 2016). Two months after inoculation, the nitrogen content derived from gaseous nitrogen (%Ndfa) in Pf-5 X940-treated maize and wheat plant organs was 74 and 85% for roots, 63 and 78% for leaves, and 70 and 82% for stems, respectively, indicating the assimilation of nitrogen derived from air. Plant growth promotion was also shown in various flowering plant species inoculated with Pf-5 X940 under sterile hydroponic growth-chamber conditions (Table 2). The beneficial effect might be the result of an increased ammonium excretion (Fox et al. 2016).

Confocal microscopy with green fluorescent protein-tagged Pf-5 and Pf-5 X940 demonstrated that both strains appear to colonize solely the rhizosphere and neither the endosphere nor the phyllosphere (Fox et al. 2016). Due to the functionality of the X940 cosmid in different *Pseudomonas* spp., transformation of established *Pseudomonas* strains with the X940 cosmid and application in agriculture might lead to increased plant performance and yield.

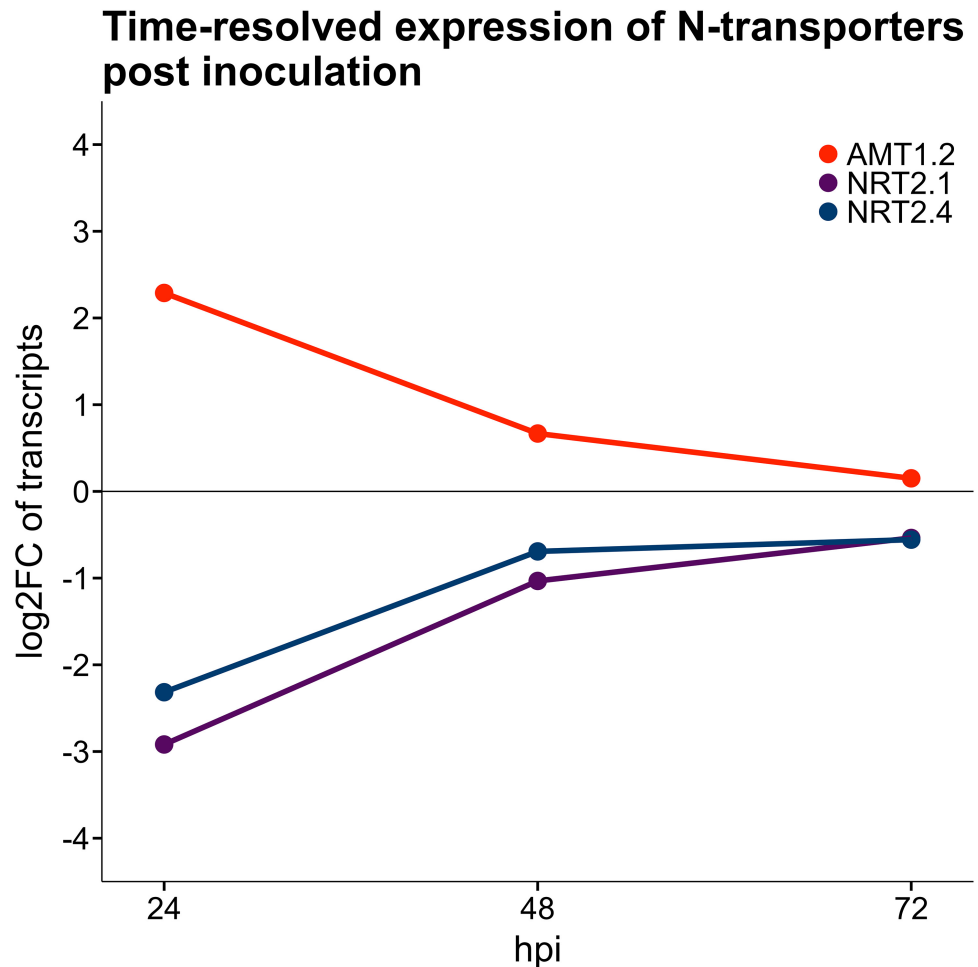
Ke et al. (2019) tested the contribution of *P. stutzeri* A1501 to BNF in well-watered and water-deficient conditions using maize. Using sterilized soil, an increase of 27.8 %Ndfa was measured in well-watered conditions, while under water defi-

ciency only 17.5 %Ndfa was observed. In absolute values, a total of 0.90 g of plant N was fixed in well-watered conditions and 0.30 g of plant N in water-deficient conditions. When grown in natural soil, the nitrogen derived from N_2 was 0.72 and 0.18 g per plant (23.6 and 14.1%) for well-watered and water-deficient conditions, respectively. Ke et al. (2019) was able to show the actual amounts of nitrogen fixed by *P. stutzeri* A1501, both in sterile and natural conditions. This shows the potential use of *P. stutzeri* A1501 to increase total N content in plants and therefore increase the biomass production (Ke et al. 2019) and underlines the importance of water supply for successful PMI.

P. psychrotolerans CS51, having genes for both denitrification and ammonification, could not only be used for plant growth promotion but also for denitrification of soils. This could mean that, in anoxic environments, such as soils containing a lot of water (like rice fields), NO_3^- could be used for denitrification, while in dry soils, respiratory ammonification occurs (Torres et al. 2016). As denitrification is not linked to plant growth promotion, the application of this strain seems to be limited to plants growing in dry soils. This strain might become more relevant with the future challenges we are facing, such as climate change and drought. Additionally, it indicates that soil properties impact the direction of the chemical reaction. Importantly, increased metabolism involving NO_3^- could remove highly abundant nitrate from the soil, resulting in a decreased nitrate leaching to ground water.

Afzal et al. (2010) shows that not only the water and nitrogen availability or N_2 -fixation play a major role in increasing the plant N content but that other nutrients are important too. The authors tested the co-inoculation of *Glycine max* (soybean) with *Bradyrhizobium japonicum* TAL 377 and *Pseudomonas* sp.

Fig. 6. Time-resolved changes on transcript level of N-related transporters postinoculation with *Pseudomonas fluorescens*. Log₂ fold changes (log₂FC) of AMT1.3, NRT2.1, NRT2.4 in *Solanum lycopersicum* roots inoculated with *P. fluorescens* 24, 48, and 72 h postinoculation (hpi). A strong early response can be observed soon after inoculation (24 hpi), which declines over time (72 hpi). During the early stage of inoculation (24 hpi), NRT2.1 and NRT2.4 are downregulated, whereas AMT1.3 is upregulated. Data from Scotti et al. (2019).



strain 54RB under varying phosphorus availability. For the pot experiments, a dose of 0.3 g of nitrogen per pot was applied in the form of urea, and different phosphorus levels were introduced by adding either no additional P or 1.35 g of P₂O₅ (50 kg per hectare) in the form of single superphosphate (SSP) to treated conditions. However, one must keep in mind that SSP also contains Ca and S, indicating that the following plant phenotypic changes are not only based on increased P but also increased Ca and S levels. Co-inoculation with both strains had positive effects in P₂O₅-treated conditions in terms of number of pods, grain yield, seed N and P, and total available P and N in soil. The available N content in soil was increased by 72% over P₂O₅-only treated plants, indicating that the availability of other nutrients (nutrient crosstalk) is also decisive for better N content in plants (Afzal et al. 2010). Observing *Pseudomonas* sp. strain 54RB promoting plant growth on its own and increasing available N in cooperation with another strain hints to its compatibility in microbial communities, and future combinations could include P-solubilizing microbes to avoid limitations, as per Liebig's law of the minimum. The exchange of nutrients and carbon between plants and microbes can occur at the plant root surface or within the plant root tissue (symplastic, apoplastic). The cumulative activity of the bacterial transmembrane transporters, the so-called transportome, plays a crucial role in PMI and determines which ecological niche is occupied in the rhizosphere (Silby et al. 2009; Larsen et al. 2015; Wilton et al. 2018). The activity of the bacterial transportome of several *Pseudomonas* spp. can lead to protection against nutrient stresses (Shinde et al. 2017; Wilton et al. 2018).

Moreover, the ability of many *Pseudomonas* spp. to grow at lower temperatures ensures propagation and survivability in fields, despite changing temperatures of the soils (Kwon et al. 2003). An outstanding example is *Pseudomonas migulae*. *P. migulae* was isolated from the Chhiplakot region, in the Western Indian Himalaya (Suyal et al. 2014). This N₂-fixing strain has adapted to different abiotic stresses, including cold tempera-

ture, height, and oxidative stress, which made it possible to fix N at temperatures of 5 to 10°C (Suyal et al. 2014). This shows once more that testing different strains from various geographical locations is valuable, as it gives insight into the mechanistic acclimation to varying environmental factors (*P. stutzeri* tested from different geographical locations [Venieraki et al. 2014]). Consequently, beneficial *Pseudomonas* species could be collected, applicable for fields in various geo-climatic regions.

Conclusions and Open Questions

A number of plant species were tested with *Pseudomonas* spp. and have shown beneficial responses that can be linked to improved N content in the plant. This encourages the further study of the use of *Pseudomonas* spp. for future agricultural applications, to ultimately reduce the application of N fertilizer while maintaining the required amount of biomass. Due to the ubiquitous distribution of the genus in the world soils and, inherently, to the adaptation to most global conditions, strains can be found that will work in fields across the globe. Despite the potential depicted, we here note that many of the mentioned studies tested the plant growth-promoting effects in natural soil but not directly in the field. Field trials come with additional challenges, like ever-changing conditions and microbial communities, compared with controlled environments. Nevertheless, *P. stutzeri* A1501 stands out as a good candidate for plant growth promotion in conditions with limited water supply (Ke et al. 2019). One additional gap is clear understanding of how these strains would perform in field microbial communities and under a variety of abiotic stresses.

In terms of yield, no clear evidence is displayed in this review, leaving the question open. Furthermore, we must keep in mind that, although we focus on N-fixation, *Pseudomonas* spp. (as other strains) have the potential to promote plant growth by promoting a greater root system, which in turn will reflect in better nutrient scavenging. An important example for this was recently

Table 2. Summary of plant phenotype responses upon inoculation with various *Pseudomonas* spp.^a

Plant species	Inoculant	Sterile	Plant response (inoculated vs. control)			Citation
			Nutrient content	Biomass ^a	Root phenotype	
<i>Zea mays</i> (Pannar BIOGENE BG6607YR)	PF-X940	X	Shoot: +170% (N) Seed: +556% (N)		Bacteria contribution to N: increased	Fox et al. 2016
<i>Triticum aestivum</i> (Bobwhite 26)	PF-X940	X	Shoot: +85% (N) Seed: +379% (N)		Bacteria contribution to N: increased	Fox et al. 2016
Maize	<i>P. stutzeri</i> A1501	X	Shoot: +14.1–23.6% (N)	SDW: +20.2% RDW: +31.2%		Ke et al. 2019
	<i>P. stutzeri</i> A1501 (natural growth conditions)	✓	Shoot: +17.5–27.8% (N)	SDW: +59% RDW: +93%		Ke et al. 2019
Rice (Super Basmati)	<i>Pseudomonas</i> sp. strain K1	X		SDW: +100% Seed: +55%		Mirza et al. 2006
Rice (Super Basmati 385)	<i>Pseudomonas</i> sp. strain K1	X		SDW: +59% Seed: +93%		Mirza et al. 2006
<i>Brassica juncea</i> (brown mustard)	<i>P. aeruginosa</i> (seed-coated)	X	Whole-plant: +40.61% (N); +100% (P)		Root length: +25%	Roychowdhury et al. 2019
	<i>P. aeruginosa</i> (rhizosphere-inoculation)	X	Whole plant: +19.9% (N)		Root length: +6.25%	Roychowdhury et al. 2019
<i>Phaseolus vulgaris</i> L. (common bean)	<i>Rhizobium</i> sp. + <i>Pseudomonas</i> sp. strain Luc2	X	Shoot: –8% (N) Bacteria contribution to N: –31.4% (N)	SDW: –1.25% RDW: +5.76%	Root length: +21%	Stajkovic et al. 2011
<i>Phaseolus vulgaris</i> L. (common bean)	<i>Rhizobium</i> sp. + <i>Pseudomonas</i> sp. strain LG	X	Shoot: +29.1% (N) Bacteria contribution to N: +113.8% (N)	SDW: +27.9% Root: –2.2%	Root length: +13.4%	Stajkovic et al. 2011
<i>Glycine max</i> (soybean)	<i>Pseudomonas</i> sp. strain 54RB	X	Seed: +17.4% (N); +11.9% (P)	Seed: +75.6% Shoot: +29.5% Root: +21.7%		Afzal et al. 2010

^a SDW = shoot dry weight; RDW = root dry weight.

published for a different clade of bacteria, certain *Oxalobacteraceae* spp., particularly of the genus *Massilia*, that affect lateral root development of maize and thereby increase N acquisition under N-limitation without bacterial N₂ fixation (Yu et al. 2021). Interestingly, only certain maize genotypes were able to attract and stimulate the propagation of these bacteria by secreting distinct flavones under N limitation, suggesting that crops can influence the abundance of root-associated microbiota via exudation of specific compounds (Yu et al. 2021). This, in consequence, suggests that root-rhizobacteria interactions cannot only be established by inoculation of plants with beneficial microbes but, potentially, more robustly, by targeted plant breeding, which we propose should be investigated for crops other than maize.

We note a gap in understanding the plant responses on the protein level and through plant development (e.g., from moment of inoculation) as this was only addressed in a few studies. In further approaches, key regulatory genes, peptides, proteins, enzymes, signaling molecules, and metabolites and lipids could be investigated and used for testing potential conserved plant growth-promoting domains throughout the *Pseudomonas* genus. In the ideal case, this knowledge could be transferred to other genera of bacteria.

Literature Cited

- Afzal, A., Bano, A., and Fatima, M. 2010. Higher soybean yield by inoculation with N-fixing and P-solubilizing bacteria. *Agron. Sustain. Dev.* 30:487-495.
- Bakkou, N. 2011. Characterization of the endosymbiotic forms of *Sinorhizobium* sp. strain NGR234. Ph.D. dissertation. University of Geneva, Geneva, Switzerland.
- Beier, M. P., Fujita, T., Sasaki, K., Kanno, K., Ohashi, M., Tamura, W., Konishi, N., Saito, M., Imagawa, F., Ishiyama, K., Miyao, A., Yamaya, T., and Kojima, S. 2019. The urea transporter DUR3 contributes to rice production under nitrogen-deficient and field conditions. *Physiol. Plant.* 167:75-89.
- Ben Hassen, T., and El Bilali, H. 2022. Impacts of the Russia-Ukraine war on global food security: Towards more sustainable and resilient food systems? *Foods* 11:2301.
- Bindel, N., and Neuhäuser, B. 2021. High-affinity ammonium transport by *Arabidopsis thaliana* AMT1;4. *Acta Physiol. Plant.* 43:1-5.
- Bock, E., and Wagner, M. 2001. Oxidation of inorganic nitrogen compounds as an energy source. Pages 457-495 in *The Prokaryotes: A Handbook on the Biology of Bacteria*, M. Dworkin, S. Falkow, E. Rosenberg, K.-H. Schleifer, and E. Stackebrandt, eds. Springer, New York.
- Boddey, R. M., De Oliveira, O. C., Urquiaga, S., Reis, V. M., De Olivares, F. L., Baldani, V. L. D., and Döbereiner, J. 1995. Biological nitrogen fixation associated with sugar cane and rice: contributions and prospects for improvement. Pages 195-209 in: *Management of Biological Nitrogen Fixation for the Development of More Productive and Sustainable Agricultural Systems: Extended Versions of Papers Presented at the Symposium on Biological Nitrogen Fixation for Sustainable Agriculture at the 15th Congress of Soil Science, Acapulco, Mexico, 1994* Springer, Dordrecht, The Netherlands.
- Bueno Batista, M., and Dixon, R. 2019. Manipulating nitrogen regulation in diazotrophic bacteria for agronomic benefit. *Biochem. Soc. Trans.* 47:603-614.
- Cerezo, M., Tillard, P., Filleur, S., Muñoz, S., Daniel-Vedele, F., and Gojon, A. 2001. Major alterations of the regulation of root NO₃⁻ uptake are associated with the mutation of *Nrt2.1* and *Nrt2.2* genes in *Arabidopsis*. *Plant Physiol.* 127:262-271.
- Chaudhary, P., Khatri, P., Chaudhary, A., Maithani, D., Kumar, G., and Sharma, A. 2021. Cultivable and metagenomic approach to study the combined impact of nanogypsum and *Pseudomonas taiwanensis* on maize plant health and its rhizospheric microbiome. *PLoS One* 16: e0250574.
- Combes-Meynet, E., Pothier, J. F., Moëgne-Loccoz, Y., and Prigent-Combaret, C. 2011. The *Pseudomonas* secondary metabolite 2,4-diacetylphloroglucinol is a signal inducing rhizoplane expression of *Azospirillum* genes involved in plant-growth promotion. *Mol. Plant-Microbe Interact.* 24:271-284.
- Daims, H., Lebedeva, E. V., Pjevac, P., Han, P., Herbold, C., Albertsen, M., Jehmlich, N., Palatinszky, M., Vierheilig, J., Bulaev, A., Kirkegaard, R. H., von Bergen, M., Rattei, T., Bendinger, B., Nielsen, P. H., and Wagner, M. 2015. Complete nitrification by *Nitrospira* bacteria. *Nature* 528:504-509.
- Day, D. A., Kaiser, B. N., Thomson, R., Udvardi, M. K., Moreau, S., and Puppò, A. 2001. Nutrient transport across symbiotic membranes from legume nodules. *Funct. Plant Biol.* 28:669-676.
- Dixon, R., and Paiva, N. 1995. Stress-induced phenylpropanoid metabolism. *Plant Cell* 7:1085-1097.
- Egamberdieva, D. 2009. Alleviation of salt stress by plant growth regulators and IAA producing bacteria in wheat. *Acta Physiol. Plant.* 31:861-864.
- Erisman, J. W., Sutton, M. A., Galloway, J., Klimont, Z., and Winiwarer, W. 2008. How a century of ammonia synthesis changed the world. *Nat. Geosci.* 1:636-639.
- Etesami, H., and Adl, S. M. 2020. Can interaction between silicon and non-rhizobial bacteria benefit in improving nodulation and nitrogen fixation in salinity-stressed legumes? A review. *Rhizosphere* 100229.
- Filleur, S., Dorbe, M.-F., Cerezo, M., Orsel, M., Granier, F., Gojon, A., and Daniel-Vedele, F. 2001. An *Arabidopsis* T-DNA mutant affected in *Nrt2* genes is impaired in nitrate uptake. *FEBS Lett.* 489:220-224.
- Fox, A. R., Soto, G., Valverde, C., Russo, D., Lagares, A., Zorreguieta, Á., Alleva, K., Pascuan, C., Frare, R., Mercado-Blanco, J., Dixon, R., and Ayub, N. D. 2016. Major cereal crops benefit from biological nitrogen fixation when inoculated with the nitrogen-fixing bacterium *Pseudomonas protegens* Pf-5×940: Robust biological nitrogen fixation in major cereal crops. *Environ. Microbiol.* 18:3522-3534.
- Frache, C., Lindström, K., and Elmerich, C. 2009. Nitrogen-fixing bacteria associated with leguminous and non-leguminous plants. *Plant Soil* 321:35-59.
- Fröhlich, A., Buddrus-Schiemann, K., Durner, J., Hartmann, A., and Von Rad, U. 2012. Response of barley to root colonization by *Pseudomonas* sp. DSMZ 13134 under laboratory, greenhouse, and field conditions. *J. Plant Interact.* 7:1-9.
- Gautrat, P., Laffont, C., Frugier, F., and Ruffel, S. 2020. Nitrogen systemic signaling: From symbiotic nodulation to root acquisition. *Trends Plant Sci.* 26:392-406.
- Giehl, R. F., Laginha, A. M., Duan, F., Rentsch, D., Yuan, L., and von Wirén, N. 2017. A critical role of AMT2;1 in root-to-shoot translocation of ammonium in *Arabidopsis*. *Mol. Plant* 10 1449-1460.
- Girin, T., Lejay, L., Wirth, J., Widiez, T., Palenchar, P. M., Nazoa, P., Touraine, B., Gojon, A., and Lepetit, M. 2007. Identification of a 150-bp cis-acting element of the AtNRT2.1 promoter involved in the regulation of gene expression by the N and C status of the plant: Identification of cis-elements involved in the regulation of NO₃⁻ uptake. *Plant Cell Environ.* 30:1366-1380.
- Gerke, C., Daumann, M., Niopek-Witz, S., Möhlmann, T. 2014. Nucleobase and nucleoside transport and integration into plant metabolism. *Front. Plant Sci.* 5:e00443.
- Glick, B. R. 1995. The enhancement of plant growth by free-living bacteria. *Can. J. Microbiol.* 41:109-117.
- Glick, B. R. 2014. Bacteria with ACC deaminase can promote plant growth and help to feed the world. *Microbiol. Res.* 169:30-39.
- Glick, B. R., and Bashan, Y. 1997. Genetic manipulation of plant growth-promoting bacteria to enhance biocontrol of phytopathogens. *Biotechnol. Adv.* 15:353-378.
- Glick, B. R., Holguin, G., Patten, C. L., and Penrose, D. M. 1999. *Biochemical and Genetic Mechanisms Used By Plant Growth Promoting Bacteria*. World Scientific, London.
- Hahlbrock, K., and Scheel, D. 1989. Physiology and molecular biology of phenylpropanoid metabolism. *Ann. Rev. Plant Biol.* 40:347-369.
- He, S., Chen, M., Xie, Z., Yan, Y., Li, H., Fan, Y., Ping, S., Lin, M., and Elmerich, C. 2008. Involvement of GlnK, a PII protein, in control of nitrogen fixation and ammonia assimilation in *Pseudomonas stutzeri* A1501. *Arch. Microbiol.* 190:1-10.
- Hirel, B., Tétu, T., Lea, P. J., and Dubois, F. 2011. Improving nitrogen use efficiency in crops for sustainable agriculture. *Sustainability* 3:1452-1485.
- Howitt, S. M., and Udvardi, M. K. 2000. Structure, function and regulation of ammonium transporters in plants. *BBA-Biomembranes* 1465:152-170.
- Iniguez, A. L., Dong, Y., and Triplett, E. W. 2004. Nitrogen fixation in wheat provided by *Klebsiella pneumoniae* 342. *Mol. Plant-Microbe Interact.* 17:1078-1085.
- Jagtap, S., Trollman, H., Trollman, F., Garcia-Garcia, G., Parra-López, C., Duong, L., Martindale, W., Munekata, P. E. S., Lorenzo, J. M., Hdaifeh, A., Hassoun, A., Salonitis, K., and Afy-Shararah, M. 2022. The Russia-Ukraine conflict: Its implications for the global food supply chains. *Foods* 11:2098.
- Jiménez, J. A., Novinscak, A., and Fillion, M. 2020. Inoculation with the plant-growth-promoting rhizobacterium *Pseudomonas fluorescens* lbm677 impacts the rhizosphere microbiome of three oilseed crops. *Front. Microbiol.* 11:569366.

- Kang, S.-M., Asaf, S., Khan, A. L., Lubna, Khan, A., Mun, B.-G., Khan, M. A., Gul, H., and Lee, I.-J. 2020. Complete genome sequence of *Pseudomonas psychrotolerans* CS51, a plant growth-promoting bacterium, under heavy metal stress conditions. *Microorganisms* 8:382.
- Ke, X., Feng, S., Wang, J., Lu, W., Zhang, W., Chen, M., and Lin, M. 2019. Effect of inoculation with nitrogen-fixing bacterium *Pseudomonas stutzeri* A1501 on maize plant growth and the microbiome indigenous to the rhizosphere. *Syst. Appl. Microbiol.* 42:248-260.
- Klessig, D. F., and Malamy, J. 1994. The salicylic acid signal in plants. *Plant Mol. Biol.* 26:1439-1458.
- Klimczyk, M., Siczek, A., and Schimmelpfennig, L. 2021. Improving the efficiency of urea-based fertilization leading to reduction in ammonia emission. *Sci. Total Environ.* 771:145483.
- Klopper, J. W., Lifshitz, R., and Zablutowicz, R. M. 1989. Free-living bacterial inocula for enhancing crop productivity. *Trends Biotechnol.* 7:39-44.
- Kwon, S. W., Kim, J. S., Park, I. C., Yoon, S. H., Park, D. H., Lim, C. K., and Go, S. J. 2003. *Pseudomonas korensis* sp. nov., *Pseudomonas umsongensis* sp. nov. and *Pseudomonas jinjuensis* sp. nov., novel species from farm soils in Korea. *Int. J. Syst. Evol. Microbiol.* 53:21-27.
- Lam, H.-M., Coschigano, K. T., Oliveira, I. C., Melo-Oliveira, R., and Coruzzi, G. M. 1996. The molecular-genetics of nitrogen assimilation into amino acids in higher plants. *Annu. Rev. Plant. Physiol. Plant. Mol. Biol.* 47:569-593.
- Larsen, P. E., Collart, F. R., and Dai, Y. 2015. Predicting ecological roles in the rhizosphere using metabolome and transportome modeling. *PLoS One* 10:e0132837.
- Lejay, L., Tillard, P., Lepetit, M., Olive, F. D., Filleur, S., Daniel-Vedele, F., and Gojon, A. 1999. Molecular and functional regulation of two NO₃⁻ uptake systems by N- and C-status of *Arabidopsis* plants. *Plant J.* 18:509-519.
- Li, W., Wang, Y., Okamoto, M., Crawford, N. M., Siddiqi, M. Y., and Glass, A. D. M. 2007. Dissection of the *AtNRT2.1:AtNRT2.2* inducible high-affinity nitrate transporter gene cluster. *Plant Physiol.* 143:425-433.
- Liu, L. H., Ludewig, U., Frommer, W. B., and von Wirén, N. 2003. AtDUR3 encodes a new type of high-affinity urea/H⁺ symporter in Arabidopsis. *Plant Cell* 15:790-800.
- Liu, R., Zhang, Y., Chen, P., Lin, H., Ye, G., Wang, Z., Ge, C., Zhu, B., and Ren, D. 2017. Genomic and phenotypic analyses of *Pseudomonas psychrotolerans* PRS08-11306 reveal a turneractin biosynthesis gene cluster that contributes to nitrogen fixation. *J. Biotechnol.* 253:10-13.
- Mantelin, S., Desbrosses, G., Larcher, M., Tranbarger, T. J., Cleyet-Marel, J.-C., and Touraine, B. 2006. Nitrate-dependent control of root architecture and N nutrition are altered by a plant growth-promoting *Phyllobacterium* sp. *Planta* 223, 591-603.
- Mérigout, P., Gaudon, V., Quilleré, I., Briand, X., and Daniel-Vedele, F. 2008. Urea use efficiency of hydroponically grown maize and wheat. *J. Plant Nutr.* 31:427-443.
- Mifflin, B. J., and Lea, P. J. 1980. Ammonia assimilation. Pages 169-202 in: *Amino Acids and Derivatives*. Academic Press, New York.
- Mirza, M. S., Mehnaz, S., Normand, P., Prigent-Combaret, C., Moënnelocoz, Y., Bally, R., and Malik, K. A. 2006. Molecular characterization and PCR detection of a nitrogen-fixing *Pseudomonas* strain promoting rice growth. *Biol. Fertil. Soils* 43:163-170.
- Mirza, M. S., Rasul, G., Mehnaz, S., Ladha, J. K., So, R. B., Ali, S., and Malik, K. A. 2000. Beneficial effects of inoculated nitrogen-fixing bacteria on rice. Pages 191-204 in: *The Quest for Nitrogen Fixation in Rice*. J. K. Ladha and P. M. Reddy, eds. International Rice Research Institute, Los Baños, Philippines.
- Muratore, C., Espen, L., and Prinsi, B. 2021. Nitrogen uptake in plants: The plasma membrane root transport systems from a physiological and proteomic perspective. *Plants* 10:681.
- Mustafa, S. E. 2022. The importance of Ukraine and the Russian Federation for global agricultural markets and the risks associated with the current conflict. High Level Panel of Experts on Food Security and Nutrition, Food and Agriculture Organization of the United Nations, Rome.
- Nadeem, S. M., Zahir, Z. A., Naveed, M., and Ashraf, M. 2010. Microbial ACC-deaminase: Prospects and applications for inducing salt tolerance in plants. *Crit. Rev. Plant Sci.* 29:360-393.
- Okamoto, M., Kumar, A., Li, W., Wang, Y., Siddiqi, M. Y., Crawford, N. M., and Glass, A. D. M. 2006. High-affinity nitrate transport in roots of *Arabidopsis* depends on expression of the *NAR2*-like gene *AtNRT3.1*. *Plant Physiol.* 140:1036-1046.
- Oliveira, A. D., Urquiaga, S., Döbereiner, J., and Baldani, J. I. 2002. The effect of inoculating endophytic N₂-fixing bacteria on micropropagated sugarcane plants. *Plant Soil* 242:205-215.
- Orsel, M., Chopin, F., Leleu, O., Smith, S. J., Krapp, A., Daniel-Vedele, F., and Miller, A. J. 2006. Characterization of a two-component high-affinity nitrate uptake system in *Arabidopsis*. *Physiology and protein-protein interaction. Plant Physiol.* 142:1304-1317.
- Owen, A. G., and Jones, D. L. 2001. Competition for amino acids between wheat roots and rhizosphere microorganisms and the role of amino acids in plant N acquisition. *Soil Biol. Biochem.* 33:651-657.
- Padilla, F. M., Gallardo, M., and Manzano-Agugliaro, F. 2018. Global trends in nitrate leaching research in the 1960–2017 period. *Sci. Total Environ.* 643:400-413.
- Panpatte, D. G., Shukla, Y. M., Shelat, H. N., Vyas, R. V., and Jhala, Y. K. 2017. Bacterial volatile organic compounds: A new insight for sustainable agriculture. Pages 151-166 in: *Microorganisms for Green Revolution*. Springer, Singapore.
- Podile, A. R., and Kishore, G. K. 2007. Plant growth-promoting rhizobacteria. Pages 195-230 in: *Plant-Associated Bacteria*. S. S. Gnanamanickam, ed. Springer, Dordrecht, The Netherlands.
- Poitout, A., Martinière, A., Kucharczyk, B., Queruel, N., Silva-Andia, J., Mashkooor, S., Gamet, L., Varoquaux, F., Paris, N., Sentenac, H., Touraine, B., and Desbrosses, G. 2017. Local signaling pathways regulate the Arabidopsis root developmental response to *Mesorhizobium loti* inoculation. *J. Exp. Bot.* 68:1199-1211.
- Pratelli, R., and Pilot, G. 2014. Regulation of amino acid metabolic enzymes and transporters in plants. *J. Exp. Bot.* 65:5535-5556.
- Prusiner, S., and Stadtman, E. R. 1973. *The Enzymes of Glutamine Metabolism*. Academic Press, New York.
- Ramamoorthy, V., Viswanathan, R., Raguchander, T., Prakasam, V., and Samiyappan, R. 2001. Induction of systemic resistance by plant growth promoting rhizobacteria in crop plants against pests and diseases. *Crop Prot.* 20:1-11.
- Ranathunge, K., El-Kereamy, A., Gidda, S., Bi, Y. M., and Rothstein, S. J. 2014. AMT1;1 transgenic rice plants with enhanced NH₄⁺ permeability show superior growth and higher yield under optimal and suboptimal NH₄⁺ conditions. *J. Exp. Bot.* 65:965-979.
- Ravishankara, A. R., Daniel, J. S., and Portmann, R. W. 2009. Nitrous oxide (N₂O): The dominant ozone-depleting substance emitted in the 21st century. *Science* 326:123-125.
- Raymond, J., Siefert, J. L., Staples, C. R., and Blankenship, R. E. 2004. The natural history of nitrogen fixation. *Mol. Biol. Evol.* 21:541-554.
- Remans, T., Nacry, P., Pervent, M., Girin, T., Tillard, P., Lepetit, M., and Gojon, A. 2006. A central role for the nitrate transporter NRT2.1 in the integrated morphological and physiological responses of the root system to nitrogen limitation in *Arabidopsis*. *Plant Physiol.* 140:909-921.
- Richardson, A. E. 2001. Prospects for using soil microorganisms to improve the acquisition of phosphorus by plants. *Funct. Plant Biol.* 28:897-906.
- Rodionov, D. A., Dubchak, I. L., Arkin, A. P., Alm, E. J., and Gelfand, M. S. 2005. Dissimilatory metabolism of nitrogen oxides in bacteria: Comparative reconstruction of transcriptional networks. *PLoS Comput. Biol.* 1:e55.
- Roychowdhury, R., Qaiser, T. F., Mukherjee, P., and Roy, M. 2019. Isolation and characterization of a *Pseudomonas aeruginosa* strain PGP for plant growth promotion. *P. Natl. A. Sci. India B* 89:353-360.
- Rubio, L. M., and Ludden, P. W. 2005. Maturation of nitrogenase: A biochemical puzzle. *J. Bacteriol.* 187:405-414.
- Rubio, L. M., and Ludden, P. W. 2008. Biosynthesis of the iron-molybdenum cofactor of nitrogenase. *Annu. Rev. Microbiol.* 62:93-111.
- Ryu, C., Hu, C., Reddy, M. S., and Klopper, J. W. 2003. Different signaling pathways of induced resistance by rhizobacteria in *Arabidopsis thaliana* against two pathogens of *Pseudomonas syringae*. *New Phytol.* 160:413-420.
- Saharan, B., and Nehra, V. 2011. Plant Growth Promoting Rhizobacteria: A Critical Review. *Life Sci. Med. Res.* 21:1-30.
- Sajjad Mirza, M., Ahmad, W., Latif, F., Haurat, J., Bally, R., Normand, P., and Malik, K. A. 2001. Isolation, partial characterization, and the effect of plant growth-promoting bacteria (PGPB) on micro-propagated sugarcane in vitro. *Plant Soil* 237:47-54.
- Sanford, R. A., Wagner, D. D., Wu, Q., Chee-Sanford, J. C., Thomas, S. H., Cruz-García, C., Rodríguez, G., Massol-Deyá, A., Krishnani, K. K., Ritalahti, K. M., Nissen, S., Konstantinidis, K. T., and Löffler, F. E. 2012. Unexpected nondenitrifier nitrous oxide reductase gene diversity and abundance in soils. *Proc. Natl. Acad. Sci. U.S.A.* 109:19709-19714.
- Scotti, R., D'Agostino, N., and Zaccardelli, M. 2019. Gene expression profiling of tomato roots interacting with *Pseudomonas fluorescens* unravels the molecular reprogramming that occurs during the early phases of colonization. *Symbiosis* 78:177-192.
- Setten, L., Soto, G., Mozzicafreddo, M., Fox, A. R., Lisi, C., Cuccioloni, M., Angeletti, M., Pagano, E., Díaz-Paleo, A., and Ayub, N. D. 2013.

- Engineering *Pseudomonas protegens* Pf-5 for nitrogen fixation and its application to improve plant growth under nitrogen-deficient conditions. *PLoS One* 8:e63666.
- Shinde, S., Cumming, J. R., Collart, F. R., Noirot, P. H., and Larsen, P. E. 2017. *Pseudomonas fluorescens* transportome is linked to strain-specific plant growth promotion in aspen seedlings under nutrient stress. *Front. Plant Sci.* 8:348.
- Sieciechowicz, K. A., Joy, K. W., and Ireland, R. J. 1988. The metabolism of asparagine in plants. *Phytochemistry* 27:663-671.
- Silby, M. W., Cerdeño-Tárraga, A. M., Vernikos, G. S., Giddens, S. R., Jackson, R. W., Preston, G. M., Zhang, X. X., Moon, C. D., Gehrig, S. M., Godfrey, S. A., Knight, C. G., Malone, J. G., Robinson, Z., Spiers, A. J., Harris, S., Challis, G. L., Yaxley, A. M., Harris, D., Seeger, K., Murphy, L., Rutter, S., Squares, R., Quail, M. A., Saunders, E., Mavromatis, K., Brettin, T. S., Bentley, S. D., Hothersall, J., Stephens, E., Thomas, C. M., Parkhill, J., Levy, S. B., Rainey, P. B., and Thomson, N. R. 2009. Genomic and genetic analyses of diversity and plant interactions of *Pseudomonas fluorescens*. *Genome Biol.* 10:1-16.
- Smercina, D. N., Evans, S. E., Friesen, M. L., and Tiemann, L. K. 2019. To fix or not to fix: Controls on free-living nitrogen fixation in the rhizosphere. *Appl. Environ. Microbiol.* 85:e02546-18.
- Smith, C., Hill, A. K., and Torrente-Murciano, L. 2020. Current and future role of Haber-Bosch ammonia in a carbon-free energy landscape. *Energy Environ. Sci.* 13:331-344.
- Smith, C. J., Nedwell, D. B., Dong, L. F., and Osborn, A. M. 2007. Diversity and abundance of nitrate reductase genes (*narG* and *napA*), nitrite reductase genes (*nirS* and *nrfA*), and their transcripts in estuarine sediments. *Appl. Environ. Microb.* 73:3612-3622.
- Song, B., and Tobias, C. R. 2011. Molecular and stable isotope methods to detect and measure anaerobic ammonium oxidation (anammox) in aquatic ecosystems. *Meth. Enzymol.* 496:63-89.
- Sopanen, T., Burston, D., and Matthews, D. M. 1977. Uptake of small peptides by the scutellum of germinating barley. *FEBS Lett.* 79: 4-7.
- Srivastava, S., Chaudhry, V., Mishra, A., Chauhan, P. S., Rehman, A., Yadav, A., Tuteja, N., and Nautiyal, C. S. 2012. Gene expression profiling through microarray analysis in *Arabidopsis thaliana* colonized by *Pseudomonas putida* MTCC5279, a plant growth promoting rhizobacterium. *Plant Signal. Behav.* 7:235-245.
- Stajkovic, O., Delic, D., Josic, D., Kuzmanovic, D., Rasulic, N., and Knezevic-Vukcevic, J. 2011. Improvement of common bean growth by co-inoculation with *Rhizobium* and plant growth-promoting bacteria. *Rom. Biotech. Lett.* 16:5919-5926.
- Suyal, D. C., Yadav, A., Shouche, Y., and Goel, R. 2014. Differential proteomics in response to low temperature diazotrophy of Himalayan psychrophilic nitrogen fixing *Pseudomonas migulae* S10724 strain. *Curr. Microbiol.* 68:543-550.
- Torres, M. J., Simon, J., Rowley, G., Bedmar, E. J., Richardson, D. J., Gates, A. J., and Delgado, M. J. 2016. Nitrous oxide metabolism in nitrate-reducing bacteria. *Adv. Microb. Physiol.* 68: 353-432.
- Trinh, C. S., Lee, H., Lee, W. J., Lee, S. J., Chung, N., Han, J., Kim, J., Hong, S.-W., and Lee, H. 2018. Evaluation of the plant growth-promoting activity of *Pseudomonas nitroreducens* in *Arabidopsis thaliana* and *Lactuca sativa*. *Plant Cell Rep.* 37:873-885.
- Trivedi, P., Leach, J. E., Tringe, S. G., Sa, T., and Singh, B. K. 2020. Plant-microbiome interactions: From community assembly to plant health. *Nat. Rev. Microbiol.* 18:607-621.
- Urquhart, A. A., and Joy, K. W. 1981. Use of phloem exudate technique in the study of amino acid transport in pea plants. *Plant Physiol.* 68:750-754.
- Venieraki, A., Dimou, M., Vezyri, E., Vamvakas, A., Katinaki, P.-A., Chatzipavlidis, I., Tampakaki, A., and Katinakis, P. 2014. The nitrogen-fixation island insertion site is conserved in diazotrophic *Pseudomonas stutzeri* and *Pseudomonas* sp. isolated from distal and close geographical regions. *PLoS One* 9:e105837.
- Vessey, J. K. 2003. Plant growth promoting rhizobacteria as biofertilizers. *Plant Soil* 255:571-586.
- Walter, A., Römheld, V., Marschner, H., and Crowley, D. E. 1994. Iron nutrition of cucumber and maize: Effect of *Pseudomonas putida* YC 3 and its siderophore. *Soil Biol. Biochem.* 26:1023-1031.
- Wang, H., Deng, N., Wu, D., and Hu, S. 2017. Quantitative response relationships between net nitrogen transformation rates and nitrogen functional genes during artificial vegetation restoration following agricultural abandonment. *Sci. Rep.* 7:7752.
- Waterworth, W. M., and Bray, C. M. 2006. Enigma variations for peptides and their transporters in higher plants. *Ann Bot.* 98:1-8.
- Wilton, R., Ahrendt, A. J., Shinde, S., Sholto-Douglas, D. J., Johnson, J. L., Brennan, M. B., and Kemner, K. M. 2018. A new suite of plasmid vectors for fluorescence-based imaging of root colonizing pseudomonads. *Front. Plant Sci.* 8:2242.
- Yan, Y., Ping, S., Peng, J., Han, Y., Li, L., Yang, J., Dou, Y., Li, Y., Fan, H., Fan, Y., Li, D., Zhan, Y., Chen, M., Lu, W., Zhang, W., Cheng, Q., Jin, Q., and Lin, M. 2010. Global transcriptional analysis of nitrogen fixation and ammonium repression in root-associated *Pseudomonas stutzeri* A1501. *BMC Genomics* 11:1-13.
- Yan, Y., Yang, J., Dou, Y., Chen, M., Ping, S., Peng, J., Lu, W., Zhang, W., Yao, Z., Li, H., Liu, W., He, S., Geng, L., Zhang, X., Yang, F., Yu, H., Zhan, Y., Li, D., Lin, Z., Wang, Y., Elmerich, C., Lin, M., and Jin, Q. 2008. Nitrogen fixation island and rhizosphere competence traits in the genome of root-associated *Pseudomonas stutzeri* A1501. *Proc. Natl. Acad. Sci. U.S.A.* 105:7564-7569.
- Yang, Z., Han, Y., Ma, Y., Chen, Q., Zhan, Y., Lu, W., Cai, L., Hou, M., Chen, S., Yan, Y., and Lin, M. 2018. Global investigation of an engineered nitrogen-fixing *Escherichia coli* strain reveals regulatory coupling between host and heterologous nitrogen-fixation genes. *Sci. Rep.* 8:10928.
- Yu, P., He, X., Baer, M., Beirinckx, S., Tian, T., Moya, Y. A. T., Zhang, X., Deichmann, M., Frey, F. P., Bresgen, V., Li, C., Razavi, B. S., Schaaf, G., von Wirén, N., Su, Z., Bucher, M., Tsuda, K., Goormachtig, S., Chen, X., and Hochholdinger, F. 2021. Plant flavones enrich rhizosphere Oxalobacteraceae to improve maize performance under nitrogen deprivation. *Nat. Plants* 7:481-499.
- Zhang, T., Yan, Y., He, S., Ping, S., Alam, K. M., Han, Y., Liu, X., Lu, W., Zhang, W., Chen, M., Xiang, W., Wang, X., and Lin, M. 2012. Involvement of the ammonium transporter AmtB in nitrogenase regulation and ammonium excretion in *Pseudomonas stutzeri* A1501. *Res. Microbiol.* 163:332-339.
- Zhuo, D., Okamoto, M., Vidmar, J. J., and Glass, A. D. 1999. Regulation of a putative high-affinity nitrate transporter (*Nrt2; 1At*) in roots of *Arabidopsis thaliana*. *Plant J.* 17 563-568.

MEETING REVIEW

12th Japan-US Seminar in Plant Pathology Meeting Report

Yumino Sasaki,^{1,†} Juliana González-Tobón,¹ Yuta Hino,² Chujia Jin,³ Tianrun Li,⁴ Tan Anh Nhi Nguyen,⁵ Blake Oakley,⁶ and Danielle Stevens⁴

¹ Plant Pathology and Plant-Microbe Biology Section, School of Integrative Plant Science, Cornell University, Ithaca, NY 14853, U.S.A.

² Graduate School of Bioagricultural Sciences, Nagoya University, Nagoya, Japan

³ Laboratory of Plant Pathology, Graduate School of Agriculture, Kyoto University, Kyoto, Japan

⁴ Department of Plant Pathology, University of California, Davis, Davis, CA 95616, U.S.A.

⁵ Department of Life Sciences, Graduate School of Arts and Sciences, The University of Tokyo, Tokyo, Japan

⁶ Department of Plant Pathology, University of Georgia, Athens, GA 30602, U.S.A.

Accepted for publication 24 April 2023.

The 12th iteration of the Japan-US Seminar in Plant Pathology was held in Ithaca, New York at Cornell University in the fall of 2022. Presentations covered a range of topics under the theme “Remodeling of the Plant-Microbe Environment During Disease, Defense, and Mutualism,” and the meeting included a panel discussion of best practices in science communication. This report presents highlights of the meeting, from the perspective of early career participants of the seminar.

Keywords: effectors, mutualism, NLR, plant immunity, PRR

The 12th Japan-US Seminar in Plant Pathology, “Remodeling of the Plant-Microbe Environment During Disease, Defense, and Mutualism”, was convened August 28 through September 2, 2022, at Cornell University. Since the last Japan-US Seminar in 2015, there have been profound leaps in our understanding of both sides of plant-microbe interactions. Approximately 100 scientists from various institutions shared the latest developments toward understanding the multi-layered interactions that occur at the interface of the plant and microbe. A poster session, a panel discussion on science communication, and networking activities supplemented the presentations. In this report, we, early career scientists, highlight presented studies that, in our view, are addressing critical knowledge gaps in the molecular interactions of plants with pathogens and mutualists. We also present key takeaways from the science communication panel and propose questions for future investigation.

Defense

Plants carry two major classes of immune receptors, cell surface pattern-recognition receptors (PRRs) and intracellular

nucleotide-binding leucine-rich repeat (LRR) receptors (NLRs). PRRs with or without a kinase domain, receptor-like kinases (RLKs) or receptor-like proteins (RLPs), respectively, have various ectodomains to detect diverse ligands, including microbe-, plant cell damage-, and herbivore-associated molecular patterns, to induce pattern-triggered immunity (PTI) (Ge et al. 2022). NLRs recognize pathogen-secreted effectors or effector-mediated perturbations of host targets inside the plant cell, inducing effector-triggered immunity (ETI) that generally culminates in cell death via the hypersensitive reaction (HR) (Yuan et al. 2021). Characterizing the diversity of these immune receptors and their underlying molecular mechanisms is necessary for understanding the co-evolutionary plant-pathogen arms race and engineering disease resistance in crop plants.

Adam Steinbrenner (University of Washington) reported on an evolutionary trajectory through which novel immune receptor functions can emerge. Several phaseoloid legume species recognize the caterpillar-associated molecular pattern inceptin (In11) by the RLP Inceptin receptor (INR). By analyzing the INR locus, Dr. Steinbrenner showed that, over the course of about 53 million years, an initial insertion event followed by diversification gave rise to a subset of phaseoloid species evolving a functional INR. Reconstruction and functional analysis of ancestral and chimeric INRs showed that In11 detection is mediated by a few amino acid differences in the INR LRR domain (Snoeck et al. 2022). These findings provide a model of how plants can evolve detection of pathogen patterns through immune receptor diversification and localized mutation. Additionally, this advance serves as a promising foundation for engineering INRs in legume crops such as soybean and chickpea that do not carry a functional INR.

Greg Martin (Cornell University) reported on an NLR, Ptr1, from a wild tomato relative that can detect the proteolytic activity of the type III effector AvrRpt2, present in *Pseudomonas syringae* pv. *tomato* race 1 strains. Race 1 strains lack effectors AvrPto and AvrPtoB that induce the widely used Pto/Prf-based resistance in cultivated tomatoes. No qualitative resistance to *P. syringae* pv. *tomato* race 1 had been identified. Remarkably, Ptr1 has convergently evolved with two other NLRs from *Arabidopsis* and apple to recognize the proteolytic activity of AvrRpt2, an effector widely distributed in phytopathogenic bacteria (Mazo-Molina et al. 2020). The discovery of Ptr1 and its addition to the list of NLRs detecting AvrRpt2 activity provides new insights into the selective pressures that drive NLR evolution and will pave the way for editing existing tomato cultivars,

†Corresponding author: Y. Sasaki; ys494@cornell.edu

Funding: Authors participated in the conference through support from the National Science Foundation award IOS-2034212 (to A. Bogdanove, Cornell University).

The author(s) declare no conflict of interest.



Copyright © 2023 The Author(s). This is an open access article distributed under the CC BY-NC-ND 4.0 International license.

which carry a pseudogenized Ptr1 ortholog, for resistance against emerging *P. syringae* pv. *tomato* race 1 strains (Mazo-Molina et al. 2019).

Instead of acting alone to detect pathogen effectors or effector perturbations, some NLRs function in pairs. NLR pairs consist of a sensor and a helper NLR, in which the sensor NLRs recognize pathogen effectors and interact with the cognate helper NLRs to cooperatively induce plant immune responses. Ryohei Terauchi (Kyoto University and Iwate Biotechnology Research Center) presented the latest findings on the molecular interactions between paired rice NLRs and their cognate *Magnaporthe oryzae* avirulence (AVR) genes. The rice genome contains almost 500 NLR-like genes, although how most of these NLRs work, individually or in pairs, is largely unknown (Baggs et al. 2017). Dr. Terauchi reported on the diverse non-canonical integrated domains (IDs) of rice sensor NLRs that bait *M. oryzae* effectors by mimicking their plant host targets (Fujisaki et al. 2017; Grund et al. 2019; Maqbool et al. 2015; Ortiz et al. 2017). Evidence was presented that *M. oryzae* effector AVR-Pik is capable of binding and stabilizing host small HMA (heavy metal-associated) proteins, some of which were shown to be susceptibility factors. The sensor NLR Pik-1, in turn, evolved an HMA ID that acts as bait for the effector. This finding provides new insight into the co-evolutionary arms race between rice and *M. oryzae* (Oikawa et al. 2020). Dr. Terauchi also expanded on recent work investigating how NLR pairs evolve. By comparing NLR pair alleles at the Pia/Pias locus across diverse *Oryza* species, a picture for divergent evolution of sensor and helper NLRs emerges, in which the helpers have undergone purifying and sensors have undergone balancing selection (Shimizu et al. 2022). These findings support a model in which the adoption of diverse IDs contributes to the evolution of sensor NLRs to keep pace with the rapid evolution of pathogen effectors that target host proteins. This understanding may enable engineering of sensor NLR IDs to expand AVR recognition specificity.

Immune responses from PRRs and NLRs must be strictly regulated to balance the tradeoff between defense and growth. Plant peptides called phyto cytokines have recently been implicated in fine-tuning of immune responses (Rzemieniewski and Stegmann 2022). However, the molecular mechanisms of their regulatory functions remain unclear. Libo Shan (Texas A&M University) reported on a group of small phyto cytokines regulating defense and water loss (SCREWs), recognized by the LRR-RLK plant screw unresponsive receptor (NUT). The perception of SCREWs by NUTs induces stomatal reopening after bacterial pathogen invasion, leading to reduced apoplastic water potential, which ultimately inhibits pathogen multiplication. SCREW and NUT expression is specifically upregulated after pathogen invasion and during PTI (Liu et al. 2022). These results suggest that precise and localized regulation of stomatal activity ensures a swift change of the host micro-environment to limit bacterial proliferation.

Plant-derived C-terminally encoded peptides (CEPs) are also known for modulating immune outputs (Fitrianti et al. 2022; Zhu et al. 2020). Kazuhiro Toyoda (Okayama University) reported that the exogenous application of the *Arabidopsis* CEP5 suppresses PTI. Pretreatment of *Arabidopsis* plants with purified CEP5 also enhances disease susceptibility to non-adapted and avirulent pathogens like *Colletotrichum tropicale* and *Pseudomonas syringae* pv. *tabaci* (Fitrianti et al. 2022). Furthermore, Chiaki Itoh and Haruka Hasegawa, students in Dr. Toyoda's lab, presented evidence for salicylic acid treatment- and PTI/ETI-induced expression of some CEPs. Although the CEP5 receptor and mechanism of CEP-mediated immunity attenuation remain unclear, these new data support a model in which CEPs modulate PTI/ETI pathways and prevent excessive immunity.

In addition to peptides that modulate specific responses to pathogens or inhibit immunity, NLRs themselves can regulate inappropriate activation of immunity. Hiroaki Adachi (Kyoto University) reported on an atypical NLR that plays this role in the context of an NLR network. NLR networks comprise multiple helper and sensor NLRs, often encoded throughout the host genome, that work together to induce immunity. Mismatches between helpers and sensors can lead to inappropriate expression, autoimmunity, and growth defects. In asterid plants, NLRs required for cell death (NRCs) are helper NLRs that form key nodes of the NLR network, typically harboring an N-terminal MADA motif associated with the ability to induce the HR (Adachi et al. 2019). Dr. Adachi described NRCX, a novel NRC that lacks a functional MADA motif and is unable to induce cell death like other NRCs do (Adachi et al. 2023). Interestingly, when NRCX is silenced, *N. benthamiana* shows a dwarf phenotype partially dependent on key network helpers NRC2 and NRC3, suggesting NRCX acts as a negative regulator of NRC2- and NRC3-mediated autoimmunity (Adachi et al. 2023). Building on the relatively recent discovery of sensor and helper NLRs and NLR networks, the findings on NRCX expand the diversity of known NLR functions to include maintaining network homeostasis and normal plant development. A better understanding of immune regulation will reveal how plants defend against a myriad of pathogen pressures and will be critical for future engineering of robust disease resistance in plants.

Responses downstream of immune receptor activation were also highlighted. Hirofumi Yoshioka (Nagoya University) reported on the dynamics of mitogen-activated protein kinase (MAPK) activity and reactive oxygen species (ROS) production in response to pathogen and insect attacks. After pathogen sensing, MAPKs phosphorylate WRKY transcription factors, master regulators of plant immunity. In *N. benthamiana*, defense-related MAPKs interact with NbWRKY8 dependent on its D domain and phosphorylate serine residues within the proline-directed serine (SP) cluster (Ishihama et al. 2011). The Yoshioka lab developed a FRET-based MAPK sensor using the D domain and SP cluster of NbWRKY8 and used it to visualize MAPK activity spatiotemporally. Dr. Yoshioka reported the exciting finding that MAPK activation propagates cell-to-cell in response to pathogen and chewing insect attacks. RBOH-dependent ROS production is also a crucial event for plant immunity. Activated NbWRKY8 induces gene expression of NbRBOHB and robust ROS production during ETI (Adachi et al. 2015). Hydrogen peroxide (H₂O₂) leads to sulfenylation, an oxidative post-translational modification, of cysteine residues of ROS sensor proteins (Kimura et al. 2017). Dr. Yoshioka also described the identification, through proteomic screening of sulfenylated proteins, of a candidate ROS sensor protein that positively regulates immune responses. Altogether, the findings presented support the model that the interplay between the MAPK-WRKY pathway and ROS production is a pivotal signaling event in plant immunity, and they provide a view of the complex downstream responses of immune receptor activation.

Disease

PRRs and NLRs are key components of the multilayered plant defense system pathogens face during infection. Throughout the co-evolutionary arms race, pathogens have acquired diverse effectors to overcome immunity mediated by these receptors (Jones and Dangl 2006). In addition to effector proteins, small RNAs (sRNAs) and secondary metabolites (e.g., phyto toxins, phytohormones) play key roles in virulence (Zhang et al. 2022).

Hailing Jin (University of California, Riverside) reported on fungal sRNAs delivered by extracellular vesicles that can hijack plant RNA interference (RNAi) machinery to repress host immune responses (Weiberg et al. 2013). Interestingly, sRNA trafficking is bidirectional; *Arabidopsis* sRNAs can be transferred to pathogenic *Botrytis cinerea* to silence *B. cinerea* virulence genes (Cai et al. 2018). The Jin group successfully expressed modified sRNAs in *Arabidopsis* to silence specific genes of the pathogen responsible for sRNA generation and virulence (Wang et al. 2016). These findings point to custom anti-fungal sRNAs as a promising tool for disease control.

Effector proteins and sRNAs may contribute generally to virulence by suppressing host immune responses, but they can also determine host specificity, as is the case for some bacterial type III effectors (Angot et al. 2006; Bocsanczy et al. 2012; Poueymiro et al. 2009). Through comparative genomic analysis of putative effector content, Danielle Stevens (University of California, Davis) identified candidate determinants of host specificity across several *Clavibacter* spp., which cause severe diseases in crop plants with high host-specificity. The ability of candidates to elicit the HR in non-host plants was tested, implicating the serine proteases ChpG and Pat-1 of *Clavibacter michiganensis* as determinants. This finding suggests that the non-host recognition of these effectors underlies host specificity (Verma and Teper 2022). The work also highlights the power of comparative “effectoromics” to elucidate host range determinants of pathogenic bacteria, which may serve as a foundation for pathogen control strategies. Yoshitaka Takano and Ru Zhang (Kyoto University) reported on host-determining effectors and transcription factors of *Colletotrichum orbiculare*. This pathogen can infect cucurbits as well as distantly related Solanaceae such as *N. benthamiana*. The newly identified effectors, named EPC1 to EPC4, are regulated by the transcription factor TFV1 as well as its closest homolog TVL1 and are critical for full virulence toward the cucurbits but not *N. benthamiana*. The distinct ways effectors can contribute to host specificity, illustrated by the findings shared in these two presentations, raise the interesting question of how different selective forces shape effector evolution and distribution.

Mutualism

Presentations on mutualism delved into mechanisms and co-evolution. Of particular interest was a presentation by Kei Hiruma (The University of Tokyo) that highlighted the dynamic and environmentally dependent nature of some interactions. The ascomycete *Colletotrichum tofieldiae* has been described as a beneficial endophyte that transfers phosphorus to *Arabidopsis*, enhancing plant growth under phosphate-starved conditions (Hiruma et al. 2016). Dr. Hiruma reported on a pathogenic *Colletotrichum tofieldiae* strain isolated in Japan, Ct3, that is closely related to a previously isolated endophytic strain but inhibits *Arabidopsis thaliana* growth by producing abscisic acid (ABA) under phosphate-limited conditions. The Ct3 ABA biosynthesis genes are clustered and co-activated with those for botrydial (BOT), a secondary metabolite that promotes virulence in *B. cinerea* (Hiruma et al. 2022; Siewers et al. 2005). By perturbing ABA signaling, Ct3 represses genes related to nutrient uptake in the host. Interestingly, knock-out of the ABA-BOT cluster or its silencing by increased temperature renders Ct3 beneficial for plant growth in low phosphate conditions (Hiruma et al. 2022). This modulation of the plant host metabolism by Ct3, which occurs only in certain environmental conditions, serves as an example of the dynamic interactions that can exist between fungi and their hosts, ranging from pathogenicity to mutualism. The results also suggest a potential method for redirecting

pathogenic fungi toward mutualistic relationships through targeted modulation of secondary metabolite biosynthesis.

New findings on interactions involving multiple microbes and a host plant in field contexts were also reported. Tan Anh Nhi Nguyen (The University of Tokyo) described another interesting strain of *Colletotrichum tofieldiae*, Ct4, which enhances the growth of *Brassica* plants in nitrogen-limited (unfertilized) fields in Japan. The results of 16S metagenomic analysis of the rhizosphere microbiome revealed that Ct4 attracts beneficial bacteria onto Ct4-colonized roots, providing insight into a mechanism through which mutualists could benefit plants. This finding also highlights the importance of understanding the complexity of interactions within the plant-associated microbiome in the native context in order, for example, to use fungal endophytes for plant growth enhancement.

Science Communication

Student moderators Juliana González-Tobón, Yuta Watanabe, and Yumino Sasaki moderated a panel discussion on “Best Practices for Sharing Science” with Maria Fernanda Alvarez (Rice Program Leader, Crops for Nutrition and Health, Alliance of Biodiversity International and International Center for Tropical Agriculture), Morgan Carter (Assistant Professor of Biology, University of North Carolina at Charlotte), Jeanne Harris (Professor of Plant Biology, University of Vermont and Editor-in-Chief of *Molecular Plant-Microbe Interactions*), Sophien Kamoun (Group Leader, The Sainsbury Laboratory), Laura Boykin Okalebo (Senior TED Fellow and Senior Scientific Consultant and Computational Biologist at Bioteam), Yoshitaka Takano (Professor of Plant Pathology, Kyoto University), and Mary Williams (Features Editor at Plant Cell and Plant Physiology, Developer of Teaching Tools in Plant Biology) as panelists.

Discussions focused on the role of social media in science and how it has spurred a “nonstop academic conference for all” (Foell 2021). Panelists illustrated the potential of social media as an educational tool and a gateway for collaboration and professional development. Social media can also expand and diversify networks, draw attention to inequities, and amplify research contributions and ideas from members of underrepresented groups, serving as a powerful tool for marginalized communities in the sciences (Polk and Diver 2020). The usefulness of academic social networks (ResearchGate, Google Scholar, ORCID), especially to early career scientists, was also emphasized. Panelists expressed a preference for open source, public platforms to guard against paywalls that could give rise to unequal access. Panelists also advocated for scientists to establish a searchable and transparent presence on the internet.

For-profit publishers, journal impact factors, and the rise of open science and preprints were also discussed. Importantly, “gatekeeping” by journals and the “publish or perish” model of scientific funding that has led to increased research misconduct were discussed and decried. Panelists praised open access and increasing implementation of preprints by journals, expressing how incorporation of preprints into science policy and research practices could promote open data and easier accessibility to new findings.

Knowing what to share in science was emphasized as being as important as knowing how to share. Audience member Fumiaki Katagiri (University of Minnesota) proposed that scientists should share searchable, organized metadata for each experiment to accurately compare results between labs working on highly context-dependent systems. Literature corrections and retractions were also addressed. Panelists spoke about how publishing a correction or retracting a paper should be normalized. Corrections and retractions should not be viewed as the consequence of “bad” science, but rather, a product of

“good” science, i.e., the continued effort of multiple scientists, including the original authors, to validate and build on previous results.

Scientific journals communicate research findings to a specialized audience in a way that is often inaccessible to scientists from outside the field and to the lay audience. Panelists emphasized the value of science communication skills and ability to share information formatted for diverse audiences. In an increasingly connected world, effective science communication is vital, not only to engage more broadly with other scientists but to promote equitable participation in science, to combat misinformation, and to help people make informed decisions in their daily lives. If science is communicated effectively, the benefits of our research will be better understood and realized, and will ensure science is responsive to societal needs.

A recording of the panel can be found on the Cornell University website (https://vod.video.cornell.edu/media/20220831_Best%20practices%20for%20sharing%20science/1_240bsitm).

Status and Future Directions of Molecular Plant-Microbe Interaction Research

Since its inception in the 1960s, the Japan-US Seminars in Plant Pathology have encapsulated the latest developments in the field and have led to many fruitful international collaborations (Ouchi 2006). This seminar, the 12th in the series, highlighted recent progress across a diversity of exciting topics, only a selection of which we have highlighted here. Further, and new to the seminar, the panel discussion illustrated how effective science communication can facilitate better research, establish connections between scientific fields, reduce misinformation, and foster equity in science. The presentations at this seminar give rise to new questions for the field of molecular plant-microbe interactions. How do the diverse array of characterized immune receptors induce downstream physiological responses? How do PRRs and NLRs cooperate to induce these responses, and do effectors interfere at that step? How are effectors shaping pathogen host specificity, and how are host selective pressures in turn shaping effectors? If plants are reprogramming components of their metabolic pathways for beneficial organisms, how do they simultaneously balance inhibition of pathogens? How can this knowledge of plant-microbe interactions be applied to agriculturally relevant plants? Addressing these questions will benefit from international collaborations fostered through meetings such as the Japan-US Seminar. We look forward to its continuation and to work presented at future seminars addressing these questions.

Acknowledgments

We thank A. Bogdanove and G. Coaker for comments on a draft of this report. We apologize to the presenters whose work we were not able to highlight.

Literature Cited

Adachi, H., Contreras, M. P., Harant, A., Wu, C. H., Derevnina, L., Sakai, T., Duggan, C., Moratto, E., Bozkurt, T. O., Maqbool, A., and Win, J. 2019. An N-terminal motif in NLR immune receptors is functionally conserved across distantly related plant species. *Elife* 8:e49956.

Adachi, H., Nakano, T., Miyagawa, N., Ishihama, N., Yoshioka, M., Katou, Y., Yaeno, T., Shirasu, K., and Yoshioka, H. 2015. WRKY transcription factors phosphorylated by MAPK regulate a plant immune NADPH oxidase in *Nicotiana benthamiana*. *Plant Cell* 27:2645-2663.

Adachi, H., Sakai, T., Harant, A., Pai, H., Honda, K., Toghiani, A., Claeys, J., Duggan, C., Bozkurt, T. O., Wu, C. H., and Kamoun, S. 2023. An atypical NLR protein modulates the NRC immune receptor network in *Nicotiana benthamiana*. *PLoS Genet.* 19:e1010500.

Angot, A., Peeters, N., Lechner, E., Vailleau, F., Baud, C., Gentzittel, L., Sartorel, E., Genschik, P., Boucher, C., and Genin, S. 2006. *Ralstonia solanacearum* requires F-box-like domain-containing type III effectors to promote disease on several host plants. *Proc. Natl. Acad. Sci. U.S.A.* 103:14620-25.

Baggs, E., Dagdas, G., and Krasileva, K. 2017. NLR diversity, helpers and integrated domains: Making sense of the NLR IDentity. *Curr. Opin. Plant Biol.* 38:59-67.

Bocsanczy, A. M., Schneider, D. J., DeClerck, G. A., Cartinhour, S., and Beer, S. V. 2012. HopX1 in *Erwinia amylovora* functions as an avirulence protein in apple and is regulated by HrpL. *J. Bacteriol.* 194:553-560.

Cai, Q., Qiao, L., Wang, M., He, B., Lin, F.-M., Palmquist, J., Huang, S.-D., and Jin, H. 2018. Plants send small RNAs in extracellular vesicles to fungal pathogens to silence virulence genes. *Science* 360:1126-29.

Fitrianti, A. N., Mai, T. L., Phuong, L. T., Monden, H., Shiiba, N., Matsui, H., Noutoshi, Y., Yamamoto, M., Ichinose, Y., Shiraiishi, T., and Toyoda, K. 2022. CEP peptide induces susceptibility of *Arabidopsis thaliana* to non-adapted pathogens. *J. Gen. Plant Pathol.* 88:287-292.

Foell, J. 2021. Social media science communication is a nonstop academic conference for all. *Nat. Hum. Behav.* 5:812.

Fujisaki, K., Abe, Y., Kanzaki, E., Ito, K., Utsushi, H., Saitoh, H., Bialas, A., Banfield, M. J., Kamoun, S., and Terauchi, R. 2017. An unconventional NOI/RIN4 domain of a rice NLR protein binds host EXO70 protein to confer fungal immunity. *bioRxiv*.

Ge, D., Yeo, I.-C., and Shan, L. 2022. Knowing me, knowing you: Self and non-self recognition in plant immunity. *Essays Biochem.* 66:447-458.

Grund, E., Tremousaygue, D., and Deslandes, L. 2019. Plant NLRs with integrated domains: Unity makes strength. *Plant Physiol.* 179:1227-1235.

Hiruma, K., Aoki, S., Utami, Y. D., Okamoto, M., Kawamura, N., Nakamura, M., Ohmori, Y., Sugita, R., Tanoi, K., Sato, T., Iwasaki, W., and Saijo, Y. 2022. A fungal secondary metabolism gene cluster enables mutualist-pathogen transition in root endophyte *Colletotrichum tofieldiae*. *bioRxiv*.

Hiruma, K., Gerlach, N., Sacristán, S., Nakano, R. T., Hacquard, S., Kracher, B., Neumann, U., Ramírez, D., Bucher, M., O'Connell, R. J., and Schulze-Lefert, P. 2016. Root endophyte *Colletotrichum tofieldiae* confers plant fitness benefits that are phosphate status dependent. *Cell* 165:464-474.

Ishihama, N., Yamada, R., Yoshioka, M., Katou, S., and Yoshioka, H. 2011. Phosphorylation of the *Nicotiana benthamiana* WRKY8 transcription factor by MAPK functions in the defense response. *Plant Cell* 23:1153-1170.

Jones, J. D. G., and Dangl, J. L. 2006. The plant immune system. *Nature* 444:323-329.

Kimura, S., Waszczak, C., Hunter, K., and Wrzaczek, M. 2017. Bound by fate: The role of reactive oxygen species in receptor-like kinase signaling. *Plant Cell* 29:638-654.

Liu, Z., Hou, S., Rodrigues, O., Wang, P., Luo, D., Munemasa, S., Lei, J., Liu, J., Ortiz-Morea, F. A., Wang, X., Nomura, K., Yin, C., Wang, H., Zhang, W., Zhu-Salzman, K., He, S. Y., He, P., and Shan, L. 2022. Phyto cytokine signaling reopens stomata in plant immunity and water loss. *Nature* 605:332-339.

Maqbool, A., Saitoh, H., Franceschetti, M., Stevenson, C., Uemura, A., Kanzaki, H., Kamoun, S., Terauchi, R., and Banfield, M. 2015. Structural basis of pathogen recognition by an integrated HMA domain in a plant NLR immune receptor. *Elife*. 4:e08709.

Mazo-Molina, C., Mainiero, S., Haefner, B. J., Bednarek, R., Zhang, J., Feder, A., Shi, K., Strickler, S. R., and Martin, G. B. 2020. Ptr1 evolved convergently with RPS2 and Mr5 to mediate recognition of AvrRpt2 in diverse solanaceous species. *Plant J.* 103:1433-1445.

Mazo-Molina, C., Mainiero, S., Hind, S. R., Kraus, C. M., Vachev, M., Maviane-Macia, F., Lindeberg, M., Saha, S., Strickler, S. R., Feder, A., Giovannoni, J. J., Smart, C. D., Peeters, N., and Martin, G. B. 2019. The *Ptr1* locus of *Solanum lycopersicoides* confers resistance to race 1 strains of *Pseudomonas syringae* pv. tomato and to *Ralstonia pseudosolanacearum* by recognizing the type III effectors AvrRpt2 and RipBN. *Mol. Plant-Microbe Interact.* 32:949-960.

Oikawa, K., Fujisaki, K., Shimizu, M., Takeda, T., Saitoh, H., Hirabuchi, A., Hiraka, Y., Bialas, A., Langner, T., Kellner, R., and Bozkurt, T. O. 2020. The blast pathogen effector AVR-Pik binds and stabilizes rice heavy metal-associated (HMA) proteins to co-opt their function in immunity. *bioRxiv*.


Ortiz, D., Guillen, K., Cesari, S., Chalvon, V., Gracy, J., Padilla, A., and Kroj, T. 2017. Recognition of the *Magnaporthe oryzae* effector AVR-Pia by the decoy domain of the rice NLR immune receptor RGA5. *Plant Cell* 29:156-168.

Ouchi, S. 2006. A retrospective of an unconventionally trained plant pathologist: Plant diseases to molecular plant pathology. *Annu. Rev. Phytopathol.* 44:1-17.

- Polk, E., and Diver, S. 2020. Situating the scientist: Creating inclusive science communication through equity framing and environmental justice. *Front. Commun.* 5:1-10.
- Poueymiro, M., Cunnac, S., Barberis, P., Deslandes, L., Peeters, N., Cazale-Noel, A.-C., Boucher, C., and Genin, S. 2009. Two type III secretion system effectors from *Ralstonia solanacearum* GMI1000 determine host-range specificity on tobacco. *Mol. Plant-Microbe Interact.* 22: 538-550.
- Rzemieniewski, J., and Stegmann, M. 2022. Regulation of pattern-triggered immunity and growth by phytochemicals. *Curr. Opin. Plant Biol.* 68: 102230.
- Shimizu, M., Hirabuchi, A., Sugihara, Y., Abe, A., Takeda, T., Kobayashi, M., Hiraka, Y., Kanzaki, E., Oikawa, K., Saitoh, H., and Langner, T. 2022. A genetically linked pair of NLR immune receptors shows contrasting patterns of evolution. *Proc. Natl. Acad. Sci.* 119:e2116896119.
- Siewers, V., Viaud, M., Jimenez-Teja, D., Collado, I. G., Gronover, C. S., Pradier, J. M., Tudzynski, B., and Tudzynski, P. 2005. Functional analysis of the cytochrome P450 monooxygenase gene *bcbot1* of *Botrytis cinerea* indicates that botrydial is a strain-specific virulence factor. *Mol. Plant-Microbe Interact.* 18:602-612.
- Snoeck, S., Abramson, B. W., Garcia, A. G. K., Egan, A. N., Michael, T. P., and Steinbrenner, A. D. 2022. Evolutionary gain and loss of a plant pattern-recognition receptor for HAMP recognition. *bioRxiv*.
- Verma, R. K., and Teper, D. 2022. Immune recognition of the secreted serine protease ChpG restricts the host range of *Clavibacter michiganensis* from eggplant varieties. *Mol. Plant Pathol.* 23:933-946.
- Wang, M., Weiberg, A., Lin, F.-M., Thomma, B. P. H. J., Huang, H.-D., and Jin, H. 2016. Bidirectional cross-kingdom RNAi and fungal uptake of external RNAs confer plant protection. *Nat. Plants* 2: 16151.
- Weiberg, A., Wang, M., Lin, F.-M., Zhao, H., Zhang, Z., Kaloshian, I., Huang, H.-D., and Jin, H. 2013. Fungal small RNAs suppress plant immunity by hijacking host RNA interference pathways. *Science* 342: 118-123.
- Yuan, M., Jiang, Z., Bi, G., Nomura, K., Liu, M., Wang, Y., Cai, B., Zhou, J.-M., He, S. Y., and Xin, X.-F. 2021. Pattern-recognition receptors are required for NLR-mediated plant immunity. *Nature* 592:105-109.
- Zhang, S., Li, C., Si, J., Han, Z., and Chen, D. 2022. Action Mechanisms of Effectors in Plant-Pathogen Interaction. *Int. J. Mol. Sci.* 23: 6758.
- Zhu, F., Deng, J., Chen, H., Liu, P., Zheng, L., Ye, Q., Li, R., Brault, M., Wen, J., Frugier, F., Dong, J., and Wang, T. 2020. A CEP peptide receptor-like kinase regulates auxin biosynthesis and ethylene signaling to coordinate root growth and symbiotic nodulation in *Medicago truncatula*. *Plant Cell* 32:2855-2877.

SHORT COMMUNICATION

Targeting Disease Susceptibility Genes in Wheat Through Wide Hybridization with Maize Expressing Cas9 and Guide RNA

Anil Karmacharya,¹ Dandan Li,¹ Yueqiang Leng,¹ Gongjun Shi,¹ Zhaohui Liu,¹  Shengming Yang,² Yang Du,³ Wenhao Dai,⁴ and Shaobin Zhong^{1,†} 

¹ Department of Plant Pathology, North Dakota State University, Fargo, ND 58102, U.S.A.

² USDA-ARS Cereal Crops Research Unit, Edward T. Schafer Agricultural Research Center, Fargo, ND 58102, U.S.A.

³ Department of Computer Systems and Software Engineering, Valley City State University, Valley City, ND 58072, U.S.A.

⁴ Department of Plant Sciences, North Dakota State University, Fargo, ND 58102, U.S.A.

Accepted for publication 2 April 2023.

Two genes (*TaHRC* and *Tsn1*) conferring susceptibility to Fusarium head blight and tan spot, Septoria nodorum blotch, and spot blotch in wheat were targeted through wide hybridization with maize expressing Cas9 and guide RNA (gRNA). For each gene, two target sites were selected and corresponding gRNA expression cassettes were synthesized and cloned into a binary vector carrying the CRISPR/Cas9-mediated genome editing machinery. The constructed binary vectors were used to transform the hybrid maize Hi-II through an *Agrobacterium*-mediated approach to generate T0 and T1 plants, which were used to cross with wheat variety Dayn for targeting *Tsn1* or the susceptible allele (*TaHRC-S*) of *TaHRC* as well as with the near-isogenic line (*Day-Fhb1*) of Dayn for targeting the resistant allele (*TaHRC-R*) of *TaHRC*. Haploid embryos were rescued in vitro from the wide crosses to generate haploid plants. PCR amplification and sequencing indicated that 15 to 33% of the haploid plants contained the target gene with mutations at the target sites. This wheat × maize hybridization combined with genome editing approach provides a useful alternative tool, not only for targeting susceptibility genes to improve disease resistance without regulatory issues, but also for understanding gene function in wheat.

†Corresponding author: S. Zhong; shaobin.zhong@ndsu.edu

A. Karmacharya, D. Li, and Y. Leng contributed equally to this study.

Current address for D. Li: USDA-ARS Cereal Crops Research Unit, Edward T. Schafer Agricultural Research Center, Fargo, ND 58102, U.S.A.

Any opinions, findings, conclusions, or recommendations expressed in this publication are those of the authors and do not necessarily reflect the view of the United States Department of Agriculture.

Funding: This study was partially supported by the North Dakota Wheat Commission and the United States Department of Agriculture, under agreement number 59-0206-0-162. This is a cooperative project with the U.S. Wheat and Barley Scab Initiative.

e-Xtra: Supplementary material is available online.

The author(s) declare no conflict of interest.

Keywords: Cas9, CRISPR, disease susceptibility gene, genome editing, guide RNA, *TaHRC*, *Tsn1*, wheat

CRISPR/Cas9-mediated genome editing technology is a powerful tool for targeted mutagenesis of disease susceptibility genes to improve disease resistance in crops (Chen et al. 2022; Zaidi et al. 2018). In wheat, most of the genome editing studies so far have directly or indirectly relied on callus induction and plant regeneration from explants receiving gene construct or pre-assembled Cas9/guide RNA (gRNA) ribonucleoprotein complex delivered by particle bombardment or *Agrobacterium*-mediated methods. Unfortunately, the efficiency of callus induction and plant regeneration is low for most wheat genotypes except for only a few, such as Bobwhite and Fielder, limiting the application of genome editing in many commercially grown wheat varieties. Recently, a new genome editing approach has emerged, which combines haploid induction with the CRISPR/Cas9-mediated genome editing technology for targeted gene mutagenesis in plants (Kelliher et al. 2019). This haploid inducer-mediated genome editing (or HI-Edit) approach relies on the expression of Cas9/gRNA of the haploidy inducer inside the transient zygote after fertilization, and then, chromosomes of the haploidy inducer are eliminated, leading to generation of gene-edited haploid plants without transgenes introduced. In wheat, haploid plants can be generated through intergeneric crossing with maize (Laurie and Bennett 1986) and doubled haploid plants can be produced from the haploid plants after chromosome doubling treatment (Laurie and Bennett 1988). In the initial report of Kelliher et al. (2019), only two wheat haploid plants with the target gene mutated were obtained from several hundreds of haploid plants derived from the intergeneric crosses with maize expressing Cas9 and gRNA, thus the efficiency was low (<1%). Later, Budhagatapalli et al. (2020) crossed different wheat varieties with maize transgenics with high Cas9 and gRNA expression for targeting two genes for BRASSINOSTEROID-INSENSITIVE 1 (BR1) and SEMI-DWARF 1 (SD1), which regulate plant height in wheat, and obtained a high frequency (3.6 to 50%) of haploid and doubled haploid wheat plants with mutations at the two targeted genes. However, no disease-susceptibility genes have been targeted in wheat using this approach. Here, we report precisely targeted mutagenesis of two genes, *TaHRC* and *Tsn1*, which are involved in susceptibility to Fusarium head blight (FHB) and



Copyright © 2023 The Author(s). This is an open access article distributed under the CC BY-NC-ND 4.0 International license.

three foliar diseases (tan spot, *Septoria nodorum* blotch, and spot blotch), respectively, in wheat, using HI-Edit.

FHB is a devastating disease caused by *Fusarium* species worldwide in cereal crops. Previous studies indicate that a major quantitative trait locus (*Fhb1*) confers FHB resistance in wheat variety Sumai3 and its derivatives (Anderson et al. 2001; Bai et al. 1999; Waldron et al. 1999; Su et al. 2018). Recently, three studies (Rawat et al. 2016; Li et al. 2019; Su et al. 2019) have identified two genes (*TaPFT* and *TaHRC*) conferring FHB resistance/susceptibility at the *Fhb1* locus. *TaPFT* encodes a pore-forming toxin-like protein (Rawat et al. 2016), while *TaHRC* encodes a histidine-rich calcium-binding protein (Li et al. 2019; Su et al. 2019). Both Li et al. (2019) and Su et al. (2019) rejected the notion that *TaPFT* is the causal gene for *Fhb1* resistance and showed that a deletion mutation at *TaHRC* gives rise to *Fhb1* resistance in wheat. However, Su et al. (2019) conclude that the wild-type allele (*TaHRC-S*) is a susceptibility factor and that the resistant allele (*TaHRC-R*) conferring the *Fhb1* resistance is the result of a knockout mutation caused by the large deletion in *TaHRC-S*, whereas Li et al. (2019) report that the deletion at *TaHRC-S* creates a new upstream translation start codon encoding a functional TaHRC-R protein 14 amino acids longer than TaHRC-S. To determine if the *Fhb1*-mediated resistance is the result of a loss-of-function mutation of *TaHRC-S* or a gain of function of *TaHRC-R*, we attempted to knock out both alleles (*TaHRC-S* and *TaHRC-R*) of *TaHRC*. We se-

lected two sites (TaHRC-T1 and TaHRC-T2) from exon 3 of the *TaHRC* gene (Fig. 1A) for targeted mutagenesis. The two 20-nt target oligo sequences (GCAAGCACAGGTCAAAGAGG and GAAGGAAGAAGCACTCGCAC) are conserved across the two alleles (*TaHRC-S* and *TaHRC-R*) of *TaHRC*. Two gRNA expression cassettes, each consisting of a promoter (either the rice U3 promoter OsU3p or the wheat U3 promoter TaU3p), gRNA scaffold with the target site sequence, and terminator (OsU3t) were synthesized by Twist Bioscience (South San Francisco, CA, U.S.A.), and were then cloned into the *BsaI* sites of the vector pBue411 (Xing et al. 2014) (Supplementary Material). The resulting binary vector (pBue411-TaHRC-T1-T2) (Fig. 1C) was used for *Agrobacterium*-mediated transformation of the maize hybrid variety Hi-II, conducted by the Plant Transformation Facility at Iowa State University (Ames, IA, U.S.A.). A total of 160 T₀ plants were generated from 23 independent transformation events and were subjected to quantitative reverse transcription (qRT-PCR) analysis (Fig. 1D) (Supplementary Material). T₀ plants with high Cas9 and gRNA expression were used for self-pollination to produce T₁ seeds and were, meanwhile, used to pollinate the wheat variety Dayn (carrying *TaHRC-S*), generating 20 wheat haploid plants from rescued embryos. Three (Dayn-14-6, Dayn-15-6, and Dayn-7-1) of the 20 (15%) haploid plants had an insertion or deletion mutation at *TaHRC-S* (Fig. 1E). T₁ transgenic maize plants were grown and used to pollinate Dayn and a near-isogenic line Dayn-*Fhb1* (carrying

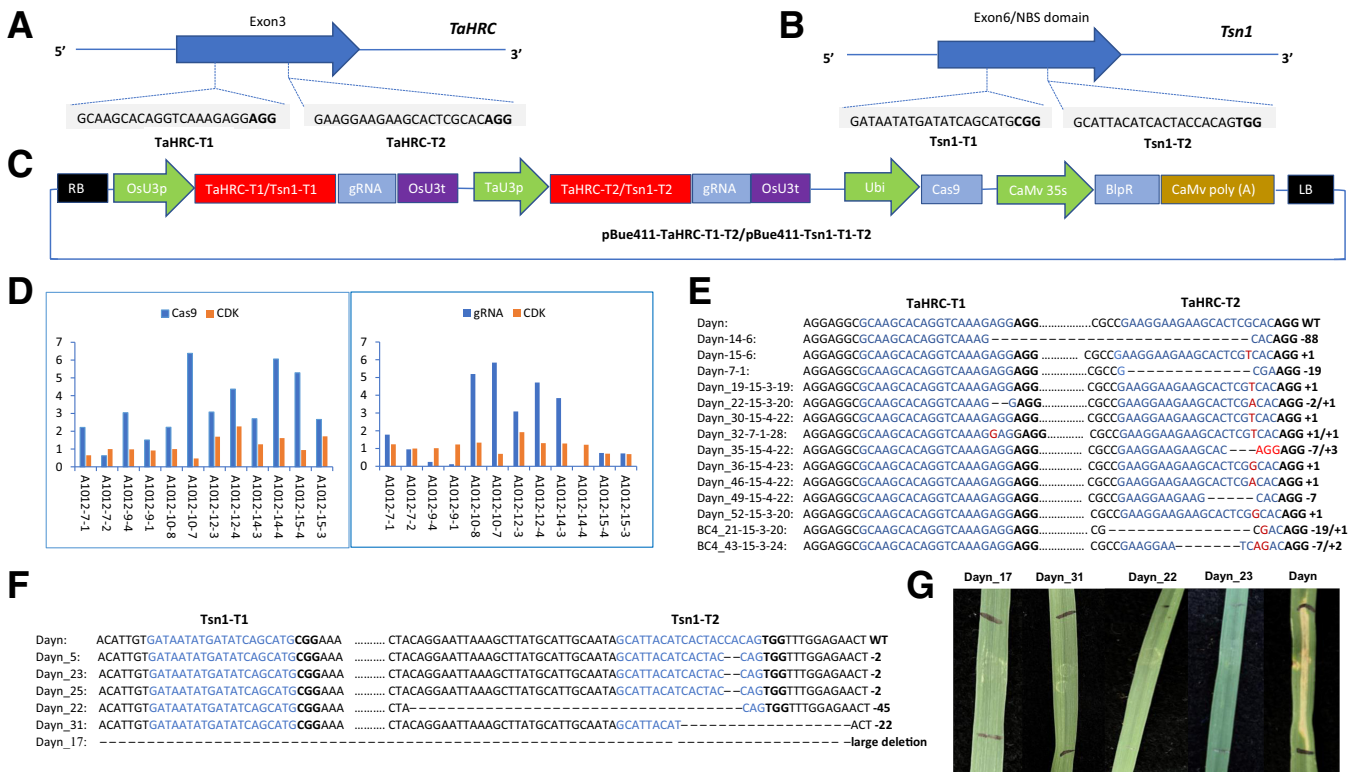


Fig. 1. Targeted genome editing of disease susceptibility genes (*TaHRC* and *Tsn1*) in wheat via haploid induction coupled with CRISPR/Cas9 genome editing. **A**, Two different target sites (TaHRC-T1 and TaHRC-T2) at exon 3 of the *TaHRC* gene. **B**, Two different target sites (Tsn1-T1 and Tsn1-T2) at exon 6 of the *Tsn1* gene. **C**, Schematic of binary plasmid vectors (pBue411-TaHRC-T1-T2 and pBue411-Tsn1-T1-T2) used for *Agrobacterium*-mediated transformation of Hi-II maize. OsU3p = rice U3 promoter, OsU3t = rice U3 terminator, TaU3p = wheat U3 promoter, Ubi = maize ubiquitin promoter, CaMV 35S = cauliflower mosaic virus 35S promoter, BfpR = bialaphos resistance gene, LB = T-DNA left border sequence, RB = T-DNA right border sequence. **D**, Expression of Cas9, gRNA (guide RNA), and CDK (cyclin-dependent kinase) with reference to the actin gene in representative transgenic maize plants used for targeting the *TaHRC* gene. **E**, Partial sequences of the *TaHRC* gene showing mutations at TaHRC-T1 and TaHRC-T2 sites in haploid plants derived from wide crosses with transgenic maize expressing Cas9 and gRNA. Sequence in red indicates insertion mutation, a plus symbol (+) indicates insertion, and a minus symbol (-) indicates deletion. WT = wild type. Sequences in blue indicate the target sites (20 nt) of *TaHRC*, bold letters indicate the protospacer adjacent motif (PAM). **F**, Partial sequences of the *Tsn1* gene showing mutations at the Tsn1-T2 site in different haploid plants derived from Dayn × maize crosses. Sequences in blue indicate the target site (20 nt) of *Tsn1*, bold letters indicate the PAM, and a minus symbol (-) indicates deletion. **G**, ToxA infiltration assay (Supplementary Material) on haploid plants derived from wide crosses with transgenic maize expressing Cas9 and gRNA targeting *Tsn1*. Photos were taken 5 days after the ToxA infiltration.

TaHRC-R), which was derived from a cross with wheat cultivar Alsen (carrying *Fhb1*) and four cycles of backcrosses with Dayn. Thirty-three and six haploid plants were produced from the wide crosses with Dayn and Dayn-*Fhb1*, respectively. Of the total 33 haploid plants from crosses with Dayn, 9 (approximately 27%) had mutations at either or both target sites of *TaHRC-S* (Fig. 1E). Two (BC4_21-15-3-20 and BC4_43-15-3-24) of the six (approximately 33%) haploid plants from the crosses with Dayn-*Fhb1* had mutations at the *TaHRC-T2* site of *TaHRC-R*. Among the total 14 haploid mutant plants, only three had mutations occurring at the *TaHRC-T1* site, while all of them had indels at the *TaHRC-T2* site. This result indicates the gRNA cassette driven by *TaU3p* had a higher efficiency for gene editing than the one driven by *OsU3p*. The resulting doubled haploid lines with homozygous mutated *TaHRC-S* or *TaHRC-R* alleles will be evaluated for FHB resistance to confirm if *TaHRC-S* is a susceptibility factor or *TaHRC-R* is a gain of function gene conferring the FHB resistance at the *Fhb1* locus.

Tan spot, Septoria nodorum blotch, and spot blotch are three important wheat diseases caused by *Pyrenophora tritici-repentis*, *Parastagonospora nodorum*, and *Bipolaris sorokiniana*, respectively. These fungal pathogens can produce a proteinaceous necrotrophic effector (ToxA) interacting with a wheat gene (*Tsn1*) to cause the diseases in wheat (Faris et al. 2010; Friesen et al. 2006; McDonald et al. 2018). *Tsn1* encodes a protein with a serine/threonine protein kinase domain and a nucleotide-binding site leucine-rich repeat domain (Faris et al. 2010). Removal of *Tsn1* in a wheat genotype can be achieved by the traditional breeding method through crossing with the genotype with *tsn1* and multiple cycles of backcrossing and marker-assisted selection against *Tsn1*, but the process is time-consuming and labor-intensive. To overcome the problem, we aimed to knock out *Tsn1* via HI-Edit, which enables direct editing of the gene in any elite wheat lines by a single cross. We selected two target sites (*Tsn1-T1* and *Tsn1-T2*) of *Tsn1* at exon 6 of chromosome 5BL (Fig. 1B) for synthesis of the corresponding gRNA expression cassettes, which were cloned into pBue411 (Xing et al. 2014) to generate the binary vector pBue411-Tsn1-T1-T2 (Fig. 1C) (Supplementary Material). pBue411-Tsn1-T1-T2 was sent to the Plant Transformation Facility at Iowa State University for *Agrobacterium*-mediated transformation of the hybrid maize variety Hi-II. Fifty-seven T_0 maize plants were generated from 15 independent transformation events and were analyzed by qRT-PCR for Cas9 and gRNA expression (Supplementary Material). T_0 plants with high Cas9 and gRNA expression were self-pollinated to produce T_1 seeds, which were grown and used to pollinate the wheat variety Dayn (carrying *Tsn1* and sensitive to ToxA). From the wide crosses, 34 haploid plants were generated. PCR amplification and DNA sequencing of the *Tsn1* sequence indicated that six of the haploid plants (approximately 18%) had mutations at the *Tsn1-T2* site, while other haploid plants had the same sequence as the wild type (Fig. 1F). No mutations were identified at the *Tsn1-T1* site. Again, this result further indicates the wheat U3 promoter (*TaU3p*) is a better choice for driving gRNA expression to achieve a high efficiency of gene editing than the rice U3 promoter (*OsU3p*). A ToxA infiltration assay (Supplementary Material) indicated that the six haploid plants with mutation at *Tsn1* were insensitive to ToxA, whereas the wild type (Dayn) and the haploid plants without mutations at *Tsn1* were sensitive to ToxA (Fig. 1G). The doubled haploid lines to be developed from the ToxA-insensitive haploid mutants are isogenic lines of Dayn and would be used as elite germplasm for resistance to the three wheat diseases caused by *P. tritici-repentis*, *P. nodorum*, and *B. sorokiniana*, respectively.

In conclusion, we successfully knocked out two wheat disease susceptibility genes (*TaHRC* and *Tsn1*) through wheat × maize hybridization coupled with CRISPR/Cas9 genome editing

technology. The efficiency for generating mutant haploid plants ranged from 15 to 33%. A higher frequency of mutations was achieved at the sites targeted by the gRNAs driven by the wheat U3 promoter (*TaU3p*) than those driven by the rice U3 promoter (*OsU3p*). The maize transgenics for targeting *TaHRC* and *Tsn1* would be useful tools for creating new and transgene-free homozygous wheat genotypes through a single cross without regulatory concerns. Evaluation of doubled haploid plants derived from the haploid mutants of *TaHRC-S* and *TaHRC-R* for FHB resistance may provide clarification on the function of *TaHRC* at the *Fhb1* locus. Further research is needed to enhance Cas9 and gRNA expression of transgenes on the maize chromosome, in the zygotic stage, for achieving higher genome editing efficiency in wheat genomes, and to increase frequency of doubled haploid production for selection of desirable homozygous mutants.

Acknowledgments

The *Pichia pastoris* strain used to produce ToxA was kindly provided by T. Friesen from the USDA-ARS Edward T. Schafer Agricultural Research Center in Fargo, North Dakota.

Literature Cited

- Anderson, J. A., Stack, R. W., Liu, S., Waldron, B. L., Fjeld, A. D., Coyne, C., Moreno-Sevilla, B., Mitchell Fetch, J., Song, Q. J., Cregan, P. B., and Froberg, R. C. 2001. DNA markers for Fusarium head blight resistance QTLs in two wheat populations. *Theor. Appl. Genet.* 102:1164-1168.
- Bai, G., Kolb, F. L., Shaner, G., and Domier, L. L. 1999. Amplified fragment length polymorphism markers linked to a major quantitative trait locus controlling scab resistance in wheat. *Phytopathology* 89:343-348.
- Budhagatapalli, N., Halbach, T., Hiekel, S., Büchner, H., Müller, A. E., and Kumlhehn, J. 2020. Site-directed mutagenesis in bread and durum wheat via pollination by cas9/guide RNA-transgenic maize used as haploidy inducer. *Plant Biotechnol. J.* 18:2376.
- Chen, H., Su, Z., Tian, B., Liu, Y., Pang, Y., Kavetskiy, V., Trick, H. N., and Bai, G. 2022. Development and optimization of a *Barley stripe mosaic virus*-mediated gene editing system to improve Fusarium head blight resistance in wheat. *Plant Biotechnol. J.* 20:1018-1020.
- Faris, J. D., Zhang, Z., Lu, H., Lu, S., Reddy, L., Cloutier, S., Fellers, J. P., Meinhardt, S. W., Rasmussen, J. B., Xu, S. S., Oliver, R. P., Simons, K. J., and Friesen, T. L. 2010. A unique wheat disease resistance-like gene governs effector-triggered susceptibility to necrotrophic pathogens. *Proc. Natl. Acad. Sci. U.S.A.* 107:13544-13549.
- Friesen, T. L., Stukenbrock, E. H., Liu, Z., Meinhardt, S., Ling, H., Faris, J. D., Rasmussen, J. B., Solomon, P. S., McDonald, B. A., and Oliver, R. P. 2006. Emergence of a new disease as a result of interspecific virulence gene transfer. *Nat. Genet.* 38:953-956.
- Kelliher, T., Starr, D., Su, X., Tang, G., Chen, Z., Carter, J., Wittich, P. E., Dong, S., Green, J., Burch, E., McCuiston, J., Gu, W., Sun, Y., Strebe, T., Roberts, J., Bate, N. J., and Que, Q. 2019. One-step genome editing of elite crop germplasm during haploid induction. *Biotechnol. J.* 27:287-292.
- Laurie, D. A., and Bennett, M. D. 1986. Wheat × maize hybridization. *Can. J. Genet. Cytol.* 28:313-316.
- Laurie, D. A., and Bennett, M. D. 1988. The production of haploid wheat plants from wheat × maize crosses. *Theor. Appl. Genet.* 76:393-397.
- Li, G., Zhou, J., Jia, H., Gao, Z., Fan, M., Luo, Y., Zhao, P., Xue, S., Li, N., Yuan, Y., Ma, S., Kong, Z., Jia, L., An, X., Jiang, G., Liu, W., Cao, W., Zhang, R., Fan, J., Xu, X., Liu, Y., Kong, Q., Zheng, S., Wang, Y., Qin, B., Cao, S., Ding, Y., Shi, J., Yan, H., Wang, X., Ran, C., and Ma, Z. 2019. Mutation of a histidine-rich calcium-binding-protein gene in wheat confers resistance to Fusarium head blight. *Nat. Genet.* 51:1106-1112.
- McDonald, M. C., Ahren, D., Simpfendorfer, S., Milgate, A., and Solomon, P. S. 2018. The discovery of the virulence gene *ToxA* in the wheat and barley pathogen *Bipolaris sorokiniana*. *Mol. Plant Pathol.* 19:432-439.
- Rawat, N., Pumphrey, M. O., Liu, S., Zhang, X., Tiwari, V. K., Ando, K., Trick, H. N., Bockus, W. W., Akhunov, E., Anderson, J. A., and Gill, B. S. 2016. Wheat *Fhb1* encodes a chimeric lectin with agglutinin domains and a pore-forming toxin-like domain conferring resistance to Fusarium head blight. *Nat. Genet.* 48:1576-1580.
- Su, Z., Bernardo, A., Tian, B., Chen, H., Wang, S., Ma, H., Cai, S., Liu, D., Zhang, D., Li, T., Trick, H., St Amand, P., Yu, J., Zhang, Z., and Bai, G. 2019. A deletion mutation in *TaHRC* confers *Fhb1* resistance to Fusarium head blight in wheat. *Nat. Genet.* 51:1099-1105.

- Su, Z., Jin, S., Zhang, D., and Bai, G. 2018. Development and validation of diagnostic markers for *Fhb1* region, a major QTL for *Fusarium* head blight resistance in wheat. *Theor. Appl. Genet.* 131:2371-2380.
- Waldron, B. L., Moreno-Sevilla, B., Anderson, J. A., Stack, R. W., and Froberg, R. C. 1999. RFLP mapping of QTL for *Fusarium* head blight resistance in wheat. *Crop Sci.* 39:805-811.
- Xing, H. L., Dong, L., Wang, Z. P., Zhang, H. Y., Han, C. Y., Liu, B., Wang, X. C., and Chen, Q. J. 2014. A CRISPR/Cas9 toolkit for multiplex genome editing in plants. *BMC Plant Biol.* 14:327.
- Zaidi, S. S., Mukhtar, M. S., and Mansoor, S. 2018. Genome editing: Targeting susceptibility genes for plant disease resistance. *Trends Biotechnol.* 36:898-906.

Grapevine Fanleaf Virus RNA1-Encoded Proteins 1A and 1B^{Hel} Suppress RNA Silencing

Jiyeong Choi,^{1,†} Samira Pakbaz,² Luz Marcela Yepes,¹ Elizabeth Jeannette Cieniewicz,³ Corinne Schmitt-Keichinger,^{4,5} Rossella Labarile,⁶ Serena Anna Minutillo,⁷ Michelle Heck,^{8,9} Jian Hua,¹⁰ and Marc Fuchs¹

¹ Plant Pathology and Plant-Microbe Biology Section, School of Integrative Plant Science, Cornell University, Cornell AgriTech, Geneva, NY 14456, U.S.A.

² Plant Pathology Department, Faculty of Agriculture and Natural Resources, Lorestan University, Khorramabad, Iran

³ Department of Plant and Environmental Sciences, College of Agriculture, Forestry, and Life Sciences, Clemson University, Clemson, SC 29634, U.S.A.

⁴ CNRS, IBMP UPR 2357, Université de Strasbourg, 67000 Strasbourg, France

⁵ INRAE, SVQV UMR 1131, Université de Strasbourg, 68000 Colmar, France

⁶ National Research Council (CNR), Institute of Chemical-Physical Processes, Via Amendola 165/A, 70126 Bari, Italy

⁷ International Center for Advanced Mediterranean Agronomic Studies - Institute of Bari (CIHEAM-Bari), 70010 Valenzano, Italy

⁸ Plant Pathology and Plant-Microbe Biology Section, School of Integrative Plant Science, Cornell University, Ithaca, NY 14853, U.S.A.

⁹ Emerging Pests and Pathogens Research Unit, USDA Agricultural Research Service, Robert W. Holley Center for Agriculture and Health, Ithaca, NY 14853, U.S.A.

¹⁰ Plant Biology Section, School of Integrative Plant Science, Cornell University, Ithaca, NY 14853, U.S.A.

Accepted for publication 29 March 2023.

Grapevine fanleaf virus (GFLV) (genus *Nepovirus*, family *Secoviridae*) causes fanleaf degeneration, one of the most damaging viral diseases of grapevines. Despite substantial advances at deciphering GFLV-host interactions, how this virus overcomes the host antiviral pathways of RNA silencing is poorly understood. In this study, we identified viral suppressors of RNA silencing (VSRs) encoded by GFLV, using fluorescence assays, and tested their capacity at modifying host gene expression in transgenic *Nicotiana benthamiana* expressing the enhanced green fluorescent protein gene (*EGFP*). Results revealed that GFLV RNA1-encoded protein 1A, for which a function had yet to be assigned, and protein 1B^{Hel}, a putative helicase, reverse systemic RNA silencing either individually or as a fused form (1A^{Hel}) predicted as an intermediary product of RNA1 polyprotein proteolytic processing. The GFLV VSRs differentially altered the expression of plant host genes involved in RNA silencing, as shown by reverse transcription-quantitative PCR. In a co-infiltration assay with an *EGFP* hairpin construct, protein 1A upregulated *NbDCL2*, *NbDCL4*, and *NbRDR6*, and proteins 1B^{Hel} and 1A+1B^{Hel} upregulated *NbDCL2*, *NbDCL4*,

NbAGO1, *NbAGO2*, and *NbRDR6*, while protein 1A^{Hel} upregulated *NbAGO1* and *NbRDR6*. In a reversal of systemic silencing assay, protein 1A upregulated *NbDCL2* and *NbAGO2* and protein 1A^{Hel} upregulated *NbDCL2*, *NbDCL4*, and *NbAGO1*. This is the first report of VSRs encoded by a nepovirus RNA1 and of two VSRs that act either individually or as a predicted fused form to counteract the systemic antiviral host defense, suggesting that GFLV might devise a unique counterdefense strategy to interfere with various steps of the plant antiviral RNA silencing pathways during infection.

Keywords: grapevine fanleaf virus, nepovirus, RNA silencing, viral suppressor of RNA silencing

†Corresponding author: J. Choi; jc3398@cornell.edu

Funding: This work was partially supported by the California Department of Food and Agriculture Pierce's Disease & Glassy-Winged Sharpshooter Board Research & Outreach Program (awards 21-0269-000-SA and 22-0550-000-SA) and Cornell AgriTech Venture Funds.

e-Xtra: Supplementary material is available online.

The author(s) declare no conflict of interest.



Copyright © 2023 The Author(s). This is an open access article distributed under the CC BY-NC-ND 4.0 International license.

RNA silencing is a conserved, sequence-specific, gene-regulation mechanism that plays a pivotal role in plant development, growth, and adaptation to various abiotic and biotic stressors (El-Sappah et al. 2021; Jin et al. 2022; Lopez-Gomollon and Baulcombe 2022). RNA silencing also functions as a strong and adaptive plant antiviral defense (Jin et al. 2022; Lopez-Gomollon and Baulcombe 2022). Mechanistically, RNA silencing is induced by double-stranded RNA (dsRNA) intermediates produced, for instance, during replication of most plant viruses. Its pathway is initiated by the host RNase III-type Dicer-like (DCL) endoribonuclease that cleaves dsRNA molecules into 21 to 24 nt-long duplex short interfering RNAs (siRNAs), resulting in the production of virus-derived siRNAs (vsiRNAs) (Gaffar and Koch 2019; Jin et al. 2022; Lopez-Gomollon and Baulcombe 2022). Then, the guide strand of the vsiRNA duplex and Argonaute (AGO) protein form an RNA-induced silencing complex (RISC) that targets and cleaves viral RNA transcripts complementary to the guide strand, leading to the degradation of viral RNAs and inhibition of translation (Gaffar and Koch 2019; Jin

et al. 2022; Lopez-Gomollon and Baulcombe 2022). This cleavage activity by RISC results in single-stranded RNA (ssRNA) fragments that serve as templates for the host RNA-dependent RNA polymerase (RdRP) to synthesize dsRNAs, which are processed by DCLs, producing secondary vsRNAs involved in systemic silencing movement and amplification (Csorba et al. 2015; Lopez-Gomollon and Baulcombe 2022; Stavolone et al. 2020).

To counteract the antiviral RNA silencing defense response in plants, viruses encode proteins referred to as viral suppressors of RNA silencing (VSRs). The VSRs interfere with one or more specific steps of the host RNA silencing pathways (Csorba et al. 2015; Lopez-Gomollon and Baulcombe 2022; Stavolone et al. 2020). Numerous plant virus VSRs have been identified and characterized, including the well-studied polerovirus protein P0 with AGO destabilization activity and the potyvirus helper component protease (HC-Pro) with multiple functions, such as siRNA sequestering and HUA ENHANCER 1 protein binding (Barrios Barón et al. 2021; Csorba et al. 2015; del Toro et al. 2017; Fusaro et al. 2012; Jamous et al. 2011; Sanobar et al. 2021; Stavolone et al. 2020).

Knowledge of VSRs encoded by plant virus species belonging to the genus *Nepovirus* of the family *Secoviridae* remains limited. The only reported nepovirus VSR is the coat protein (CP) of tomato ringspot virus (ToRSV) (Karran and Sanfaçon 2014). No other nepovirus VSR has been identified, although artichoke Italian latent virus (AILV) interferes with the cell-to-cell movement of the RNA silencing signal (Santovito et al. 2014).

Grapevine fanleaf virus is a species of the genus *Nepovirus* in the family *Secoviridae* (Fuchs et al. 2022). Grapevine fanleaf virus (GFLV) causes fanleaf degeneration, one of the most damaging viral diseases of grapevines in most viticultural regions of the world (Andret-Link et al. 2004; Martelli 2019; Schmitt-Keichinger et al. 2017). GFLV is transmitted by the dagger nematode *Xiphinema index* (Andret-Link et al. 2004; Fuchs et al. 2017; Schmitt-Keichinger et al. 2017) and can be propagated in *Nicotiana benthamiana* (Roy and Fuchs 2022). In this systemic herbaceous host, most GFLV strains cause an asymptomatic infection, while vein clearing symptoms are transiently apparent in apical leaves of plants infected with strain GHu (Osterbaan et al. 2019; Vigne et al. 2013).

The GFLV genome is composed of two positive-sense ssRNAs called RNA1 and RNA2 (Fuchs et al. 2017; Schmitt-Keichinger et al. 2017). The polyprotein encoded by each genomic RNA is proteolytically processed by the RNA1-encoded

protease (1D^{Pro}) upon its monocistronic translation to produce mature and functional proteins. RNA1 encodes polyprotein P1 (253 kDa), which is cleaved in *cis* into five mature proteins: protein 1A (46 kDa) of unknown function, putative helicase (1B^{Hel}) (88 kDa), viral protein genome-linked protein 1C^{VPg} (3 kDa), viral cysteine protease 1D^{Pro} (25 kDa), and putative RdRP 1E^{Pol} (92 kDa) (Schmitt-Keichinger et al. 2017) (Fig. 1). Protein 1E^{Pol} is also a symptom determinant in *N. benthamiana* (Osterbaan et al. 2019; Vigne et al. 2013). RNA2 encodes polyprotein P2 (122 kDa), which is cleaved in *trans* by protein 1D^{Pro} into three mature proteins: a homing protein, 2A^{HP} (28 kDa), that directs RNA2 to the virus replication sites; a movement protein, 2B^{MP} (38 kDa); and a CP, 2C^{CP} (56 kDa) (Andret-Link et al. 2004; Fuchs et al. 2017; Schmitt-Keichinger et al. 2017) (Fig. 1). In addition to mature, fully cleaved proteins, intermediaries of GFLV polyprotein proteolytic processing have been reported. For example, the RNA1-encoded 1C^{VPg}-1D^{Pro} (Margis et al. 1994), the RNA2-encoded 2A^{HP}-2B^{MP} (Margis et al. 1993), and several other unidentified, intermediate polyproteins (Margis et al. 1993, 1994; Pinck et al. 1988) have been detected by in-vitro translation experiments (Fig. 1). No function has been attributed to any of these intermediate polyproteins.

Despite advanced knowledge of the biology of GFLV (Fuchs et al. 2017; Schmitt-Keichinger et al. 2017), a VSR profile is yet to be revealed for this economically relevant virus. In this study, we examined the silencing suppression activity of GFLV-encoded protein constructs in transgenic *N. benthamiana* plants expressing the enhanced green fluorescent protein gene (*EGFP*) and report the identification and characterization of two RNA1-encoded VSRs.

Results

Transient expression of pHELLSGATE8-EGFP induces systemic silencing of EGFP in transgenic *N. benthamiana* plants expressing EGFP.

Wild-type (WT) and transgenic *N. benthamiana* plants expressing *EGFP* (*EGFP* plants) were used in this study. Silencing of *EGFP* in transgenic *EGFP* plants was achieved by *Agrobacterium tumefaciens*-mediated delivery of a pHELLSGATE8-EGFP (pHELL-EGFP) construct encoding *EGFP* hairpin at the five- to seven-leaf development stage. Local silencing of *EGFP* was observed at 3 to 4 days postinfiltration (dpi) in leaves treated

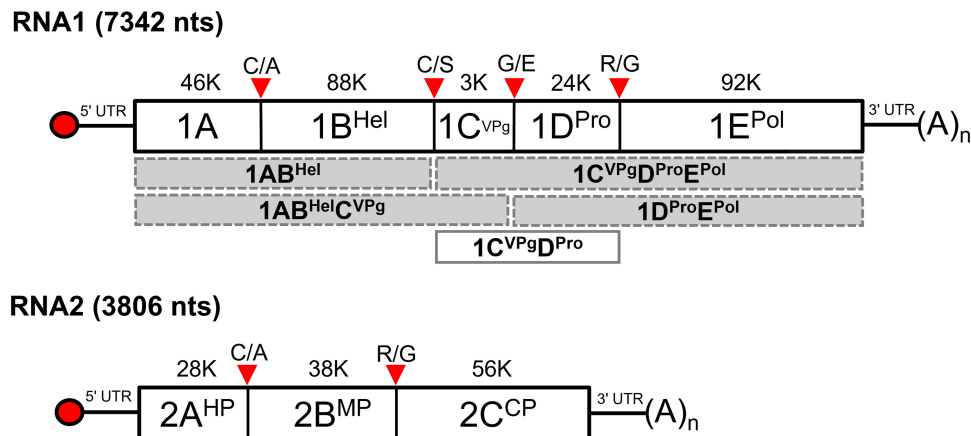


Fig. 1. Genomic structure of grapevine fanleaf virus (GFLV) strain GHu: 1A, function unknown at the start of this study; 1B^{Hel}, putative helicase; 1C^{VPg}, viral genome-linked protein; 1D^{Pro}, proteinase; 1E^{Pol}, predicted RNA-dependent RNA polymerase; 2A^{HP}, homing protein; 2B^{MP}, movement protein; and 2C^{CP}, coat protein. Some hypothetical intermediates of RNA1-encoded polyprotein (P1) proteolytic processing are shown in gray boxes with dotted lines. An intermediary of P1 proteolytic processing detected by in vitro experiments (Margis et al. 1994) is shown in an empty box with gray solid lines. The red arrows indicate proteolytic cleavage sites (A = alanine, C = cysteine, E = glutamic acid, G = glycine, R = arginine, and S = serine). The 5' and 3' untranslated regions (UTR) are represented by black lines. The poly-A tail is represented by (A)_n at the 3' end, and the VPg is represented by a red circle at the 5' end.

with pHELL-EGFP. Monitoring a total of 858 plants indicated the onset of systemic silencing of *EGFP* as early as 4 dpi, with fully silenced apical leaves observed at 6 to 8 dpi (Supplementary Fig. S1A). In comparison, plants treated with tobacco rattle virus (TRV) carrying *EGFP* (TRV-EGFP) (Vigne et al. 2013) developed fully silenced apical leaves starting at 5 dpi and produced multiple silenced apical leaves at 6 to 8 dpi (Supplementary Fig. S1A). Additionally, apical leaves of pHELL-EGFP- or TRV-EGFP-treated transgenic *EGFP* plants and WT plants exhibited significantly lower ($P < 0.001$) EGFP fluorescence intensity units at 6 to 8 dpi in comparison with untreated *EGFP* plants and infiltration buffer-treated (mock) plants (Supplementary Fig. S1B). These results revealed that pHELL-EGFP, like TRV-EGFP, caused systemic silencing of *EGFP* in *EGFP* plants.

The ability of pHELL-EGFP at inducing systemic RNA silencing was confirmed by quantifying the relative abundance of *EGFP* transcripts via reverse transcription-quantitative PCR (RT-qPCR), followed by relative quantification ($2^{-\Delta\Delta C_t}$) with *F-BOX* used as an internal control (Liu et al. 2012). *F-BOX* was chosen as the host housekeeping gene in this study because the abundance of its transcripts was consistent across treatments, with an average quantification cycle (Cq) value of 24.92 ± 0.66 (Supplementary Fig. S2A). In addition, comparative analyses of qPCR standard curve assays revealed optimal amplification efficiency (102.9%) and high coefficient determination (R^2) value (0.999) for *F-BOX* relative to four other housekeeping gene candidates (*ACT*, *CDC2*, *EF1 α* , and *PP2A*) tested in RT-qPCR (Supplementary Table S1). Furthermore, the relative expression of three host genes (*NbAGO1*, *NbDCLA*, and *NbRDR6*) and *EGFP* in transgenic *EGFP* plants normalized against *F-BOX* and *PP2A* (Liu et al. 2012) showed similar patterns, although the detectable amount of *PP2A* transcripts was dramatically increased in plants treated with p24 of grapevine leafroll-associated virus 2 (GLRaV 2) that was used as a positive VSR control (Li et al. 2018; Osterbaan et al. 2018) (Supplementary Fig. S2B). These results supported the use of *F-BOX* as a suitable internal control for RT-qPCR quantification of host gene expression.

Coinciding with the EGFP fluorescence intensity results (Supplementary Fig. S1B), the relative *EGFP* expression level was significantly lower ($P < 0.001$) in apical leaves of pHELL-EGFP- or TRV-EGFP-treated *EGFP* plants at 6 to 8 dpi and of WT plants in comparison with apical leaves of untreated and mock-infiltrated plants (Supplementary Fig. S1C). These results showed that *A. tumefaciens*-mediated transient expression of an *EGFP* hairpin construct by pHELL-EGFP induced strong systemic silencing of *EGFP* in transgenic *N. benthamiana* *EGFP* plants. Nonetheless, the systemic silencing strength by pHELL-EGFP varied across biological replicates (plants) with approximately half of the treated plants (53%, 159 of 300) exhibiting strong systemic silencing of *EGFP* and the other half (47%, 141 of 300) displaying weak systemic silencing of *EGFP* (Supplementary Fig. S3). Therefore, only *EGFP* plants that developed strong systemic silencing of *EGFP* in the apical leaves upon agroinfiltration with pHELL-EGFP, as determined by fluorescence imaging, were selected for subsequent experiments.

GFLV suppresses systemic RNA silencing in *N. benthamiana* *EGFP* plants.

To determine whether GFLV contains a VSR, reversal of systemic *EGFP* silencing was assessed by first inducing systemic RNA silencing of *EGFP* in *N. benthamiana* *EGFP* plants with the pHELL-EGFP construct and then mechanically inoculating systemically silenced plants with GFLV strains GHu or F13 (Osterbaan et al. 2019; Vigne et al. 2013) at 7 to 8 dpi. Plants were monitored for systemic suppression of *EGFP* and disease symptoms. Mock-inoculated plants were used as negative controls.

Systemic suppression of RNA silencing was observed in *EGFP*-silenced *N. benthamiana* *EGFP* plants inoculated with GFLV strain GHu (GFLV-GHu) (Fig. 2I to L). GFLV infection was confirmed in these plants by double-antibody sandwich enzyme-linked immunosorbent assay with specific antibodies (data not shown). Plants infected with GFLV-GHu progressively displayed a reversal of RNA silencing in apical leaves over time, as observed at 6 to 15 days post-mechanical inoculation (dpmi) (Fig. 2I to L). In addition, systemic silencing of *EGFP* was inhibited in petioles of the top youngest leaves in infected plants (Fig. 2I to L). Leaves of GFLV-GHu-infected *EGFP* plants (Fig. 2L) appeared similar at 15 dpmi to the corresponding leaves of untreated *EGFP* plants (Fig. 2D), when observed with an orange filter under a Dark Reader light in the dark. As anticipated, fluorescence was strong in untreated *EGFP* plants (Fig. 2A to D), while mock-treated plants exhibited systemic silencing of *EGFP* (Fig. 2E to H). A reversal of systemic *EGFP* silencing was also observed in transgenic plants mechanically inoculated with GFLV strain F13 (Supplementary Fig. S4). These results showed that two GFLV strains suppress systemic RNA silencing in *N. benthamiana* *EGFP* plants, suggesting the existence of at least one VSR encoded by this virus.

Association between suppression of systemic RNA silencing in *N. benthamiana* *EGFP* plants and symptom development by GFLV strain GHu.

A temporal analysis of *EGFP* expression upon GFLV-GHu infection revealed suppression of systemic RNA silencing in apical leaves as early as 5 to 6 dpmi (Fig. 2I). Suppression became stronger at 9 and 11 dpmi (Fig. 2J and K, respectively), with the silencing movement limited to a few lateral and sublateral veins near the apex (Fig. 2K). Systemic suppression induced by GFLV-GHu was strongest at 15 dpmi (Fig. 2L). Concurrently, GFLV-GHu caused vein clearing symptoms around 6 dpmi (Fig. 2M). Symptoms started to fade around 9 dpmi (Fig. 2N) and were no longer apparent around 11 dpmi (Fig. 2O), confirming previous reports (Osterbaan et al. 2019; Vigne et al. 2013). No symptoms were observed on plants infected with GFLV-F13 (Supplementary Fig. S4), as expected (Osterbaan et al. 2019; Vigne et al. 2013). These results revealed that the onset of reversal of *EGFP* silencing in GFLV-GHu-inoculated *EGFP* plants (Fig. 2I) coincided with the initiation of vein clearing symptom development in apical leaves (Fig. 2M), while the maximal reversal of systemic RNA silencing (Fig. 2L) corresponded with full plant recovery from vein clearing symptoms (Fig. 2P).

Selection of GFLV VSR candidates.

Preliminary research conducted in our laboratory showed that GFLV proteins 1A, 1B^{Hel}, and 1AB^{Hel}, a predicted intermediary product of proteolytic processing of the RNA1-encoded polyprotein, bear silencing suppression activity (Fig. 1; Supplementary Fig. S5). Other GFLV-encoded proteins, including RNA2-encoded proteins 2A, 2B^{MP}, and 2C^{CP} and RNA1-encoded proteins 1D^{Pro} and 1E^{Pol}, did not exhibit silencing suppression potential (Supplementary Fig. S5). Therefore, the suppression activities performed in this study focused on pEarleyGate100 constructs (Earley et al. 2006) of GFLV-GHu proteins 1A, 1B^{Hel}, and 1AB^{Hel}, with GFLV-GHu protein 1D^{Pro} used as a non-VSR control and GLRaV 2 p24 as a positive VSR control (Li et al. 2018; Osterbaan et al. 2018). The expression of the pEarleyGate100-GFLV clones was confirmed in infiltrated leaves of WT *N. benthamiana*, at the transcript level, via RT-qPCR (Supplementary Fig. S6) with specific primers (Supplementary Table S1). Validating the expression of these constructs at the protein level was unsuccessful because polyclonal antibodies raised against several synthetic GFLV

1A and 1B^{Hel} peptides failed to detect immunoreactive viral proteins in planta via Western blot assays (data not shown).

GFLV 1A and 1B^{Hel} reverse systemic RNA silencing individually or as a fused form.

To examine the ability of GFLV 1A and 1B^{Hel} to reverse systemic RNA silencing, the hairpin pHELL-EGFP construct was used to induce systemic silencing of *EGFP* in *EGFP* plants at the five- to seven-leaf development stage. Then, at 6 to 8 dpi, *EGFP*-silenced plants were infiltrated with pEarleyGate100-GFLV 1A (1A), pEarleyGate100-GFLV 1B^{Hel} (1B^{Hel}), pEarleyGate100-GFLV 1AB^{Hel} (1AB^{Hel}), or pEarleyGate100-GFLV 1A and pEarleyGate100-GFLV 1B^{Hel} mixed at a 1:1 ratio (1A+1B^{Hel}) (Fig. 3A). To verify if plasmids and a non-VSR-encoded GFLV protein construct affect suppression of systemic RNA silencing, *EGFP*-silenced plants were untreated (negative) or treated with infiltration buffer (mock), empty pEarleyGate100 vector (pV), and pEarleyGate100-GFLV 1D^{Pro} (1D^{Pro}). GLRaV 2 p24 (p24)

was used as a positive control (Li et al. 2018). Suppression of systemic RNA silencing was examined by fluorescence imaging and fluorescence measurements in *EGFP*-silenced leaves infiltrated with a GFLV protein constructs at 3 to 4 dpi and in uninfiltrated apical leaves at 7 to 11 dpi (Fig. 3A).

No reversal of *EGFP* silencing was convincingly observed in leaves infiltrated with 1A, 1B^{Hel}, 1A+1B^{Hel}, and 1AB^{Hel}, although the reversal of RNA silencing was observed in the midrib by fluorescence imaging at 3 to 4 dpi in GFLV 1B^{Hel}-infiltrated leaves (Fig. 4A). GFLV 1B^{Hel}-infiltrated leaves exhibited both significantly higher ($P < 0.05$) fluorescence intensity (Fig. 4B) and *EGFP* expression (Fig. 4C) in comparison with control plants that maintained silencing of *EGFP* (negative, mock, pV, and 1D^{Pro}). Western blot analyses of EGFP accumulation revealed that GFLV protein construct-treated leaves exhibited relatively higher EGFP protein quantity than did those in 1D^{Pro}- and pV-treated leaves (Fig. 4D), in agreement with fluorescence intensity quantification assays (Fig. 4B). As anticipated, p24 re-

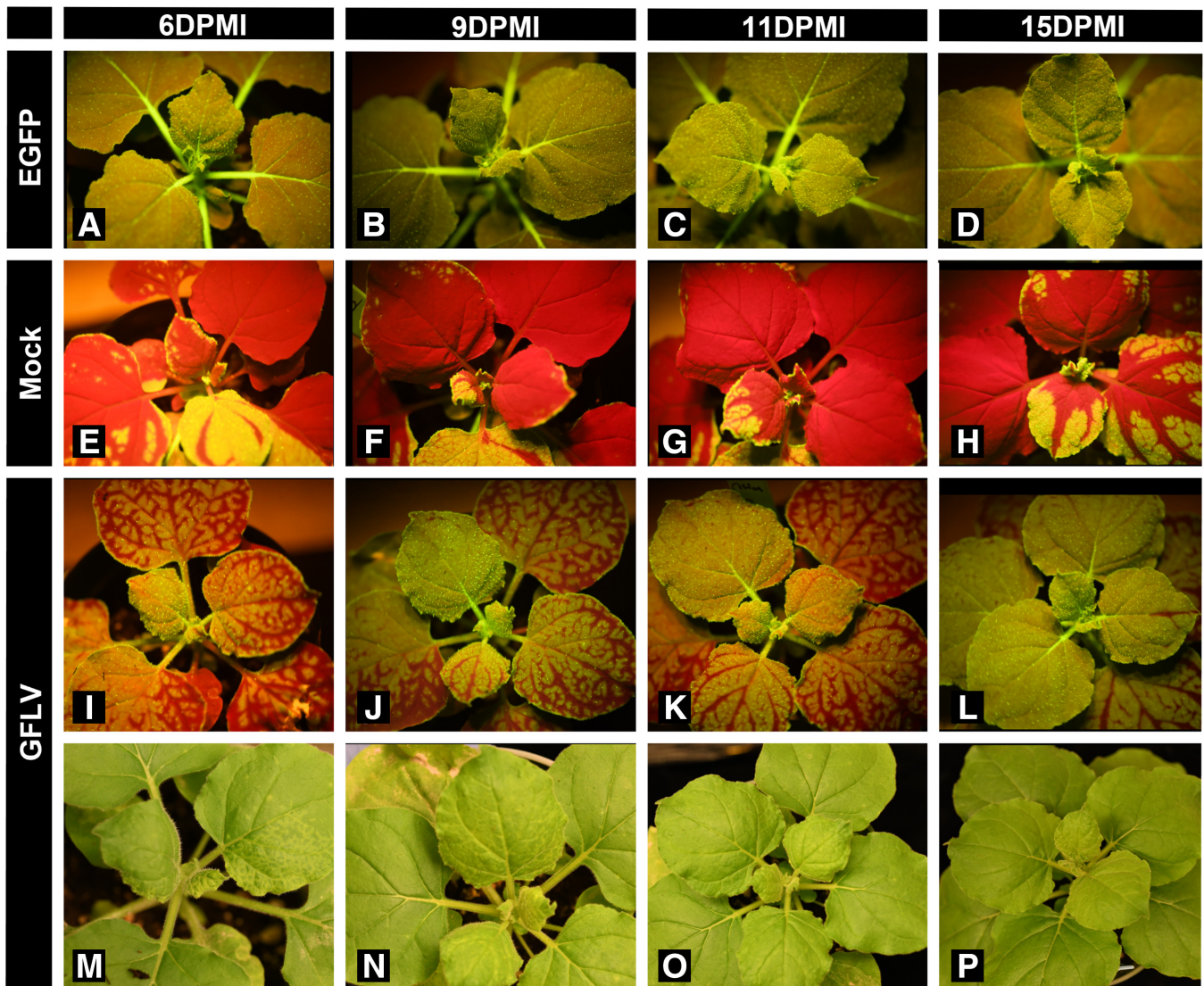


Fig. 2. Systemic suppression of enhanced green fluorescent protein gene (*EGFP*) silencing by grapevine fanleaf virus (GFLV) strain GHu (GFLV-GHu) in transgenic *Nicotiana benthamiana* expressing *EGFP*. Transgenic *N. benthamiana* *EGFP* plants that developed strong systemic *EGFP* silencing upon agroinfiltration with pHELLSGATE8-*EGFP* were mechanically inoculated at 7 to 8 days postinfiltration with GFLV-GHu-infected *N. benthamiana* tissue. **A to D**, Fluorescence photos of untreated transgenic *EGFP* plants. **E to H**, Fluorescence photos of systemically silenced transgenic *EGFP* plants inoculated with buffer (Mock). **I to L**, Fluorescence photos showing various degrees of reversal of systemic *EGFP* silencing by GFLV-GHu in transgenic *EGFP* plants. Eight biological replicates (plants) were analyzed. **M to P**, Light field photos of plants shown in I to L, showing development and loss of vein clearing symptoms over time. Photos were taken at 6, 9, 11, and 15 days post-mechanical inoculation (DPMI), using a NIKON D850 digital camera with an orange filter under a Dark Reader light (A to L) or indoor LED light (M to P).

versed RNA silencing in infiltrated leaves, as shown by both qualitative and quantitative data of EGFP and *EGFP* expression (Fig. 4A to D). These results provided weak evidence of the capacity of GFLV 1B^{Hel} at reversing systemic RNA silencing in infiltrated leaves at 3 to 4 dpi. However, due to discrepancies among EGFP protein quantification analyses (Fig. 4A, B, and D), no conclusion could be confidently reached on its suppression activity in this assay.

In uninfiltrated apical leaves, systemic suppression of *EGFP* silencing by GFLV 1A, 1B^{Hel}, 1A+1B^{Hel}, and 1AB^{Hel} was observed at 7 to 11 dpi in the top three youngest apical leaves (Fig. 5A). The EGFP fluorescence intensity and the relative *EGFP* transcript abundance were significantly higher ($P < 0.05$) in *EGFP*-silenced plants treated with GFLV 1A, 1B^{Hel}, 1A+1B^{Hel}, and 1AB^{Hel} in comparison with the other treatments (pV and GFLV 1D^{Pro}) and the negative controls (negative and mock) (Fig. 5B and C). As expected, p24 induced a significant increase ($P < 0.05$) in fluorescence intensity and relative *EGFP* transcript accumulation, in agreement with fluorescence imaging (Fig. 5A to C). Additionally, the apical leaves of negative control plants and those treated with pV and GFLV 1D^{Pro} maintained systemic silencing of *EGFP* expression, as anticipated (Fig. 5A to C).

Suppression of systemic RNA silencing in uninfiltrated apical leaves by GFLV 1A and 1B^{Hel} was observed around 7 dpi, similarly to p24. Interestingly, systemic suppression by GFLV 1A+1B^{Hel} and 1AB^{Hel} was always delayed by 2 to 4 days in comparison with individual GFLV 1A and 1B^{Hel} treatment. Noticeably, 1B^{Hel} induced the most consistent suppression of systemic

RNA silencing in apical leaves, but its suppression strength was variable across biological replicates (plants), with 64% (seven of 11) of the 1B^{Hel}-treated plants developing strong suppression and 36% (four of 11) of them developing relatively weak suppression, as determined by qualitative and quantitative analyses of *EGFP* expression (Supplementary Fig. S7). Together, these results showed that GFLV 1A and 1B^{Hel} suppress systemic RNA silencing independently or as a fused form (1AB^{Hel}).

GFLV 1A and 1B^{Hel} differentially alter the expression of plant host genes involved in RNA silencing.

Some VSRs can alter host gene expression to interfere with RNA silencing and antiviral defense (Azevedo et al. 2010; Jin et al. 2022; Pertermann et al. 2018; Stabolone et al. 2020). To gain insights into the ability of GFLV 1A and 1B^{Hel} to modulate the expression of five host genes involved in RNA silencing and antiviral defense in *N. benthamiana* (*NbAGO1*, *NbAGO2*, *NbDCL2*, *NbDCL4*, and *NbRDR6*) (Li et al. 2017; Ludman and Fátýol 2021; Pérez-Cañamás et al. 2021; Scholthof et al. 2011), changes in host RNA silencing gene expression profiles were quantified in infiltrated leaves at 3 to 4 dpi and in uninfiltrated apical leaves at 7 to 11 dpi of *EGFP*-silenced plants via RT-qPCR using specific primers (Supplementary Table S1).

In infiltrated leaves at 3 to 4 dpi, GFLV 1B^{Hel} and 1A+1B^{Hel} significantly upregulated ($P < 0.05$) the relative expression of the five host genes tested (Fig. 4E to I) with *NbDCL2* and *NbDCL4* expression being the most upregulated. GFLV 1AB^{Hel} signifi-

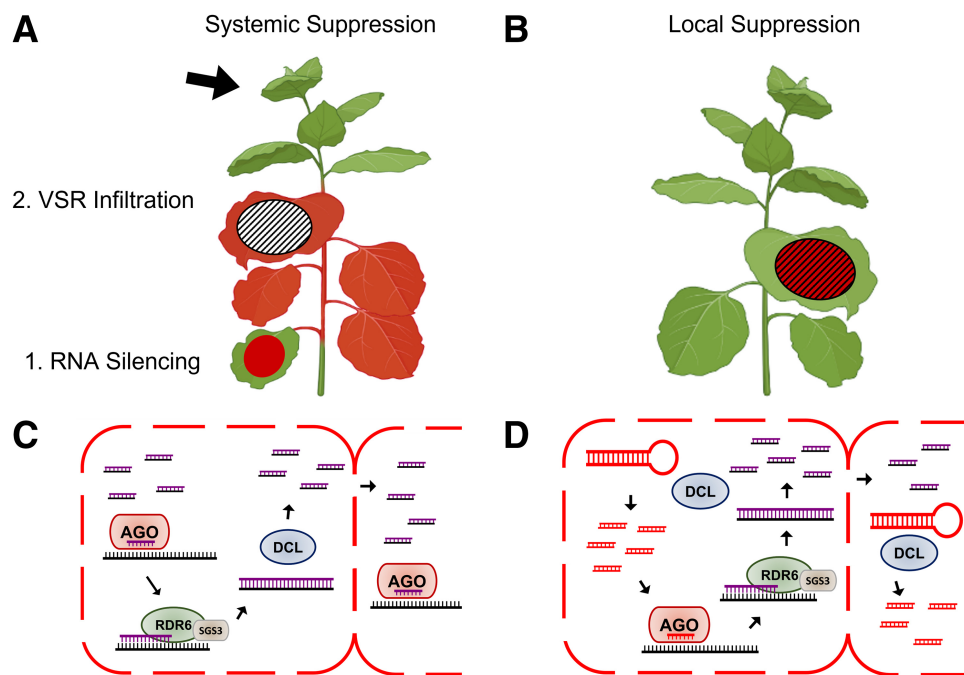


Fig. 3. A schematic representation of two RNA silencing suppression assays with grapevine fanleaf virus (GFLV) 1A, 1B^{Hel}, 1A+1B^{Hel}, and 1AB^{Hel} in transgenic *Nicotiana benthamiana* expressing enhanced green fluorescent protein gene (*EGFP*). The solid red circle without a border line represents the leaf area infiltrated with an *EGFP* hairpin construct. A lined circle with dashes represents the leaf area infiltrated with GFLV viral suppressor of RNA silencing (VSR) constructs. **A**, In the reversal of RNA silencing assay, systemic RNA silencing was triggered with an *EGFP* hairpin construct (red circle without border line) (step 1, RNA silencing), then, systemically silenced leaves were infiltrated with GFLV VSR constructs (circle with black border line and dashes) at 6 to 8 days postinfiltration (dpi) (step 2, VSR infiltration) and were analyzed for suppression of RNA silencing in infiltrated leaves 3 to 4 days later and in uninfiltrated apical leaves (shown by dark arrow) 7 to 11 days later. **B**, In the co-infiltration assay, leaves were simultaneously infiltrated with an *EGFP* hairpin construct and a GFLV VSR construct to examine local suppression at 3 to 4 dpi (red circle with black border line and dashes). **C**, For the reversal of silencing assay (A), short interfering RNA (siRNA) precursor molecules are limited to RDR6-SGS3-generated double-stranded RNA. Secondary siRNA duplexes (depicted in purple) produced by transitivity from *EGFP* hairpin infiltrated cells (step 1) move via plasmodesmata- and phloem-mediated transport and initiate RDR6-SGS3- and Dicer-like (DCL)-mediated production of secondary siRNAs in distal leaves (step 2). The produced secondary siRNAs transit via plasmodesmata-mediated movement to the adjacent cell. **D**, For the co-infiltration assay (B), two different types of siRNA duplex precursor molecules are present. Primary siRNA duplexes (shown in red) are produced from an *EGFP* hairpin construct, and secondary siRNAs (shown in purple) are generated by RDR6-SGS3 and DCL. Resulting siRNAs transit via plasmodesmata-mediated movement to the adjacent cell. The figure was created in BioRender and Adobe Photoshop 2022.

cantly upregulated ($P < 0.05$) the relative expression of *NbDCL4* and *NbAGO2* (Fig. 4F and H). GLRaV 2 p24 significantly upregulated ($P < 0.05$) the relative expression of all four host genes (Fig. 4E to H), including *NbAGO1*, confirming previous reports (Li et al. 2018).

In uninfiltrated apical leaves at 7 to 11 dpi, the relative expression of *NbDCL2* was significantly higher ($P < 0.01$) in plants treated with GFLV 1A and 1A^{H_{hel}} (Fig. 5D). GFLV 1A^{H_{hel}} significantly upregulated ($P < 0.001$) the relative expression of *NbDCL4* (Fig. 5E) and *NbAGO1* ($P = 0.048$) (Fig. 5F), while GFLV 1A significantly upregulated ($P < 0.01$) the relative expression of *NbDCL2* (Fig. 5D) and *NbAGO2* (Fig. 5G). The relative *NbRDR6* expression level was not altered ($P > 0.05$) by the GFLV protein constructs in the apical leaves (Fig. 5H). GLRaV 2 p24 significantly upregulated *NbDCL2*, *NbDCL4*, and *NbAGO1* expression ($P < 0.01$) (Fig. 5D to F).

These results showed that GFLV 1A and 1A^{H_{hel}} differentially affect the expression of host genes involved in RNA silencing when expressed individually or as a fused form (Table 1).

GFLV 1A and 1A^{H_{hel}} do not suppress hairpin-induced RNA silencing in co-infiltration assays.

To determine whether GFLV 1A and 1A^{H_{hel}} suppress hairpin-induced RNA silencing at the local level, leaves of *EGFP* plants were co-infiltrated with a mixture of pHELL-EGFP and one of the GFLV VSR protein constructs (Fig. 3B). Plants treated with

pHELL-EGFP and empty pV were used as infiltration controls. GFLV 1D^{Pro} was used as a non-VSR control and p24 was utilized as a positive VSR control. Untreated and mock-treated *EGFP* plants were used as negative controls.

Results showed that GFLV 1A, 1A^{H_{hel}}, 1A+1A^{H_{hel}}, and 1A^{H_{hel}} did not suppress hairpin-induced RNA silencing in co-infiltration assays at 3 to 4 dpi, as shown by fluorescence imaging (Fig. 6A) and EGFP fluorescence intensity (Fig. 6B). These results were confirmed by quantification analyses of relative *EGFP* transcript abundance (Fig. 6C) and Western blot analyses of EGFP protein (Fig. 6D). As expected, p24 induced strong suppression of RNA silencing (Fig. 6A to D), and the expression of EGFP and *EGFP* transcripts was high in negative controls (untreated and mock-treated *EGFP* plants) (Fig. 6A to D). Additionally, a red border line was observed at the outer edge of the area infiltrated with the GFLV VSRs and the other treatments, illustrating short-distance movement of RNA silencing (Voinnet and Baulcombe 1997) (Fig. 6A). In contrast, a thinner red border line was observed in p24-treated leaves, showing limited short-distance movement of RNA silencing (Fig. 6A).

GFLV 1A and 1A^{H_{hel}} alter the expression of host genes involved in RNA silencing in co-infiltration assays.

Although GFLV 1A and 1A^{H_{hel}} did not suppress RNA silencing in a co-infiltration assay with pHELL-EGFP, we examined their ability to alter the expression of host RNA silencing genes.

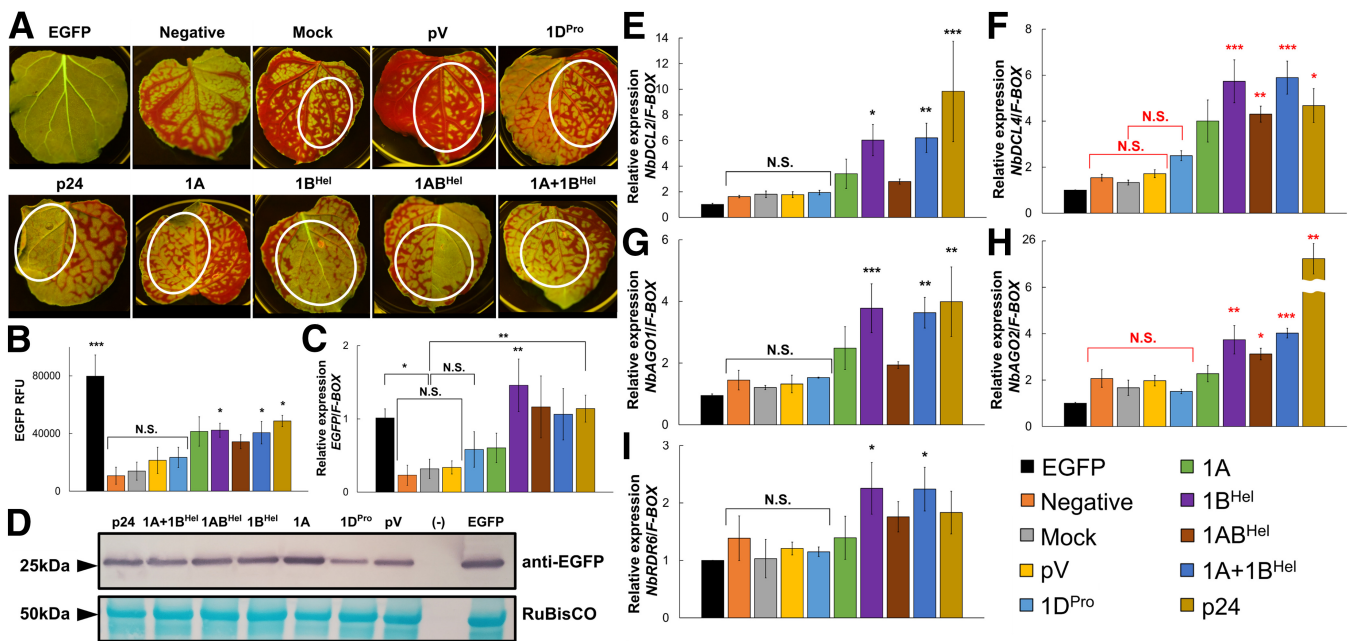
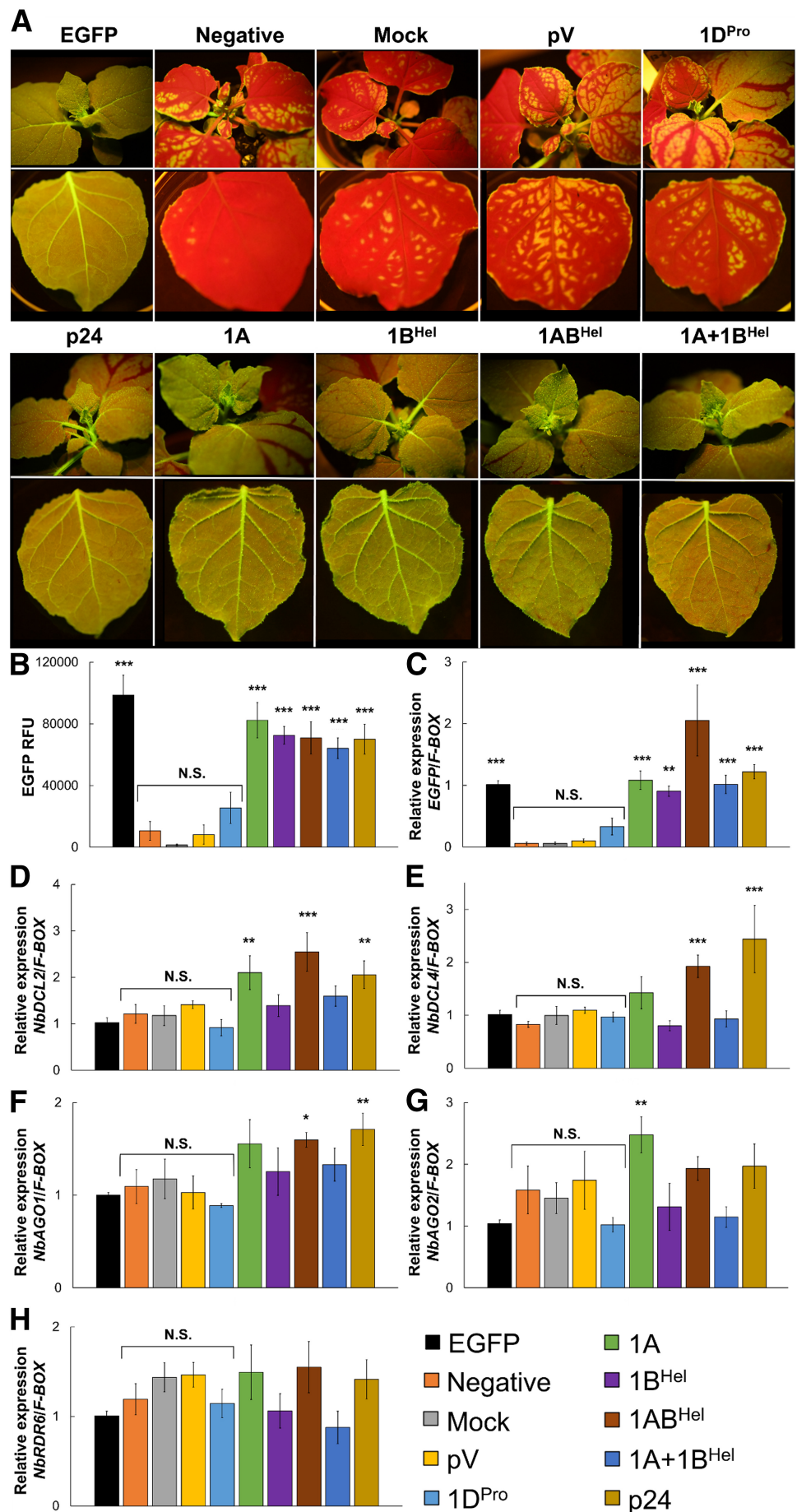


Fig. 4. Reversal of enhanced green fluorescent protein gene (*EGFP*) silencing assays by grapevine fanleaf virus (GFLV) 1A and 1A^{H_{hel}} in transgenic *Nicotiana benthamiana* expressing *EGFP*. Transgenic *EGFP* plants were first agroinfiltrated with pHELLSGATE8-EGFP for systemic silencing and were then subjected to the following treatments at 6 to 8 days postinfiltration (dpi): none (Negative), infiltration buffer (Mock), empty pEarleyGate100 vector (pV), grapevine leafroll-associated virus 2 p24 (p24) as positive control, GFLV 1D^{Pro} as negative control, GFLV 1A, GFLV 1A^{H_{hel}}, GFLV 1A+1A^{H_{hel}}, and GFLV 1A+1A^{H_{hel}} infiltrated after mixing the two constructs at a 1:1 ratio on the same leaf (1A+1A^{H_{hel}}). Untreated control *N. benthamiana* plants expressing *EGFP* are labeled EGFP. **A**, Fluorescence photos of infiltrated leaves at 3 to 4 dpi under a Dark Reader light with an orange filter, using a NIKON D850 digital camera. Photos show the abaxial surface of individual infiltrated leaves with white circles representing the infiltrated areas. **B**, Quantification of EGFP fluorescence intensity emitted at 530 nm. The fluorescence intensity is shown as relative fluorescence unit (RFU) after the background fluorescence obtained from the extraction buffer was subtracted. **C**, Relative quantification of *EGFP* transcripts via reverse transcription-quantitative PCR (RT-qPCR). **D**, Western blot analysis of total *N. benthamiana* protein showing the accumulation of EGFP (approximately 27 kDa) using a specific monoclonal antibody (anti-EGFP). The extraction buffer (–) was used as a negative loading control. The bottom panel shows the loading control RuBisCO stained with the Pierce Reversible Protein Stain kit. **E**, Relative gene expression level of *NbDCL2*, **F**, *NbDCL4*, **G**, *NbAGO1*, **H**, *NbAGO2*, and **I**, *NbRDR6* via RT-qPCR with specific primers. The gene expression was normalized against the housekeeping gene *F-BOX* and was calibrated to untreated transgenic *EGFP* plants. N.S. with a bracket indicates no significant difference ($P > 0.05$). Asterisks denote significant differences (one asterisk [*], $P < 0.05$; two [**], $P < 0.01$; and three [***] $P < 0.001$) of treatments compared with the average value from negative, mock, pV, and GFLV 1D^{Pro} treatments, according to a Dunnett's post hoc test (asterisks in black) or pairwise Wilcoxon test (asterisks in red). The bars exhibit means \pm standard error. This experiment was repeated at least twice with two to five plants per treatment. Two technical replicates per plant were used for EGFP fluorescence intensity analyses, and three technical replicates per plant were used for gene expression analyses via RT-qPCR.

Fig. 5. Systemic suppression analyses of enhanced green fluorescent protein gene (*EGFP*) silencing by grapevine fanleaf virus (GFLV) 1A and 1B^{Hel} in transgenic *Nicotiana benthamiana* expressing *EGFP*. Transgenic *EGFP* plants were first infiltrated with pHELLSGATE8-*EGFP* for systemic silencing and were then subjected to the following treatments at 6 to 8 days postinfiltration (dpi): none (Negative), infiltration buffer (Mock), empty pEarleyGate100 vector (pV), grapevine leafroll-associated virus 2 p24 (p24) as positive control, GFLV 1D^{Pro} as negative control, GFLV 1A, GFLV 1B^{Hel}, GFLV 1A^{B^{Hel}}, and GFLV 1A and GFLV 1B^{Hel} infiltrated after mixing the two constructs at a 1:1 ratio on the same leaf (1A+1B^{Hel}). Untreated control *N. benthamiana* plants expressing *EGFP* are labeled *EGFP*. **A**, Fluorescence photos of treated leaves at 7 to 11 dpi under a Dark Reader light with an orange filter using a NIKON D850 digital camera. The top panel shows whole plants, while the bottom panel shows the abaxial surface of individual apical leaves. **B**, Quantification of *EGFP* fluorescence intensity emitted at 530 nm. The fluorescence intensity is shown as relative fluorescence unit (RFU) after the background fluorescence obtained from the extraction buffer was subtracted. **C**, Relative gene expression level of *EGFP*, **D**, *NbDCL2*, **E**, *NbDCL4*, **F**, *NbAGO1*, **G**, *NbAGO2*, and **H**, *NbRDR6* via reverse transcription-quantitative PCR (RT-qPCR) with specific primers. The gene expression was normalized against the housekeeping gene *F-BOX* and was calibrated to untreated transgenic *EGFP* plants. The asterisks denote significant differences (one [*], $P < 0.05$; two [**], $P < 0.01$, and three [***], $P < 0.001$) compared with the average value of Negative, Mock, pV, and 1D^{Pro} treatments according to the post hoc test. N.S. with a bracket indicates no significant difference ($P > 0.05$). The bars exhibit means \pm standard error. This experiment was repeated at least twice with two to five plants per treatment. Two technical replicates per plant were used for *EGFP* fluorescence intensity analyses, while three technical replicates per plant were used for gene expression analyses via RT-qPCR.



GFLV 1B^{Hel} and 1A+1B^{Hel} significantly upregulated ($P < 0.05$) the relative expression of *NbDCL2*, *NbDCL4*, *NbAGO1*, *NbAGO2*, and *NbRDR6* in comparison with the other treatments (pHELL-EGFP, pV, and 1D^{Pro}), while 1A^{Hel} significantly upregulated ($P < 0.05$) the relative expression of *NbAGO1* and *NbRDR6* (Fig. 6E to I). GFLV 1A upregulated the relative ex-

pression of *NbDCL2*, *NbDCL4*, and *NbRDR6* (Fig. 6E, F, and I). Interestingly, all the GFLV VSR constructs significantly upregulated ($P < 0.05$) the relative *NbRDR6* expression (Fig. 6I). GLRaV 2 p24 significantly upregulated ($P < 0.05$) the relative expression of *NbDCL2* and *NbAGO2* in addition to *NbAGO1*, confirming a previous report (Li et al. 2018) (Fig. 6E to I). As an-

Table 1. Effect of grapevine fanleaf virus (GFLV) proteins 1A and 1B^{Hel} on the expression of five host RNA silencing genes in transgenic *Nicotiana benthamiana* expressing the enhanced green fluorescent protein gene (*EGFP*)

GFLV VSR	<i>NbDCL2</i> ^a			<i>NbDCL4</i>			<i>NbAGO1</i>			<i>NbAGO2</i>			<i>NbRDR6</i>		
	SS	SS-a	LS	SS	SS-a	LS	SS	SS-a	LS	SS	SS-a	LS	SS	SS-a	LS
1A	–	Up ^b	Up	–	–	Up	–	–	–	–	Up	–	–	–	Up
1B ^{Hel}	Up	–	Up	Up	–	Up	Up	–	Up	Up	–	Up	Up	–	Up
1A ^{Hel}	–	Up	–	Up	Up	–	–	Up	Up	Up	–	–	–	–	Up
1A+1B ^{Hel}	Up	–	Up	Up	–	Up	Up	–	Up	Up	–	Up	Up	–	Up

^a Host gene expression level was assessed in i) leaves of *EGFP*-silenced plants that were infiltrated with one or more GFLV viral suppressors of RNA silencing (VSRs) to assess reversal of systemic silencing (SS) at 3 to 4 days postinfiltration (dpi), ii) uninfiltrated apical leaves of SS to assess reversal of systemic silencing in the apical leaves (SS-a) at 7 to 11 dpi, and iii) leaves of *EGFP* plants that were co-infiltrated with pHELLSGATE8-EGFP and one or more GFLV VSRs to assess local suppression (LS) at 3 to 4 dpi.

^b Significant upregulation (up) of relative gene expression ($P < 0.05$) by different combinations of GFLV VSRs (1A, 1B^{Hel}, 1A^{Hel}, and 1A+1B^{Hel}) compared with the average value of other treatments (empty pEarleyGate100 vector, GFLV 1D^{Pro}, and negative and mock treatments for SS and SS-a or pHELLSGATE8-EGFP treatment for LS) is shown. – indicates no significant difference ($P > 0.05$).

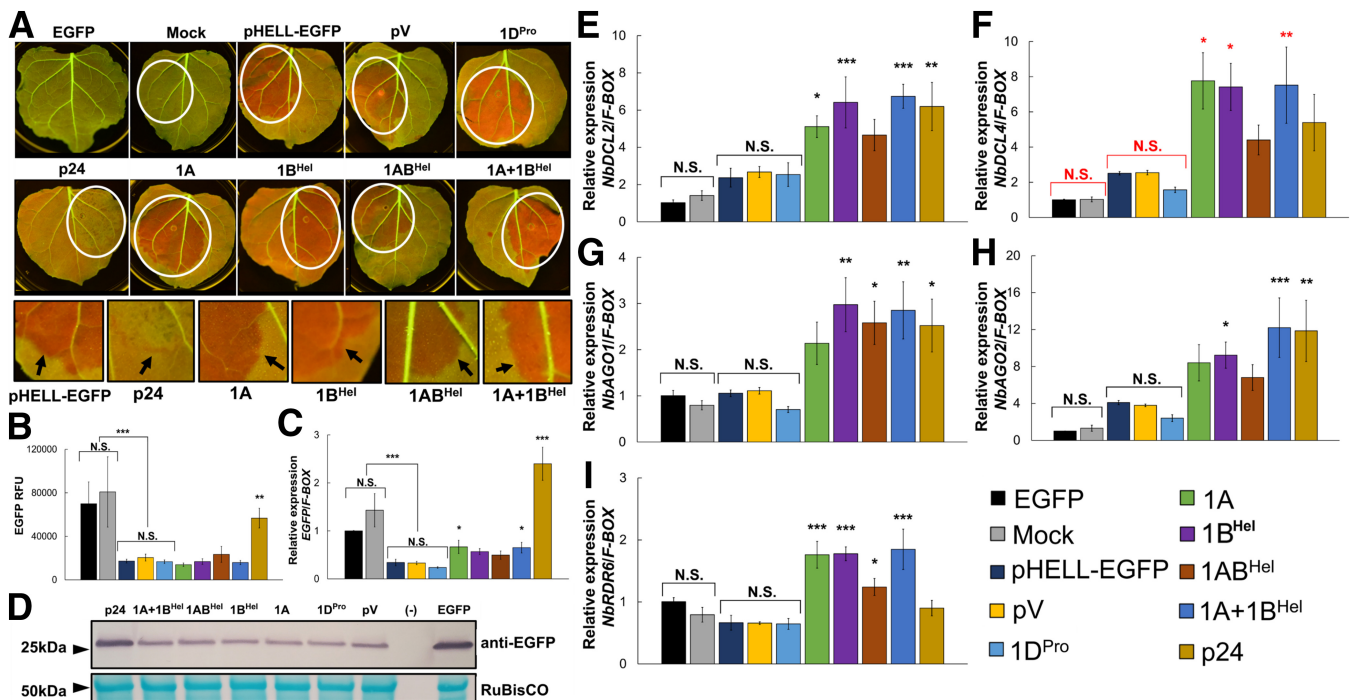


Fig. 6. Co-infiltration assay of local suppression of enhanced green fluorescent protein gene (*EGFP*) silencing by grapevine fanleaf virus (GFLV) 1A and 1B^{Hel} in transgenic *Nicotiana benthamiana* expressing *EGFP*. Transgenic *EGFP* plants were co-infiltrated with a mixture of agrobacteria containing pHELLSGATE8-EGFP and the empty pEarleyGate100 vector (pV) or GFLV 1D^{Pro} as negative control, or grapevine leafroll-associated virus 2 p24 (p24) as positive control, or GFLV 1A, 1B^{Hel}, 1A^{Hel}, or a mixture of 1A and 1B^{Hel} at a 1:1 ratio (1A+1B^{Hel}). Plants treated with infiltration buffer (Mock) or agroinfiltrated with pHELLSGATE8-EGFP only (pHELL-EGFP) were used as additional negative controls. Untreated control *N. benthamiana* plants expressing *EGFP* are labeled EGFP. **A**, Fluorescence photos of infiltrated leaves at 3 to 4 days postinfiltration under a Dark Reader light with an orange filter, using a NIKON D850 digital camera. Photos show the abaxial surface of individual infiltrated leaves with white circles representing the infiltrated areas. The bottom panel shows the red border line developed at the outer edge of infiltration sites marked by the dark arrow, indicating short-distance movement of RNA silencing. **B**, Quantification of EGFP fluorescence intensity emitted at 530 nm. The fluorescence intensity is shown as relative fluorescence unit (RFU) after the background fluorescence obtained from the extraction buffer was subtracted. **C**, Relative quantification of *EGFP* transcripts via reverse transcription-quantitative PCR (RT-qPCR) with specific primers. **D**, Western blot analysis of total *N. benthamiana* proteins showing the accumulation of EGFP (approximately 27 kDa) using a specific monoclonal antibody (anti-EGFP). The extraction buffer (–) was used as a negative loading control. The bottom panel shows the loading control RuBisCO stained with the Pierce Reversible Protein Stain kit. **E**, Relative gene expression level of *NbDCL2*, **F**, *NbDCL4*, **G**, *NbAGO1*, **H**, *NbAGO2*, and **I**, *NbRDR6* via RT-qPCR. The gene expression was normalized against the housekeeping gene *F-BOX* and was calibrated to untreated transgenic *EGFP* plants. N.S. with a bracket indicates no significant difference ($P > 0.05$). Asterisks denote significant differences (one [*], $P < 0.05$; two [**], $P < 0.01$, and three [***], $P < 0.001$) of treatments compared with the average value of pHELL-EGFP, pV, and GFLV 1D^{Pro} treatments, according to a Dunnett's post hoc test (asterisks in black) or pairwise Wilcoxon test (asterisks in red). The bars exhibit means \pm standard error. This experiment was repeated at least twice with two to four plants per treatment. Two technical replicates per plant were used for EGFP fluorescence intensity analyses, and three technical replicates per plant were used for gene expression analyses via RT-qPCR.

anticipated, there were no significant ($P > 0.05$) differences among the non-GFLV VSR treatments (pHELL-EGFP, pV, and GFLV 1D^{Pro}) and between the two negative controls (untreated and mock-treated *EGFP* plants) (Fig. 6E to I).

Together, these results revealed that GFLV 1A, 1B^{Hel}, 1A+1B^{Hel}, and 1AB^{Hel} altered the relative expression level of five plant RNA silencing genes, although they did not suppress RNA silencing when concomitantly expressed with an RNA silencing-inducing *EGFP* hairpin construct in the co-infiltration assay (Fig. 6; Table 1).

Discussion

In this study, we identified two VSRs encoded by GFLV that map to the N-terminus amino acid sequence of the RNA1-encoded polyprotein P1: 1A, with a hitherto unidentified function, and the putative helicase 1B^{Hel}. In addition, we explored the host RNA silencing gene expression profile influenced by GFLV VSRs. GFLV constructs 1A or 1B^{Hel}, individually, together (1A+1B^{Hel}), or as a predicted precursor of proteolytic processing (1AB^{Hel}), suppressed systemic RNA silencing in transgenic *N. benthamiana* expressing *EGFP*. To our knowledge, this is the first report of a putative intermediary product of polyprotein proteolytic cleavage (1AB^{Hel}) composed of two individual VSRs, 1A and 1B^{Hel} (Fig. 1), that suppresses systemic RNA silencing. No equivalent has been described among VSRs of viruses of plants, animals, and insects (Bonnard and Saleh 2021; Csorba et al. 2015; Jin et al. 2022; Maillard et al. 2019). Nonetheless, since the expression of the protein construct 1AB^{Hel} could not be confirmed by Western blot, despite experimental evidence of its VSR function, other approaches such as epitope tag-mediated detection should be considered to ascertain in planta expression of this fused protein product.

The first GFLV VSR identified in this study was protein 1A. GFLV 1A is the foremost N-terminal product obtained upon proteolytic cleavage of the RNA1-encoded polyprotein P1 by protease 1D^{Pro} (Schmitt-Keichinger et al. 2017). This protein is referred to as protein X1 in ToRSV (Han and Sanfaçon 2003) and arabis mosaic virus (Wetzel et al. 2008), a nepovirus closely related to GFLV (Sanfaçon 2022). Like protein 1A, the function of X1 remains elusive. Our study is the first to assign a function to GFLV protein 1A. It would be interesting to determine if protein X1 of other nepoviruses also functions as a VSR. Protein 1A suppressed systemic RNA silencing in uninfiltrated apical leaves (Fig. 5) of transgenic *N. benthamiana* expressing *EGFP* but not in infiltrated leaves in a silencing reversal assay (Fig. 4) or in leaves co-infiltrated with an *EGFP* hairpin construct (Fig. 6). Nonetheless, GFLV 1A upregulated the expression of some plant genes involved in RNA silencing at the local level (*NbDCL2*, *NbDCL4*, and *NbRDR6*) and in uninfiltrated apical leaves (*NbAGO2* and *NbDCL2*). Other examples of VSRs that induce systemic silencing without interfering at the local level, like GFLV protein 1A, include protein 2b of asparagus virus 2 (genus *Iilarvirus*, family *Bromoviridae*) (Shimura et al. 2013), P50 of apple chlorotic leaf spot virus (ACLSV) (genus *Trichovirus*, family *Betaflexiviridae*) (Yaegashi et al. 2007a), TGBp1 of potato virus M (genus *Carlavirus*, family *Betaflexiviridae*) (Senshu et al. 2011), and one of the three capsid proteins, Vp20, of apple latent spherical virus (ALSV) (genus *Cheravirus*, family *Secoviridae*) (Yaegashi et al. 2007b). These VSRs do not inhibit siRNA accumulation at the local level and their mode of action remains largely unknown, although P50 of ACLSV interferes with long-distance RNA silencing movement without the ability to bind to synthetic 25-nt ss-siRNA or ds-siRNA (Yaegashi et al. 2008). It would be interesting to investigate if GFLV 1A interferes with systemic movement of siRNA molecules.

The second GFLV VSR identified in this study was protein 1B^{Hel}. GFLV 1B^{Hel} is obtained upon proteolytic cleavage at the N-terminus of the RNA1-encoded polyprotein P1 by protease 1D^{Pro} (Schmitt-Keichinger et al. 2017). GFLV protein 1B^{Hel} suppressed systemic RNA silencing (Fig. 5) and induced the most potent restoration of *EGFP* transcripts, compared with the other GFLV VSR constructs (Fig. 4). These results suggested that GFLV 1B^{Hel} may act as a first responder to counteract host antiviral RNA silencing. Systemic suppression by GFLV 1B^{Hel} was sometimes weak and slightly delayed compared with GFLV 1A (Supplementary Fig. S7), suggesting a dynamic, spatiotemporal interaction among 1B^{Hel} and host RNA silencing proteins. In addition, protein 1B^{Hel} upregulated the expression of five plant RNA silencing genes (*NbDCL2*, *NbDCL4*, *NbAGO1*, *NbAGO2*, and *NbRDR6*) in infiltrated leaves in both a reversal of systemic RNA silencing assay and a co-infiltration assay (Table 1). It would be interesting to explore how GFLV 1B^{Hel} upregulates the expression of host genes and if these mechanisms are associated with its ability to reverse systemic RNA silencing.

GFLV 1B^{Hel} was recently predicted to be cleaved at a non-canonical site (M/G) into 21- and 67-kDa proteins (Sanfaçon 2022). These two putative proteins correspond to protein X2 and the NTB coding region of ToRSV (Sanfaçon 2022) and ArMV (Wetzel et al. 2008). If this cleavage prediction is validated for GFLV through protein expression and maturation assays, a new layer of complexity would be added to our limited understanding of the functionality of GFLV protein 1B^{Hel} and its role in counterdefense against host antiviral response.

GFLV 1A and 1B^{Hel} functioned as VSRs when present together in uninfiltrated apical leaves in the reversal of systemic RNA silencing assay (Fig. 5). They also upregulated the relative expression of the five plant genes involved in RNA silencing at the local level in the co-infiltration assay and in infiltrated leaves in a silencing reversal assay (Figs. 4 and 6).

The predicted GFLV fusion product 1AB^{Hel} suppressed systemic RNA silencing in a silencing reversal assay (Fig. 5) but did not reverse or inhibit RNA silencing in infiltrated leaves (Figs. 4 and 6). Additionally, GFLV 1AB^{Hel} was the only GFLV VSR construct to upregulate the expression of three host genes (*NbDCL2*, *NbDCL4*, and *NbAGO1*) in uninfiltrated apical leaves in a silencing reversal assay (Fig. 5).

Varying suppression activities in different assays were documented for VSRs of other members of the family *Secoviridae*, to which GFLV belongs. For example, the glutamic protease (Pro2Glu) and P28 of strawberry mottle virus (SMoV) (genus *Stramovirus*, family *Secoviridae*) (Fan et al. 2022) and the large CP (LCP) of broad bean wilt virus 2 (BBWV-2) (genus *Fabavirus*, family *Secoviridae*) (Kong et al. 2014) failed to suppress RNA silencing induced by dsRNA but not by ssRNA at the local level. The host targets of these VSRs are unknown, although BBWV-2 LCP showed binding to long ssRNAs (Kong et al. 2014).

Overall, each of the GFLV VSR forms (1A, 1B^{Hel}, 1A+1B^{Hel}, and 1AB^{Hel}) differentially altered the relative expression of the plant genes involved in RNA silencing that were tested in this study (Table 1). Systemic suppression of RNA silencing by GFLV 1A+1B^{Hel} or 1AB^{Hel} was often observed in the apical leaves 2 to 4 days after suppression by individual proteins 1A and 1B^{Hel}, suggesting distinct, temporal roles for each GFLV VSR during virus infection.

GFLV VSRs altered the relative expression of *NbDCL2* and *NbDCL4* (Table 1). A reduced *DCL4* expression promotes robustness of systemic RNA silencing, while a decrease in *DCL2* expression has an opposite effect in *N. benthamiana* (Chen et al. 2018). To date, only a few VSRs have been reported to hinder the function or expression of *DCL2* or *DCL4* (Gaffar and Koch

2019; Jin et al. 2022; Lopez-Gomollon and Baulcombe 2022; Stavolone et al. 2020). It remains to be tested whether GFLV VSRs interfere with DCLs directly or indirectly through other pathways (Montavon et al. 2016).

GFLV VSRs upregulated the relative expression of *NbAGO1* and *NbAGO2* to various degrees (Table 1). AGO1 and AGO2 are drivers of antiviral RNA silencing that act hierarchically in plants (Carbonell and Carrington 2015). Numerous VSRs targeting AGOs have been identified (Jin et al. 2022; Lopez-Gomollon and Baulcombe 2022; Stavolone et al. 2020). It would be interesting to explore whether GFLV VSRs disrupt AGO homeostasis through direct protein interaction or by upregulating antagonistic microRNA as documented in other VSRs, such as polerovirus P0 (Barrios Barón et al. 2021) and tombusvirus p19 (Várallyay et al. 2010).

All GFLV VSRs upregulated the relative expression of *NbRDR6* in the co-infiltration assay (Table 1). The RDR6-dependent secondary siRNA production leads to amplification of systemic RNA silencing in plants (Stavolone et al. 2020). The ability of GFLV VSRs to upregulate *NbRDR6* expression is distinctive from other VSRs that reduce *RDR6* expression (Ren et al. 2010; Zhang et al. 2008). Further research exploring the mechanisms utilized by GFLV VSRs to alter the expression of host genes would enhance our understanding of how this virus interferes with the host antiviral immune system and what role each GFLV VSR contributes for successful infection and invasion of the host. Similarly, exploring how GFLV VSRs impact the abundance and diversity of mobile small RNA will provide insights into their interference mechanism against systemic RNA silencing.

In infiltrated leaves of silenced *EGFP* plants, the relative abundance of EGFP protein via Western blotting and relative *EGFP* transcripts was not correlated (Fig. 4B and D). This may be due to interference with RNA silencing being foremost observed at the transcript level rather than at the protein level. Another explanation for this discrepancy may be related to systemic silencing not being uniformly assimilated in these leaves by the time of tissue collection for analyses, causing spatial variations in RNA silencing intensity across the leaf tissue. Nonetheless, the different assays revealed distinct variation in suppression of RNA silencing (Figs. 4 and 5) and host gene expression alteration by GFLV VSRs (Table 1). In the reversal of systemic RNA silencing assay, GFLV VSRs were introduced in leaves with pre-established silencing initiated by secondary siRNA from transitivity (Fig. 3A). Thus, the availability of siRNA precursors in these leaves was limited to dsRNAs produced by RDR6-suppressor of gene silencing 3 (SGS3) (Fig. 3C). This is different from co-infiltration assays in which no GFLV VSR induced suppression when concomitantly infiltrated into leaves with an *EGFP* hairpin construct (Fig. 3B). In this assay, two different siRNA precursors were present, *EGFP* hairpin molecules for primary siRNA production and dsRNAs generated by RDR6-SGS3 for secondary siRNA production (Fig. 3D). Therefore, even if the interference with RDR6-SGS3-dependent dsRNA production of siRNA is occurring, it would not be sufficient to inhibit RNA silencing due to the presence of *EGFP* hairpin molecules.

GFLV belongs to the family *Secoviridae* (Fuchs et al. 2017, 2022; Schmitt-Keichinger et al. 2017) for which VSRs include the small CP of cowpea mosaic virus (genus *Comovirus*) (Liu et al. 2004), Vp20 of ALSV (Yaegashi et al. 2007b), the CP of ToRSV (Karran and Sanfaçon 2014), p51 of maize chlorotic dwarf virus (MCDV) (genus *Waikavirus*) (Stewart et al. 2017), Pro2Glu and P28 of SMoV (Fan et al. 2022), and VP53, VP37, and LCP of BBWV-2 (Kong et al. 2014). All these VSRs map to the RNA2-encoded polyprotein (Fan et al. 2022; Karran and Sanfaçon 2014; Kong

et al. 2014; Liu et al. 2004; Yaegashi et al. 2007b) or the polyprotein encoded by the monopartite RNA genome of MCDV (Stewart et al. 2017). GFLV is the first member of the family *Secoviridae* with a bipartite RNA genome for which VSRs map to the RNA1-encoded polyprotein. This unique feature of GFLV adds to the overall biological and molecular diversity of the family *Secoviridae* (Sanfaçon 2022; Thompson 2020). Nonetheless, limited information is available on how VSRs of members in the family *Secoviridae* interact with host proteins for RNA silencing suppression. The only exception is the CP of ToRSV that suppresses RNA silencing via mediation of AGO1 degradation and inhibition of its translation repression without altering *NbAGO1* mRNA and siRNA levels (Karran and Sanfaçon 2014).

The counterdefense response of GFLV strain GHu against RNA silencing in *N. benthamiana* was associated with symptom recovery. Vein clearing symptoms developed shortly after the onset of systemic RNA silencing suppression in the emerging leaves and first two youngest leaves (Fig. 2). Interestingly, systemic suppression of RNA silencing progressed over time as the plants fully recovered from the vein clearing symptoms. The direct association between viral symptom recovery and RNA silencing for nepoviruses was first demonstrated with tomato black ring virus (genus *Nepovirus*, family *Secoviridae*) (Ratcliff et al. 1997). For AILV, infection of transgenic *N. tabacum* expressing heterologous VSR HC-Pro led to an increased AILV titer and abolished or delayed symptom recovery (Santovito et al. 2014). The nepovirus symptom recovery phenomenon is not always associated with a reduction in viral titer, as shown for ToRSV, for which symptom recovery is associated with a reduced translation of RNA2 (Ghoshal and Sanfaçon 2014). In our study, a correlation between progression of symptom recovery and suppression robustness was observed over time in *EGFP*-silenced transgenic *N. benthamiana* *EGFP* plants infected with GFLV-GHu (Fig. 2). Since vein clearing symptom development by GFLV-GHu in *N. benthamiana* is determined by protein 1E^{Pol} (Osterbaan et al. 2019), and GFLV 1E^{Pol} is potentially interacting with GFLV 1B^{Hel}, as suggested by coimmunoprecipitation assays (Osterbaan et al. 2021), it is possible that GFLV-GHu symptom recovery may be related to interactions among GFLV VSR 1B^{Hel}, 1E^{Pol}, and host proteins.

In conclusion, our study revealed two VSRs encoded by GFLV RNA1, namely, 1A and 1B^{Hel}. These two VSRs suppress systemic RNA silencing individually or as a fused form and differently alter the relative expression of host genes involved in the antiviral pathways of RNA silencing. These findings suggested that GFLV might utilize multiple discrete strategies, specific to each VSR, to interfere with RNA silencing for coordinated opportunities to counteract the innate antiviral plant defense pathways.

Materials and Methods

Plant materials and growth condition.

Wild-type *N. benthamiana* and transgenic *N. benthamiana* expressing *EGFP* were used in this study. The transgenic *N. benthamiana* line expressing *EGFP* was developed in our laboratory via *A. tumefaciens*-mediated transformation of leaf explants. Both plant types were grown and maintained in a growth chamber at 25°C with a 16-h light cycle.

Construct design.

The *EGFP* hairpin construct pHELL-EGFP was generated via Gateway cloning technology (Invitrogen, Waltham, MA, U.S.A.), according to the manufacturer instructions and protocols previously described (Wesley et al. 2004). Briefly, the Gateway *attB* sites were added to the 5' and 3' end of the *EGFP*

gene derived from pEGFP (Clontech TaKaRa Bio, San Jose, CA, U.S.A.) via PCR with *attB1*- and *attB2-EGFP* primers (Supplementary Table S1). The BP Clonase II reaction was performed with pDNOR221 (Invitrogen) as a donor vector, and the resulting entry clone pDNOR221-EGFP was heat-shocked into *Escherichia coli* DH5 α cells (New England Biolabs, Ipswich, MA, U.S.A.). To verify the integrity of recombinant clones, Sanger sequencing was conducted at the Cornell Biotechnology Resource Center (BRC) to verify the insert with universal M13 forward and reverse primers, using purified plasmid (E.Z.N.A. Plasmid DNA mini kit; Omega Bio-Tek, Norcross, GA, U.S.A.) of pDNOR221-EGFP. The LR Clonase II reaction was performed with sequence-verified pDNOR221-EGFP and hairpin interference binary vector pHELLSGATE8 (Helliwell and Waterhouse 2003), obtained from the Commonwealth Scientific and Industrial Research Organisation (Canberra, Australia). Colony screening was carried out using enzyme digestion with *AgeI*-HF/*StuI* (New England Biolabs), and the resulting expression clone pHELL-EGFP was verified via high-throughput sequencing at the Center for Computational & Integrative Biology (CCIB) DNA Core at Massachusetts General Hospital (MGH; Cambridge, MA, U.S.A.). The confirmed construct pHELL-EGFP was then electroporated into *A. tumefaciens* GV3101 for delivery in planta via agroinfiltration. *A. tumefaciens* GV3101 containing TRV-EGFP (Vigne et al. 2013) was used as a positive control for RNA silencing.

Plasmid DNA with full-length wild-type GFLV strain GHu RNA1 in pCLEAN-GHu-1 (Osterbaan et al. 2019) was used as a template to amplify GFLV-1A, GFLV-1B^{Hel}, GFLV-1AB^{Hel}, and GFLV-1D^{Pro} via PCR, using specific *attB1* and *attB2* primers (Supplementary Table S1). The BP Clonase II reaction was performed with pDNOR207 (Invitrogen) as a donor vector, and then, the resulting entry clones were heat-shocked into *E. coli* DH5 α cells. Purified plasmids of recombinant entry clones pDNOR207-GFLV-1A, pDNOR207-GFLV-1B^{Hel}, and pDNOR207-GFLV-1AB^{Hel}, and pDNOR207-GFLV-1D^{Pro} were analyzed to verify the integrity of the insert via restriction digestion, using restriction endonucleases *ApaI*, *ApaI/AgeI*-HF, *AgeI*-HF, and *ApaI/KpnI*-HF, respectively (New England Biolabs). The validated recombinant entry clones were then used to perform the LR Clonase II reaction with destination vector pEarleyGate100 (Earley et al. 2006). Purified plasmids of expression clones pEarleyGate100-GFLV-1A, pEarleyGate100-GFLV-1B^{Hel}, pEarleyGate100-GFLV-1AB^{Hel}, and pEarleyGate100-GFLV-1D^{Pro} were analyzed and verified via restriction digestion with *KpnI*-HF/*XbaI*. In addition, the inserts were characterized by Sanger sequencing at Cornell BRC with specific primers, and recombinant plasmids were sequenced at the CCIB DNA Core at MGH. The sequence-verified expression clones were then electroporated into competent *A. tumefaciens* GV3101 for agroinfiltration. DNASTAR/Lasergene (v. 15.3) and SnapGene (v. 5) were both used to design Gateway cloning primers and simulate outcomes of Gateway BP and LR reactions.

The binary vector pGA482G containing p24 of GLRaV 2 (Osterbaan et al. 2018; Vigne et al. 2013) was electroporated into competent *A. tumefaciens* C58Z707 and was used as a positive control for silencing suppression experiments.

Plant transformation and agroinfiltration.

A. tumefaciens GV3101 containing pHELL-EGFP (per liter, gentamicin 30 mg and spectinomycin 100 mg) and TRV-EGFP (per liter, gentamicin 30 mg, kanamycin 50 mg, and rifampicin 15 mg) were grown in Luria-Bertani liquid media, supplemented with 100 μ M acetosyringone and appropriate antibiotics, at 28°C, with shaking at 225 rpm for no more than 2 days. The bacterial cultures were then diluted with infiltration buffer (10 mM MES-KOH, pH 5.6, 10 mM MgCl₂, and 200 μ M acetosyringone)

to an optical density at 600 nm (OD₆₀₀) of 0.7 for pHELL-EGFP and OD₆₀₀ of 0.2 for TRV-EGFP and were incubated for 3 h with gentle shaking prior to agroinfiltration. Transgenic *N. benthamiana* plants expressing *EGFP* were agroinfiltrated at the five- to seven-leaf development stage with pHELL-EGFP ($n = 858$) onto the abaxial surface of three to four leaves per plant using 3-ml needleless syringes. The positive control TRV-EGFP and mock control with infiltration buffer were similarly delivered. Only plants that developed strong systemic *EGFP* silencing upon infiltration with pHELL-EGFP were used for systemic suppression analysis to identify and characterize GFLV VSRs (Supplementary Figs. S1 and S3). Four to six biological replicates (plants) per treatment were used for quantitative analyses of *EGFP* spectrometry and *EGFP* RT-qPCR to validate that strong *EGFP* silencing has occurred.

For systemic RNA silencing suppression assays, *A. tumefaciens* GV3101 containing the empty vector pEarleyGate100 (pV) and GFLV protein constructs (pEarleyGate100-GFLV-1A, pEarleyGate100-GFLV-1B^{Hel}, pEarleyGate100-GFLV-1AB^{Hel}, and pEarleyGate100-GFLV-1D^{Pro}) and *A. tumefaciens* C58Z707 containing pGA482G-GLRaV 2 p24 (Osterbaan et al. 2018) were grown, as described above, with appropriate antibiotics (per liter, gentamicin 30 mg, kanamycin 50 mg, and rifampicin 15 mg, for pEarleyGate100 constructs, and gentamicin 30 mg and kanamycin 50 mg, for pGA482G construct). The agrobacterial cultures were then diluted with infiltration buffer to a final OD₆₀₀ of 0.3 to 0.4, and were next incubated for 3 h with gentle shaking prior to agroinfiltration. Three to four apical leaves of transgenic *N. benthamiana* plants expressing *EGFP* that developed systemic *EGFP* silencing around 6 to 8 dpi were agroinfiltrated as described above according to the following treatments: GFLV 1A, 1B^{Hel}, 1AB^{Hel}, 1A+1B^{Hel}, and positive control p24. For GFLV 1A+1B^{Hel} treatment, agrobacteria containing pEarleyGate100-GFLV-1A and pEarleyGate100-GFLV-1B^{Hel} were agroinfiltrated on the same leaf after being mixed at a 1:1 ratio (vol/vol). The *EGFP*-silenced plants that received empty vector pV and GFLV 1D^{Pro} were included as agroinfiltration and non-VSR controls, while those that received no treatment (negative) and infiltration buffer (mock) were used as negative controls. Untreated *EGFP* plants were used as control plants. Each experiment had two to five biological replicates (plants) per treatment and was repeated at least twice.

For co-infiltration assays, agrobacterial culture containing pHELL-EGFP (OD₆₀₀ of 0.7) were mixed at 1:1 ratio with agrobacterial culture containing one of the treatments (OD₆₀₀ of 0.3 to 0.4) described above (GFLV-1A, GFLV-1B^{Hel}, GFLV-1AB^{Hel}, GFLV-1A+1B^{Hel}, GFLV-1D^{Pro}, pV, and positive control p24). Mixed agrobacteria cultures were infiltrated onto abaxial surfaces of three to four leaves per plant using 3-ml needleless syringes. For this assay, transgenic *N. benthamiana* plants expressing *EGFP* at the six- to eight-leaf development stage were used. Plants that received no treatment or infiltration buffer (mock) were used as negative controls as well as pHELL-EGFP as agroinfiltration control. The co-infiltration experiments were repeated at least twice with two to four biological replicates (plants) per treatment.

Mechanical inoculation of GFLV.

Leaf tissue of wild-type *N. benthamiana* plants systemically infected with GFLV strains GHu and F13 were used as inoculum sources. GFLV strain GHu causes vein clearing symptoms in *N. benthamiana*, while strain F13 causes a symptomless infection in this herbaceous host (Vigne et al. 2013). Infected plant tissue was ground using a mortar and a pestle with inoculation buffer (15 mM KH₂PO₄, 35 mM Na₂HPO₄, pH 7.4). Transgenic *N. benthamiana* plants expressing *EGFP* infiltrated

with pHELL-EGFP and developing strong systemic silencing of *EGFP* were selected to be mechanically inoculated with GFLV-GHu or GFLV-F13. The adaxial surface of third, fourth, and fifth leaves of selected plants were coated with a thin layer of Carborundum powder and were gently rubbed with plant sap, using a pestle. Eight independent biological replicates (plants) were used for inoculation. The plants were monitored for the development of systemic suppression of RNA silencing and disease symptoms caused by GFLV-GHu. This was repeated with GFLV-F13.

EGFP imaging and sample collection.

For suppression of RNA silencing experiments, all control and treated plants were monitored for EGFP fluorescence, starting at 2 dpi with naked eyes, under a hand-held Dark Reader lamp (400 to 500 nm, Clare Chemical Research; Dolores, CO, U.S.A.) with orange filter, and photos were taken using a digital NIKON D850 camera.

A cork borer (no. 4) was used to collect leaf disc samples from apical leaves of agroinfiltrated plants at 6 to 8 dpi for systemic RNA silencing experiments. Leaf disc samples were similarly collected from infiltrated (Fig. 3A) or co-infiltrated leaves (Fig. 3B) at 3 to 4 dpi and from uninfiltrated apical leaves (Fig. 3A) at 7 to 11 dpi for suppression of RNA silencing experiments. The collected leaf disc samples were used for EGFP spectrometry and RT-qPCR of *EGFP* and known plant RNA-silencing genes with specific primers (Supplementary Table S1). Leaf disc samples were stored at -80°C until further processing. Additional leaves were collected for Western blot analysis of EGFP protein accumulation.

Spectrometry of EGFP.

Total soluble proteins were extracted from two leaf discs (one disc from one side of the midrib of one leaf and another disc from the other side of the midrib of the same leaf) per biological replicate (plant) for each treatment, as previously described by Dong et al. (2019) with modifications. The two frozen leaf discs were lysed at 30 Hz for 2 min with a TissueLyser II (Qiagen, Germantown, MD, U.S.A.), were suspended in extraction buffer (50 mM Tris-HCl, pH 8.0, 150 mM NaCl, and 10 mM EDTA) at a 1:4 ratio, and were incubated for 10 min in ice before centrifuging at 4°C for 15 min at $12,000 \times g$. The resulting supernatant was loaded in duplicate per biological replicate (plant) in a microtiter plate for measurement of EGFP fluorescence at 485 nm with a 20-nm bandpass excitation filter and at 530 nm with a 25-nm bandpass emission filter, using a Synergy2 microplate reader (BioTek, Winooski, VT, U.S.A.).

Total RNA extraction and RT-qPCR.

Total RNA was extracted from two leaf discs (one disc from one side of the midrib of one leaf and another disc from the other side of the midrib of the same leaf) of *N. benthamiana* per biological replicate (plant), using the E.Z.N.A. Plant RNA kit (Omega Bio-Tek), and were treated with DNase-I according to manufacturer instructions. Extracted RNAs with a minimum A260/A280 ratio of 2.0 were selected for RT-qPCR using the SYBR Green-based Luna Universal One-Step RT-qPCR kit (New England Biolabs) and specific primers on a CFX96 Touch thermocycler (Bio-Rad, Hercules, CA, U.S.A.). A minimum of three technical replicates was loaded per biological replicate (plant). The thermocycler conditions were set according to the manufacturer protocol. The expression levels of target genes were calculated using the $2^{-\Delta\Delta\text{Ct}}$ method, as described by Livak and Schmittgen (2001). The Cq values of target genes were normalized against the Cq values of the housekeeping gene *F-BOX* and were calibrated to the untreated transgenic *N. benthamiana* plants expressing *EGFP*. The primers used in this study and their

efficiency properties, calculated using the standard curves, are listed in Supplementary Table S1.

To determine the expression of the GFLV protein constructs 1A, 1B^{Hel}, 1AB^{Hel}, and 1D^{Pro} at the transcript level, total RNA was similarly extracted from infiltrated leaves of *EGFP* plants and was used for RT-qPCR analyses with specific primers (Supplementary Table S1). PrimerQuest (Integrated DNA Technologies, Coralville, IA, U.S.A.), Multiple Primer Analyzer (Thermo Fisher Scientific, Waltham, MA, U.S.A.), and Primer3 (v. 4.1.0) were used to design primers used in this study.

SDS-PAGE and Western blot.

Leaf tissue of *N. benthamiana* collected from biological replicates (plants) of the same treatment was used for protein extraction. Frozen leaf tissue was lysed using TissueLyser II (Qiagen, Germantown, MD, U.S.A.) and suspended in dithiothreitol (DTT)-containing lysis buffer (50 mM HEPES-KOH, pH 7.4, 110 mM KOAc, 2 mM MgCl₂, 0.4% TritonX-100, 2.5 mM DTT, and 1× protease inhibitor cocktail from Invitrogen) at a 1:5 ratio (wt/vol) (DeBlasio et al. 2015; Osterbaan et al. 2021). The protein supernatants were mixed at a 1:1 ratio (vol/vol) with loading buffer (2× Laemmli sample buffer [Bio-Rad] with 5% β-mercaptoethanol), and were incubated at 95°C for 5 min before being loaded onto 4 to 20% Mini-PROTEAN TGX precast gels (Bio-Rad). Loading buffer was used as a loading blank, and the Precision Plus Protein Dual Xtra Standards (Bio-Rad) were used as a protein ladder. Proteins were separated by electrophoresis on a Mini-PROTEAN Tetra Cell (Bio-Rad) and were then wet-transferred to 0.45 μm nitrocellulose membranes (Bio-Rad) at 4°C . An anti-EGFP mouse monoclonal antibody (F56-6A1.2.3 from Invitrogen) was used as a primary antibody at a 1:1,000 dilution, and alkaline phosphatase-conjugated goat anti-mouse immunoglobulin G (H+L) (Invitrogen) was used as a secondary antibody, at a 1:5,000 dilution with nitroblue tetrazolium and 5-bromo-4-chloro-3-indolyl phosphate substrates.

Statistical analyses.

The spectrometry and RT-qPCR data were imported into the software R (R Core Team 2022) and were analyzed for statistical significance tests. First, the normality of sample mean distribution was assessed, using the normal quantile-quantile plot and histogram of one-way analysis of variance (ANOVA). Next, based on sample mean normality, an appropriate statistical significance test was carried out to determine the significance ($P < 0.05$) among treatment groups and controls. For the normally distributed data set, parametric analysis was used via one-way ANOVA followed by Dunnett's post hoc multiple comparison test. For the abnormally distributed data set, nonparametric analysis was used via a Kruskal-Wallis test followed by pairwise Wilcoxon post hoc test.

Acknowledgments

We thank the Commonwealth Scientific and Industrial Research Organisation for providing pHELLSGATE8 vector. We are grateful to M. Thomas from the Cornell Statistical Consulting Unit for his guidance with statistical analyses.


Literature Cited

- Andret-Link, P., Laporte, C., Valat, L., Ritzenthaler, C., Demangeat, G., Vigne, E., Laval, V., Pfeiffer, P., Stussi-Garaud, C., and Fuchs, M. 2004. *Grapevine fanleaf virus*: Still a major threat to the grapevine industry. *J. Plant Pathol.* 86:183-195.
- Azevedo, J., Garcia, D., Pontier, D., Ohnesorge, S., Yu, A., Garcia, S., Braun, L., Bergdoll, M., Hakimi, M. A., Lagrange, T., and Voinnet, O. 2010. Argonaute quenching and global changes in Dicer homeostasis caused by a pathogen-encoded GW repeat protein. *Genes Dev.* 24:904-915.

- Barrios Barón, M. P., Delfosse, V. C., Agrofoglio, Y. C., Nahiriak, V., Almasia, N. I., Vazquez Rovere, C., and Distéfano, A. J. 2021. Argentinian potato leafroll virus P0 protein: Novel activities for a previously known suppressor. *Plant Pathol.* 70:259-274.
- Bonning, B. C., and Saleh, M.-C. 2021. The interplay between viruses and RNAi pathways in insects. *Annu. Rev. Entomol.* 66:61-79.
- Carbonell, A., and Carrington, J. C. 2015. Antiviral roles of plant ARGONAUTES. *Curr. Opin. Plant Biol.* 27:111-117.
- Chen, W., Zhang, X., Fan, Y., Li, B., Ryabov, E., Shi, N., Zhao, M., Yu, Z., Qin, C., Zheng, Q., Zhang, P., Wang, H., Jackson, S., Cheng, Q., Liu, Y., Gallusci, P., and Hong, Y. 2018. A genetic network for systemic RNA silencing in plants. *Plant Physiol.* 176:2700-2719.
- Csorba, T., Kontra, L., and Burgyán, J. 2015. Viral silencing suppressors: Tools forged to fine-tune host-pathogen coexistence. *Virology* 479-480:85-103.
- DeBlasio, S. L., Johnson, R., Mahoney, J., Karasev, A., Gray, S. M., MacCoss, M. J., and Cilia, M. 2015. Insights into the poliovirus-plant interactome revealed by coimmunoprecipitation and mass spectrometry. *Mol. Plant-Microbe Interact.* 28:467-481.
- del Toro, F. J., Donaire, L., Aguilar, E., Chung, B.-N., Tenllado, F., and Canto, T. 2017. *Potato virus Y* HC-Pro suppression of antiviral silencing in *Nicotiana benthamiana* plants correlates with its ability to bind *in vivo* to 21- and 22-nucleotide small RNAs of viral sequence. *J. Virol.* 91:e00367-17.
- Dong, J., Ding, X., and Wang, S. 2019. Purification of the recombinant green fluorescent protein from tobacco plants using alcohol/salt aqueous two-phase system and hydrophobic interaction chromatography. *BMC Biotechnol.* 19:86.
- Earley, K. W., Haag, J. R., Pontes, O., Opper, K., Juehne, T., Song, K., and Pikaard, C. S. 2006. Gateway-compatible vectors for plant functional genomics and proteomics. *Plant J.* 45:616-629.
- El-Sappah, A. H., Yan, K., Huang, Q., Islam, M. M., Li, Q., Wang, Y., Khan, M. S., Zhao, X., Mir, R. R., Li, J., El-Tarabily, K. A., and Abbas, M. 2021. Comprehensive mechanism of gene silencing and its role in plant growth and development. *Front. Plant Sci.* 12:705249.
- Fan, L., He, C., Gao, D., Xu, T., Xing, F., Yan, J., Zhan, B., Li, S., and Wang, H. 2022. Identification of silencing suppressor protein encoded by strawberry mottle virus. *Front. Plant Sci.* 13:786489.
- Fuchs, M., Hily, J.-M., Petrzik, K., Sanfaçon, H., Thompson, J. R., van der Vlugt, R., and Wetzel, T., and 2022. ICTV Report Consortium. 2022. ICTV virus taxonomy profile: *Secoviridae*. *J. Gen. Virol.* 103: 001807.
- Fuchs, M., Schmitt-Keichinger, C., and Sanfaçon, H. 2017. A renaissance in nepovirus research provides new insights into their molecular interface with hosts and vectors. Pages 61-105 in: *Advances in Virus Research*, M. Kielian, T. C. Mettenleiter, and M. J. Roossinck, eds. Academic Press, Cambridge, MA, U.S.A.
- Fusaro, A. F., Correa, R. L., Nakasugi, K., Jackson, C., Kawchuk, L., Vaslin, M. F. S., and Waterhouse, P. M. 2012. The *enamovirus* P0 protein is a silencing suppressor which inhibits local and systemic RNA silencing through AGO1 degradation. *Virology* 426:178-187.
- Gaffar, F. Y., and Koch, A. 2019. Catch me if you can! RNA silencing-based improvement of antiviral plant immunity. *Viruses* 11:673.
- Ghoshal, B., and Sanfaçon, H. 2014. Temperature-dependent symptom recovery in *Nicotiana benthamiana* plants infected with tomato ringspot virus is associated with reduced translation of viral RNA2 and requires ARGONAUTE 1. *Virology* 456-457:188-197.
- Han, S., and Sanfaçon, H. 2003. Tomato ringspot virus proteins containing the nucleoside triphosphate binding domain are transmembrane proteins that associate with the endoplasmic reticulum and cofractionate with replication complexes. *J. Virol.* 77:523-534.
- Helliwell, C., and Waterhouse, P. 2003. Constructs and methods for high-throughput gene silencing in plants. *Methods* 30:289-295.
- Jamous, R. M., Boonrod, K., Fuellgrabe, M. W., Ali-Shtayeh, M. S., Krczal, G., and Wassenegger, M. 2011. The helper component-proteinase of the *Zucchini yellow mosaic virus* inhibits the Hua Enhancer 1 methyltransferase activity *in vitro*. *J. Gen. Virol.* 92:2222-2226.
- Jin, L., Chen, M., Xiang, M., and Guo, Z. 2022. RNAi-based antiviral innate immunity in plants. *Viruses* 14:432.
- Karran, R. A., and Sanfaçon, H. 2014. *Tomato ringspot virus* coat protein binds to ARGONAUTE1 and suppresses the translation repression of a reporter gene. *Mol. Plant-Microbe Interact.* 27:933-943.
- Kong, L., Wang, Y., Yang, X., Sunter, G., and Zhou, X. 2014. Broad bean wilt virus 2 encoded VP53, VP37 and large capsid protein orchestrate suppression of RNA silencing in plant. *Virus Res.* 192: 62-73.
- Li, F., Zhao, N., Li, Z., Xu, X., Wang, Y., Yang, X., Liu, S.-S., Wang, A., and Zhou, X. 2017. A calmodulin-like protein suppresses RNA silencing and promotes geminivirus infection by degrading SGS3 via the autophagy pathway in *Nicotiana benthamiana*. *PLoS Pathog.* 13:e1006213.
- Li, M., Zhang, J., Feng, M., Wang, X., Luo, C., Wang, Q., and Cheng, Y. 2018. Characterization of silencing suppressor p24 of *Grapevine leafroll-associated virus 2*. *Mol. Plant Pathol.* 19:355-368.
- Liu, D., Shi, L., Han, C., Yu, J., Li, D., and Zhang, Y. 2012. Validation of reference genes for gene expression studies in virus-infected *Nicotiana benthamiana* using quantitative real-time PCR. *PLoS One* 7:e46451.
- Liu, L., Grainger, J., Cañizares, M. C., Angell, S. M., and Lomonosoff, G. P. 2004. Cowpea mosaic virus RNA-1 acts as an amplicon whose effects can be counteracted by a RNA-2-encoded suppressor of silencing. *Virology* 323:37-48.
- Livak, K. J., and Schmittgen, T. D. 2001. Analysis of relative gene expression data using real-time quantitative PCR and the $2^{-\Delta\Delta CT}$ method. *Methods* 25:402-408.
- Lopez-Gomollon, S., and Baulcombe, D. C. 2022. Roles of RNA silencing in viral and non-viral plant immunity and in the crosstalk between disease resistance systems. *Nat. Rev. Mol. Cell Biol.* 23:645-662.
- Ludman, M., and Fátýol, K. 2021. Targeted inactivation of the AGO1 homologues of *Nicotiana benthamiana* reveals their distinct roles in development and antiviral defence. *New Phytol.* 229:1289-1297.
- Maillard, P. V., van der Veen, A. G., Poirier, E. Z., and Reis e Sousa, C. 2019. Slicing and dicing viruses: Antiviral RNA interference in mammals. *EMBO J.* 38:e100941.
- Margis, R., Ritzenthaler, C., Reinbolt, J., Pinck, M., and Pinck, L. 1993. Genome organization of grapevine fanleaf nepovirus RNA2 deduced from the 122K polyprotein P2 *in vitro* cleavage products. *J. Gen. Virol.* 74:1919-1926.
- Margis, R., Viry, M., Pinck, M., Bardonnet, N., and Pinck, L. 1994. Differential proteolytic activities of precursor and mature forms of the 24K proteinase of grapevine fanleaf nepovirus. *Virology* 200:79-86.
- Martelli, G. P. 2019. Virus diseases of grapevine. In: *Encyclopedia of Life Sciences*. John Wiley & Sons, Ltd., Hoboken, NJ, U.S.A.
- Montavon, T., Kwon, Y., Zimmermann, A., Hammann, P., Vincent, T., Cognat, V., Michel, F., and Dunoyer, P. 2016. A specific dsRNA-binding protein complex selectively sequesters endogenous inverted-repeat siRNA precursors and inhibits their processing. *Nucleic Acids Res.* 45:1330-1344.
- Osterbaan, L. J., Choi, J., Kenney, J., Flasco, M., Vigne, E., Schmitt-Keichinger, C., Rebelo, A. R., Heck, M., and Fuchs, M. 2019. The identity of a single residue of the RNA-dependent RNA polymerase of grapevine fanleaf virus modulates vein clearing in *Nicotiana benthamiana*. *Mol. Plant-Microbe Interact.* 32:790-801.
- Osterbaan, L. J., Hoyle, V., Curtis, M., DeBlasio, S., Rivera, K. D., Heck, M., and Fuchs, M. 2021. Identification of protein interactions of grapevine fanleaf virus RNA-dependent RNA polymerase during infection of *Nicotiana benthamiana* by affinity purification and tandem mass spectrometry. *J. Gen. Virol.* 102:001607.
- Osterbaan, L. J., Schmitt-Keichinger, C., Vigne, E., and Fuchs, M. 2018. Optimal systemic grapevine fanleaf virus infection in *Nicotiana benthamiana* following agroinoculation. *J. Virol. Methods* 257:16-21.
- Pérez-Cañamás, M., Hevia, E., Katsarou, K., and Hernández, C. 2021. Genetic evidence for the involvement of Dicer-like 2 and 4 as well as Argonaute 2 in the *Nicotiana benthamiana* response against *Pelargonium* line pattern virus. *J. Gen. Virol.* 102.
- Pertermann, R., Tamilarasan, S., Gursinsky, T., Gambino, G., Schuck, J., Weinholdt, C., Lilie, H., Grosse, I., Golbik, R. P., Pantaleo, V., and Behrens, S. E. 2018. A viral suppressor modulates the plant immune response early in infection by regulating microRNA activity. *mBio* 9:e00419-18.
- Pinck, L., Fuchs, M., Pinck, M., Ravelonandro, M., and Walter, B. 1988. A satellite RNA in grapevine fanleaf virus strain F13. *J. Gen. Virol.* 69:233-239.
- R Core Team. 2022. R: A language and environment for statistical computing. R Foundation for Statistical Computing, Vienna.
- Ratcliff, F., Harrison, B. D., and Baulcombe, D. C. 1997. A similarity between viral defense and gene silencing in plants. *Science* 276:1558-1560.
- Ren, B., Guo, Y., Gao, F., Zhou, P., Wu, F., Meng, Z., Wei, C., and Li, Y. 2010. Multiple functions of *Rice dwarf phyto-reovirus* Pns10 in suppressing systemic RNA silencing. *J. Virol.* 84:12914-12923.
- Roy, B. G., and Fuchs, M. 2022. Herbaceous plant hosts as supermodels for grapevine viruses: A historical perspective. *J. Plant Pathol.*
- Sanfaçon, H. 2022. Re-examination of nepovirus polyprotein cleavage sites highlights the diverse specificities and evolutionary relationships of nepovirus 3C-like proteases. *Arch. Virol.* 167:2529-2543.
- Sanobar, N., Lin, P.-C., Pan, Z.-J., Fang, R.-Y., Tjita, V., Chen, F.-F., Wang, H.-C., Tsai, H.-L., Wu, S.-H., Shen, T.-L., Chen, Y.-H., and Lin, S.-S. 2021. Investigating the viral suppressor HC-Pro inhibiting small RNA

- methylation through functional comparison of HEN1 in angiosperm and bryophyte. *Viruses* 13:1837.
- Santovito, E., Mascia, T., Siddiqui, S. A., Minutillo, S. A., Valkonen, J. P. T., and Gallitelli, D. 2014. Infection cycle of *Artichoke Italian latent virus* in tobacco plants: Meristem invasion and recovery from disease symptoms. *PLoS One* 9:e99446.
- Schmitt-Keichinger, C., Hemmer, C., Berthold, F., and Ritzenthaler, C. 2017. Molecular, cellular, and structural biology of grapevine fanleaf virus. Pages 83-107 in: *Grapevine Viruses: Molecular Biology, Diagnostics, and Management*. B. Meng, G. P. Martelli, D. A. Golino, and M. Fuchs, eds. Springer International Publishing, Cham.
- Scholthof, H. B., Alvarado, V. Y., Vega-Arreguin, J. C., Ciomperlik, J., Odokonyero, D., Brosseau, C., Jaubert, M., Zamora, A., and Moffett, P. 2011. Identification of an ARGONAUTE for antiviral RNA silencing in *Nicotiana benthamiana*. *Plant Physiol.* 156:1548-1555.
- Senshu, H., Yamaji, Y., Minato, N., Shiraishi, T., Maejima, K., Hashimoto, M., Miura, C., Neriya, Y., and Namba, S. 2011. A dual strategy for the suppression of host antiviral silencing: Two distinct suppressors for viral replication and viral movement encoded by potato virus M. *J. Virol.* 85:10269-10278.
- Shimura, H., Masuta, C., Yoshida, N., Sueda, K., and Suzuki, M. 2013. The 2b protein of *Asparagus virus 2* functions as an RNA silencing suppressor against systemic silencing to prove functional synteny with related cucumoviruses. *Virology* 442:180-188.
- Stavolone, L., Prigigallo, M. I., and Cillo, F. 2020. Plant viruses against RNA silencing-based defenses: Strategies and solutions. Pages 225-250 in: *Applied plant biotechnology for improving resistance to biotic stress*. P. Poltronieri and Y. Hong, eds. Academic Press, London.
- Stewart, L. R., Jarugula, S., Zhao, Y., Qu, F., and Marty, D. 2017. Identification of a maize chlorotic dwarf virus silencing suppressor protein. *Virology* 504:88-95.
- Thompson, J. R. 2020. Secoviruses (*Secoviridae*). Pages 692-702 in: *Encyclopedia of Virology*, D. H. Bamford and M. Zuckerman, eds. Academic Press, London.
- Várallyay, E., Válóczy, A., Agyi, A., Burgyán, J., and Havelda, Z. 2010. Plant virus-mediated induction of miR168 is associated with repression of ARGONAUTE1 accumulation. *EMBO J.* 29:3507-3519.
- Vigne, E., Gottula, J., Schmitt-Keichinger, C., Komar, V., Ackerer, L., Belval, L., Rakotomalala, L., Lemaire, O., Ritzenthaler, C., and Fuchs, M. 2013. A strain-specific segment of the RNA-dependent RNA polymerase of grapevine fanleaf virus determines symptoms in *Nicotiana* species. *J. Gen. Virol.* 94:2803-2813.
- Voynet, O., and Baulcombe, D. C. 1997. Systemic signalling in gene silencing. *Nature* 389:553.
- Wesley, S. V., Helliwell, C., Wang, M. B., and Waterhouse, P. 2004. Posttranscriptional gene silencing in plants. *Methods Mol. Biol.* 265:117-129.
- Wetzel, T., Chisholm, J., Bassler, A., and Sanfaçon, H. 2008. Characterization of proteinase cleavage sites in the N-terminal region of the RNA1-encoded polyprotein from *Arabidopsis mosaic virus* (subgroup A nepovirus). *Virology* 375:159-169.
- Yaegashi, H., Takahashi, T., Isogai, M., Kobori, T., Ohki, S., and Yoshikawa, N. 2007a. Apple chlorotic leaf spot virus 50 kDa movement protein acts as a suppressor of systemic silencing without interfering with local silencing in *Nicotiana benthamiana*. *J. Gen. Virol.* 88:316-324.
- Yaegashi, H., Tamura, A., Isogai, M., and Yoshikawa, N. 2008. Inhibition of long-distance movement of RNA silencing signals in *Nicotiana benthamiana* by apple chlorotic leaf spot virus 50 kDa movement protein. *Virology* 382:199-206.
- Yaegashi, H., Yamatsuta, T., Takahashi, T., Li, C., Isogai, M., Kobori, T., Ohki, S., and Yoshikawa, N. 2007b. Characterization of virus-induced gene silencing in tobacco plants infected with apple latent spherical virus. *Arch. Virol.* 152:1839-1849.
- Zhang, X., Du, P., Lu, L., Xiao, Q., Wang, W., Cao, X., Ren, B., Wei, C., and Li, Y. 2008. Contrasting effects of HC-Pro and 2b viral suppressors from *Sugarcane mosaic virus* and *Tomato aspermy cucumovirus* on the accumulation of siRNAs. *Virology* 374:351-360.

VdTps2 Modulates Plant Colonization and Symptom Development in *Verticillium dahliae*

Luyao Xiao,¹ Chen Tang,¹ Steven J. Klosterman,² and Yonglin Wang^{1,†} 

¹ State Key Laboratory of Efficient Production of Forest Resources, Beijing Key Laboratory for Forest Pest Control, College of Forestry, Beijing Forestry University, Beijing, China

² United States Department of Agriculture, Agricultural Research Service, Salinas, U.S.A.

Accepted for publication 27 March 2023.

The trehalose biosynthesis pathway is a potential target for anti-fungal drugs development. Trehalose phosphate synthase (TPS) and phosphatase are widely conserved components of trehalose biosynthesis in fungi. However, the role of trehalose biosynthesis in the vascular plant-pathogenic fungus *Verticillium dahliae* remains unclear. Here, we investigated the functions of the TPS complex, including VdTps1, VdTps2, and VdTps3 in *V. dahliae*. Unlike VdTps2, deletion of VdTps1 or VdTps3 did not alter any phenotypes compared with the wild-type strain. In contrast, the Δ VdTps2 strain showed severely depressed radial growth due to the abnormal swelling of the hyphal tips. Further, deletion of VdTps2 increased microsclerotia formation, melanin biosynthesis, and resistance to cell-wall perturbation and high-temperature stress. Virulence assays and quantification of fungal biomass revealed that deletion of VdTps2 delayed disease symptom development, as evident by the reduced virulence and decreased biomass of the Δ VdTps2 strain in plant stem tissue following inoculation. Additionally, increases in penetration peg formation observed in the Δ VdTps2 strain in the presence of H₂O₂ suggested that VdTps2 suppresses initial colonization. Our results also revealed the role of VdTps2 as a regulator of autophagy. Together, these results indicate that VdTps2 contributes to plant colonization and disease development.

Keywords: melanized microsclerotia, penetration peg, ROS stress, *Verticillium dahliae*, virulence

Trehalose is a nonreducing disaccharide that consists of two glucose units that are linked in an α , α -1,1-glycosidic linkage (Elbein et al. 2003). Trehalose plays a major role in cellular protection against desiccation, dehydration, and temperature stresses. The trehalose biosynthesis pathway widely exists in fungi but not in humans (Elbein et al. 2003; Thammahong et al. 2017). Thus, this pathway has been considered a promising target for developing broad-spectrum fungicides that may not have any harmful impacts on humans (Chen et al. 2020; Thammahong

et al. 2017). The components of trehalose phosphate synthase/trehalose phosphate phosphatase (TPS/TPP) pathway are currently well-described in fungi. In *Saccharomyces cerevisiae*, trehalose synthase is composed of four subunits, including the trehalose-6-phosphate (T6P) synthase Tps1, the T6P phosphatase Tps2, and two regulatory proteins, Tps3 and Tsl1. Tps1 catalyzes formation of T6P from the substrates UDP-glucose and glucose-6-phosphate (G6P). T6P is dephosphorylated by Tps2 to produce trehalose (Bell et al. 1992; De Virgilio et al. 1993). Additionally, Tps1 and Tps2 regulate other biological processes such as autophagy (Kim et al. 2021).

Analyses of the roles of the trehalose biosynthesis machinery have previously revealed the importance of the TPS complex in the virulence of some pathogenic fungi. In filamentous fungal pathogens such as *Magnaporthe oryzae*, there are only three TPS complex subunits, including Tps1, Tps2, and Tps3 (Wilson et al. 2007). In *M. oryzae*, Δ MoTps1 and Δ MoTps2 strains showed attenuated virulence resulting from a defect in the development of the infection structure (Chen et al. 2021; Foster et al. 2003). MoTps3 was important for the activation of MoTps1 and was also involved in virulence (Wilson et al. 2007). In the wheat head blight pathogen *Fusarium graminearum*, FgTps1 and FgTps2 affected mycotoxin production and pathogenicity and FgTps2 has been considered as a new pesticide target (Song et al. 2014; Xu et al. 2021). Deletion of Tps2 caused a significant defect in dissemination of the animal pathogen *Candida albicans* within the host (Van Dijck et al. 2002; Zaragoza et al. 2002). Thus, the TPS complex plays important roles in host-pathogen interactions.

Vascular wilt disease caused by *Verticillium dahliae* affects more than 400 dicotyledonous plant species worldwide, leading to substantial economic losses of crops and ornamental plants (Klosterman et al. 2009). In China, *V. dahliae* is not only a major threat to various crops but also causes severe devastation to stands of ornamental woody plants, such as reported on smoke trees (*Cotinus coggygria*) within the Xiangshan Park in Beijing (Wang et al. 2013). *V. dahliae* is a soilborne fungus and forms melanized resting structures known as microsclerotia, and these structures may remain viable in the soil for up to 14 years without a suitable host (Fradin and Thomma 2006; Inderbitzin et al. 2011b; Klosterman et al. 2009; Santhanam and Thomma 2013; Wilhelm 1955). Melanin, 8-dihydroxy naphthalene melanin (DHN-melanin), is deposited during microsclerotia development, and this has a major effect in the protection of *V. dahliae* from various stress including UV irradiation, elevated temperature extremes, enzymatic lysis, and fungicidal activities (Bell and Wheeler 1986; Wang et al. 2018; Wheeler 1982; Xiong et al. 2014). The microsclerotia germinate to form infectious hyphae that adhere to the root surfaces and invade via hyphopodia (Fradin and Thomma 2006; Klosterman et al. 2009; Zhao et al.

[†]Corresponding author: Y. Wang; ylwang@bjfu.edu.cn

L. Xiao and C. Tang contributed equally to this work.

Funding: This research was supported by the National Natural Science Foundation of China (grant 31971657).

e-Xtra: Supplementary material is available online.

The author(s) declare no conflict of interest.



Copyright © 2023 The Author(s). This is an open access article distributed under the CC BY-NC-ND 4.0 International license.

2014). After successful invasion, *V. dahliae* produces conidia that spread within the sap stream inside the vascular tissue of the host plant, leading to chlorosis, necrosis, stunted growth, and wilting (Inderbitzin et al. 2011a; Klosterman et al. 2009; Sink and Grey 1999).

Considering the roles of the TPS complex in pathogenicity of other fungi (Chen et al. 2021; Foster et al. 2003), genetic analyses of the TPS complex in *V. dahliae* may yield additional insight into the regulation of pathogenicity in *V. dahliae*. Herein, we identified component members of the TPS complex in *V. dahliae*, including *VdTps1*, *VdTps2*, and *VdTps3*, and demonstrated the involvement of *VdTps2* in pathogenesis. The $\Delta VdTps2$ strain depressed vegetative growth as well as conidia production and delayed disease symptom development but increased microsclerotia formation, melanin biosynthesis, and stress resistance. *VdTps2* affects pathogenicity by inhibiting the formation of infection structures and increasing its dissemination in the plant vascular tissue.

Results

VdTps2 mutants exhibit morphological defects.

To identify components of the TPS complex in *V. dahliae*, three TPS-encoding genes *VdTps1* (VDAG_02853), *VdTps2* (VDAG_02281), and *VdTps3* (VDAG_03989) were identified by BLASTP search using the amino acid (aa) sequence of *MoTps1*, *MoTps2*, and *MoTps3*, respectively (Chen et al. 2021), and the genome of strain VdLs.17 of *V. dahliae* (Klosterman et al. 2011). *VdTps1*, *VdTps2*, and *VdTps3* encoded predicted proteins of 525, 974, and 911 aa, and a Glyco_transf_20 domain, a PRK14501 superfamily domain, and two domains of the GT20_TPS and OtsB superfamily, respectively (Supplementary Fig. S1). Phylogenetic analysis demonstrated that the TPS complex was conserved in filamentous fungi (Supplementary Fig. S1). To determine the functions of these TPS genes in *V. dahliae*, three independent deletion mutants were obtained

for each gene using *Agrobacterium tumefaciens*-mediated transformation and verified by PCR (Supplementary Fig. S2A and B). Mutants were complemented by the introduction of the wild-type copies of *VdTps1*, *VdTps2*, and *VdTps3* into the respective mutant strains (Supplementary Fig. S2C, D, and E).

To determine the roles of *VdTps1*, *VdTps2*, and *VdTps3* in vegetative growth, radial growth of the wild-type strain XS11, mutants, and complemented strains was recorded from 3 to 12 days postinoculation (dpi) on potato dextrose agar (PDA) plates at 25°C. The $\Delta VdTps1$ and $\Delta VdTps3$ strains showed similar radial growth to the XS11 strain on PDA, while the radial growth of the $\Delta VdTps2$ strain was significantly reduced compared with that of the XS11 strain (Fig. 1A and B). Considering the relationship between the TPS complex and trehalose biosynthesis, the content of trehalose in all strains was measured. The $\Delta VdTps1$ and $\Delta VdTps3$ strains exhibited no differences with the XS11 strain, while the content of trehalose of the $\Delta VdTps2$ strain was depressed by 50% that of the XS11 strain (Supplementary Fig. S3A). We further tested the content of T6P in XS11, $\Delta VdTps2$, and complemented strains. The result showed that the content of T6P in the $\Delta VdTps2$ was more than 20 times that of the XS11 (Supplementary Fig. S3B). We speculated that the reduced radial growth after *VdTps2* deletion was due to the decrease in trehalose synthesis. However, the use of exogenous trehalose as the sole carbon source did not relieve the growth defects of the $\Delta VdTps2$ strain (Supplementary Fig. S3C and D). These results indicated that *VdTps2* is involved in radial growth but this is not attributable to trehalose content. In *V. dahliae*, the abnormal swelling of hyphal tips led to defects in radial growth (Tian et al. 2017). Thus, we observed the hyphal tips in all strains on glass slides covered with PDA. The $\Delta VdTps1$ and $\Delta VdTps3$ strains showed normal hyphal morphology like the XS11 strain and all the complemented strains, but the hyphal tips of the $\Delta VdTps2$ strain showed abnormal swelling (Fig. 1C). This result suggested that deletion of *VdTps2* caused the abnormal swelling of the hyphae, which probably led to the observed growth defect.

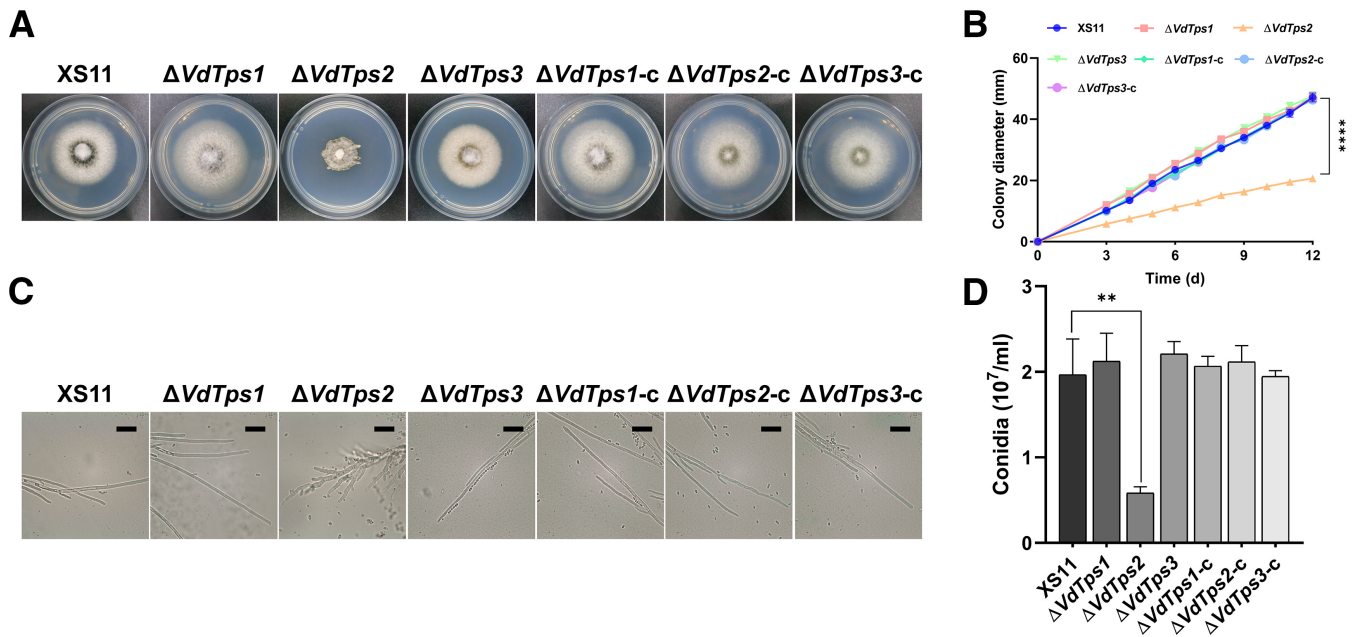


Fig. 1. *VdTps2* regulates growth and conidia production in *Verticillium dahliae*. **A**, Deletion of *VdTps2* inhibits the radial growth of *V. dahliae*. The wild type XS11, $\Delta VdTps1$, $\Delta VdTps2$, and $\Delta VdTps3$ strains were cultured on PDA plates at 25°C for 10 days. **B**, The diameter of the colonies of all strains cultured on PDA plates measured at 3 to 12 dpi. Asterisk indicates a significant difference according to Student's *t*-test between the XS11 strain and $\Delta VdTps2$ strain at 12 dpi, $P < 0.0001$ (****). **C**, All strains were cultured on glass slides dipped on PDA at 25°C for 7 days and photographed under microscopy. Scale bar = 10 μ m. **D**, The number of conidia of all strains was calculated using a hemocytometer to obtain conidia counts of equivalent volumes. Error bars represent the standard deviation based on at least three independent biological replicates. Asterisks indicate a significant difference according to Student's *t*-test, $P < 0.01$ (**).

Statistical analysis of conidia production indicated that the number of conidia of the $\Delta VdTps2$ strain decreased almost threefold compared with that of the XS11 strain, while deletion of *VdTps1* and *VdTps3* did not impact conidia production in *V. dahliae* (Fig. 1D). The conidia production of all the complemented strains was similar to that of the XS11 strain (Fig. 1D). Taken together the results revealed that *VdTps2*, but not *VdTps1* or *VdTps3*, regulates radial growth, trehalose biosynthesis, and conidia production in *V. dahliae*.

Deletion of *VdTps2* promotes microsclerotia formation and melanin biosynthesis in *V. dahliae*.

The microsclerotia of *V. dahliae* are survival structures resistant to environmental extremes (Hall and Ly 1972; Heale and Isaac 1965; Wang et al. 2018). To determine the roles of the TPS complex in microsclerotia formation, we incubated the XS11 strain, the three mutants, and the complemented strains on glass slides covered with basal medium (BM). The density of melanized microsclerotia of the $\Delta VdTps2$ strain was significantly higher than that of the XS11 strain (Fig. 2A and B). The other two mutants and the complemented strains showed no obvious differences in numbers of melanized microsclerotia compared with the XS11 strain. For further examination, the conidial suspensions of all strains were uniformly spread over BM plates with pre-covered cellulose membranes, respectively. Consistent with the melanin quantification, the $\Delta VdTps2$ strain formed more melanized microsclerotia than the XS11 strain (Fig. 2C). These results indicated that *VdTps2* negatively regulates microsclerotia formation.

Melanin deposition is tightly coupled with microsclerotia development (Fang et al. 2019). To study the roles of *VdTps2* in melanin biosynthesis, we examined melanin deposition of microsclerotia using cellulose membranes overlaid on BM plates. All strains formed melanized microsclerotia at 7 dpi. However, the $\Delta VdTps2$ exhibited increased melanin deposition when compared with the XS11 strain (Fig. 2D). We further examined the relative expression of key genes involved in the DHN-melanin biosynthesis pathway of *V. dahliae* (Wang et al. 2018). Deletion of *VdTps2* resulted in the upregulation of melanin biosynthesis gene expression levels (Fig. 2E). These results showed that the deletion of $\Delta VdTps2$ enhanced melanin biosynthesis.

***VdTps2* regulates the resistance to cell-wall perturbation and high-temperature stresses in *V. dahliae*.**

Since melanin is involved in cell-wall integrity in fungi (Howard and Valent 1996), the resistance to cell-wall stresses of $\Delta VdTps$ deletion strains were tested using Calcofluor-white (CFW) and Congo red (CR), which are known agents that perturb the cell wall. On CFW- or CR-containing media, the $\Delta VdTps2$ strain exhibited lower (approximately 66 and 80%, respectively) inhibition rates than the XS11 strain (Fig. 3A and B). The sensitivities of the $\Delta VdTps1$ and $\Delta VdTps3$ strains were similar compared with those of XS11 and the complemented strains (Fig. 3A and B).

Melanin plays a critical role in the resistance to high-temperature stress in *V. dahliae* (Wang et al. 2018). Thus, we analyzed the effects of the TPS complex on response to high-temperature stresses in *V. dahliae*. The growth of all strains was strongly decreased under high-temperature stress, especially at 30°C, and the growth inhibition rates of the $\Delta VdTps1$ and $\Delta VdTps3$ strains were similar to that of the XS11 strain at 28 and 30°C (Fig. 3C and D). However, the resistance of the $\Delta VdTps2$ strain was significantly stronger than that of the XS11 strain under high-temperature stress (Fig. 3C and D). The sensitivity of all the complemented strains was similar to that of the XS11 strain. These results indicated that *VdTps2* regulates the resistance to high-temperature stresses in *V. dahliae*.

***VdTps2* is involved in pathogenesis in *V. dahliae*.**

To determine the relevance of *VdTps1*, *VdTps2*, and *VdTps3* in pathogenicity, tobacco seedlings were inoculated XS11, the three *VdTps* deletion mutants, and the complemented strains. Deletion of *VdTps1* and *VdTps3* did not affect the virulence of *V. dahliae* (Fig. 4A to F). However, the deletion of *VdTps2* strongly delayed disease symptom development (Fig. 4A to F). At 30 dpi, all plants showed severe wilt symptoms except for the plants inoculated with the $\Delta VdTps2$ strain and the negative controls (Fig. 4A and D). At 40 dpi, the mortality rate of plants inoculated with the $\Delta VdTps2$ strain was significantly lower than that inoculated with the XS11 strain (Fig. 4B and E). The tobacco seedlings inoculated with the $\Delta VdTps2$ strain died at 50 dpi (Fig. 4C and F). These results indicated that deletion of *VdTps2* delayed disease symptom development but did not affect the overall virulence of *V. dahliae*.

To further study the reason for the delayed disease symptom development, we cultured XS11 and all *VdTps* mutants and complemented strains on onion epidermal tissue, to gain insights on plant penetration. The $\Delta VdTps2$, $\Delta VdTps1$, $\Delta VdTps3$ strains successfully penetrated the onion epidermis at 36 h postincubation (hpi), similar to the penetration observed at 36 hpi for XS11 and complemented strains (Supplementary Fig. S4A). In addition, the conidial adhesion was tested by washing the Hybond-N⁺ membrane that was uniformly sprayed with the conidia and incubated on PDA plates for 18 h. The ability of all strains to adhere on the membrane was similar (Supplementary Fig. S4B). We next quantified fungal biomass by quantitative PCR (qPCR) in plants inoculated with conidia at different timepoints to compare the colonization of all strains. As anticipated, the fungal biomass of the $\Delta VdTps2$ strain in the stem of the plants was reduced relative to XS11 at 25 dpi but was not different at 50 dpi compared with that of XS11 (Fig. 4G and H). These results suggested that the $\Delta VdTps2$ strain failed to normally spread in the vascular tissue of hosts like XS11, leading to delayed disease symptom development. It is noteworthy that the fungal biomass of the $\Delta VdTps2$ strain in plant roots at 36 hpi was significantly higher than that of the XS11 strain (Fig. 4I). The fungal biomass of all strains except the $\Delta VdTps2$ strain showed no obvious differences with that of the XS11 strain at 25 dpi, 50 dpi, and 36 hpi (Fig. 4G, H, and I).

***VdTps2* promotes reactive oxygen species (ROS) resistance and penetration peg formation.**

ROS, like hydrogen peroxide (H₂O₂), produced by plants during the plant-pathogen interactions play crucial roles in the resistance to *V. dahliae* (Jia et al. 2007). To further determine the roles of *VdTps2* in the infection, we examined whether *VdTps2* is necessary for the resistance to H₂O₂. The XS11, $\Delta VdTps2$, and complemented strains were grown on PDA plates and PDA supplemented with various concentrations of H₂O₂. The colony diameters of all strains on PDA supplemented with H₂O₂ were significantly suppressed, but the inhibition rate of the $\Delta VdTps2$ strain was reduced 14 and 47% compared with that of the XS11 strain at concentrations of 7.5 and 10 mM H₂O₂, respectively (Fig. 5A and B). We also tested the content of H₂O₂ in hyphae of the XS11, $\Delta VdTps2$, and the complemented strains. The content of H₂O₂ in the hyphae of the $\Delta VdTps2$ strain was reduced 48% compared with that of the XS11 strain and the *VdTps2* complemented strain (Fig. 5C). The results indicated the $\Delta VdTps2$ strain is resistant to H₂O₂ stress and *VdTps2* promotes the neutralization of exogenous H₂O₂.

To further study the roles of enhanced ROS resistance of the $\Delta VdTps2$ strain in infection, XS11, $\Delta VdTps2$, and complemented strains were cultured on minimal medium (MM) and MM with various concentrations of H₂O₂. The plates were also overlaid with a cellophane membrane to examine penetra-

tion. We found that all strains successfully penetrated the cellophane membrane at 3 dpi regardless of the H₂O₂ concentration (Fig. 5D). Further, the number of penetration pegs formed by the $\Delta VdTps2$ strain was similar to that of XS11 and complemented strains without H₂O₂ treatment (Fig. 5E). However, the number of penetration pegs of the $\Delta VdTps2$ strain was

1.46 and 1.50 times higher than that of the XS11 strain in the presence of 0.5 or 1.0 mM H₂O₂, respectively (Fig. 5E). The $VdTps2$ -complemented strain was similar to XS11 in numbers of penetration pegs, under all concentrations of H₂O₂ examined. These results indicated that H₂O₂ reduces formation of penetration pegs in *V. dahliae* and $VdTps2$ controls

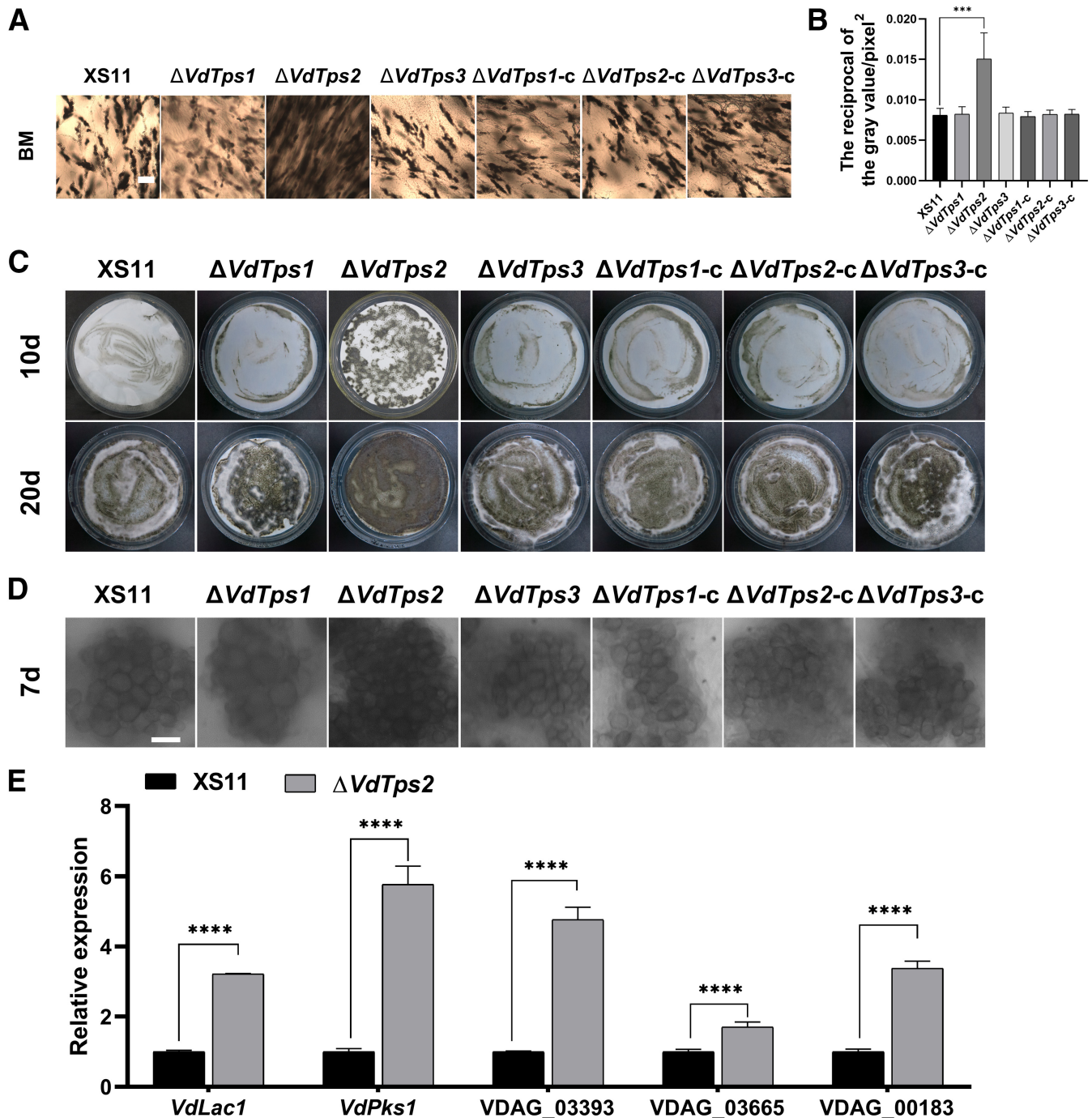


Fig. 2. Assays for microsclerotia formation and melanin biosynthesis of *VdTps* mutant strains of *Verticillium dahliae*. **A**, The wild-type XS11, and mutant strains $\Delta VdTps1$, $\Delta VdTps2$, and $\Delta VdTps3$ were cultured on glass slides coated with BM at 25°C for 7 days and photographed with a microscope. Scale bar = 10 μ m. **B**, Melanin deposition of microsclerotia of all strains cultured on BM for 7 days was measured by ImageJ. The reciprocal of grayscale value/pixel² represents the density of melanized microsclerotia. Error bars represent the standard deviation based on at least three independent biological replicates. Asterisks indicate a significant difference according to Student's *t*-test, $P < 0.001$ (***). **C**, Conidia (10^6 /ml) of all strains were spread on BM plates pre-covered with cellulose membrane and cultured at 25°C. Photographs were taken after 10 days and 20 days. **D**, Microscopic observations of melanin deposition of microsclerotia in all strains after 7 days. Scale bar = 20 μ m. **E**, Relative expression analysis of melanin-related genes in the XS11 strain and the $\Delta VdTps2$ strain by reverse transcription-quantitative PCR. All samples were collected 10 days after incubation in liquid BM at 25°C. The β -tubulin gene was used as an internal reference. Error bars indicate standard deviation derived from three independent experiments consisting of three replicates each. Asterisks indicate significant differences according to Student's *t*-test, $P < 0.0001$ (****).

penetration peg formation via the regulation of the oxidative resistance.

***VdTps2* is involved in autophagy in *V. dahliae*.**

In the budding yeast, loss of *Tps2* results in the decrease of *Atg8* expression and impaired autophagic flux under nitrogen starvation (Kim et al. 2021). Given that autophagy is involved in plant colonization and melanin biosynthesis of *V. dahliae* (Fang et al. 2019; Zhou et al. 2013), we introduced an autophagy marker fusion gene *VdAtg8-GFP* into both the $\Delta VdTps2$ strain and the XS11 strain to analyze autophagic flux by epifluorescence microscopy. When grown in liquid complete medium (CM), the strong punctate *VdAtg8-GFP* green fluorescence was observed within the hyphal cytoplasm of XS11 and $\Delta VdTps2$ strains (Fig. 6A). When starved for nitrogen in MM minus nitrogen (MM-N) for 6 h, the *VdAtg8-GFP* green fluorescence of the XS11 strain appeared as faint punctate structures in the cytosol, but strongly green, fluorescent punctate structures were detected in the $\Delta VdTps2$ strain (Fig. 6A). At 12 h, the punctate green structures were undetectable in the cytosol and all fluorescence was detected inside the vacuoles in the XS11 strain (Fig. 6A). However, in the $\Delta VdTps2$ strain, the punctate green structures were detected in the cytosol (Fig. 6A). Quantification of *VdAtg8-GFP* localization and fluorescence intensity at different timepoints showed that the degradation of *VdAtg8* was reduced in the $\Delta VdTps2$ strain (Fig. 6B and C). These results suggest that *VdTps2* is involved in the regulation of autophagy and the deletion of *VdTps2* inhibits the degradation of *VdAtg8* in *V. dahliae*.

Discussion

In this study, we identified three TPS subunits in *V. dahliae* and found that deletion of *VdTps1* and *VdTps3* did not influence morphogenesis, microsclerotia formation, stress responses, or virulence in *V. dahliae*. However, *VdTps2* is involved in morphogenesis, impacts resistance to stresses, and negatively regulates microsclerotia formation as well as melanin biosynthesis. Additionally, the deletion of *VdTps2* delayed disease symptom development, probably via reduced growth and conidia production but did not impact the overall virulence of *V. dahliae*. *VdTps2* also inhibits penetration peg formation by regulating the neutralization of excess H_2O_2 . Finally, *VdTps2* is a positive regulator of autophagy in *V. dahliae*. We concluded that *VdTps2* modulates virulence by regulating the balance of growth and stress resistance in *V. dahliae*.

Tps2 affects hyphal morphogenesis in multiple fungi, potentially providing insight into *VdTps2* function. For example, in *F. graminearum*, deletion of *FgTps2* depressed fungal radial growth due to altered cell polarity and the hyphae of the mutant strain were thick, hyperbranched, and swollen (Song et al. 2014). Loss of *MoTps2* resulted in excessive cell-wall polymer deposition at the hyphal tips and consequently altered hyphal morphology and radial growth in *M. oryzae* (Chen et al. 2021). Herein, deletion of *VdTps2* in *V. dahliae* also reduced colony diameter and the $\Delta VdTps2$ strain exhibited swollen hyphae (Fig. 1C). Interestingly, the $\Delta VdMsn2$ deletion strain displayed similar hyphal morphology, leading to depressed radial growth (Tian et al. 2017). Regardless of a potential functional linkage between in *VdMsn2* and *VdTps2*, the depressed growth of the $\Delta VdTps2$

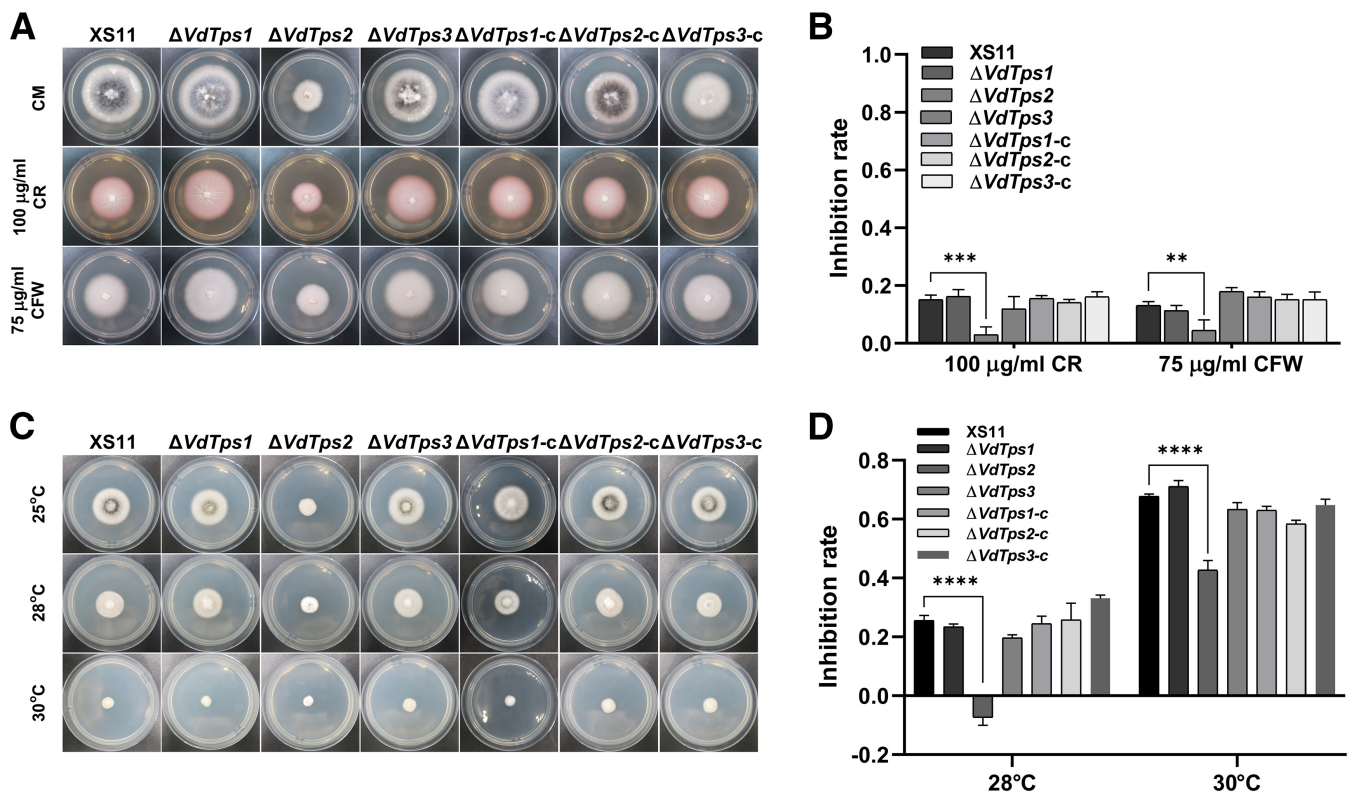


Fig. 3. Effect of the TPS complex deletion on the cell-wall integrity and resistance to high-temperature stress in *Verticillium dahliae*. **A**, The wild-type XS11, and mutant strains $\Delta VdTps1$, $\Delta VdTps2$, and $\Delta VdTps3$ were cultured on complete media (CM), CM with 100 µg/ml Congo red (CR) and CM with 75 µg/ml calcofluor-white (CFW) at 25°C for 10 days. **B**, Graph showing the inhibition rates of all strains incubated with different agents that perturb the cell-wall perturbation. Error bars represent the standard deviation based on at least three independent biological replicates. Asterisks indicate significant differences according to Student's *t*-test, $P < 0.01$ (**), $P < 0.001$ (***). **C**, All strains were cultured on PDA plates at 25, 28 and 30°C for 7 days. **D**, Graph showing the inhibition rates of all strains cultured at different temperatures. Error bars represent the standard deviation based on at least three independent biological replicates. Asterisks indicate significant differences according to Student's *t*-test, $P < 0.0001$ (****).

strain is likely caused by abnormal hyphal tip swelling. T6P level has been shown to affect morphogenesis (Chary et al. 2008). In *M. oryzae*, elevated intracellular T6P levels in a $\Delta MoTps2$ strain led to defects in cellular morphogenesis. Herein, our results showed that T6P accumulated in the cells of the $\Delta VdTps2$ strain (Supplementary Fig. S3B), but we did not investigate whether T6P level affects cell morphogenesis in *V. dahliae*.

Previous studies indicated that *Tps2* mediates several cellular stress responses. Deletion of *Tps2* impaired cell-wall integrity by disrupting cell-wall assembly and chitin biosynthesis in some pathogens, such as *M. oryzae*, *F. graminearum*, and *Aspergillus fumigatus* (Chen et al. 2021; Puttikamonkul et al. 2010; Song et al. 2014). *Tps2* also has a positive effect on fungal resistance to high temperatures by accumulating trehalose (Thammahong et al. 2017). For instance, *UmTps2* promoted resistance to heat stress by regulating trehalose accumulation in *Ustilago maydis* (Salmerón-Santiago et al. 2011). In *Candida albicans*, the *Tps2* deletion strain was unable to grow at elevated temperatures (Miao et al. 2016). However, the deletion of *VdTps2* enhanced resistance to cell-wall perturbations and high-temperature stress in *V. dahliae*, which is contrary to the roles of *Tps2* (and its orthologues) in these above-named fungi. We speculate that the observed resistance to stress is attributed to the increased production of melanized microsclerotia in the $\Delta VdTps2$ strain.

In *V. dahliae*, melanin protects against various stresses and as is evident in the analyses of strains defective in the melanin biosynthesis pathway (Gordee and Porter 1961; Griffiths 1970). *VdCmr1* affects the survival of *V. dahliae* in response to high-temperature stress via regulation of melanogenesis (Fang et al. 2019; Wang et al. 2018). Hyphae and conidia can be killed after heat treatment at 47°C for 5 min, but higher temperatures and more time are required to kill the melanized microsclerotia (Hawke and Lazarovits 1994). Additionally, melanin is implicated in the maintenance of cell-wall structure (Howard and Valent 1996). In *A. fumigatus*, melanin is an essential component for the correct assembly of the cell walls in conidia (Pihet et al. 2009). In *Colletotrichum graminicola*, melanin enhanced cell-wall rigidity, despite it not being necessary for turgor generation (Ludwig et al. 2014). In *V. dahliae*, melanin is deposited in the cell wall of microsclerotia that thickens with microsclerotia development (Fang et al. 2019). Thus, melanin might be involved in the resistance to high temperature and cell-wall perturbations. The $\Delta VdTps2$ strain showed enhanced transcription levels of genes related to melanin biosynthesis compared with the XS11 strain (Fig. 2D). These results supported the hypothesis that *VdTps2* restrains resistance to cell-wall perturbations and high-temperature stress via inhibiting melanin biosynthesis in *V. dahliae*. Further study is required to examine the mechanism by which *VdTps2* inhibits melanin biosynthesis.

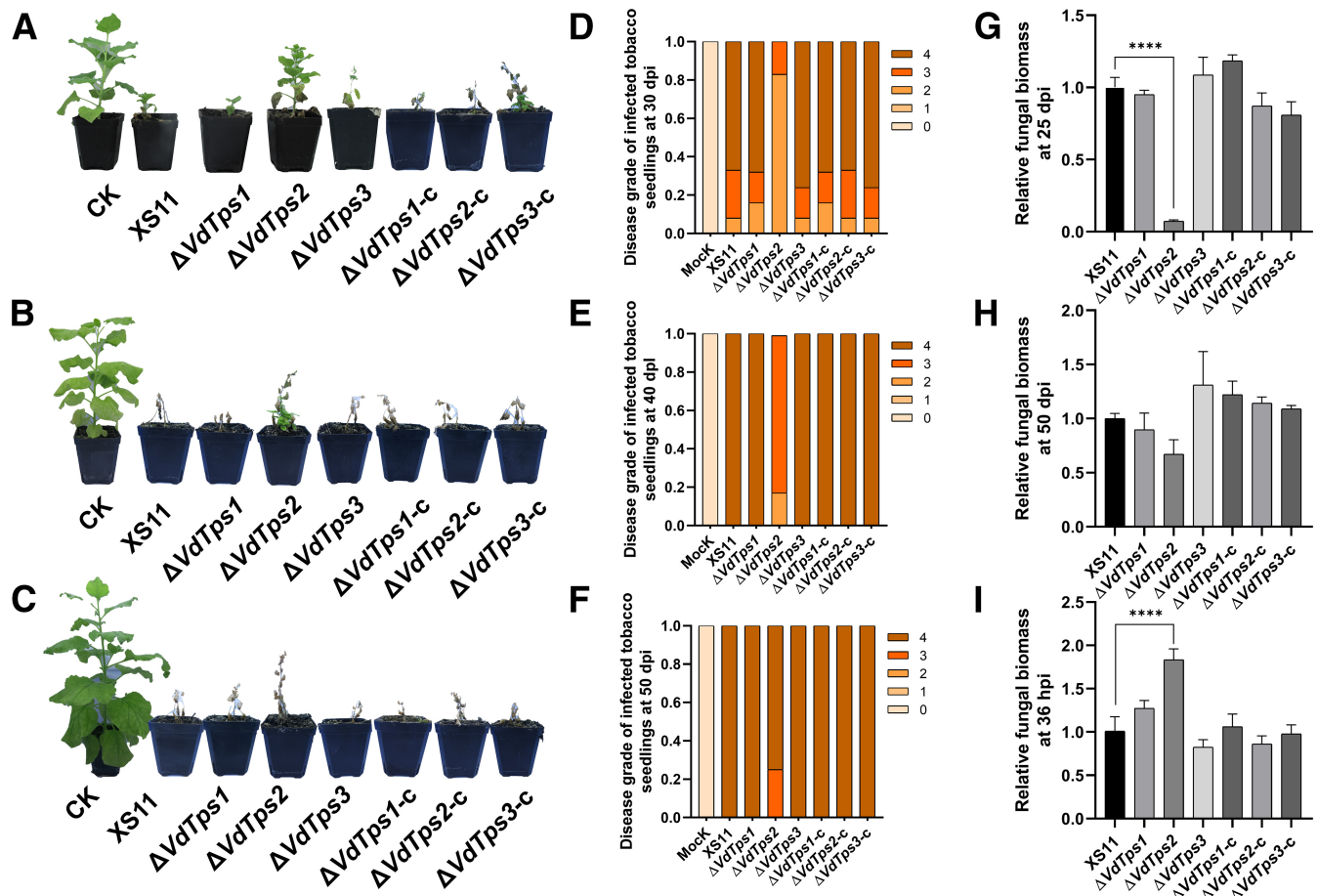


Fig. 4. Pathogenicity tests of *VdTps* mutant strains of *Verticillium dahliae*. **A to C**, Twelve 1-month-old tobacco seedlings (*Nicotiana benthamiana*) were used for virulence assays, and the assays were repeated at least 3 times. Plant roots were dipped in conidial suspensions (10^6 conidia/ml) of the wild-type XS11, and mutant strains $\Delta VdTps1$, $\Delta VdTps2$, and $\Delta VdTps3$ for 10 mins and replanted into sterilized soil at 25°C. Controls were mock-inoculated with sterile water. Disease symptoms of tobacco seedlings inoculated with different pathogens or control were photographed at 30 dpi, 40 dpi and 50 dpi. **D to F**, Disease indices on tobacco seedlings were scored visually on four levels from 0 to 4 according to the ratio of symptomatic leaves and total leaves, where 0 represents the host has no symptom, 1 represents 1 to 33%, 2 represents 34 to 50%, 3 represents 51 to 67%, and 4 represents 68 to 100%. **G to I**, Three tobacco seedling roots or stems of per treatment group were used for DNA extraction for quantification of fungal biomass at 25 dpi, 50 dpi, and 36 hpi. Error bars represent the standard deviation based on at least three independent biological replicates. Asterisks indicate significant differences according to Student's *t*-test, $P < 0.0001$ (****).

Tps2 has important roles in host-pathogen interactions and virulence in filamentous fungal pathogens like *M. oryzae*, *F. graminearum*, and *C. albicans* (Chen et al. 2021; Foster et al. 2003; Song et al. 2014; Van Dijck et al. 2002; Xu et al. 2021; Zaragoza et al. 2002). In this study, the deletion of *VdTps2* delayed disease symptom development but did not affect the overall virulence of *V. dahliae*. There are many factors affecting the virulence of *V. dahliae*. Conidia produced by *V. dahliae* spread within xylem fluid inside the vascular tissue of plant hosts, causing systemic infection (Inderbitzin et al. 2011b; Klosterman et al. 2009). Excess germinating conidia may plug the transpiration stream and disturb nutrient and water transport to the plant, resulting in disease symptoms (Carroll et al. 2018; Fradin and Thomma 2006; Klosterman et al. 2009; Zhang et al. 2022). Virulence of the $\Delta VdVell$ deletion strain was decreased due to reductions in the numbers of conidia, and the knockout of *VdSkn7* exhibited a virulence defect due to reduced penetration capability and conidiation (Höfer et al. 2021). Additionally, the development of

disease symptoms may be accompanied by an increase in fungal biomass. For example, *VdPKS9* promotes virulence via the regulation of hyphal growth in *V. dahliae* (Li et al. 2022). Herein, the growth rate and conidia production were both reduced after deleting *VdTps2*, and the fungal biomass was decreased in plants inoculated with the $\Delta VdTps2$ strain at 25 dpi (Figs. 1 and 4G). Therefore, we speculate that *VdTps2* might regulate virulence by affecting colonization in the plant vascular tissue by regulation of hyphal growth and conidia production. The increase of fungal biomass of the $\Delta VdTps2$ strain in hosts may be explained by the enhanced ability of the $\Delta VdTps2$ strain to eliminate H_2O_2 (Fig. 5A and B). Presumably, this effect contributes to the $\Delta VdTps2$ strain overcoming plant immune response to promote fungal biomass accumulation in hosts.

Paradoxically, the fungal biomass of the $\Delta VdTps2$ strain in the roots of plants was significantly higher than that of the XS11 strain at 36 hpi (Fig. 4I). For successful colonization to plant hosts, *V. dahliae* forms infection structures to enter plant root

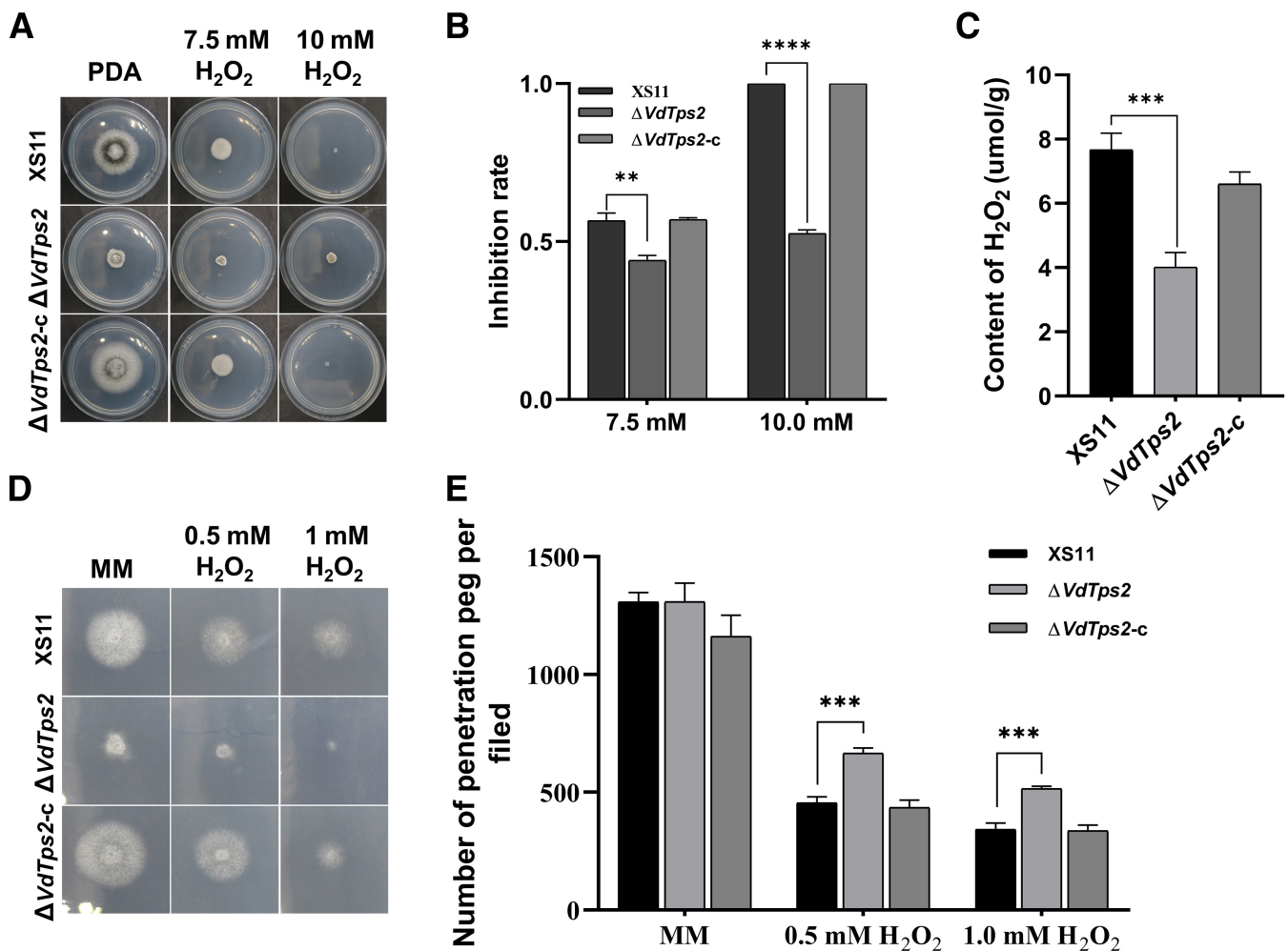


Fig. 5. Oxidative stress responses and penetration peg development of the $\Delta VdTps2$ strain of *Verticillium dahliae*. **A**, The wild-type XS11 strain, the $\Delta VdTps2$ strain, and the complemented strain were cultured on PDA, PDA supplemented with 7.5mM H_2O_2 and PDA supplemented with 10 mM H_2O_2 at 25°C for 10 days. **B**, Graph showing the inhibition rates of the three *V. dahliae* strains under different concentrations of H_2O_2 . Error bars represent the standard deviation based on at least three independent biological replicates. Asterisks indicate significant differences according to Student's *t*-test, $P < 0.01$ (**), $P < 0.0001$ (****). **C**, Graph showing the content of H_2O_2 in the hyphae of all strains. The wild-type XS11 strain, the $\Delta VdTps2$ strain, and the complemented strain were grown in CM for 3 days before being treated with 5 mM H_2O_2 for 5 h. Error bars indicate standard deviation derived from three independent experiments consisting of three replicates in each sampling. Asterisks indicate a significant difference according to Student's *t*-test, $P < 0.001$ (***). **D**, All strains successfully penetrated the cellophane membrane at 3 dpi. The wild-type XS11 strain, the $\Delta VdTps2$ strain, and the complemented strain were grown on minimal medium (MM) overlaid with a cellophane layer for 3 days, and the plates were further incubated for 3days after removing the cellophane layer and photographed. **E**, Quantification of the number of penetration peg formation. The wild-type XS11 strain, the $\Delta VdTps2$ strain, and the complemented strain were grown on MM overlaid with a cellophane layer at 3 dpi, and the number of penetration pegs was counted per strain. Error bars represent the standard deviation based on at least three independent biological replicates. Asterisks indicate significant differences according to Student's *t*-test, $P < 0.001$ (***).

epidermal cells (Fradin and Thomma 2006; Klosterman et al. 2009). Deletion of *VdTps2* may have enhanced the penetration capability of *V. dahliae*. Several mutants in *V. dahliae* have been characterized that display defective penetration peg formation or reduced numbers of penetration pegs leading to impaired virulence (Tang et al. 2020; Yang et al. 2022). Formation of the fungal infection structures is often regulated by endogenous ROS in filamentous pathogenic fungi (Zhu et al. 2021). NADPH oxidases (NOX) are responsible for endogenous ROS production in cells, and the $\Delta VdNoxB$ deletion mutants of *V. dahliae* were incapable of producing ROS, leading to defective hyphodia and penetration pegs (Lambeth 2004; Scott 2015; Sumimoto 2008; Zhao

et al. 2016). Meanwhile, excess ROS production is one of the earliest responses in plant-pathogen interactions, which means exogenous ROS is likely to restrain fungal penetration (Kadota et al. 2014; Li et al. 2014). However, the roles of exogenous ROS in infection structure formation remain unclear. Herein, the H_2O_2 treatment decreased the number of penetration pegs in the XS11 strain, providing direct evidence that exogenous ROS can inhibit the capability of *V. dahliae* to penetrate the host (Fig. 5E). However, the number of penetration pegs in the $\Delta VdTps2$ strain was more than those observed in the XS11 strain when treated by H_2O_2 , suggesting a higher resistance of the $\Delta VdTps2$ strain to H_2O_2 (Fig. 5E). Coincidentally, the deletion of *VdTps2* enhanced resistance to H_2O_2 by neutralizing exogenous H_2O_2 and the effect promoted penetration peg formation in *V. dahliae* (Fig. 5A, B, and C). Additionally, there is no difference in the number of penetration pegs between both XS11 and the $\Delta VdTps2$ strains growing on MM without H_2O_2 . The results indicated that penetration peg formation in *V. dahliae* is not directly regulated by *VdTps2*. The increase of the number of penetration pegs of the $\Delta VdTps2$ strain growing on MM with H_2O_2 is due to the enhanced ability to eliminate ROS of the mutant. Overall, we uncovered an important function of *VdTps2* to modulate the formation of penetration pegs under ROS stress, demonstrating the complexity of *VdTps2* regulation of virulence.

Melanin protects certain pathogenic fungi from ROS released by their respective hosts (Gessler et al. 2014). In *A. fumigatus*, DHN-melanin protects against ROS by eliminating excess ROS generated by hosts (Perez-Cuesta et al. 2020). Melanin in *M. oryzae* is also required to protect the fungus from plant ROS (Aver'yanov et al. 2013; Gessler et al. 2014). Our previous study revealed that the $\Delta VdMRTF1$ strain of *V. dahliae* exhibited increased melanin biosynthesis, thereby promoting the elimination of exogenous ROS and enhancing pathogenicity (Lai et al. 2022). In this study, melanin biosynthesis was enhanced in the $\Delta VdTps2$ strain; meanwhile, this strain showed improved ROS resistance as well as increased ability to neutralize H_2O_2 (Figs. 2D and 5A, B, and C). Therefore, the deletion of *VdTps2* enhanced gene expression associated with melanin biosynthesis to promote melanin production and possibly the elimination of ROS. Examining more precisely the roles of melanin in scavenging excess ROS in the *VdTps2* mutant strain will be an additional future objective.

The results indicate that *VdTps2* promotes autophagy in *V. dahliae*. In *S. cerevisiae*, deletion of *Tps2* results in the decrease of *Atg8* expression and the reduction of autophagic flux when grown under nitrogen-starvation conditions, and the effect is not related to the trehalose synthesis function of *Tps2* (Kim et al. 2021). A previous study showed that ROS involved autophagy initiation (Dunn et al. 2015) and, once activated, autophagy removes excessive ROS (Zhang et al. 2016). In mammals, the mTOR (mechanistic target of rapamycin) pathway is regulated by ROS concentration, and ROS and autophagy constitute a negative feedback mechanism (Qin et al. 2019). Oxidized lipoprotein (a), an arteriosclerotic factor, induces autophagy via a ROS-dependent PAPR-1-LKB1-AMPK-mTOR pathway in human umbilical vein endothelial cells, and the induced effect is inhibited by exogenous superoxide dismutase (Li et al. 2015). These results indicated that the induction of autophagy is related to ROS concentrations. The regulatory mechanisms between ROS and the mTOR pathway remain unclear in plant-pathogenic fungi. In *Alternaria alternata*, autophagy is triggered by H_2O_2 and deletion of *Atg8* failed to effectively detoxify ROS produced by hosts, leading to ROS accumulation (Wu et al. 2022). In this study, we showed that *VdTps2* inhibits the elimination of ROS and promotes autophagy in *V. dahliae* (Fig. 6). The inhibition of autophagy of the $\Delta VdTps2$ strain is presumably related to low-level ROS in its cells.

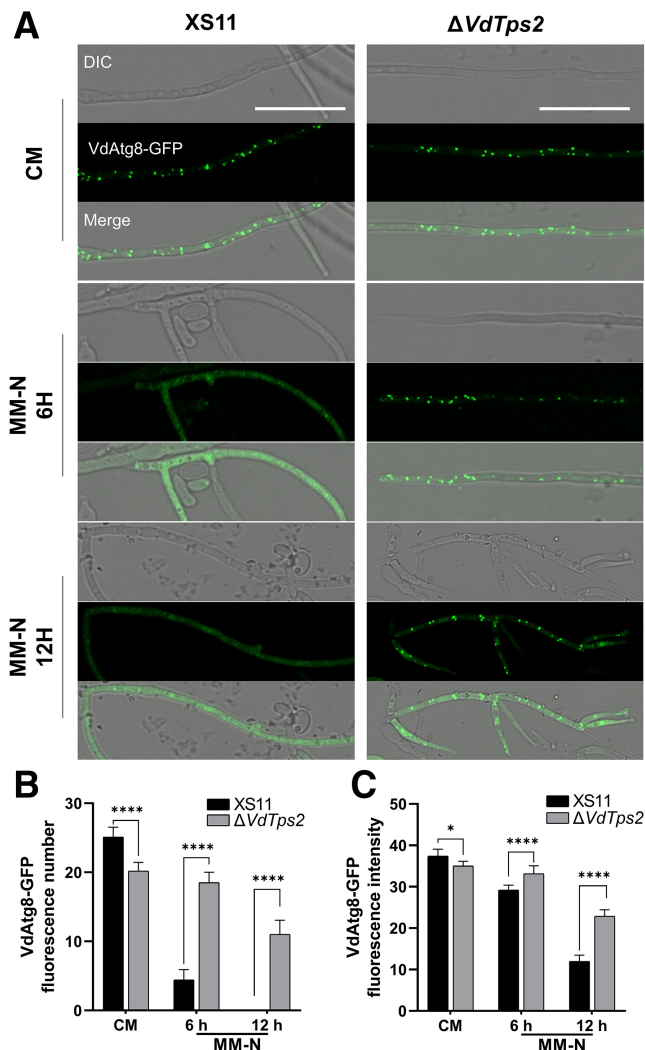


Fig. 6. Functional analyses of the *VdTps2* in autophagy in *Verticillium dahliae*. **A**, Epifluorescence micrographs of autophagosomes. The autophagy marker fusion gene *VdAtg8-GFP* was introduced into both the $\Delta VdTps2$ and wild type XS11 strains for analyses by epifluorescence microscopy. All strains were grown in liquid CM for 48 h, and for 48 h before transferred into MM minus nitrogen (MM-N) for the indicated time. Scale bar = 10 μ m. **B**, *VdAtg8-GFP* fluorescence number within hyphae. The mean *VdAtg8-GFP* fluorescence number was calculated from at least 10 hyphal segments with a length of 50 μ m. Error bars represent the standard deviation based on at least ten independent biological replicates. Asterisks indicate significant differences according to Student's *t*-test, $P < 0.0001$ (****). **C**, Fluorescence intensity of *VdAtg8-GFP*. The mean value of GFP fluorescence intensity was calculated from at least 10 hyphal segments with a length of 50 μ m using ImageJ under default setting. Error bars represent the standard deviation based on at least ten independent biological replicates. Asterisks indicate significant differences according to Student's *t*-test, $P < 0.05$ (*), $P < 0.0001$ (****).

In conclusion, we have identified *VdTps2* in *V. dahliae* and determined that it regulates microsclerotia formation, melanin biosynthesis, and pathogenicity in *V. dahliae*. *VdTps2* affects plant colonization and disease symptom development by regulating the neutralization of ROS, thereby inhibiting penetration peg formation, and by regulating the spread of *V. dahliae* in the host above the crown. Furthermore, our data presented in this study support previous findings of the protective effect of melanin against high-temperature stress (Wang et al. 2018) but also indicated that melanin of *V. dahliae* has potential roles in regulating the resistance to cell-wall perturbations and is involved in scavenging excess ROS. Since *VdTps2* deletion in *V. dahliae* leads to pleiotropic effects, there may be more than one avenue of *VdTps2*-mediated control of *Verticillium* wilt to explore. As suggested by others, the trehalose biosynthesis pathway may be a promising target for developing safe and broad-spectrum fungicides (Chen et al. 2021; Thammahong et al. 2017).

Materials and Methods

Fungal strains and culture conditions.

The *V. dahliae* wild-type strain XS11 was isolated from a smoke tree in Fragrant Hills, Beijing (Wang et al. 2013). All strains were grown on PDA (200 g of potato, 20 g of glucose, and 15 g of agar per liter) plates at 25°C for 10 days for experimentation. Mycelial masses (approximately 3 mm) used for inoculation were cut from these plates with a sterile scalpel. Conidial suspensions of all strains were obtained by flooding 10-day-old colonies on PDA plates with water, collecting, and storing at -80°C in 50% glycerol.

Preparation of gene knockout strains and mutant complementation.

The gene deletion vectors were constructed as follows. The upstream and downstream flanking sequences of *VdTps* were amplified by PCR from genomic DNA (gDNA) of the XS11 strain, using sequence-specific primer pairs with adapter sequences (Supplementary Table S1). The plasmid pDHt2 was linearized by restriction endonuclease *RcoRI* or *XbaI*, and the upstream and downstream flanking sequences of *VdTps* were attached to both the ends of the hygromycin resistance gene cassette by homologous recombination (ClonExpress MultiS One Step Cloning Kit, Vazyme) (Zhou et al. 2013). Subsequently, the deletion vectors were transformed into *Agrobacterium tumefaciens* AGL-1. *Agrobacterium tumefaciens* AGL-1 was used for fungal transformations on PDA plates pre-covered with the cellulose membrane at 25°C (Li et al. 2022; Maruthachalam et al. 2011). Selection of strains resistant to the antibiotic hygromycin (Sigma) was carried out by inoculating the respective transformant strain on PDA plates supplemented with 50 µg of hygromycin per milliliter. To verify the putative mutants, PCR amplifications were performed using internal and combinatorial primer pairs (Supplementary Table S1).

To complement the $\Delta VdTps$ strain, sequence-specific primer pairs were used to amplify the fragment containing the *VdTps* coding sequence from the XS11 strain. The geneticin sequence and the amplified sequences verified by sequencing were used for protoplast transformation directly (Wang et al. 2013). To screen the complemented strain, the diagnostic PCR using internal specific primer pairs of *Tps* were carried out. Primer pairs used are listed in Supplementary Table S1.

Analyses of growth, melanin production, and stress responses.

To observe vegetative growth and conidia production, radial growth of all strains was recorded from 3 to 13 days after incu-

bation of the inoculated PDA plates for 10 days at 25°C. Conidia were harvested by flooding the PDA plates with 1 ml of sterile deionized water and pipetting. Spore concentrations were calculated using a hemocytometer. These experiments were repeated three times.

To observe microsclerotia development, 0.5 µl of conidial suspensions (1×10^5 conidia per milliliter) of all strains were dropped on a glass slide coated with BM (10 g of glucose, 0.2 g of sodium nitrate, 0.52 g of KCl, 0.52 g of $MgSO_4 \cdot 7H_2O$, 1.52 g of KH_2PO_4 , 3 µM thiamine HCl, 0.1 µM biotin, and 15 g of agar per liter) and were incubated at 25°C for 7 days. Melanin deposition of microsclerotia was measured using ImageJ under default settings (Li et al. 2022). The reciprocal of grayscale value/pixel² represents the density of melanized microsclerotia. *P* value < 0.5 was considered statistically significant. To further observe microsclerotia development and melanin biosynthesis, 50-µl conidial suspensions (1×10^6 conidia per milliliter) of all strains were uniformly spread on a cellulose membrane overlaid onto BM plates and incubated at 25°C for 7, 10, and 20 days. Melanin biosynthesis of microsclerotia was observed under light microscopy (DM2500, Leica) after 7 days. At 10 and 20 days, microsclerotia formation were documented by photography. These experiments were repeated three times.

To test high-temperature stress, all strains were cultured on PDA plates at 25, 28, and 30°C for 7 days. The colony diameter was measured after 7 dpi. Inhibition rate is calculated as the difference between the colony diameter of the experimental group (28 and 30°C treatment) and the control group (25°C treatment) divided by the colony diameter of the control group. For cell-wall integrity assays, all strains were cultured in CM (50 ml 20× nitrate salts [NS, 120 g of $NaNO_3$, 10.4 g of KCl, 10.4 g of $MgSO_4 \cdot 7H_2O$, and 30.4 g of KH_2PO_4 per liter], 1 ml of 1,000× trace elements, 10 g of glucose, 2 g of peptone, 1 g of yeast extract, 1 g of casamino acids, 1 ml of vitamin solution, and 15 g of agar per liter) and CM containing 100 µg of CR per milliliter or 75 µg of CFW per milliliter at 25°C for 10 days. The colony diameter was measured after 10 dpi. Inhibition rate is calculated as the difference between the colony diameter of the experimental group (CR and CFW treatment) and the control group divided by the colony diameter of the control group. To test oxidative stresses, all strains were cultured on PDA plates and PDA plates supplemented with 7.5 or 10.0 mM H_2O_2 at 25°C for 10 days. The colony diameter was measured after 10 dpi. Inhibition rate is calculated as the difference between the colony diameter of the experimental group (7.5 or 10.0 mM H_2O_2 treatment) and the control group divided by the colony diameter of the control group. For growth tests on trehalose as the sole carbon source, all strains were cultured for 10 days on MM without glucose (6 g of $NaNO_3$, 1.52 g of KH_2PO_4 , 0.52 g of KCl, 0.152 g of $MgSO_4 \cdot 7H_2O$, 3 µM of thiamine HCl, and 15 g of agar per liter) containing 1% (wt/vol) trehalose at 25°C. The colony diameter was measured after 10 dpi. These experiments were repeated three times.

To examine penetration peg formation under ROS stress, the XS11 strain, the $\Delta VdTps2$ strain, and the complemented strain were cultured on MM (6 g of $NaNO_3$, 1.52 g of KH_2PO_4 , 0.52 g of KCl, 0.52 g of $MgSO_4 \cdot 7H_2O$, 20 mM L-glutamic acid, and 15 g of agar per liter) plates with or without 0.5 or 1.0 mM H_2O_2 . These were pre-covered with a cellophane membrane and were incubated at 25°C for 3 days. The cellophane was removed after the 3-day period and the presence of the fungus was documented by photographs following an additional 3 days of incubation. Penetration pegs were counted using ImageJ, under threshold of 100 from three independent replicates (Tang et al. 2020). *P* value < 0.5 was considered statistically significant. These experiments were repeated three times.

RNA extraction and gene expression analysis.

Fresh mycelia of the XS11 and $\Delta VdTps2$ strains were grown in liquid BM in shake culture, 150 rpm at 25°C, for 10 days. Total RNA was extracted by RNA Easy Fast plant tissue kit (Tiangen). RNA was reverse transcribed using ABScript III RT master mix for qPCR and gDNA Remove (ABclonal). Reverse-transcription quantitative real-time PCR was performed with the SuperReal PreMix Plus (SYBR Green) (Tiangen) and a CFX Connect real-time system (Bio-Rad). The β -tubulin gene was used as an internal reference. The transcription levels of the target genes relative to the β -tubulin gene were quantified using the $2^{-\Delta\Delta C_q}$ method (Livak and Schmittgen 2001) in three independent experiments. All primers used for these assays are listed in Supplementary Table S1. These experiments were repeated three times.

Virulence assays and quantification of fungal biomass.

All strains were grown in liquid CM at 25°C for 5 days, and conidia were filtered through two layers of Mira cloth (Millipore) and were then diluted to 10^6 conidia per milliliter in sterile water. Twelve 1-month-old tobacco seedlings (*Nicotiana benthamiana*) were used for virulence assays. All plant roots were dipped in 10^6 conidia per milliliter of each of the conidial suspensions from the different strains for 10 mins and were subsequently replanted into sterilized soil in a greenhouse maintained at 25°C. Control plants were mock-inoculated with distilled water. All plants were observed at 30, 40, and 50 dpi. Pathogenicity experiments were repeated three times.

Onion epidermal strips were soaked in 75% ethanol for 7 days prior to examination of *V. dahliae* infections. Aseptic onion epidermal strips were soaked in sterile deionized water for 30 mins and the hydrophobic surface was placed upwards on 0.8% water agar plates. A 1- μ l drop of a 1×10^5 conidia per milliliter suspension was placed on the onion epidermis for each the strains under examination. Infection processes were observed under light microscopy (DM2500, Leica) at 36 hpi. The experiments were repeated three times.

Examinations of the ability of conidia to adhere to surfaces were as follows. Conidial suspensions (1×10^7 per milliliter) of all strains were uniformly sprayed on Hybond-N⁺ membranes (GE Healthcare) overlaid onto PDA plates and were incubated at 25°C for 18 h, before the membranes were gently washed with 1 ml of sterile deionized water. Fifty microliters of the conidial suspensions were used to coat the PDA plates and suspensions were incubated at 25°C for 5 days before determining the number of colonies (Xiong et al. 2016). The experiments were repeated three times.

Three tobacco seedling roots or stems per treatment group were used for DNA extractions (Plant Genomic DNA kit, Tiangen) for quantification of fungal biomass at 36 hpi, 25 dpi, and 50 dpi. The roots or stems were washed carefully with sterile water prior to extraction. Kits used for qPCR were the same as the above used for analysis of melanin-related genes expression. The qPCR assays for fungal biomass estimations were conducted by targeting the *Verticillium* internal transcribed spacer gene, while the *N. benthamiana GAPDH* gene served as the endogenous plant control (Wang et al. 2022). All primers used in this assay are listed in Supplementary Table S1. These experiments were repeated three times.

Assays of trehalose, T6P, and cellular H₂O₂ contents.

The mycelia of all strains for the trehalose assay were obtained after culturing for 3 days in liquid CM at 25°C. Trehalose and T6P concentration was determined according to the instructions of the Trehalose Content Detection kit (Sangon) and the Fungus T6P ELISA kit (Yilaisa), respectively.

The mycelia of the XS11 strain and the $\Delta VdTps2$ strain were grown in liquid CM for 3 days before being treated with 5 mM

H₂O₂ for 5 h. Cellular H₂O₂ levels were determined according to the instructions of the Hydrogen Peroxide (H₂O₂) Content Detection kit (Solarbio).

Confocal microscopy.

To monitor the autophagic process in *V. dahliae*, a *VdAtg8*-GFP fusion gene with the native promoter was transformed into the XS11 strain and the $\Delta VdTps2$ strain. To observe fluorescence, the XS11 strain and the transformed *VdAtg8*-GFP strain were grown in liquid CM (50 ml of 20 \times NS, 1 ml of 1,000 \times trace elements, 10 g of glucose, 2 g of peptone, 1 g of yeast extract, 1 g of casamino acids, and 1 ml of vitamin solution per liter) for 48 h and for 48 h in CM before switching to liquid MM-N (1.98 g glucose, 1.52 g KH₂PO₄, 0.52 g KCl, 0.152 g MgSO₄·7H₂O, and 3 μ M thiamine HCl per liter) for 6 and 12 h. Fluorescence imaging of the GFP fusion protein was conducted using a Leica Application Suite X (Leica) with excitation and emission wavelengths of 488 and 580 nm, respectively.

Statistical analysis.

Data are expressed as mean \pm standard error of the mean and were analyzed with one-way analysis of variance independent-samples Tukey's range test using GraphPad Prism for Windows version 8.0.1. *P* values < 0.5 were considered statistically significant, and asterisks are used to indicate *P* < 0.05 (*), *P* < 0.01 (**), *P* < 0.001 (***), *P* < 0.0001 (****).

Literature Cited

- Aver'yanov, A., Zakharenkova, T., Lapikova, V., Pasechnik, T., Gaivoron-skaya, L., and Baker, C. 2013. Exogenous superoxide dismutase may lose its antidotal ability on rice leaves. *Russ. J. Plant. Physiol.* 60:270-278.
- Bell, A. A., and Wheeler, M. H. 1986. Biosynthesis and functions of fungal melanins. *Annu. Rev. Phytopathol.* 24:411-451.
- Bell, W., Klaassen, P., Ohnacker, M., Boller, T., Herweijer, M., Schoppink, P., Vanderzee, P., and Wiemken, A. 1992. Characterization of the 56-kDa subunit of yeast trehalose-6-phosphate synthase and cloning of its gene reveal its identity with the product of CIF1, a regulator of carbon catabolite inactivation. *Eur. J. Biochem.* 209:951-959.
- Carroll, C. L., Carter, C. A., Goodhue, R. E., Lawell, C.-Y. C. L., and Subbarao, K. V. 2018. A review of control options and externalities for *Verticillium* wilts. *Phytopathology* 108:160-171.
- Chary, S. N., Hicks, G. R., Choi, Y. G., Carter, D., and Raikhel, N. V. 2008. Trehalose-6-phosphate synthase/phosphatase regulates cell shape and plant architecture in *Arabidopsis*. *Plant Physiol.* 146:97-107.
- Chen, X., Abubakar, Y. S., Yang, C., Wang, X., Miao, P., Lin, M., Wen, Y., Wu, Q., Zhong, H., and Fan, Y. 2021. Trehalose phosphate synthase complex-mediated regulation of trehalose 6-phosphate homeostasis is critical for development and pathogenesis in *Magnaporthe oryzae*. *Msyste.ms* 6:e00462-00421.
- Chen, X., Zhang, Z., Chen, Z., Li, Y., Su, S., and Sun, S. 2020. Potential antifungal targets based on glucose metabolism pathways of *Candida albicans*. *Front Microbiol.* 11:296.
- De Virgilio, C., Bärckert, N., Bell, W., Jenö, P., Boller, T., and Wiemken, A. 1993. Disruption of TPS2, the gene encoding the 100-kDa subunit of the trehalose-6-phosphate synthase/phosphatase complex in *Saccharomyces cerevisiae*, causes accumulation of trehalose-6-phosphate and loss of trehalose-6-phosphate phosphatase activity. *Eur. J. Biochem.* 212: 315-323.
- Dunn, J. D., Alvarez, L. A., Zhang, X., and Soldati, T. 2015. Reactive oxygen species and mitochondria: A nexus of cellular homeostasis. *Redox. Biol.* 6:472-485.
- Elbein, A. D., Pan, Y., Pastuszak, I., and Carroll, D. 2003. New insights on trehalose: A multifunctional molecule. *Glycobiology* 13:17R-27R.
- Fang, Y., Klosterman, S. J., Tian, C., and Wang, Y. 2019. Insights into VdCmr1-mediated protection against high temperature stress and UV irradiation in *Verticillium dahliae*. *Environ. Microbiol.* 21:2977-2996.
- Foster, A. J., Jenkinson, J. M., and Talbot, N. J. 2003. Trehalose synthesis and metabolism are required at different stages of plant infection by *Magnaporthe grisea*. *EMBO J.* 22:225-235.
- Fradin, E. F., and Thomma, B. P. 2006. Physiology and molecular aspects of *Verticillium* wilt diseases caused by *V. dahliae* and *V. albo-atrum*. *Mol. Plant Pathol.* 7:71-86.

- Gessler, N., Egorova, A., and Belozerskaya, T. 2014. Melanin pigments of fungi under extreme environmental conditions. *Appl. Biochem. Microbiol.* 50:105-113.
- Gordee, R., and Porter, C. 1961. Structure, germination, and physiology of microsclerotia of *Verticillium albo-atrum*. *Mycologia* 53:171-182.
- Griffiths, D. 1970. The fine structure of developing microsclerotia of *Verticillium dahliae* Kleb. *Archiv für Mikrobiologie* 74:207-212.
- Hall, R., and Ly, H. 1972. Development and quantitative measurement of microsclerotia of *Verticillium dahliae*. *Can. J. Bot.* 50:2097-2102.
- Hawke, M., and Lazarovits, G. 1994. Production and manipulation of individual microsclerotia of *Verticillium dahliae* for use in studies of survival. *Phytopathology* 84:883-890.
- Heale, J. B., and Isaac, I. 1965. Environmental factors in the production of dark resting structures in *Verticillium albo-atrum*, *V. dahliae* and *V. tricorpus*. *T. Brit. Mycol. Soc.* 48:35-50, IN7.
- Höfer, A. M., Harting, R., Aßmann, N. F., Gerke, J., Schmitt, K., Starke, J., Bayram, Ö., Tran, V.-T., Valerius, O., and Braus-Stromeier, S. A. 2021. The velvet protein Vell1 controls initial plant root colonization and conidia formation for xylem distribution in *Verticillium* wilt. *PLoS Genet.* 17:e1009434.
- Howard, R. J., and Valent, B. 1996. Breaking and entering: Host penetration by the fungal rice blast pathogen *Magnaporthe grisea*. *Annu. Rev. Microbiol.* 50:491-512.
- Inderbitzin, P., Bostock, R. M., Davis, R. M., Usami, T., Platt, H. W., and Subbarao, K. V. 2011b. Phylogenetics and taxonomy of the fungal vascular wilt pathogen *Verticillium*, with the descriptions of five new species. *PLoS One* 6:e28341.
- Inderbitzin, P., Davis, R. M., Bostock, R. M., and Subbarao, K. V. 2011a. The ascomycete *Verticillium longisporum* is a hybrid and a plant pathogen with an expanded host range. *PLoS One* 6:e18260.
- Jia, Z., Yuan, H., and Li, Y. 2007. NO and H₂O₂ induced by *Verticillium dahliae* toxins and its influence on the expression of GST gene in cotton suspension cells. *Chin. Sci. Bull.* 52:1347-1354.
- Kadota, Y., Sklenar, J., Derbyshire, P., Stransfeld, L., Asai, S., Ntoukakis, V., Jones, J. D., Shirasu, K., Menke, F., and Jones, A. 2014. Direct regulation of the NADPH oxidase RBOHD by the PRR-associated kinase BIK1 during plant immunity. *Mol. Cell* 54:43-55.
- Kim, B., Lee, Y., Choi, H., and Huh, W.-K. 2021. The trehalose-6-phosphate phosphatase Tps2 regulates ATG8 transcription and autophagy in *Saccharomyces cerevisiae*. *Autophagy* 17:1013-1027.
- Klosterman, S. J., Atallah, Z. K., Vallad, G. E., and Subbarao, K. V. 2009. Diversity, Pathogenicity, and Management of *Verticillium* Species. *Annu. Rev. Phytopathol.* 47:39-62.
- Klosterman, S. J., Subbarao, K. V., Kang, S., Veronese, P., Gold, S. E., Thomma, B. P., Chen, Z., Henriessat, B., Lee, Y.-H., and Park, J. 2011. Comparative genomics yields insights into niche adaptation of plant vascular wilt pathogens. *PLoS Pathog.* 7:e1002137.
- Lai, M., Cheng, Z., Xiao, L., Klosterman, S. J., and Wang, Y. 2022. The bZip transcription factor VdMRTF1 is a negative regulator of melanin biosynthesis and virulence in *Verticillium dahliae*. *Microbiol. Spectrum* 10:e02581-02521.
- Lambeth, J. D. 2004. NOX enzymes and the biology of reactive oxygen. *Nat. Rev. Immunol.* 4:181-189.
- Li, G.-h., Lin, X.-l., Zhang, H., Li, S., He, X.-l., Zhang, K., Peng, J., Tang, Y.-l., Zeng, J.-f., and Zhao, Y. 2015. Ox-Lp (a) transiently induces HUVEC autophagy via an ROS-dependent PAPR-1-LKB1-AMPK-mTOR pathway. *Atherosclerosis* 243:223-235.
- Li, H., Wang, D., Zhang, D.-D., Geng, Q., Li, J.-J., Sheng, R.-C., Xue, H.-S., Zhu, H., Kong, Z.-Q., and Dai, X.-F. 2022. A polyketide synthase from *Verticillium dahliae* modulates melanin biosynthesis and hyphal growth to promote virulence. *BMC Biol.* 20:1-24.
- Li, L., Li, M., Yu, L., Zhou, Z., Liang, X., Liu, Z., Cai, G., Gao, L., Zhang, X., and Wang, Y. 2014. The FLS2-associated kinase BIK1 directly phosphorylates the NADPH oxidase RbohD to control plant immunity. *Cell Host Microbe* 15:329-338.
- Livak, K. J., and Schmittgen, T. D. 2001. Analysis of relative gene expression data using real-time quantitative PCR and the 2^{-ΔΔCT} method. *Methods* 25:402-408.
- Ludwig, N., Löhner, M., Hempel, M., Mathea, S., Schliebner, I., Menzel, M., Kiesow, A., Schaffrath, U., Deising, H. B., and Horbach, R. 2014. Melanin is not required for turgor generation but enhances cell-wall rigidity in appressoria of the corn pathogen *Colletotrichum graminicola*. *Mol. Plant-Microbe Interact.* 27:315-327.
- Maruthachalam, K., Klosterman, S., Kang, S., Hayes, R., and Subbarao, K. 2011. Identification of pathogenicity-related genes in the vascular wilt fungus *Verticillium dahliae* by *Agrobacterium tumefaciens*-mediated T-DNA insertional mutagenesis. *Mol. Biotechnol.* 49:209-221.
- Miao, Y., Tenor, J. L., Toffaletti, D. L., Washington, E. J., Liu, J., Shadrack, W. R., Schumacher, M. A., Lee, R. E., Perfect, J. R., and Brennan, R. G. 2016. Structures of trehalose-6-phosphate phosphatase from pathogenic fungi reveal the mechanisms of substrate recognition and catalysis. *Proc. Natl. Acad. Sci.* 113:7148-7153.
- Perez-Cuesta, U., Aparicio-Fernandez, L., Guruceaga, X., Martin-Souto, L., Abad-Diaz-de-Cerio, A., Antonan, A., Buldain, I., Hernando, F. L., Ramirez-Garcia, A., and Rementeria, A. 2020. Melanin and pyomelanin in *Aspergillus fumigatus*: From its genetics to host interaction. *Int. Microbiol.* 23:55-63.
- Pihet, M., Vandeputte, P., Tronchin, G., Renier, G., Saulnier, P., Georgeault, S., Mallet, R., Chabasse, D., Symoens, F., and Bouchara, J.-P. 2009. Melanin is an essential component for the integrity of the cell wall of *Aspergillus fumigatus* conidia. *BMC Microbiol.* 9:1-11.
- Puttikamonkul, S., Willger, S. D., Grahl, N., Perfect, J. R., Movahed, N., Bothner, B., Park, S., Paderu, P., Perlin, D. S., and Cramer Jr, R. A. 2010. Trehalose 6-phosphate phosphatase is required for cell wall integrity and fungal virulence but not trehalose biosynthesis in the human fungal pathogen *Aspergillus fumigatus*. *Mol. Microbiol.* 77:891-911.
- Qin, Q.-F., Li, X.-J., Li, Y.-S., Zhang, W. K., Tian, G.-H., Shang, H.-C., and Tang, H.-B. 2019. AMPK-ERK/CARM1 signaling pathways affect autophagy of hepatic cells in samples of liver cancer patients. *Front. Oncol.* 9:1247.
- Salmerón-Santiago, K. G., Pardo, J. P., Flores-Herrera, O., Mendoza-Hernández, G., Miranda-Arango, M., and Guerra-Sánchez, G. 2011. Response to osmotic stress and temperature of the fungus *Ustilago maydis*. *Arch. Microbiol.* 193:701-709.
- Santhanam, P., and Thomma, B. P. 2013. *Verticillium dahliae* Sge1 differentially regulates expression of candidate effector genes. *Mol. Plant-Microbe Interact.* 26:249-256.
- Scott, B. 2015. Conservation of fungal and animal nicotinamide adenine dinucleotide phosphate oxidase complexes. *Mol. Microbiol.* 95:910-913.
- Sink, K. C., and Grey, W. E. 1999. A root-injection method to assess *Verticillium* wilt resistance of peppermint (*Mentha × piperita* L.) and its use in identifying resistant somaclones of cv. Black Mitcham. *Euphytica* 106:223-230.
- Song, X.-S., Li, H.-P., Zhang, J.-B., Song, B., Huang, T., Du, X.-M., Gong, A.-D., Liu, Y.-K., Feng, Y.-N., and Agboola, R. S. 2014. Trehalose 6-phosphate phosphatase is required for development, virulence and mycotoxin biosynthesis apart from trehalose biosynthesis in *Fusarium graminearum*. *Fungal Genet. Biol.* 63:24-41.
- Sumimoto, H. 2008. Structure, regulation and evolution of Nox-family NADPH oxidases that produce reactive oxygen species. *FEBS J.* 275:3249-3277.
- Tang, C., Li, T., Klosterman, S. J., Tian, C., and Wang, Y. 2020. The bZIP transcription factor VdAtf1 regulates virulence by mediating nitrogen metabolism in *Verticillium dahliae*. *New Phytol.* 226:1461-1479.
- Thammahong, A., Puttikamonkul, S., Perfect, J. R., Brennan, R. G., and Cramer, R. A. 2017. Central role of the trehalose biosynthesis pathway in the pathogenesis of human fungal infections: Opportunities and challenges for therapeutic development. *Microbiol. Mol. Biol. Rev.* 81:e00053-00016.
- Tian, L., Yu, J., Wang, Y., and Tian, C. 2017. The C₂H₂ transcription factor VdMsn2 controls hyphal growth, microsclerotia formation, and virulence of *Verticillium dahliae*. *Fungal biology* 121:1001-1010.
- Van Dijk, P., De Rop, L., Szlufcik, K., Van Ael, E., and Thevelein, J. M. 2002. Disruption of the *Candida albicans* TPS2 gene encoding trehalose-6-phosphate phosphatase decreases infectivity without affecting hypha formation. *Infect. Immun.* 70:1772-1782.
- Wang, H., Tang, C., Deng, C., Li, W., Klosterman, S. J., and Wang, Y. 2022. Septins regulate virulence in *Verticillium dahliae* and differentially contribute to microsclerotial formation and stress responses. *Phytopathol. Res.* 4:1-14.
- Wang, Y., Hu, X., Fang, Y., Anchieta, A., Goldman, P. H., Hernandez, G., and Klosterman, S. J. 2018. Transcription factor VdCmr1 is required for pigment production, protection from UV irradiation, and regulates expression of melanin biosynthetic genes in *Verticillium dahliae*. *Microbiology* 164:685.
- Wang, Y., Xiao, S., Xiong, D., and Tian, C. 2013. Genetic transformation, infection process and qPCR quantification of *Verticillium dahliae* on smoke-free *Cotinus coggygria*. *Australas. Plant Path.* 42:33-41.
- Wheeler, M. H. 1982. Melanin biosynthesis in *Verticillium dahliae*: Dehydration and reduction reactions in cell-free homogenates. *Exp. Mycol.* 6:171-179.
- Wilhelm, S. 1955. Longevity of the *Verticillium* wilt fungus in the laboratory and field. *Phytopathology* 45.
- Wilson, R. A., Jenkinson, J. M., Gibson, R. P., Littlechild, J. A., Wang, Z. Y., and Talbot, N. J. 2007. Tps1 regulates the pentose phosphate

- pathway, nitrogen metabolism and fungal virulence. *EMBO J.* 26: 3673-3685.
- Wu, P. C., Choo, C. Y. L., Lu, H. Y., Wei, X. Y., Chen, Y. K., Yago, J. I., and Chung, K. R. 2022. Pexophagy is critical for fungal development, stress response, and virulence in *Alternaria alternata*. *Mol. Plant Pathol.* 23:1538-1554.
- Xiong, D., Wang, Y., Ma, J., Klosterman, S. J., Xiao, S., and Tian, C. 2014. Deep mRNA sequencing reveals stage-specific transcriptome alterations during microsclerotia development in the smoke tree vascular wilt pathogen, *Verticillium dahliae*. *BMC Genomics* 15:1-19.
- Xiong, D., Wang, Y., Tian, L., and Tian, C. 2016. MADS-box transcription factor VdMcm1 regulates conidiation, microsclerotia formation, pathogenicity, and secondary metabolism of *Verticillium dahliae*. *Front Microbiol.* 7:1192.
- Xu, C., Chen, H., Wu, Q., Wu, Y., Daly, P., Chen, J., Yang, H., Wei, L., and Zhuang, Y. 2021. Trehalose-6-phosphate phosphatase inhibitor: N-(phenylthio) phthalimide, which can inhibit the DON biosynthesis of *Fusarium graminearum*. *Pestic. Biochem. Physiol.* 178:104917.
- Yang, X., Guo, C., Chen, C., Hu, Z., Zheng, X., Xu, S., Yang, X., and Xie, C. 2022. A kinesin VdKin2 required for vacuole formation, mycelium growth, and penetration structure formation of *Verticillium dahliae*. *J. Fungi* 8:391.
- Zaragoza, O., de Virgilio, C., Pontón, J., and Gancedo, C. 2002. Disruption in *Candida albicans* of the *TPS2* gene encoding trehalose-6-phosphate phosphatase affects cell integrity and decreases infectivity. *Microbiology* 148:1281-1290.
- Zhang, D. D., Dai, X. F., Klosterman, S. J., Subbarao, K. V., and Chen, J. Y. 2022. The secretome of *Verticillium dahliae* in collusion with plant defence responses modulates *Verticillium* wilt symptoms. *Biol. Rev.* 97:1810-1822.
- Zhang, X., Yu, L., and Xu, H. 2016. Lysosome calcium in ROS regulation of autophagy. *Autophagy* 12:1954-1955.
- Zhao, P., Zhao, Y.-L., Jin, Y., Zhang, T., and Guo, H.-S. 2014. Colonization process of *Arabidopsis thaliana* roots by a green fluorescent protein-tagged isolate of *Verticillium dahliae*. *Protein Cell* 5:94-98.
- Zhao, Y.-L., Zhou, T.-T., and Guo, H.-S. 2016. Hyphopodium-specific VdNoxB/VdPls1-dependent ROS-Ca²⁺ signaling is required for plant infection by *Verticillium dahliae*. *PLoS Pathog.* 12:e1005793.
- Zhou, L., Zhao, J., Guo, W., and Zhang, T. 2013. Functional analysis of autophagy genes via *Agrobacterium*-mediated transformation in the vascular wilt fungus *Verticillium dahliae*. *J. Genet. Genom.* 40:421-431.
- Zhu, X., Sayari, M., Islam, M. R., and Daayf, F. 2021. NOXA is important for *Verticillium dahliae*'s penetration ability and virulence. *J. Fungi* 7:814.

Host Specificity Controlled by *PWL1* and *PWL2* Effector Genes in the Finger Millet Blast Pathogen *Magnaporthe oryzae* in Eastern Africa

Hosea Isanda Masaki,¹ Santie de Villiers,^{1,2,†} Peng Qi,^{3,4} Kathryn A. Prado,³ Davies Kiambi Kaimenyi,^{1,2} Kassahun Tesfaye,^{5,6} Tesfaye Alemu,⁵ John Takan,⁷ Mathews Dida,⁸ Justin Ringo,⁹ Wilton Mbinda,¹ Chang Hyun Khang,³ and Katrien M. Devos^{3,4}

¹ Pwani University, Department of Biochemistry and Biotechnology, Kilifi, Kenya

² Pwani University Biosciences Research Centre (PUBReC), Kilifi, Kenya

³ University of Georgia, Department of Plant Biology, Athens, GA 30602, U.S.A.

⁴ Institute of Plant Breeding, Genetics and Genomics Department of Crop and Soil Sciences, University of Georgia, Athens, GA 30602, U.S.A.

⁵ Addis Ababa University, Addis Ababa, Ethiopia

⁶ Ethiopian Biotechnology Institute, Addis Ababa, Ethiopia

⁷ National Semi-Arid Resources Research Institute Serere, Soroti, Uganda

⁸ Maseno University, Maseno, Kenya

⁹ Tanzania Agricultural Research Institute, Illonga, Tanzania

Accepted for publication 12 April 2023.

Magnaporthe oryzae, a devastating pathogen of finger millet (*Eleusine coracana*), secretes effector molecules during infection to manipulate host immunity. This study determined the presence of avirulence effector genes *PWL1* and *PWL2* in 221 *Eleusine* blast isolates from eastern Africa. Most Ethiopian isolates carried both *PWL1* and *PWL2*. Kenyan and Ugandan isolates largely lacked both genes, and Tanzanian isolates carried either *PWL1* or lacked both. The roles of *PWL1* and *PWL2* towards pathogenicity on alternative chloridoid hosts, including weeping lovegrass (*Eragrostis curvula*), were also investigated. *PWL1* and *PWL2* were cloned from Ethiopian isolate E22 and were transformed separately into Ugandan isolate U34, which lacked both genes. Resulting transformants harboring either gene gained varying degrees of avirulence on *Eragrostis curvula* but remained virulent on finger millet. Strains carrying one or both *PWL1* and *PWL2* infected the chloridoid species *Sporobolus phyllotrichus* and *Eleusine tristachya*, indicating the absence of cognate resistance (*R*) genes for *PWL1* and *PWL2* in these species. Other chloridoid grasses, however, were fully resistant, regardless of the presence of one or both

PWL1 and *PWL2*, suggesting the presence of effective *R* genes against *PWL* and other effectors. Partial resistance in some *Eragrostis curvula* accessions to some blast isolates lacking *PWL1* and *PWL2* also indicated the presence of other interactions between fungal avirulence (*AVR*) genes and host resistance (*R*) genes. Related chloridoid species thus harbor resistance genes that could be useful to improve finger millet for blast resistance. Conversely, loss of *AVR* genes in the fungus could expand its host range, as demonstrated by the susceptibility of *Eragrostis curvula* to finger millet blast isolates that had lost *PWL1* and *PWL2*.

Keywords: blast disease, chloridoid grasses, *Eleusine coracana*, *Eragrostis curvula*, host resistance, *Magnaporthe oryzae*, *PWL1*, *PWL2*

The filamentous ascomycete fungus *Magnaporthe oryzae* causes blast disease, one of the most devastating diseases affecting more than 50 grass species, including finger millet (*Eleusine coracana*). In endemic areas, complete yields can be lost, especially if blast infections occur in combination with abiotic stresses (Senthil et al. 2012). The fungus infects finger millet at all developmental stages, but infection of the panicle (head blast) and peduncle (neck blast) are the most destructive (Ramakrishnan et al. 2016; Takan et al. 2012). The most cost-effective solution for small holder farmers to manage blast disease is to deploy tolerant plant varieties that carry resistance (*R*) genes against the infecting blast strain (Vleeshouwers and Oliver 2014). However, because of their adaptability, fungal pathogens often overcome resistance in newly deployed cultivars within a few years (Orbach et al. 2000).

Individual strains of *M. oryzae* are host-specific and have been classified into distinct subgroups according to their pathogenicity on a variety of plants, such as *Eleusine* pathotypes that infect finger millet, *Setaria* pathotypes on foxtail millet, *Oryza* pathotypes on rice, and *Triticum* pathotypes on wheat (Kato et al. 2000). The fungus utilizes a hemibiotrophic infection strategy

†Corresponding author: S. de Villiers; santiedevilliers@gmail.com

C. H. Khang and K. M. Devos contributed equally to the research.

Funding: The research was supported by a Bill & Melinda Gates Foundation PEARL grant OPP1131765 “Unraveling the molecular genetics of finger millet blast disease and the existing resistance for the development of high-yielding resilient varieties” and National Science Foundation BREAD ABRDC award IOS-1543901 “Development of Essential Genetic and Genomic Resources for Finger Millet”.

e-Xtra: Supplementary material is available online.

The author(s) declare no conflict of interest.



Copyright © 2023 The Author(s). This is an open access article distributed under the CC BY 4.0 International license.

to interact with the host plant. During the initial biotrophic phase, it colonizes living tissues, from which it acquires nutrients before switching to a necrotrophic phase when it acquires nutrients from the dead cells (Jones et al. 2021; Park et al. 2009; Vleeshouwers and Oliver 2014). To subvert the host defense mechanisms and cellular activities, *M. oryzae* secretes effector proteins that facilitate host colonization (Valent and Khang 2010; Yoshida et al. 2016). Some effectors exhibit avirulence properties (Zhang and Xu 2014) and are recognized by host plant R proteins (De Wit et al. 2009), resulting in a rapid and effective hypersensitive response (Yoshida et al. 2009).

To date, a limited number of *M. oryzae* avirulence (*AVR*) effector genes have been identified and analyzed for mutations that can affect avirulence, including *AVR-Pita1* (Khang et al. 2008; Orbach et al. 2000), *ACE1* (Böhnert et al. 2004), *AvrPiz-t* (Li et al. 2009), *Avr-Pia* (Yoshida et al. 2009), *Avr-Pii* and *Avr-Pik/km/kp* (Yoshida et al. 2009), *Avr-CO39* (Ribot et al. 2013), and *PWL* (Kang et al. 1995; Sweigard et al. 1995). Of these, *AVR-Pita1* was shown to be linked to the subtelomeric region in a Chinese rice field isolate, O-137, indicating that loss of chromosome tips could result in gain of virulence (Orbach et al. 2000). Previous studies of *M. oryzae* have revealed that the fungus employs gene gain or loss to change its host specificity (Sone et al. 2013; Yoshida et al. 2016). This process often involves transposable elements, which can generate gene duplications, gene disruptions, recombination, mutations, and the adaptive evolution of blast fungal effector genes (Chuma et al. 2011; Khang et al. 2008; Gómez Luciano et al. 2019; Thon et al. 2006; Wang et al. 2017).

The diversified, rapidly evolving *PWL* gene family in *M. oryzae*, which determines pathogenicity in weeping lovegrass (*Eragrostis curvula*), includes four genes—*PWL1*, *PWL2*, *PWL3*, and *PWL4*. *PWL1* was identified from a cross between *Eleusine* isolate WGG-FA40 and weeping lovegrass isolate K76-79 (Valent et al. 1986) and was subsequently cloned (Kang et al. 1995). The second gene, *PWL2*, was identified and cloned from a cross between two laboratory strains virulent on rice, of which one strain (4224-7-8) was virulent and the other (6043) avirulent on weeping lovegrass (Sweigard et al. 1995). *PWL3* and *PWL4* were found not to confer avirulence in weeping lovegrass, although *PWL4* became functional when its expression was driven by the promoter of either *PWL1* or *PWL2* (Kang et al. 1995).

In this study, we cloned and transferred *PWL1* and *PWL2* from the Ethiopian finger millet blast (FMB) isolate E22, which is avirulent on weeping lovegrass, to the Ugandan strain U34, which lacks both *PWL1* and *PWL2*, and used the transformants as well as native isolates in infection assays to determine the role of *PWL1* and *PWL2* in pathogenicity on eight chloridoid species, including finger millet. In addition, PCR amplification of *PWL1* and *PWL2* in 221 *Eleusine* isolates collected across Ethiopia, Kenya, Tanzania, and Uganda was used to investigate the presence of *PWL1* and *PWL2* genes in *M. oryzae* across eastern Africa.

Results

Distribution of *PWL1* and *PWL2* genes across FMB isolates from eastern Africa.

To determine the presence in FMB strains of *PWL1* and *PWL2*, which have been shown to mediate resistance of weeping lovegrass to rice blast strains (Kang et al. 1995; Sweigard et al. 1995), a collection of 221 *Eleusine M. oryzae* isolates were investigated in this study. The 221 strains were isolated from blast-infected finger millet tissues collected between 2015 and 2017 from Ethiopia (E isolates), Kenya (K), Tanzania (T), and Uganda (U). PCR amplification with gene-specific primers (Table 1), bioinformatic mining of resequencing data, or both revealed that

PWL1 and *PWL2* were present either alone or in combination in 89 isolates (Table 2). Thirty-six isolates contained only *PWL1*, three contained only *PWL2*, and 50 had both. The remaining 132 isolates, which included all those from Uganda and most Kenyan isolates, lacked both *PWL1* and *PWL2* (Table 2). The isolates were subsequently grouped into four groups, based on whether they contained neither *PWL1* nor *PWL2* (FMB-1), both *PWL1* and *PWL2* (FMB-2), *PWL1* only (FMB-3), or *PWL2* only (FMB-4). In FMB-1, 76.5% of the isolates had been collected from Kenya and Uganda; in FMB-2, 90.0% originated in Ethiopia; and in FMB-3, 83.3% originated in Tanzania. Presence of *PWL2* only was found in only three isolates, all originating from Tanzania. Tanzanian isolates were mainly present in groups FMB-1 (34.5%) and FMB-3 (51.7%) (Table 2).

Nucleotide sequence comparison of *PWL1* and *PWL2* with those from other *Eleusine coracana* and rice blast isolates.

We compared the level of sequence conservation between the FMB *PWL1* (444 bp) and *PWL2* (438 bp) open reading frames (ORFs) cloned from Ethiopian isolate E22 with those reported in GenBank and with resequencing data for both genes in a subset of the 221 FMB isolates we collected from eastern Africa. The *PWL1* sequence isolated from E22 (this study; GenBank accession MT669814) was identical to those from the Japanese FMB strains reported by Asuke et al. (2019) (GenBank accession AB480169) and Gómez Luciano et al. (2019) (GenBank accession CP034204.1). Similarly, no variants were identified upon alignment of resequencing reads from 49 Ethiopian, 35 Tanzanian, and two Kenyan strains to *PWL1* of strain E22. Ten single base substitutions, predicted to result in three amino acid substitutions, were found between *PWL1* from E22 and the orthologous sequence in a rice blast strain (GenBank accession CP091458; region 363,360 to 363,803) (Supplementary Figs. S1 and S2). Two of the amino acid changes are located in the N-terminal signal peptide, but predictions by SignalP 6.0 (Teufel et al. 2022) indicated that they do not affect cleavage. The third amino acid substitution is located near the C terminus of *PWL1*.

Two synonymous and one nonsynonymous single base substitution were present between *PWL2* from FMB strain E22 (GenBank accession MT669815) and a rice blast strain (GenBank accession U26313.1) (Sweigard et al. 1995) (Supplementary Figs. S3 and S4). The amino acid substitution is located in the signal peptide and, as for *PWL1*, SignalP 6.0 predictions do not indicate an effect on cleavage. It should be noted that the amino acid substitution does not correspond to the aspartic acid to asparagine mutation that rendered *PWL2* in the rice blast fungus nonfunctional as an avirulence gene (Sweigard et al. 1995). No variants were observed for *PWL2* in resequencing data from a set of 45 Ethiopian and eight Tanzanian strains isolated from finger millet.

PWL1 and *PWL2* from *Eleusine* isolates confer avirulence on weeping lovegrass.

Using whole-plant spray inoculations, we tested the pathogenicity of select FMB-1 and FMB-2 isolates on weeping love-

Table 1. PCR primers used in this study

Primer	Sequence (5' to 3')
E22_PWL1_F	CTTAGTGGACCCTTTGTCCG
E22_PWL1_R	GGAAACTAGCGAGCGTGGTTAG
E22_PWL2_F	CCTTATCACGTGAGGTGGAG
E22_PWL2_R	CCAAACAAGCTTCGAGGC
PWL1_CDS_F	ATGAAATTCAACAAAACATATCC
PWL1_CDS_R	TTACATAATATGGCAGCCC
PWL2_CDS_F	ATGAAATGCAACAACATCATCCTCCC
PWL2_CDS_R	ACATAATATTGCAGCCCTCTTCTCGC

grass (*Eragrostis curvula* PI 197425) and found that virulence was correlated with the absence of the *PWL1* and *PWL2* genes. Two Ugandan isolates, U34 and U44 (*pwl1*⁻/*pwl2*⁻; FMB-1 group in Table 2), showed severe infections on weeping lovegrass, causing the infected leaves to completely shrivel with merged lesions (Figs. 1 and 2). This was in stark contrast to the response of PI 197425 to two Ethiopian isolates, E2-GFP (a laboratory strain carrying enhanced green fluorescent protein [FGP]) and E22 (*PWL1*⁺/*PWL2*⁺; FMB-2 group in Table 2), which caused barely visible lesions or some uniform dark brown pinpoint lesions without visible centers (typical avirulent lesions

[Valent et al. 1991]) with occasional isolated lesions with distinct tan centers surrounded by a darker brown margin.

To demonstrate that the *PWL1* and *PWL2* genes in FMB isolates indeed confer avirulence on weeping lovegrass, we first cloned *PWL2* from the avirulent isolate E22 and introduced the cloned gene into the virulent isolate U34. The resulting U34 transformants (*n* = 5) caused typical avirulent lesions with occasional small lesions, exhibiting gain of avirulence in weeping lovegrass (Fig. 1; Supplementary Table S1). Similarly, we transformed U34 with *PWL1* cloned from E22. The resulting transformants (*n* = 3) also showed gain of avirulence in weeping

Table 2. Distribution of *PWL1* and *PWL2* in *Magnaporthe oryzae* isolated from *Eleusine coracana*

Group	No. ^a	Origins	Isolate names
Lacking both <i>PWL1</i> and <i>PWL2</i> FMB-1	132 (59.7%)	Ethiopia (11; 8.3%) Kenya (43; 32.6%) Tanzania (20; 15.2%) Uganda (58; 43.9%)	E1 E3 E8 E18 E30 E32 E43 E46 E55 E61 E62 K1 K2 K3 K4 K5 K6 K7 K8 K9 K10 K11 K12 K13 K14 K15 K16 K17 K18 K19 K20 K21 K22 K23 K24 K26 K27 K28 K29 K30 K32 K33 K34 K35 K36 K37 K38 K39 K40 K41 K42 K43 K44 K45 T2 T9 T11 T14 T17 T19 T20 T23 T24 T26 T28 T34 T35 T39 T40 T46 T49 T53 T54 T58 U1 U2 U3 U4 U5 U6 U7 U8 U9 U10 U11 U12 U13 U14 U15 U16 U17 U18 U19 U20 U21 U22 U23 U24 U25 U26 U27 U28 U29 U30 U31 U32 U33 U34 U35 U36 U37 U38 U39 U40 U41 U42 U43 U44 U45 U46 U47 U48 U49 U50 U51 U52 U53 U54 U55 U56 U57 U58
Carrying both <i>PWL1</i> and <i>PWL2</i> FMB-2	50 (22.6%)	Ethiopia (45; 90.0%) Tanzania (5; 10.0%)	E2 E5 E6 E12 E13 E14 E15 E16 E17 E19 E20 E21 E22 E23 E24 E25 E26 E27 E29 E33 E34 E35 E36 E37 E38 E39 E40 E41 E42 E44 E45 E47 E48 E49 E50 E51 E52 E53 E54 E56 E57 E58 E59 E60 E63 T1 T3 T27 T37 T57
<i>PWL1</i> only FMB-3	36 (16.3%)	Ethiopia (4; 11.1%) Kenya (2; 5.6%) Tanzania (30; 83.3%)	E4 E9 E28 E31 K25 K31 T4 T5 T6 T7 T8 T10 T12 T13 T16 T18 T21 T22 T29 T30 T31 T32 T33 T36 T38 T41 T43 T44 T45 T47 T48 T50 T51 T52 T55 T56
<i>PWL2</i> only FMB-4	3 (1.4%)	Tanzania (3; 100.0%)	T15 T25 T42

^a Number of isolates (*n* = 221).

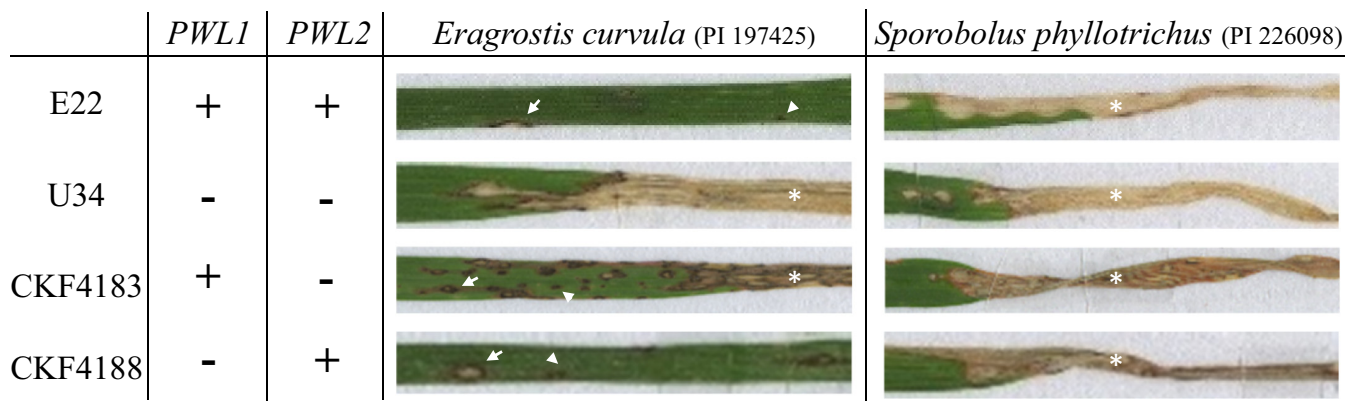


Fig. 1. Pathogenicity of finger millet blast strains on *Eragrostis curvula* and *Sporobolus phyllotrichus*. The latter was used as a susceptible control. Leaves of *Eragrostis curvula* (PI 197425) and *Sporobolus phyllotrichus* (PI 226098) at 7 days after spray inoculation with a panel of *Magnaporthe oryzae* strains; E22 and U34 are field isolates and CKF4183 and CKF4188 are transformants of U34 with *PWL1* and *PWL2*, respectively, cloned from E22. The presence or absence of *PWL1* and *PWL2* is indicated by plus (+) or minus (-), respectively. Asterisks indicate typical virulent lesions (straw-colored and shriveled leaf with merged lesions). Arrowheads indicate some avirulent lesions, and arrows indicate some isolated lesions with distinct tan centers surrounded by a darker brown margin. Consistent infection results were observed from more than eight leaves in two independent inoculations. Note that *M. oryzae* transformants carrying either *PWL1* (CKF4183) or *PWL2* (CKF4188) gained avirulence on *Eragrostis curvula*, as compared with recipient strain U34, while maintaining virulence on *S. phyllotrichus*. Bars = 0.5 cm.

lovegrass, but there was some variation among transformants; avirulent lesions were more evident in the transformant CKF4183 than the other two transformants (Fig. 1; Supplementary Table S1). While no native isolates containing solely *PWL1* (group FMB-3) or *PWL2* (group FMB-4) were tested, the expectation is these strains would yield infection results similar to those obtained with the *PWL1* and *PWL2* transformants.

PWL1- and *PWL2*-independent avirulence on weeping lovegrass.

To further explore the nature of avirulence of FMB isolates on weeping lovegrass, we tested the response of different *Eragrostis curvula* accessions to pathogens with different effector repertoires. As expected, E2-GFP (*PWL1*⁺/*PWL2*⁺) was avirulent on *Eragrostis curvula* cv. Ermelo (from Oklahoma in the United States), whereas U44 (*pwl1*⁻/*pwl2*⁻) was virulent on this cultivar (Fig. 2). This correlation between the presence of the *PWL1* and *PWL2* genes and avirulence on *Eragrostis curvula* cv. Ermelo was consistent with the results obtained with the Kenyan *Eragrostis curvula* accession PI 197425 (Fig. 1). Intriguingly, the Ugandan isolate U27, lacking both *PWL1* and *PWL2*, caused mostly avirulent lesions on *Eragrostis curvula* cv. Ermelo (Fig. 2). The lack of successful colonization of U27 and E2-GFP on *Eragrostis curvula* cv. Ermelo was not due to a lack of pathogenicity because both strains were highly virulent on the finger millet cultivar AAUFM-44 (Fig. 2). These results suggest that U27 possesses one or more *AVR* genes, other than *PWL1* and *PWL2*, which are recognized by one or more yet-to-be-characterized resistance genes in *Eragrostis curvula* cv. Ermelo.

Occurrence of additional *AVR-R* gene combinations controlling the disease response in *Eragrostis curvula* to FMB isolates was further supported by the variation found within *Eragrostis curvula* germplasm for the resistance response to FMB isolate U34 (*pwl1*⁻/*pwl2*⁻). An *Eragrostis curvula* accession from South Africa, PI 295694, displayed fewer symptoms when inoculated with U34, when compared with *Eragrostis curvula* cv. Ermelo (Fig. 3). All three *Eragrostis curvula* accessions tested in this study were resistant to E22 (*PWL1*⁺/*PWL2*⁺) (Figs. 1 and 3).

PWL1 and *PWL2* do not confer avirulence in *Sporobolus phyllotrichus* and *Eleusine tristachya*.

To test if *PWL1* and *PWL2* can confer an avirulent response against *M. oryzae* in *Eragrostis curvula*-related plant species, we inoculated another chloridoid grass, *Sporobolus phyllotrichus*, with FMB isolates as well as *PWL1* and *PWL2* transformants.

Our whole-plant spray-inoculation assays showed that both E22 (*PWL1*⁺/*PWL2*⁺) and U34 (*pwl1*⁻/*pwl2*⁻) had high infection levels on *S. phyllotrichus* (accession PI 226098) and that similar high infection levels were observed with U34 transformants carrying either *PWL1* or *PWL2* (Fig. 1). This indicates that, unlike *Eragrostis curvula* (PI 197425), *S. phyllotrichus* (PI 226098) does not recognize *PWL1* or *PWL2*.

Infection of five other chloridoid species, two of which belong to the genus *Eleusine*, with either U34 or U40, both of which lack *PWL1* and *PWL2*, showed avirulence on *Eragrostis tef* (U40), *Calamovilfa longifolia* (U34), *Dactyloctenium giganteum* (U34), and *Eleusine floccifolia* (U34), and virulence on *Eleusine tristachya* (U34) (Fig. 4). The same pathogenicity response was observed when these lines were inoculated with E2-GFP (*PWL1*⁺/*PWL2*⁺), demonstrating that *PWL1* and *PWL2* are not recognized by the *Eleusine tristachya* accession analyzed. While we cannot derive from the infection results whether *R* genes that recognize the *PWL* genes are present in the four resistant chloridoid species, we can conclude that the strains lacking the *PWL* effectors carry other effectors for which *R* genes are present in the finger millet relatives.

Discussion

Distribution of *PWL1* and *PWL2* in FMB isolates from eastern Africa.

The present study found that the 221 *Eleusine* blast isolates from eastern Africa grouped into four classes, differentiated by the absence or presence of one or both *PWL1* and *PWL2* genes. Isolates from Kenya and Uganda predominantly lacked both *PWL1* and *PWL2* (FMB-1), while the majority of Ethiopian isolates carried both genes (FMB-2) (Table 2). Around 50% of Tanzanian lines belonged to FMB-1, while the other half carried only *PWL1* (FMB-3) (Table 2). The lack of *PWL1* in Ugandan FMB isolates was also observed by Aduke et al. (2019), who classified *Eleusine* blast isolates collected from Japan, Nepal, India, and Uganda into two groups, EC-I isolates that did not contain *PWL1* and were infectious on both weeping lovegrass and finger millet and EC-II isolates that contained *PWL1* and were virulent on finger millet but avirulent on weeping lovegrass (Aduke et al. 2019). Similarly to what was observed by Aduke et al. (2019), our study shows that the FMB-1 isolates U34 and U44 (*pwl1*⁻/*pwl2*⁻) were virulent on both finger millet AAUFM-44 and *Eragrostis curvula* cv. Ermelo. The FMB-2 isolates E2-GFP and E22 (*PWL1*⁺/*PWL2*⁺), on the other hand, were avirulent on the same *Eragrostis curvula* cultivar, while they were highly virulent on finger millet. *Eragrostis curvula* originated in southern



Fig. 2. Pathogenicity of finger millet blast strains on *Eragrostis curvula* and *Eleusine coracana*. Leaves of *Eragrostis curvula* cv. Ermelo and *Eleusine coracana* cv. AAUFM-44 at 7 days after spray inoculation with E2-GFP, U27, and U44 at a concentration of 1×10^5 spores per milliliter on *Eragrostis curvula* and 1×10^4 spores per milliliter on *Eleusine coracana*. The plus (+) and minus (-) indicate, respectively, the presence or absence of *PWL1* and *PWL2*. Arrowheads indicate some of the typical avirulent lesions. Asterisks indicate typical virulent symptoms with merged lesions. Consistent infection results were observed from more than three leaves in two independent inoculations, except for U27-*Eleusine coracana*, which was tested in one experiment. Bars = 0.5 cm.

Africa and then moved northwards to eastern Africa. While the species is present in Ethiopia, our data suggest that *Eragrostis curvula* may be an alternative host to finger millet for *Eleusine* isolates in Kenya, Uganda, and some regions of Tanzania but not in Ethiopia.

We hypothesize that the presence or absence of one or both *PWL1* and *PWL2* is brought about by either the prevailing environmental conditions, co-evolution with the host, or both and that the ancestral FMB lineage carried both *PWL1* and *PWL2*. The latter is suggested by the fact that Asian (Asuke et al. 2019), Ethiopian, and about half of the Tanzanian blast isolates analyzed carried *PWL1*, either by itself or in combination with *PWL2*, and that gene loss leading to a broader host range is a more likely scenario than gene gain, which would reduce the host range. Subsequently, an adaptation strategy to survive on alternative hosts such as *Eragrostis curvula* in the absence of finger millet may have been adopted through the loss of *PWL1* and *PWL2*. Our results also show that gene loss is more likely than inactivation through the accumulation of point mutations; no variants were identified for *PWL1* or *PWL2* across the more than 50 strains tested.

Multiple mechanisms of host resistance to FMB exist in chloridoid grasses.

Previous segregation analyses showed that *PWL1* and *PWL2* determined avirulence of rice-adapted *M. oryzae* on *Eragrostis curvula* (Kang et al. 1995; Sweigard et al. 1995). Using native and transformed finger millet–adapted blast strains, we demonstrated that the mechanism of host resistance to FMB in weeping lovegrass is also governed by *PWL1* and *PWL2* and is likely the same for finger millet and rice blast. The variation seen in infection levels for different FMB-1 strains and *Eragrostis curvula* accession combinations also suggests that other genes are present in weeping lovegrass that can convey at least partial resistance to FMB isolates that lack *PWL1* and *PWL2* (Figs. 2 and 3).

However, *PWL1* and *PWL2* do not control pathogenicity on *S. phyllotrichus*, another chloridoid grass, at least not on the accession tested (PI 226098), as *PWL1* and *PWL2* transformants as well as the parental strain U34 were highly infectious on *S. phyllotrichus* accession PI 226098. This suggests that *S. phyllotrichus* lacks the genes that recognize the *PWL1* and *PWL2* effector proteins. Testing of five additional chloridoid accessions, *Eleusine tristachya*, *Eleusine floccifolia*, *C. longifolia*,

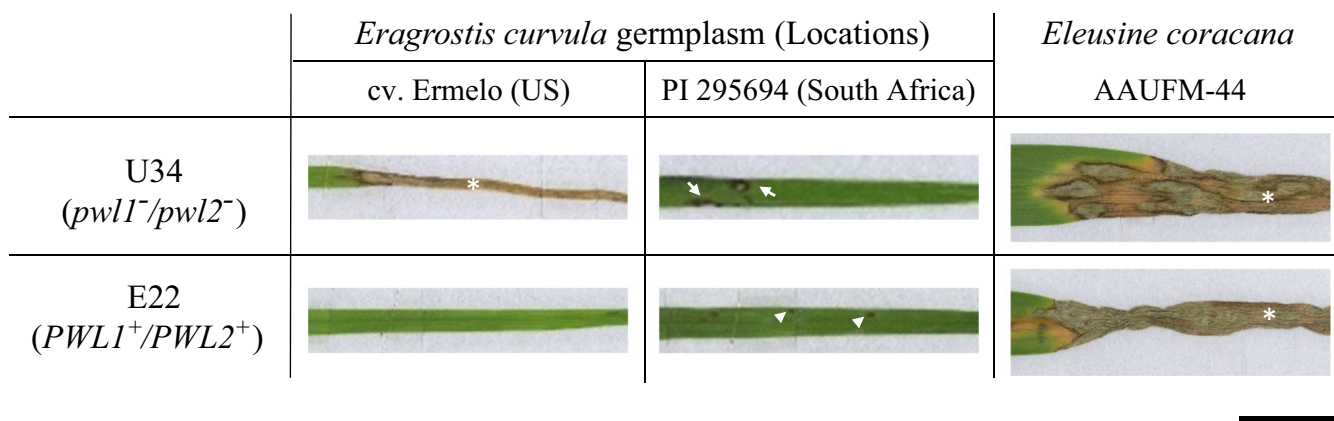


Fig. 3. *Eragrostis curvula* germplasms inoculated with U34 lacking both *PWL1* and *PWL2* or E22 carrying both genes at a concentration of 1×10^4 spores per milliliter. *Eleusine coracana* was used as a susceptible control. An asterisk indicates typical virulent symptoms with merged lesions. Arrowheads indicate some of the typical avirulent lesions, and arrows indicate some of the small isolated lesions with distinct tan centers surrounded by a darker brown margin. Consistent infection results were observed from more than three leaves in three experiments. Bar = 1 cm.

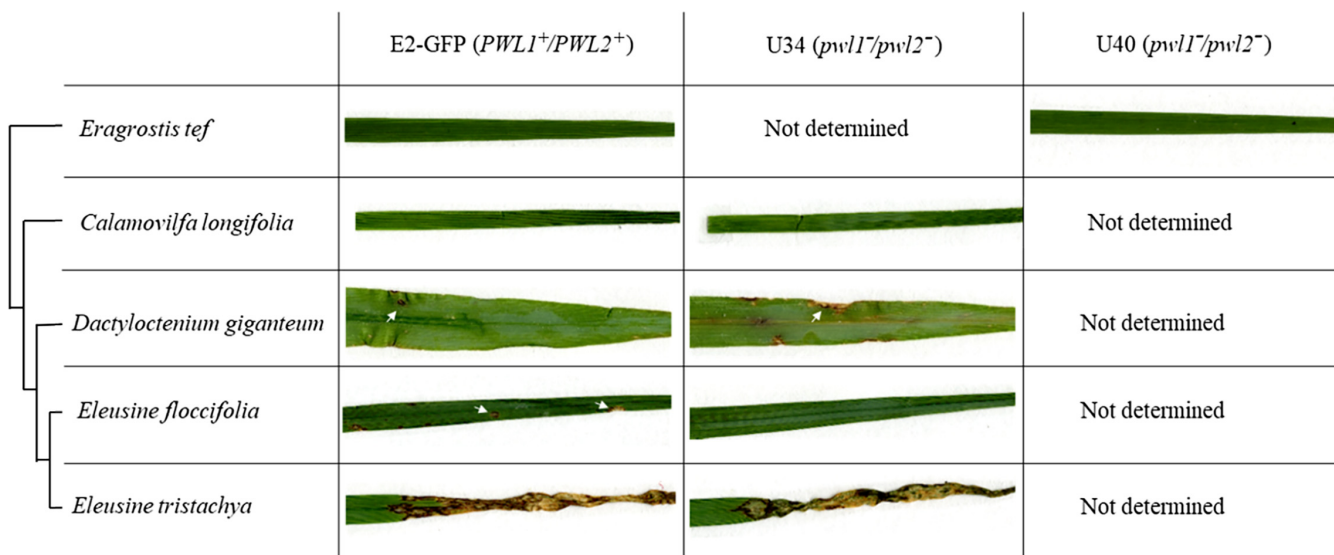


Fig. 4. Chloridoid species inoculated with finger millet blast strains carrying or lacking *PWL1* and *PWL2* with a concentration of 1×10^5 spores per milliliter. The phylogenetic relationship between the species is shown on the left hand side. Arrows indicate some of the small, isolated lesions. Asterisks indicate typical virulent symptoms with merged lesions. ‘Not determined’ indicates that the plant species was not inoculated with that particular strain in this experiment. Consistent infection results were observed from more than three leaves in one experiment.

D. giganteum, and *Eragrostis tef* with two FMB strains, one lacking *PWL1* and *PWL2* and one containing both genes, showed the same pathogenicity response, either resistance or susceptibility, to both strains. This demonstrates that the resistance genes effective to *PWL1* and *PWL2* are absent from the susceptible *Eleusine tristachya* accession tested. In the four chloridoid species that display resistant interactions, it is unknown whether *PWL1* and *PWL2* play a role in the resistance. Regardless, *R* genes, whether recognizing *PWL* effectors or other effectors in the FMB strains, must be present in those chloridoid grasses.

Importantly, our study demonstrates that, despite being considered host-specific, *M. oryzae* strains likely have alternative hosts. FMB isolates are able to infect both *Eleusine tristachya* and *S. phyllotrichus*. *Eleusine tristachya* is native to South America while *S. phyllotrichus* is native to eastern Africa. On the other hand, resistance to finger millet–adapted *M. oryzae* strains was observed in the chloridoid species *Eleusine floccifolia*, also native to eastern Africa, *C. longifolia*, native to North America, *D. giganteum*, which is found from Kenya to South Africa and in Madagascar, and *Eragrostis tef*, a cereal widely grown in Ethiopia. Based on the limited number of species analyzed, there does not appear to be a correlation between the presence of resistance in related chloridoids to finger millet–adapted *M. oryzae* strains and sympatry of the species tested with finger millet. Similarly, no obvious link was discerned between the taxonomic relatedness of the species (Peterson et al. 2010) and their resistance or lack thereof to FMB isolates (Supplementary Fig. S5).

The resistance we observed in several of the chloridoid species against finger millet infecting *M. oryzae* isolates was complete, in contrast to the resistance typically seen in finger millet accessions (Takan et al. 2012). In a recent study in *Arabidopsis*, a few susceptible transgressive segregants were found in progeny derived from intercrossing 19 parents that were resistant to white rust caused by *Albugo candida*, for which *Arabidopsis* is considered a non-host (Cevik et al. 2019). Further analysis of the segregants led to the identification of resistance genes, some of which also conferred resistance to *Albugo candida* when introduced into susceptible lines of the host species *Brassica napus* and *B. juncea* (Cevik et al. 2019). This indicated that the resistance to *Albugo candida* in *Arabidopsis* was caused by effector-triggered immunity. Similarly, the resistance of wheat to ryegrass- and oat-infecting *M. oryzae* isolates was caused by the incompatible interaction of the ryegrass blast AVR effectors PWT3 and PWT4 with the wheat resistance proteins RWT3 and RWT4. Widespread cultivation of *rwt3* wheat cultivars led to pathogenicity of ryegrass blast on wheat (Inoue et al. 2017). Our study identified the presence of at least two types of resistance in the FMB–chloridoid host system. In *Eragrostis curvula*, resistance is present against the cognate effectors *PWL1* and *PWL2*. In other chloridoid species, such as *Eleusine floccifolia*, *C. longifolia*, *D. giganteum*, and *Eragrostis tef*, resistance to finger millet–adapted *M. oryzae* is expressed in the absence of *PWL1* and *PWL2* and, hence, is targeted to as-yet-unknown AVR effectors that are present in FMB. Screening germplasm collections or intercrossed populations for susceptible genotypes will provide a way forward to genetic mapping and isolation of the genes underlying the resistance to FMB in other chloridoids. While these genes will provide novel sources of potentially durable resistance in finger millet, knowing the basis of the resistance seen in finger millet relatives will also be important for related crop species that have overlapping cultivation areas with finger millet. *Eragrostis tef*, for example, grows in sympatry with finger millet in Ethiopia but is resistant to FMB. However, *Eragrostis tef* could become vulnerable to FMB if varieties were to be bred and widely cultivated that lacked the gene or genes conferring the resistance to finger millet–adapted

blast strains or if the FMB fungus lost the corresponding AVR genes.

Conclusions.

This study confirmed that, as in rice, *PWL1*, either alone or in combination with *PWL2*, modulates the virulence of FMB fungus on *Eragrostis curvula*. Analysis of the prevalence of *PWL1* and *PWL2* across eastern Africa further showed that *Eleusine M. oryzae* isolates formed four groups based on the presence or absence of one or both *PWL1* and *PWL2*. FMB-1 isolates (lacking both genes) originated almost exclusively in Kenya and Uganda. Most Ethiopian isolates carried both *PWL1* and *PWL2* (FMB-2), while the Tanzanian lines were divided between FMB-1, FMB-3 (*PWL1* only), and FMB-4 (*PWL2* only). This suggests that FMB may use *Eragrostis curvula* as an alternative host in Kenya and Uganda but not in Ethiopia. *S. phyllotrichus*, also native to eastern Africa, may also be used as an alternative host, as the accession we tested had intermediate to high susceptibility depending on the blast isolates tested, although the resistance level was independent of the presence of *PWL1* or *PWL2*. Our study also identified resistance in species other than *Eragrostis curvula* that was not, or at least not solely, based on interaction of host resistance genes with one or both *PWL1* and *PWL2*. Elucidating the mechanisms of resistance to FMB in finger millet relatives will broaden the portfolio of resistance genes that could be introduced into finger millet to fight blast disease. Conversely, it would allow breeders to ensure that resistance is retained in other chloridoid crops that are grown in sympatry with finger millet, such as *Eragrostis tef* in Ethiopia.

Materials and Methods

Fungal strains and plant materials.

Plant accessions used for infection assays are described in Table 3. The *Eleusine M. oryzae* isolates used in infection assays are described in Table 4. This included four isolates from Uganda (U27, U34, U40, and U44), eight transformants of U34, Ethiopian isolate E22, and one laboratory strain (E2-GFP). The latter was generated by transforming Ethiopian isolate E2 with pBV126 carrying enhanced GFP under control of the *M. oryzae* ribosomal protein 27 promoter (Khang et al. 2010). *Eleusine* isolate U34 was used as the recipient for *PWL1* and *PWL2* by genetic transformation. Fungal transformants were generated using *Agrobacterium tumefaciens*–mediated transformation (Khang et al. 2006). *M. oryzae* isolates and transformants were stored dehydrated and frozen at -20°C to maintain full pathogenicity and were cultured on oatmeal agar plates at 24°C , under continuous light (Valent et al. 1991). In addition to the fungal and plant materials described above, one or both DNA samples and resequencing reads covering *PWL1* and *PWL2* from 221 *Eleusine* isolates, collected from Ethiopia, Kenya, Tanzania, and Uganda between 2015 and 2017, were made available to this study for *PWL1* and *PWL2* distribution analysis.

Table 3. Plant accessions used for infection assays

Species	Accession	Origin
<i>Calamovilfa longifolia</i>	PI 477995	United States
<i>Dactyloctenium giganteum</i>	PI 364504	South Africa
<i>Eleusine coracana</i> subsp. <i>coracana</i>	AAUFM-44	Ethiopia
<i>Eleusine floccifolia</i>	PI 196853	Ethiopia
<i>Eleusine tristachya</i>	PI 309950	Brazil
<i>Eragrostis curvula</i>	Ermelo	United States
<i>Eragrostis curvula</i>	PI 197425	Kenya
<i>Eragrostis curvula</i>	PI 295694	South Africa
<i>Eragrostis tef</i>	Tsedey (DZ-Cr-37)	Ethiopia
<i>Sporobolus phyllotrichus</i>	PI 226098	Kenya

Cloning of *PWL1* and *PWL2* and their transformation in FMB strain U34.

PWL1 and *PWL2* were individually amplified from genomic DNA of *Eleusine* isolate E22 with the primers listed in Table 1 (E22_PWL1_F and E22_PWL1_R for *PWL1* amplification, E22_PWL2_F and E22_PWL2_R for *PWL2* amplification). The 1.13-kb *PWL1* fragment consisted of 444 bp of coding sequence (CDS), and 459 and 230 bp of upstream and downstream sequence from the start and stop codons, respectively. The 1.37-kb *PWL2* fragment consisted of 438 bp of CDS and 725 and 207 bp of upstream and downstream sequence, respectively. PCR was performed in 25 μ l containing 25 ng of genomic DNA, 1 \times Q5 reaction buffer, 200 μ M dNTPs, 0.5 μ M forward primer, 0.5 μ M reverse primer, and 0.02 U of Q5 high-fidelity DNA polymerase (NEB) per microliter. Reaction conditions were 30 cycles of denaturation at 98°C for 10 s, annealing at 66°C for 30 s, and extension at 72°C for 2 min. The resulting PCR products of *PWL1* and *PWL2* were individually cloned into the pMiniT PCR vector (NEB) to generate plasmids pHM1 and pHM2, respectively. *PWL1* and *PWL2* genes in these plasmids were verified by Sanger sequencing (GENEWIZ). Using *Bam*HI and *Xho*I restriction enzymes, the *PWL1* insert in pHM1 and the *PWL2* insert in pHM2 were excised and were subsequently cloned into the *Bam*HI and *Sal*I sites of pBV1 (Mullins et al. 2001) to generate plasmids pCK2104 and pCK2106, respectively. pCK2104 (carrying *PWL1*) and pCK2106 (carrying *PWL2*) were separately transformed into *Agrobacterium tumefaciens* EHA105 competent cells and were then transformed into *Eleusine M. oryzae* isolate U34, as described by Khang et al. (2006).

Infection assays.

For infection assays, spores from each fungal culture were harvested in 0.25% sterilized gelatin solution, and the spore concentrations were adjusted to 1.0×10^4 or 1.0×10^5 spores per milliliter. Five to 15 seeds of each accession (Table 3), depending on the germination rate, were sown in soil in labeled pots and were placed in a growth chamber at 28°C and 80% relative humidity. Inoculations were performed on 14-day-old seedlings placed inside plastic bags. Each bagged seedling was sprayed with 5 ml of inoculum, using an artist's air brush with compressed air at 20 psi. Bags were then sealed to maintain humidity to support infection at room temperature for 24 h, after which the bags were removed and the plants were transferred to a growth chamber. Plants sprayed with the gelatin suspension without spores were used as negative controls. Seven days

Table 4. *Magnaporthe oryzae* isolates from finger millet used in infection assays

Strain	Origin	<i>PWL1</i> ^a	<i>PWL2</i> ^a
E2-GFP	Ethiopian isolate E2 transformed with enhanced green fluorescent protein	+	+
E22	Ethiopia	+	+
U27	Uganda	–	–
U34	Uganda	–	–
U40	Uganda	–	–
U44	Uganda	–	–
CKF4183	U34 transformed with <i>PWL1</i>	+	–
CKF4184	U34 transformed with <i>PWL1</i>	+	–
CKF4185	U34 transformed with <i>PWL1</i>	+	–
CKF4186	U34 transformed with <i>PWL2</i>	–	+
CKF4187	U34 transformed with <i>PWL2</i>	–	+
CKF4188	U34 transformed with <i>PWL2</i>	–	+
CKF4192	U34 transformed with <i>PWL2</i>	–	+
CKF4193	U34 transformed with <i>PWL2</i>	–	+

^a Negative and positive symbols indicate absence and presence, respectively, of either *PWL1* or *PWL2*.

postinoculation, leaves were harvested, scored, and scanned. Severity of infection was rated according to six progressive grades from 0 to 5 with 0 = no visible symptoms, 1 = pin-point spots, 2 = small lesions (<1.5 mm), 3 = intermediate sized lesions (<3 mm), 4 = large lesions typical of blast infection, and 5 = complete shriveling of leaf blades (Supplementary Fig. S6). Raw data generated from more than three leaves in one or two independent inoculations were averaged (Supplementary Table S1).

Presence of and single nucleotide polymorphism variation in *PWL1* and *PWL2* across FMB isolates.

PCR primers used to determine the presence or absence of the two *PWL* genes (*PWL1_CDS_F*, *PWL1_CDS_R*, *PWL2_CDS_F*, and *PWL2_CDS_R*) are listed in Table 1. These primers were designed to amplify the *PWL1* ORF of 444 bp and *PWL2* ORF of 438 bp, respectively. Reaction conditions were 35 cycles of denaturation at 94°C for 30 s, annealing at 62°C for 30 s, and extension at 72°C for 5 min. A 3- μ l sample from each PCR reaction was run on a 1% (wt/vol) agarose gel.

Illumina resequencing reads for 208 FMB isolates were aligned against the *PWL1* and *PWL2* gene sequences cloned from isolate E22 with Bowtie2 (Langmead and Salzberg 2012), using the parameters ‘–maxin 900 –no-discordant –no-mixed’. *PWL1* and *PWL2* were considered present if $\geq 90\%$ of their coding region was covered by Illumina reads to a depth $\geq 2 \times$.

Data availability.

The sequence data from this study can be obtained from GenBank EMBL databases under accession numbers MT669814 for *PWL1* and MT669815 for *PWL2*.

Literature Cited

- Asuke, S., Tanaka, M., Hyon, G., Inoue, Y., Thi, T., Vy, P., Niwamoto, D., Nakayashiki, H., and Tosa, Y. 2019. Evolution of an *Eleusine*-specific subgroup of *Pyricularia oryzae* through a gain of an avirulence gene. *Mol. Plant-Microbe Interact.* 33:153-165.
- Böhnert, H. U., Fudal, I., Dioh, W., Tharreau, D., Nottoghem, J. L., and Lebrun, M. H. 2004. A putative polyketide synthase/peptide synthetase from *Magnaporthe grisea* signals pathogen attack to resistant rice. *Plant Cell* 16:2499-2513.
- Cevik, V., Boutrot, F., Apel, W., Robert-Seilanianz, A., Furzer, O. J., Redkar, A., Castel, B., Kover, P. X., Prince, D. C., Holub, E. B., and Jones, J. D. G. 2019. Transgressive segregation reveals mechanisms of *Arabidopsis* immunity to *Brassica*-infecting races of white rust (*Albugo candida*). *Proc. Natl. Acad. Sci. U.S.A.* 116:2767-2773.
- Chuma, I., Isobe, C., Hotta, Y., Ibaragi, K., Futamata, N., and Kusaba, M. 2011. Multiple translocation of the *AVR-Pita* effector gene among chromosomes of the rice blast fungus *Magnaporthe oryzae* and related species. *PLoS Pathog.* 7:e1002147.
- De Wit, P. J. G. M., Mehrabi, R., Van Den Burg, H. A., and Stergiopoulos, I. 2009. Fungal effector proteins: Past, present and future. *Mol. Plant Pathol.* 10:735-747.
- Gómez Luciano, L. B., Tsai, I. J., Chuma, I., Tosa, Y., Chen, Y. H., Li, J. Y., Li, M. Y., Lu, M. J., Nakayashiki, H., and Li, W. H. 2019. Blast fungal genomes show frequent chromosomal changes, gene gains and losses, and effector gene turnover. *Mol. Biol. Evol.* 36:1148-1161.
- Inoue, Y., Vy, T. T. P., Yoshida, K., Asano, H., Mitsuoka, C., Asuke, S., Anh, V. L., Cumagun, C. J. R., Chuma, I., Terauchi, R., Kato, K., Mitchell, T., Valent, B., Farman, M., and Tosa, Y. 2017. Evolution of the wheat blast fungus through functional losses in a host specificity determinant. *Science* 357:80-83.
- Jones, K., Zhu, J., Jenkinson, C. B., Kim, D. W., and Khang, C. H. 2021. Disruption of the interfacial membrane leads to *Magnaporthe oryzae* effector re-location and lifestyle switch during rice blast disease. *Front. Cell Dev. Biol.* 9:681734.
- Kang, S., Sweigard, J. A., and Valent, B. 1995. The *PWL* host specificity gene family in the blast fungus *Magnaporthe grisea*. *Mol. Plant-Microbe Interact.* 8:939-948.
- Kato, H., Yamamoto, M., Yamaguchi-ozaki, T., Kadouchi, H., Iwamoto, Y., Nakayashiki, H., Tosa, Y., Mayama, S., and Mori, N. 2000. Pathogenicity,

- mating ability and DNA restriction fragment length polymorphisms of *Pyricularia* populations isolated from *Gramineae*, *Bambusideae* and *Zingiberaceae* plants. *J. Gen. Plant Pathol.* 66:30-47.
- Khang, C. H., Berruyer, R., Giraldo, M. C., Kankanala, P., Park, S.-Y., Czymbek, K., Kang, S., and Valent, B. 2010. Translocation of *Magnaporthe oryzae* effectors into rice cells and their subsequent cell-to-cell movement. *Plant Cell* 22:1388-1403.
- Khang, C. H., Park, S., Lee, Y., Valent, B., and Kang, S. 2008. Genome organization and evolution of the AVR-*Pita* avirulence gene family in the *Magnaporthe grisea* species complex. *Mol. Plant-Microbe Interact.* 21:658-670.
- Khang, C. H., Park, S. Y., Rho, H. S., Lee, Y. H., and Kang, S. 2006. Filamentous fungi (*Magnaporthe grisea* and *Fusarium oxysporum*). *Methods Mol. Biol.* 344:403-420.
- Langmead, B., and Salzberg, S. L. 2012. Fast gapped-read alignment with Bowtie 2. *Nat. Methods* 9:357-359.
- Li, W., Wang, B., Wu, J., Lu, G., Hu, Y., Zhang, X., Zhang, Z., Zhao, Q., Feng, Q., Zhang, H., Wang, Z., Wang, G. L., Han, B., Wang, Z., and Zhou, B. 2009. The *Magnaporthe oryzae* avirulence gene *AvrPiz-t* encodes a predicted secreted protein that triggers the immunity in rice mediated by the blast resistance gene *Piz-t*. *Mol. Plant-Microbe Interact.* 22:411-420.
- Mullins, E. D., Chen, X., Romaine, P., Raina, R., Geiser, D. M., and Kang, S. 2001. *Agrobacterium*-mediated transformation of *Fusarium oxysporum*: An efficient tool for insertional mutagenesis and gene transfer. *Phytopathology* 91:173-180.
- Orbach, M. J., Farrall, L., Sweigard, J. A., Chumley, F. G., and Valent, B. 2000. A telomeric avirulence gene determines efficacy for the rice blast resistance gene *Pi-ta*. *Plant Cell* 12:2019-2032.
- Park, J. Y., Jin, J., Lee, Y. W., Kang, S., and Lee, Y. H. 2009. Rice blast fungus (*Magnaporthe oryzae*) infects *Arabidopsis* via a mechanism distinct from that required for the infection of rice. *Plant Physiol.* 149:474-486.
- Peterson, P. M., Romaschenko, K., and Johnson, G. 2010. A classification of the *Chloridoideae* (*Poaceae*) based on multi-gene phylogenetic trees. *Mol. Phylogenet. Evol.* 55:580-98.
- Ramakrishnan, M., Ceasa, S. A., Durairamian, V., Vinod, K. K., Kalpana, K., Al-Dhabi, N. A., and Ignacimuthu, S. 2016. Tracing QTLs for leaf blast resistance and agronomic performance of finger millet (*Eleusine coracana* (L.) *gaertn.*) genotypes through association mapping and *in silico* comparative genomics analyses. *PLoS One* 11:1-23.
- Ribot, C., Césari, S., Abidi, I., Chalvon, V., Bournaud, C., Vallet, J., Lebrun, M. H., Morel, J. B., and Kroj, T. 2013. The *Magnaporthe oryzae* effector AVR1-CO39 is translocated into rice cells independently of a fungal-derived machinery. *Plant J.* 74:1-12.
- Senthil, R., Shanmugapackiam, S., and Raguchander, T. 2012. Evaluation of biocontrol agents and fungicides for the management of blast disease of finger millet. *J. Mycol. Plant Pathol.* 42:454-458.
- Sone, T., Takeuchi, S., Miki, S., Satoh, Y., Ohtsuka, K., Abe, A., and Asano, K. 2013. Homologous recombination causes the spontaneous deletion of AVR-*Pia* in *Magnaporthe oryzae*. *FEMS Microbiol. Lett.* 339:102-109.
- Sweigard, J. A., Carroll, A. M., Kang, S., Farrall, L., Chumley, F. G., and Valent, B. 1995. Identification, cloning, and characterization of *PWL2*, a gene for host species specificity in the rice blast fungus. *Plant Cell* 7:1221-1233.
- Takan, J. P., Chipili, J., Muthumeenakshi, S., Talbot, N. J., Manyasa, E. O., Bandyopadhyay, R., Sere, Y., Nutsugah, S. K., Talhinhas, P., Hossain, M., Brown, A. E., and Sreenivasaprasad, S. 2012. *Magnaporthe oryzae* populations adapted to finger millet and rice exhibit distinctive patterns of genetic diversity, sexuality and host interaction. *Mol. Biotechnol.* 50:145-158.
- Teufel, F., Almagro Armenteros, J. J., Johansen, A. R., Gislason, M. H., Pihl, S. I., Tsirigos, K. D., Winther, O., Brunak, S., von Heijne, G., and Nielsen, H. 2022. SignalP 6.0 predicts all five types of signal peptides using protein language models. *Nat. Biotechnol.* 40:1023-1025.
- Thon, M. R., Pan, H., Diener, S., Papalas, J., Taro, A., Mitchell, T. K., and Dean, R. A. 2006. The role of transposable element clusters in genome evolution and loss of synteny in the rice blast fungus *Magnaporthe oryzae*. *Genome Biol.* 7:R16.
- Valent, B., Farrall, L., and Chumley, F. G. 1991. *Magnaporthe grisea* genes for pathogenicity and virulence identified through a series of backcrosses. *Genetics* 127:87-101.
- Valent, B., and Khang, C. H. 2010. Recent advances in rice blast effector research. *Curr. Opin. Plant Biol.* 13:434-441.
- Valent, B., Mark, S. C., Weaver, C. G., and Chumley, F. G. 1986. Genetic studies of fertility and pathogenicity in *Magnaporthe grisea* (*Pyricularia oryzae*). *Iowa State J. Res.* 60:569-594.
- Vleeshouwers, V. G. A. A., and Oliver, R. P. 2014. Effectors as tools in disease resistance breeding against biotrophic, hemibiotrophic, and necrotrophic plant pathogens. *Mol. Plant-Microbe Interact.* 27:196-206.
- Wang, B., Ebbole, D. J., and Wang, Z. 2017. The arms race between *Magnaporthe oryzae* and rice: Diversity and interaction of *Avr* and *R* genes. *J. Integr. Agric.* 16:2746-2760.
- Yoshida, K., Saitoh, H., Fujisawa, S., Kanzaki, H., Matsumura, H., Yoshida, K., Tosa, Y., Chuma, I., Takano, Y., Win, J., Kamoun, S., and Terauchi, R. 2009. Association genetics reveals three novel avirulence genes from the rice blast fungal pathogen *Magnaporthe oryzae*. *Plant Cell* 21:1573-1591.
- Yoshida, K., Saunders, D. G. O., Mitsuoka, C., Natsume, S., Kosugi, S., Saitoh, H., Inoue, Y., Chuma, I., Tosa, Y., Cano, L. M., Kamoun, S., and Terauchi, R. 2016. Host specialization of the blast fungus *Magnaporthe oryzae* is associated with dynamic gain and loss of genes linked to transposable elements. *BMC Genomics* 17:1-18.
- Zhang, S., and Xu, J. R. 2014. Effectors and effector delivery in *Magnaporthe oryzae*. *PLoS Pathog.* 10:1-4.

Maize Phytocytokines Modulate Pro-Survival Host Responses and Pathogen Resistance

Maurice Koenig,¹ Daniel Moser,^{1,2} Julian Leusner,¹ Jasper R. L. Depotter,¹ Gunther Doehlemann,^{1,2,†} and Johana Misas Villamil^{1,2,†}

¹ Institute for Plant Sciences, University of Cologne, Cologne, Germany

² Cluster of Excellence on Plant Sciences (CEPLAS), University of Cologne, Cologne, Germany

Accepted for publication 23 April 2023.

Phytocytokines are signaling peptides that alert plant cells of danger. However, the downstream responses triggered by phytocytokines and their effect on plant survival are still largely unknown. Here, we have identified three biologically active maize orthologues of phytocytokines previously described in other plants. The maize phytocytokines show common features with microbe-associated molecular patterns (MAMPs), including the induction of immune-related genes and activation of papain-like cysteine proteases. In contrast to MAMPs, phytocytokines do not promote cell death in the presence of wounding. In infection assays with two fungal pathogens, we found that phytocytokines affect the development of disease symptoms, likely due to the activation of phytohormonal pathways. Collectively, our results show that phytocytokines and MAMPs trigger unique and antagonistic features of immunity. We propose a model in which phytocytokines activate immune responses partially similar to MAMPs but, in contrast to microbial signals, they act as danger and survival molecules to the surrounding cells. Future studies will focus on the components determining the divergence of signaling outputs upon phytocytokine activation.

Keywords: cell death, immune signaling, MAMPs, phytocytokines, PLCPs, PR genes

To recognize microorganisms, plants have evolved a diverse range of pattern recognition receptors (PRRs) that detect conserved patterns characteristic of infection. These PRRs can detect microbe-associated molecular patterns (MAMPs) or

damage-associated molecular patterns (DAMPs) (Peng et al. 2018; Saijo et al. 2018). MAMPs can be microbial proteins, polysaccharides, peptidoglycan, lipids, or other conserved molecules (Boller and Felix 2009; Boller and Flury 2012). A well-known MAMP is the conserved 22–amino acid peptide of bacterial flagellin (flg22), which is recognized by the leucine-rich repeat receptor-like kinase (LRR-RLK) FLAGELLIN SENSITIVE (FLS2) (Chinchilla et al. 2006). The detection of MAMPs triggers defense responses leading to MAMP-triggered immunity (MTI) (Peng et al. 2018). MTI defense response includes an increase of cytosolic Ca²⁺, production of apoplastic reactive oxygen species (ROS), and mitogen-activated protein kinase (MAPK) cascade activation (Saijo et al. 2018). These signals are quickly followed by the synthesis of phytohormones such as ethylene (ET) and salicylic acid (SA) (Boller and Felix 2009). Finally, hormonal activation induces stomatal closure, callose deposition, as well as transcriptional and metabolic reprogramming (Boller and Felix 2009; Saijo et al. 2018).

In contrast to MAMPs, DAMPs are plant-derived peptides, sugars, extracellular DNA, or other molecules that are passively released upon leakage of damaged cells into the apoplast or after degradation by microbial enzymes (Gust et al. 2017; Hou et al. 2019a; Li et al. 2020). Defense responses to DAMPs are thought to protect against mechanical or cellular damage triggering defense responses similar to MTI (Hou et al. 2019a). One example of a cell wall–derived DAMP are oligogalacturonides (OGs). These are fragments of the pectin polysaccharide homogalacturonan, a linear polymer of α -1-4–linked galacturonic acid, that assists in maintaining cell-wall integrity (Pontiggia et al. 2020). OGs can be released mechanically or by pathogen-secreted hydrolytic enzymes and can be recognized by the receptor wall-associated receptor kinase 1 (WAK1) (Brutus et al. 2010; Decreux and Messiaen 2005; Denoux et al. 2008; Pontiggia et al. 2020).

Endogenous signaling peptides were previously classified as DAMPs, but recently “danger signals” have been re-classified into molecules passively released (classical DAMPs) as well as phytocytokines, which are plant elicitor peptides being processed or secreted upon danger (Gust et al. 2017; Luo 2012). Phytocytokines are divided into two classes, depending on whether the precursor protein (propeptide) contains a signal peptide or not. The majority of phytocytokines identified to date belong to the secreted elicitor peptides (Hou et al. 2021; Li et al. 2020), including hydroxyproline-rich systemins (HypSys) (Chen et al. 2008), PAMP-induced secreted peptide 1 (PIP1) and PIP2 (Hou et al. 2014), serine-rich endogenous peptide 12 (SCOOP12) (Gully et al. 2019), phytosulfokines (PSKs) (Amano et al. 2007), plant peptide containing sulfated tyrosine 1 (PSY1) (Amano et al. 2007), inflorescence deficient in abscission (IDA) and

[†]Corresponding authors: J. Misas Villamil; jmisas@uni-koeln.de, and G. Doehlemann; gdoehlemann@uni-koeln.de

M. Koenig and D. Moser contributed equally.

Funding: We acknowledge support from the Cluster of Excellence on Plant Sciences (CEPLAS) funded by the Deutsche Forschungsgemeinschaft (DFG, German Research Foundation) under Germany’s Excellence Strategy, EXC 2048/1, project ID 390686111. Our research is funded by the DFG through SFB1403 (project number 414786233) and DFG project DO 1421/5-2. J. R. L. Depotter was supported by the Research Fellowship Programme for Postdoctoral Researchers of the Alexander von Humboldt-Stiftung.

e-Xtra: Supplementary material is available online.

The author(s) declare no conflict of interest.



Copyright © 2023 The Author(s). This is an open access article distributed under the CC BY-NC-ND 4.0 International license.

IDA-LIKE 6 (IDL6) (Butenko et al. 2003), root meristem growth factors (RGFs) and GOLVENS (GLVs) (Stegmann et al. 2022), immune-related peptide (IRP) (Wang et al. 2020), catabolite activator protein (CAP)-derived peptide (CAPE) (Chien et al. 2015), and rapid alkalization factors (RALFs) (Stegmann et al. 2017). On the contrary, systemin (McGurl et al. 1992), plant elicitor peptides (PEPs) (Huffaker et al. 2006, 2011; Nakaminami et al. 2018; Yamaguchi et al. 2011), and the *Zea mays* immune signaling peptide 1 (Zip1) (Ziemann et al. 2018) belong to the non-secreted phytochemicals (Hou et al. 2021). In contrast to DAMPs, phytochemicals are quickly transcriptionally activated, produced as propeptides and, then, the signaling peptide is actively released by plant proteases during pathogen attack or wounding. For instance, the plant elicitor peptide 1 (PEP1) is released within minutes from its precursor, ProPEP1, upon wounding of plant cells (Huffaker et al. 2006, 2011). Wounding triggers Ca^{2+} accumulation in the cytosol activating the plant protease METACASPASE 4 (MC4), which releases PEP1 from the vacuolar membrane into the extracellular space via an unknown mechanism, promoting the recognition by the bystander cells via the LRR-RLK cell surface receptors PEPR1 and PEPR2 (Hander et al. 2019; Yamaguchi et al. 2006). In addition to their role as signaling molecules in immunity, phytochemicals can also modulate developmental processes and act as cell-to-cell communication signals (Rzemieniewski and Stegmann 2022).

Conservation of phytochemicals across different plant species can be very low on the sequence level and it is rarely studied on the functional level. Some phytochemicals, such as RALFs and PEPs, are ubiquitously found in many plant species (Gust et al. 2017). Some other phytochemicals have been identified in most species of a family, such as systemin, which is only present in Solanaceae or is IRP-specific for Poacea (Li et al. 2020; Ryan and Pearce 2003). Still, others have been specifically found in one species, such as Zip1, which is specific for *Z. mays* and its wild ancestor teosinte (Depotter et al. 2022). An evolutionary arms race might have led to a sequence diversification of some phytochemicals, and it remains largely unknown if signaling peptides found in dicots also function similarly in monocots.

The plant response against exogenous and endogenous danger signals and the downstream responses, such as cell death provoked by recognition of these molecules, is a central question of our study. Using a bioinformatics pipeline, we aimed to identify maize orthologues of phytochemicals described in other species to be involved in plant immunity. We then addressed the bioactivity of candidate peptides and identified three new maize phytochemicals with functions in immune signaling and pathogen resistance. We found that maize phytochemicals trigger overlapping signaling pathways with MAMPs, but they also show unique features, such as the arrest of cell death in the co-occurrence of wounding. In summary, our study reveals that the perception of phytochemicals and MAMPs leads to distinct outcomes in plant immunity. In contrast to MAMPs, which promote cell death in the presence of wounding, phytochemicals act as danger signals but do not contribute to regulated cell death.

Results

Mining the maize genome for small signaling peptides

A literature search was performed to identify signaling peptides that are involved in plant immunity. Eighteen immune-related propeptides were found in monocots and dicots, from which 10 of 18 sequences belong to *Arabidopsis thaliana* (Table 1). The GLV2 peptide (Stegmann et al. 2022) was published during the preparation of this manuscript and, thus, it could not be included in our analysis. To identify putative peptide orthologues in maize, a database containing 78 predicted plant proteomes, including 31 monocots, 43 dicots, and four

from other phyla was generated (Supplementary Table S1). A search in this database was performed, using a position-specific iterative Basic Local Alignment Search Tool (psiBLAST), due to its sensitivity and capacity to find orthologues with lower local sequence similarity (Altschul et al. 1997). These 78 proteomes were selected to generate a position-specific score matrix covering as much proteome diversity as possible for the psiBLAST search, to identify orthologues between very distantly related species (e.g., between *A. thaliana* and *Z. mays*). In addition, a BLASTp search (Altschul et al. 1990) was performed to compare to the psiBLAST search results. After the removal of low quality (protein identities <10% and query coverage <25%) and redundant entries, the best-hit propeptide per organism was selected for further analysis, yielding a total of 964 pre-filtered candidates (Supplementary Fig. S1). Notably, the psiBLAST searches resulted in more hits compared with BLASTp searches (Supplementary Fig. S2), confirming that an iterative search can improve the sensitivity of a BLASTp to find distant orthologues. The majority of the psiBLAST searches resulted in 33 to 79 hits per queried propeptide (e.g., OsProIRP: 33, AtPrePIP1: 68, and AtProPEP1: 60 [Supplementary Fig. S1, initial filtering]). Interestingly, only a few or no hits were found in searches for the propeptides of GmProPEP890, GmProPEP914, AtProSCOOP12, and ProZip1 (Supplementary Fig. S1, length filtering), indicating that orthologues of these propeptides are encoded only in a small number of genomes. To reduce the number of false-positive hits, sequences with low sequence length similarity to the query (1.5 times longer or shorter) were removed. This filtering affected mostly hits with sequence identities below 30%, especially hits for NtPreproHypSys and SIProsystemin (Supplementary Fig. S1, length filtering). Afterward, all hits were aligned with CLUSTAL Omega (Goujon et al. 2010) and putative peptides were identified by alignment. The similarity to the queried peptide (motif score) was calculated based on the alignment of the discovered peptide to the queried peptide, using a BLOSUM62 matrix (Henikoff and Henikoff 1992) and the self-alignment of the queried peptides as reference to account for differing peptide lengths. Hits with a motif score below 10% were removed, since this was the score at which ZmPEP1 was found, via our pipeline, with AtPEP1 as a query sequence (Supplementary Fig. S1, iterative motif filtering).

To compare whether certain peptide orthologues were restricted to specific phylogenetic groups, the presence or absence of peptides in a subset of species was investigated. Ten proteomes of monocots and 13 proteomes of dicots were selected as representative crops and common plant model species. Two major clades, with 0.3 and 0.11 amino acid substitutions per site, were generated, containing the monocots (dark blue) and the dicots (light blue) (Fig. 1A). Putative orthologues of some peptides, including AtRALF23, AtPSK1, AtPIP1, and AtPSY1, were found in most monocots and dicots. For a second group, orthologues of AtPEP1, AtGRI, AtPEP3, AtPIP2, and AtPEP2 were only found in dicots. Orthologue searches for ZmPEP1 and OsIRP resulted in peptide motifs mostly specific for monocots and Zip1, NtHypSys, SISystemin, SICAPE1, GmPEP890, GmPEP914, and AtSCOOP12 appeared to be species-specific (Fig. 1B). Although ZmPEP1 and AtPEP1 showed certain similarities between their pathogenesis-related (PR)-rich N terminus and GQHN-rich C terminus, the motif score of the *Z. mays* orthologue of AtPEP1 was 10%, while, in the reverse search using psiBLAST, the orthologues of ZmPEP1 could not even be identified in *A. thaliana*. (Supplementary Fig. S3).

Altogether, six *Z. mays* phytochemical candidates, ZmIRP, ZmPIP1, ZmPSK1, ZmPEP1, ZmRALF23, and ZmPSY1, were identified as orthologues in our analysis (Table 2). All orthologues, excluding ZmPSY1 and ZmPEP1, showed strong motif conservation across all tested species, suggesting an

evolutionary diversification for these two peptides (Supplementary Fig. S4). The sequences of ZmRALF23 and ZmPEP1 have been previously described (Campbell and Turner 2017; Huffaker et al. 2011). The identified sequence of ZmPSY1 has a motif score of 37% compared with its orthologue in *A. thaliana*, whereas the sequences for ZmIRP, ZmPIP1, and ZmPSK1 have a 42, 74, and 100% motif score, respectively, towards the described orthologue (Fig. 1). To further characterize the biological function of the *Z. mays* phytocytokine candidates, the sequences of ZmIRP (GTDSWLESGVGMILTQLLLGAK), N-terminal extended ZmPSK1e (AHTDYIYTQ, non-sulfated), and ZmPIP1 (RLPAGPSPKGPGRH, without hydroxylation) were selected, due to their higher sequence similarity to the original peptide sequence and conservation motif. For further analysis, we decided to use the extended ZmPSK1e peptide, which contains the canonical five PSK1 amino acids (YIYTQ) but also four conserved amino acids at its N terminal (AHTD) (Supplementary Fig. S4).

Maize phytocytokines trigger immune responses

To investigate the potential role of ZmIRP, ZmPSK1e, and ZmPIP1 in maize, we syringe-infiltrated chemically synthesized peptides into maize leaves and tested for PR gene expression 24 h postinfiltration (hpi) as a readout for the activation of the immune response (Dolezal et al. 2014; Glazebrook 2005; Ray et al. 2016; van der Linde et al. 2012). As a positive control, the previously identified maize phytocytokine Zip1 (Ziemann et al. 2018) was used. As a negative control, we included the maize apoplastic peptide (MAP1) (formerly described as DAMP1), which was

previously shown to not trigger PR gene expression in maize (Ziemann et al. 2018). In parallel, the known MAMPs, flg22 and chitin, were used to compare the elicitation of the immune response. Both flg22 and chitin induced a significant upregulation of all tested PR genes, confirming the elicitation of a typical MAMP-immune response in our experimental conditions. The expression of PR3, PR4, PR5, and PR10.1 was significantly up-regulated in comparison with mock after treatments with ZmIRP, ZmPSK1e, and ZmPIP1 and Zip1 (Fig. 2A, B, and D; Supplementary Fig. S5). PRm6b expression was significantly induced only after ZmPSK1e and Zip1 treatments (Fig. 2C). In contrast, MAP1 did not cause a significant induction of any of the tested PR genes (Fig. 2A to D). Besides, we tested if sulfonation of PSK1 enhances PR gene expression by comparing the canonical PSK1 sequence (YIYTQ) sulfonated in tyrosines of positions 1 and 4 to our unmodified ZmPSK1e. PR gene expression was triggered with both peptides and no differences in the magnitude of the PR gene expression was observed (Supplementary Fig. S6). Together, these results show that ZmIRP, ZmPSK1e, and ZmPIP1 trigger defense gene expression in maize leaves.

Papain-like cysteine proteases (PLCPs) are hubs in maize immunity (Misas-Villamil et al. 2016). Therefore, we tested the activation of PLCPs after treatment with the newly identified phytocytokines in comparison with the MAMPs, flg22, and chitin. Total extracts of treated maize leaves were labeled with the activity-based probe DCG04-Cy5 for 3 h. DCG04-Cy5 is a fluorescently tagged derivative of E-64 that binds covalently and irreversibly to the active site of PLCPs and serves to monitor the availability of active sites in complex proteomes (Greenbaum

Table 1. Propeptides used in the BLAST search and their properties

Propeptide	Identifier	Organism	Protein/peptide length	SP ^a	Peptide sequence	Source
ProIRP	Os04t0352066-00	<i>Oryza sativa</i>	66/20	Y	GEGWLEDGIGMVVDMLGELK	Wang et al. 2020
PrePIP1	AT4G28460.1	<i>Arabidopsis thaliana</i>	72/13	N	RLASGSPSRGRGH	Hou et al. 2014
PrePIP2	AT4G37290.1	<i>Arabidopsis thaliana</i>	84/15	Y	RFVKHSGPSPSGPGH	Hou et al. 2014
Prepro-HypSys	sp Q93WP8 HSYA_TOBAC	<i>Nicotiana tabacum</i>	165/18	Y	RGANLPOOSOASSOOSKE	Chen et al. 2008
ProCAPE1	sp P04284 PR06_SOLLC	<i>Solanum lycopersicum</i>	228/11	Y	PDAGLASRAQN	Chien et al. 2015
ProGRI	NP_175721.1	<i>Arabidopsis thaliana</i>	168/20	Y	KTRLLVSHYKKIKKGMRCHV	Wrzaczek et al. 2009
ProPEP1	NP_569001.1	<i>Arabidopsis thaliana</i>	92/23	N	ATKVKAKQRGKEKVVSSGRP GQHN	Huffaker et al. 2006
ProPEP2	NP_569000.1	<i>Arabidopsis thaliana</i>	109/36	N	DNKAKSKKRDKKPKSSGRPGQ TNSVPNAAIQVYKED	Nakaminami et al. 2018
ProPEP3	NP_569002.1	<i>Arabidopsis thaliana</i>	96/23	N	EIKARGKNTKPTPSSGKG GKHN	Nakaminami et al. 2018
ProPEP890	sp K7LFIJ0.2 PP890_SOYBN	<i>Glycine max</i>	52/8	N	DLPRGGNY	Yamaguchi et al. 2011
ProPEP914	sp K7LSB9.1 PP914_SOYBN	<i>Glycine max</i>	52/8	N	DHPRGGNY	Yamaguchi et al. 2011
ProRALF23	NP_566555.1	<i>Arabidopsis thaliana</i>	138/49	Y	ATRRYISYGALRRNTIPCSRGA SYNCRRAQANPYSRGCSAI TRCRR	Stegmann et al. 2017
ProSCOOP12	NP_001119372.1	<i>Arabidopsis thaliana</i>	78/13	Y	PVRSSQSSQAGGR	Gully et al. 2019
ProSystemin	AAA34184.1	<i>Solanum lycopersicum</i>	201/18	N	AVQSKPPSKRDPKMQTD	McGurl et al. 1992
ProZip1	AC210027.3_FGT003.1	<i>Zea mays</i>	137/17	N	EGESELKLTQGASVRR	Ziemann et al. 2018
ProPSK1	NP_172816.2	<i>Arabidopsis thaliana</i>	87/5	Y	YIYTQ	Amano et al. 2007
ProPSY1	NP_200673.1	<i>Arabidopsis thaliana</i>	75/19	Y	DYGDPSANPKHDPGVPPS	Amano et al. 2007
ZmProPEP1	Zm00001d002137_P002	<i>Zea mays</i>	142/24	N	VRRRPTTPGRPREGSGGNG GNHH	Huffaker et al. 2011

^a SP = signal peptide; Y indicates the presence and N the absence of SP.

et al. 2000). Three main PLCP-specific signals can be observed between 25 and 40 kDa (Fig. 2E). Signals were quantified, values were normalized to the E-64 background (irreversible PLCP inhibitor) (Hanada et al. 1978), and the loading control and mock signals were set to 100% activity. The overall activity of PLCPs was significantly enhanced after MAMP and phyto-cytokine treatments but not after MAP1 treatment. However, different PLCPs were differentially activated, depending on the treatment; band A was significantly enhanced after Zip1, ZmIRP, and ZmPIP1 treatments, whereas band B showed stronger signals for all treatments except for ZmPIP1 and Zip1. Signals for band C were stronger after flg22 and chitin treatment as well as for all phyto-cytokines except for ZmIRP (Fig. 2E; Supple-

mentary Fig. S7). Thus, MAMPs and phyto-cytokine treatments activate distinct PLCPs, which in turn might trigger differential immune responses. Overall, these data indicate that the newly identified peptides ZmIRP, ZmPSK1e, and ZmPIP1 elicit maize defense responses and might function as phyto-cytokines in maize immunity.

Phyto-cytokines induce the upregulation of phyto-hormone-related genes

It has been previously shown that phyto-cytokines are involved in phyto-hormonal immune signaling (Hou et al. 2021). We therefore tested, which hormonal pathways become activated in response to our set of peptides 3 and 24 h after treatments. As

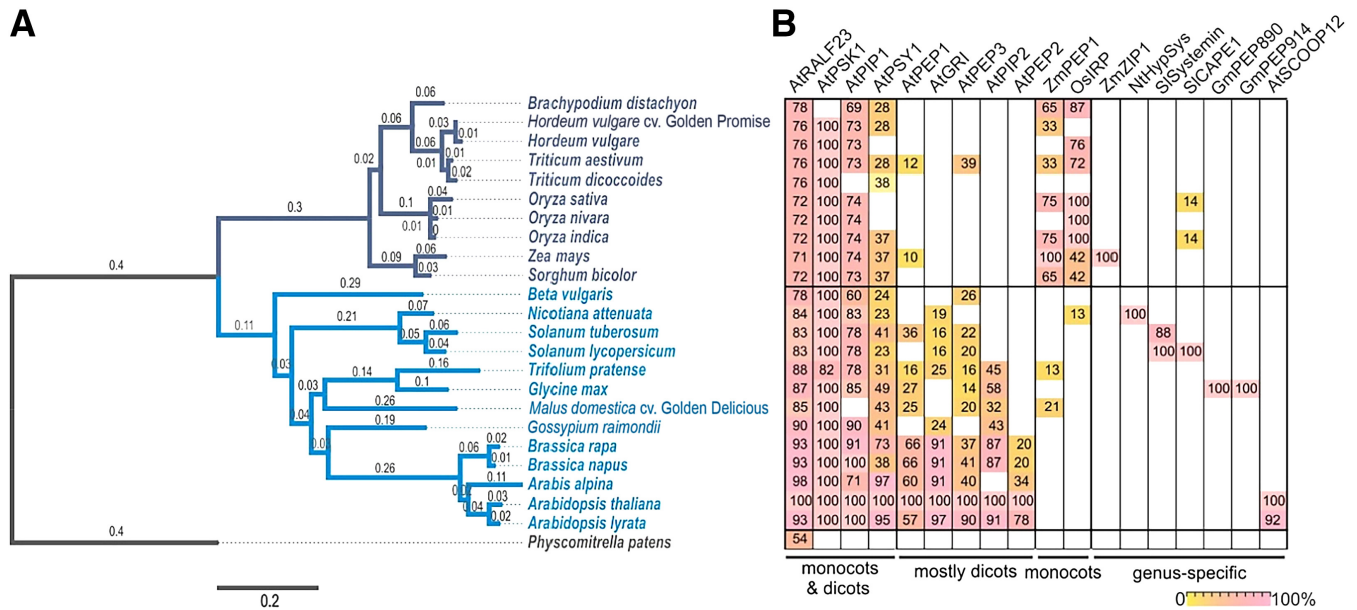


Fig. 1. Phylogenetic analysis and distribution of phyto-cytokines across monocots and dicots. **A**, Phylogenetic tree of selected crops and model plants. A total of 23 genomes were selected as representative species of monocots (dark blue) and dicots (light blue). The phylogenetic tree was generated based on BUSCO proteins (Manni et al. 2021; Seppely et al. 2019) shared by all species and with the moss *Physcomitrella patens* as outgroup. The scale bar represents the number of amino acid substitutions per site on the respective branch. **B**, Distribution of phyto-cytokines in selected plant species from 18 sequence queries of known phyto-cytokines used for the search of orthologue sequences. Colors and values in cells indicate the motif score (0 to 100%) of the identified peptide in the respective plant species. Phyto-cytokines were grouped in four categories depending in which plant species they were found: monocots and dicots, mostly dicots, only monocots, and genus-specific.

Table 2. Peptide orthologues found in *Zea mays*^a

Peptide/organism	Identifier	Peptide motif ^b	Motif score (%)	Peptide length
IRP				
<i>Oryza sativa</i>	Os04t0352066-00	GE-GWLEDGIGMVVDMGLGELK	100	20
<i>Zea mays</i>	Zm00001d004250_P001	GTDSWLESGVGMMLTQLLLGA	42.06	21
PIP1				
<i>Arabidopsis thaliana</i>	AT4G28460.1	RLASGPSRGRGH	100	13
<i>Zea mays</i>	Zm00001d021160_P001	RLPAGSPKPGPH	74.65	13
PSK1				
<i>Arabidopsis thaliana</i>	AT1G13590.1	YIYTQ	100	5
<i>Zea mays</i>	Zm00001d018727_P001	AHTDYIYTQ	100	9
PEP1				
<i>Arabidopsis thaliana</i>	AT5G64900.1	ATKVKAKQRGKEKVSSG-RPGQHN	100	23
<i>Zea mays</i>	Zm00001d002137_P002	VRR-RPTTPGRPREGSGGNGGNHH	10.17	23
RALF23				
<i>Arabidopsis thaliana</i>	AT3G16570.3	ATRRYISYGALRRNTIPCSRRGASYYNCR RGAQANPYSRGCASITRCRR	100	49
<i>Zea mays</i>	Zm00001d023856_P001	YGGGYISYGALRRDNVPCSRRGASYYNCR PGGQANPYHRGCSRITRCRG	71.96	49
PSY1				
<i>Arabidopsis thaliana</i>	AT5G58650.1	DYGDPSANPKHDPGVPPS	100	18
<i>Zea mays</i>	Zm00001d009425_P001	DYDYGGSNPKHDPRRKPG	37.38	18

^a Peptides identified in *Zea mays* as orthologues of known phyto-cytokines related to plant immunity.

^b Hyphens represent a gap in the alignment to the query peptide.

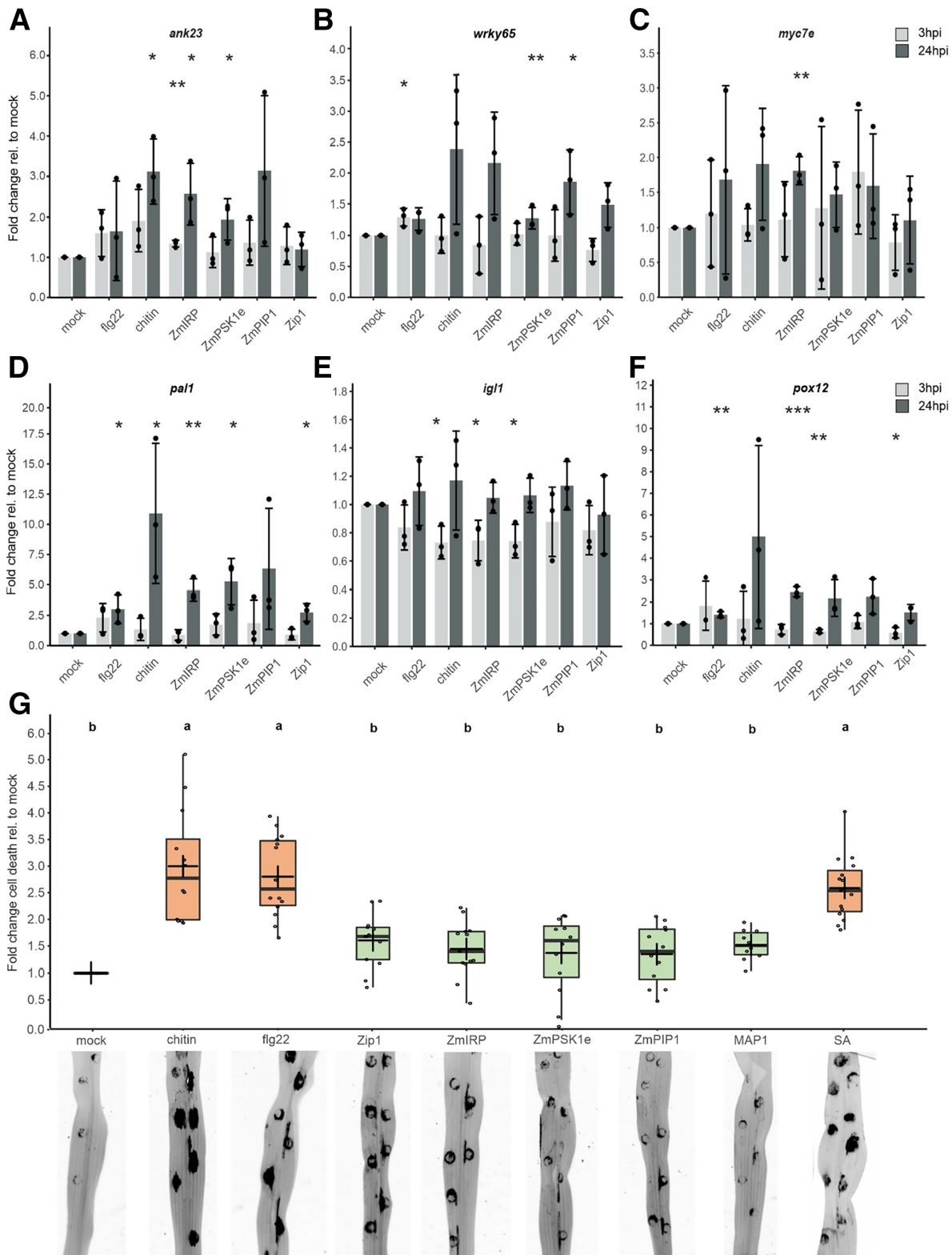


Fig. 3. Maize phytochemicals trigger phytohormonal pathways but do not promote cell death. Gene expression analysis shows differential regulation of hormonal pathways. **A**, The expression of the marker genes *ank23* (Zhang et al. 2019), **B**, *wrky65* (Huo et al. 2021), **C**, *myc7e* (Engelberth et al. 2012), **D**, *pal1* (Wang et al. 2020), **E**, *igl1* (Frey et al. 2004), and **F**, *pox12* (Hemetsberger et al. 2012) was tested after maize leaves were treated with the microbe-associated molecular patterns (MAMPs) flg22 and chitin, the phytochemicals ZmiRP, ZmPSK1, ZmPIP1, and Zip1, or the mock solution at 3 and 24 h postinfiltration (hpi). Gene expression of at least three biological replicates was normalized to *gapdh* and the fold change expression relative to mock was analyzed. Shown are at least three independent biological replicates with two technical replicates, error bars represent standard deviation; *P* values were calculated via unpaired *t* test. One asterisk (*) indicates $P < 0.05$; two (**) $P < 0.01$; three (***) $P < 0.0001$. **G**, Maize phytochemicals, in contrast to MAMPs and salicylic acid (SA), do not induce cell death in co-incidence with wounding. Cell death quantification at 24 hpi of maize leaves treated with 4 μ M flg22, 4 mg of chitin per milliliter, or 4 μ M of the synthetic peptides Zip1, ZmiRP, ZmPSK1, and ZmPIP1. Mock and MAP1 served as negative controls. Additionally, 2 μ M SA was tested. Shown are representative pictures, imaged 24 hpi with a blue epi-illumination source. Black signals represent cell death. The results of at least three independent biological replicates each, with six technical replicates were plotted. Data analyses were performed using an analysis of variance. Letters above indicate significant differences between samples ($\alpha = 0.05$, Tukey test).

of *wrky65*, a transcription factor associated to the SA signaling pathway (Fig. 3B). At 24 hpi, the SA markers *pall* and *ank23* were upregulated in response to chitin, whereas the *pall* and *pox12* induced an upregulation after flg22 treatment (Fig. 3A, D, and F). In addition, the newly identified maize phytochemicals also triggered the expression of hormonal marker genes. ZmIRP significantly triggered the upregulation of the SA marker *ank23* at 3 and 24 hpi as well as of *pall* and *pox12* at 24 hpi (Fig. 3A, D, and F). The JA marker *myc7e* was upregulated after ZmIRP treatment at 24 hpi (Fig. 3C). Besides, ZmIRP treatment caused downregulation of *Igl1* at 3 hpi (Fig. 3E), correlating to activation of SA defense responses. ZmPSK1e treatment caused an upregulation of the three SA marker genes *ank23*, *wrky65*, and *pall* at 24 hpi, although, at 3 hpi, *pox12* and *Igl1* expression was downregulated (Fig. 3A to F). ZmPIP1 treatment only upregulated the expression of *wrky65* at 24 hpi (Fig. 3B). Zip1 upregulated the SA biosynthesis gene *pall* at 24 hpi, which is in line with the previous report that Zip1 induces SA responses (Ziemann et al. 2018). Gene expression analysis of marker genes for SA- and JA-related immune pathways suggest that both MAMPs and phytochemicals activate immune components of hormonal pathways but to a different strength and often antagonistic responses.

Phytochemicals do not induce cell death in co-occurrence with damage

It was recently shown that simultaneous perception of MAMPs and cell damage triggers a strong localized immune response in *Arabidopsis* roots (Zhou et al. 2020). We speculated that leaves would also similarly react to this combination of triggers and a strong cell-death response might occur. At the same time, we asked if not only MAMPs but also phytochemicals could result in a similar output. A combination of damage and MAMPs or damage and phytochemicals was tested in syringe-infiltrated maize leaves. The syringe infiltration caused damage at the infiltrated site, which can be observed as a circular lesion in the form of a syringe without a needle (Fig. 3G). Autofluorescence was used as a measurement for the quantification of cell death 24 hpi. SA was included as an additional treatment, since a variety of phytochemicals and MAMPs trigger immunity through the SA defense pathway (Hou et al. 2021). At 24 h after treatment, flg22 and chitin caused strong cell death at the infiltration site, as compared with mock (Fig. 3G). Also, the treatment with SA induced a similar spread of cell death as the MAMP treatments (Fig. 3G). In contrast, none of the tested phytochemicals nor the control peptide MAP1 caused significant induction of cell death in comparison with the mock sample (Fig. 3G). These findings demonstrate that the combination of damage and MAMPs (or SA) trigger a cell death response in maize leaves in contrast to the phytochemicals, which did not trigger cell death. Thus, we conclude that although both MAMPs and phytochemicals activate overlapping defense responses related to phytohormonal pathways, the signaling output with regard to cell death differs between the triggers.

Phytochemicals alter virulence of biotrophic and necrotrophic pathogens

To gain further insights into the roles of the maize phytochemicals ZmIRP, ZmPSK1e, and ZmPIP1 in plant immunity, we conducted infection assays with the necrotrophic fungal pathogen *Botrytis cinerea*. To this end, *B. cinerea* conidia were applied onto the infiltrated leaf tissues 24 h after infiltration with the tested peptides. Subsequently, lesion sizes were measured at 48 h after fungal inoculation. Treatment with the MAMPs flg22 and chitin, resulted in significantly reduced lesion size, as compared with mock (Fig. 4A), due to the induction of defense responses. Similarly, ZmPSK1e treatment significantly reduced the lesion size in a similar manner as the chitin treatment, sug-

gesting that ZmPSK1e enhances resistance against *B. cinerea*. Contrarily, the phytochemicals ZmIRP and Zip1 caused a significant increase in *B. cinerea* lesion size, indicating enhanced susceptibility of the maize leaves upon treatment with these peptides. ZmPIP1 did not cause a statistically significant effect compared with the mock control or the MAP1 treatment (Fig. 4A). This experiment revealed that both MAMPs and phytochemicals alter plant susceptibility towards the necrotrophic pathogen *B. cinerea*. While both tested MAMPs as well as ZmPSK1e appeared to cause an increased resistance towards *B. cinerea*, the phytochemicals Zip1 and ZmIRP promoted infection of the necrotrophic pathogen.

To test the responses of a biotrophic pathogen to the maize phytochemicals, we made use of a “trojan horse” approach in which the fungus *Ustilago maydis* is deployed to deliver plant peptides into the leaf apoplast in vivo (van der Linde et al. 2018; Ziemann et al. 2018). *U. maydis* infects primordia of all aerial organs of maize and virulence can be evaluated by the induction of chlorosis, anthocyanin, and tumor formation (Schilling et al. 2014; Skibbe et al. 2010). We generated recombinant *U. maydis* strains secreting ZmPSK1e, ZmPIP1, and ZmIRP phytochemicals during biotrophic infection. In addition, a previously generated *U. maydis* strain that delivers the Zip1 peptide was used as a positive control. Expression constructs for the plant peptides were integrated as a single copy into the *U. maydis* genome. In addition, we selected *U. maydis* transformants that contained multiple integrations of ZmPSK1e, which allowed us to test for an eventual dose effect of the delivered phytochemical. Maize seedlings were infected with the recombinant fungal strains and the resulting disease symptoms were quantified at 12 days postinfiltration (dpi). Secretion of Zip1 resulted in a reduction of *U. maydis* disease symptoms, confirming previous results (Fig. 4B) (Ziemann et al. 2018). Similarly, ZmPSK1e had a negative impact on *U. maydis* infection, and the expression of ZmIRP resulted in an even stronger reduction of *U. maydis* virulence (Fig. 4B). In contrast, ZmPIP1 seemed to enhance *U. maydis* virulence, although not statistically significant in comparison with the SG200 infection (Fig. 4B). Thus, ZmPSK1e and ZmIRP significantly interfere with *U. maydis* infection restricting disease symptoms. Together, we observed that maize phytochemicals modulate infection of both necrotrophic and biotrophic pathogens in a differential manner. ZmIRP and Zip1 enhance resistance to the biotrophic pathogen but increase susceptibility to the necrotroph correlated to activation of SA-related defense responses. In contrast, ZmPSK1e reduces the virulence of both biotrophic and necrotrophic pathogens, whereas ZmPIP1 did not interfere with *B. cinerea* infection nor promote tumorigenesis caused by *U. maydis*.

Discussion

In this study we have used a bioinformatics pipeline to identify six maize orthologues of phytochemicals from other plant species, three of which were confirmed as biologically active signaling peptides in maize, namely, ZmIRP, ZmPIP1 and ZmPSK1e. Similar to the MAMPs flg22 and chitin, these peptides trigger maize immune responses such as PR-gene expression and PLCP activation. ZmIRP and ZmPSK1e differentially activate hormonal pathways, thus playing an important role in the plant immune response against biotrophic and necrotrophic pathogens. ZmIRP, similarly to Zip1, has been shown to activate the SA pathway in rice (Wang et al. 2020). Consequently, ZmIRP triggers the transcription of maize SA-related genes and confers resistance to the biotrophic pathogen *U. maydis* but enhances susceptibility towards the necrotroph *B. cinerea*, reflecting the antagonistic SA-JA dependency of plant resistance towards biotrophic vs. necrotrophic pathogens (Glazebrook 2005).

Thus, in our experiments, ZmIRP and Zip1 appear to have a similar impact on the maize immune response towards the activation of SA-related components.

Perception of MAMPs by membrane-localized PRR receptors leads to the activation of signaling pathways related to pathogen-triggered immunity (PTI) responses (DeFalco and Zipfel 2021; Hou et al. 2021). Some phytochemicals trigger PTI-related responses, suggesting overlapping components being involved in perception and upstream signaling. For instance, *Arabidopsis* AtPIP1 (PAMP-induced secreted peptide 1) induces MPK6 and MPK3 activation, ROS production, callose deposition, and enhanced *frk1*, *wrky53*, and *wrky33* gene expression, as well as other SA-related components (Hou et al. 2014, 2019b). Expression of *propip1* is upregulated by *flg22*, *Pseudomonas syringae* DC3000, and *Fusarium oxysporum* infection, which results in enhanced resistance against these pathogens. AtPIP1 has therefore been proposed as an amplifier of *flg22* responses (Hou et al. 2014). In maize, we found that ZmPIP1 triggers defense responses such as PR gene expression and PLCP activation, but it neither leads to a significant upregulation of SA- or JA-responsive genes nor to an altered resistance towards the tested plant pathogens. One possible explanation is that the hydroxylation of ZmPIP1 is required for pathogen resistance. It has been previously shown that the AtPIP1 unmodified peptide still has certain bioactivity as it inhibits the main root elongation, but

hydroxylation in position 6 enhances AtPIP1 bioactivity (Hou et al. 2014).

Differences in phytochemical responses could also indicate that their perception and function differ between plant species, i.e., between monocots and dicots. Indeed, PEPs were not recognized by species outside of their plant family of origin, likely due to a divergence of the PEP sequences and adaptation of the PEP receptors (Lori et al. 2015). In contrast to maize, where PEPs activate distinct signaling phytohormonal pathways such as JA, ET, volatile terpenes, and indoles (Poretsky et al. 2020), in *Arabidopsis*, the PEPs have largely redundant activities (Bartels et al. 2013; Huffaker et al. 2006). This indicates that, although PEPs are conserved as plant immune components, there are regulatory differences among species (Poretsky et al. 2020). In maize, Zip1 responses are distinct from what is described for phytochemicals in *Arabidopsis*. In particular, Zip1 does not trigger any of the canonical PTI responses but, instead, activates transcriptional reprogramming and PLCP activation largely overlapping with SA responses (Ziemann et al. 2018).

MAMP and phytochemical responses diverge in cell death

In the course of this study, we observed that maize phytochemicals activate plant defense genes similar to MAMPs, however, in co-incidence with wounding, the immune responses bifurcate. While the combination of wounding and MAMPs resulted in cell

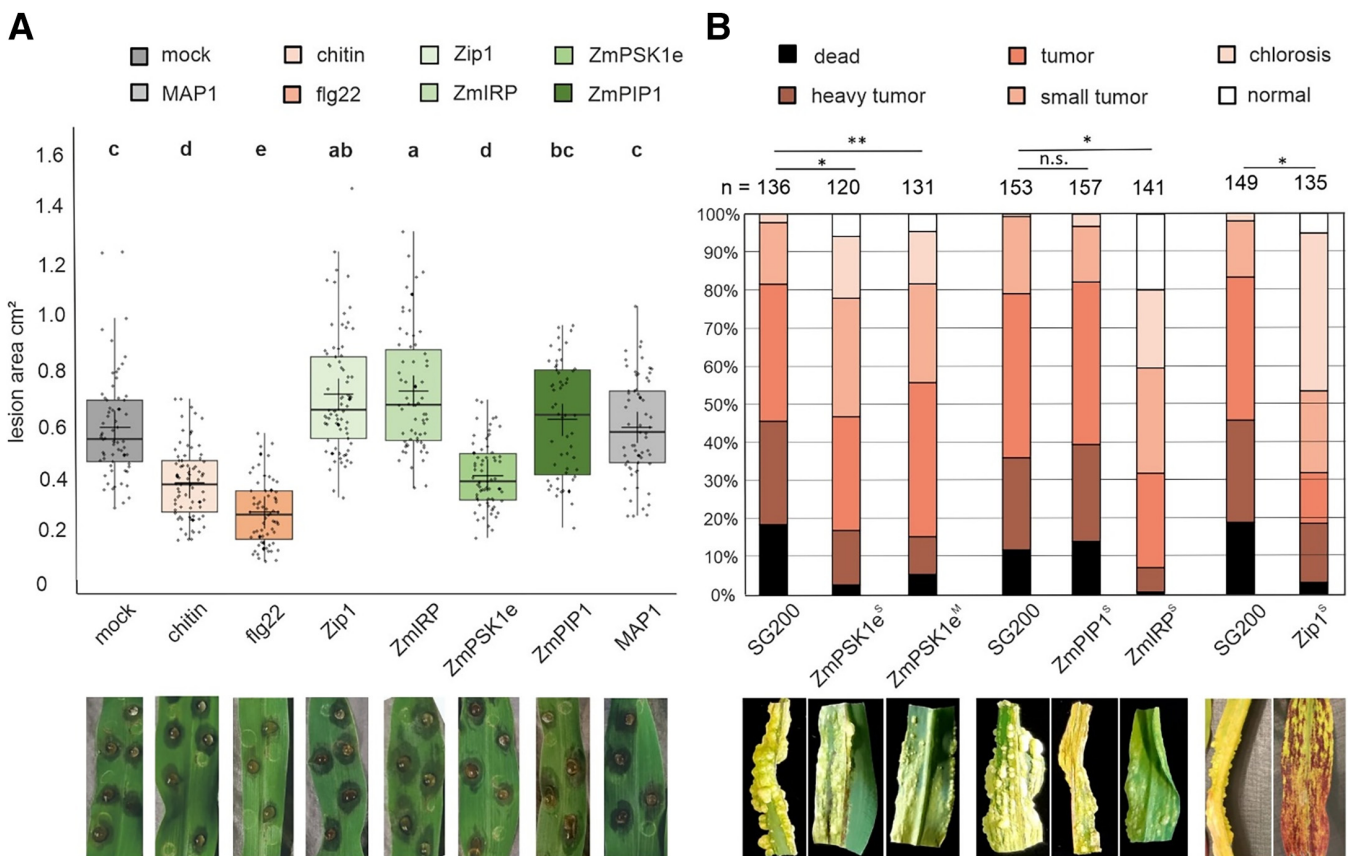


Fig. 4. Maize phytochemicals influence virulence of necrotrophic and biotrophic fungal pathogens. **A**, Maize phytochemicals alter lesion size upon *Botrytis cinerea* infection. Lesions of maize leaves treated with 4 μ M phytochemicals, microbe-associated molecular patterns, and the control peptide AMP1 were quantified 48 h postinfiltration (hpi). Shown are representative pictures of the infection at 48 hpi. This experiment was performed with at least three independent biological replicates each, with six technical replicates. Statistical analysis was performed using an analysis of variance. Letters above indicate significant differences between samples ($\alpha = 0.05$, Tukey test) **B**, The presence of maize phytochemicals affect *Ustilago maydis* virulence. Seven-day-old maize seedlings were infected with the solo-pathogenic strain SG200 and transgenic SG200 expressing the phytochemicals ZmPSK1, ZmPIP1, ZmIRP, and Zip1 under the control of the *pit2* promoter. Single (^S) and multiple (^M) integrations into the SG200 genome were tested. Disease symptoms were quantified and representative pictures of the infection were taken at 12 days postinfiltration. Statistical analyses were performed with a *t* test (one asterisk [*] indicates $P < 0.05$; two [**] $P < 0.01$; three [***] $P < 0.0001$; *n* = number of tested plants). Shown are the results of at least three independent biological replicates.

death, this was not the case for the phyto cytokines. Interestingly, in our experiments, promotion of cell death by MAMPs does not enhance susceptibility to *B. cinerea*, suggesting that the activation of immune responses even in the case of cell death is sufficient to prime the “infected” tissue enhancing resistance to necrotrophic pathogens. Activation of MAMP-triggered defense responses seen by PR gene induction and PLCP activation 24 hpi was already induced when *B. cinerea* conidia started germination. However, similar to a biotroph, a necrotroph such as *B. cinerea* also requires suppression of PTI at the (pre)penetration stage. In particular, the generation of extracellular ROS in its early infection stage prior to epidermal penetration needs to be controlled (Cessna et al. 2000). In *Arabidopsis* roots, it has been shown that damage to small cell clusters strongly upregulates PRR expression (Zhou et al. 2020). This leads to a localized immune response of otherwise non-responsive cells to beneficial bacteria, indicating that damage “switches on” local immune responses, generating more PRRs capable of sensing MAMPs. It has been proposed that the levels of signals perceived might contribute to the diversification and specificity of the immune response (Hou et al. 2021), but this also might suggest that the number of available PRRs could be the regulating factor. Indeed, perception of the tyrosine sulfated peptide RGF/GLV (AtGLV) in *Arabidopsis* promotes the stability and abundance of the FLS2 and EFR receptors (Stegmann et al. 2022), and external application of AtPIP1 also induces transcriptional upregulation of PRRs (Hou et al. 2014; Rhodes et al. 2021). After phyto cytokine perception, PRRs could be stabilized in a spatio-temporal manner making surrounding cells more responsive to the invaders and ready to further amplify the immune response. Besides, phyto cytokines could also play an important role in the healing process of the cell (Vega-Muñoz et al. 2020). Another possible scenario is that the fate of the cell is decided downstream of perception. This hypothesis is supported by a recent finding in *Arabidopsis* showing that both effector-triggered immunity and PTI defense pathways are activated downstream of BAK1 receptor recognition (Schulze et al. 2022). With the available information, one could hypothesize that phyto cytokines are used by the plant as alert signals for cell-to-cell communication, to amplify immune responses in by-stander cells as a survival mechanism (Fig. 5). Indeed, a few reports describe the existence of “death” peptides in plants. One example is the kiss-of-death (AtKOD) peptide from *Arabidopsis*, which is upregulated by biotic and abiotic stresses and whose expression causes cell death in leaves and seedlings (Blanvillain et al. 2011). Another example in *Arabidopsis* is the GRIM REAPER (AtGRI) peptide, which has been shown to be activated by the MC9 releasing an 11-amino acid peptide, which is then recognized by the receptor-like kinase PRK5, inducing ROS-dependent cell death (Wrzaczek et al. 2015). Future experiments will aim to unravel the cellular components that determine the initiation of immune-regulated cell death or, rather, promote a phyto cytokine-driven pro-life decision in immune-activated cells.

Materials and Methods

In silico identification of putative propeptides and peptide hormones

A BLAST database consisting of predicted proteomes from 78 randomly selected plants was created (Supplementary Table S1). The proteomes were obtained from the Ensemble Plants database (<https://plants.ensembl.org/>). Eighteen previously published propeptides (Table 1) were used as queries in the National Center for Biotechnology Information BLAST+ application (Camacho et al. 2009). psiBLAST searches (Altschul et al. 1997; Schäffer et al. 2001) of the queries in the database were performed with five iterations and an e-value threshold of

0.05 to detect distant relationships between proteins. A parallel BLASTp (Altschul et al. 1990) with the same settings was performed.

The results for the 18 BLAST searches were combined and unique identifiers were assigned to each hit. Redundant hits for every proteome were removed after sorting by their bit score and selecting only the hit with the highest score. Hits with less than 10% protein identities and query coverage less than 25% in the psiBLAST and BLASTp were removed. Due to sequence variance in the length of all hits, hits with amino-acid sequence length 1.5 times longer or shorter with more than 75% identity were removed. In the last step, hits were filtered according to their similarity to the query. All hits for each queried propeptide were aligned with the ClustalOmega (Goujon et al. 2010) application, and the region containing the phyto cytokine was analyzed and scored. The similarity of each alignment region containing the newly identified peptide was scored based on a BLOSUM62 matrix (Henikoff and Henikoff 1992) and low gap costs (gap: -8, extension: -1), using the Biopython package (Cock et al. 2009), with the motif score equal to 100 times the alignment score of the putative peptide with the reference peptide divided by the alignment score of the self-alignment of the reference peptide.

The final motif score was calculated taking into account the length and amino-acid composition of the peptide. Hits with motif scores lower than 10% were removed. The process of alignment, scoring, and filtering was performed three times. The phylogenetic tree was created using a customized dataset of representative crops and common plant model species. A total of 140 complete proteins present in all proteomes, either as one or as multiple copies, were selected using the BUSCO software (Manni et al. 2021; Seppey et al. 2019). If multiple copies were present, only the best hit was used to create the phylogenetic tree. The orthologs of each BUSCO protein were aligned via ClustalOmega. The alignments of all proteins were concatenated. A phylogenetic tree of the concatenated multiple sequence alignments was calculated via RAXML (Stamatakis 2014), using the “PROTCATBLOSUM62” substitution model. The phylogenetic tree was visualized with FigTree (software/figtree). Plots of results regarding peptide hormones were created with the matplotlib (Hunter 2007) and the logomaker (Tareen and Kinney 2019) packages in Python. The Venn diagram was created with the “ggvenn” package in R.

All scripts are deposited on GitHub (<https://github.com/dmoser1/phyto cytokine.git>).

Plant growth conditions

Grains of maize (*Z. mays*, cv. Golden Bantam) were placed in organic growth soil and were grown for 7 to 8 days in a plant growth chamber (15 h photoperiod at 28°C, 1 h twilight morning and evening and 7 h darkness, at 22°C).

Plant treatments

Chitin. Fifty milligrams of shrimp shell chitin (Sigma Aldrich) was ground in 2.5 ml of double-distilled water (ddH₂O) with mortar and pestle. Residues were flushed with an additional 2.5 ml of ddH₂O. The mortar was placed in a microwave for 60 s. The chitin solution was transferred to a 15-ml Falcon tube that was filled to 5 ml with ddH₂O to compensate for evaporation. The solution was sonicated using a microtip (Sonoplus) for 3 min, using pulse and 70% amplitude. The sonicate was centrifuged for 5 min at 2,500 × *g* and the supernatant (10 mg/ml) was transferred to a new tube. For the treatments, the supernatant was diluted to a final concentration of 4 mg/ml, using ddH₂O.

flg22. flg22 (1 mM) was diluted to a final concentration of 4 μM in ddH₂O.

For ZmIRP (GTDSWLESGVGMTQLLGGAK), MAP1 (IFDDGGFGEVHADPIKVER), ZmPSK1e (AHTDYIYTQ, non-sulfated), ZmPIP1 (RLPAGSPKGGPH, non-hydroxylated), and Zip1 (EGESELKLATQGASVRR), lyophilized peptide powder was diluted to stock concentrations of 0.5 mg/ml. The final concentration to treat the plants was 4 μ M each. Canonical PSK1 [Tyr(SO₃H)-Ile-Tyr(SO₃H)-Thr-Gln] was obtained from Peptanova.

The second leaf of 8-day-old maize seedlings was infiltrated, using a 1-ml needleless syringe.

Gene expression analyses

Treated leaf samples were taken at 24 hpi and were ground with liquid nitrogen. RNA was extracted using TRIzol, following the protocol of Ambion Life Technologies. RNA was treated with DNase using TURBO DNA-free reagents following the corresponding protocols. Two micrograms of RNA were transcribed to complementary DNA (cDNA) using the RevertAid

H Minus First Strand cDNA Synthesis Kit (Thermo Scientific). The oligo (dt)₁₈ primer was used for the synthesis. The obtained cDNA was diluted 1:100 using nuclease-free water. The diluted cDNA was used for quantitative reverse transcription PCR analyses with gene-specific primers (Supplementary Table S2). We used IQ SYBR Green (Promega) reagent for detection. GAPDH was used as a housekeeping gene in maize experiments. *Pr3*, *pr4*, *pr5*, *prm6b*, and *pr10.1* were included in the analysis as defense marker genes. *Igl1*, *ank23*, *myc7E*, *wrky65*, *cc9*, *pox12*, and *pall* were included in the analysis as SA or JA marker genes.

PLCP activity assay: activity-based protein profiling (ABPP)

Treated leaves were collected 24 hpi and were ground with liquid nitrogen. Equal amounts of powder were dissolved in 50 mM NaOAc buffer (pH = 6), using a VIBRAX shaker system (IKA) three times for 1 min. Samples were centrifuged with

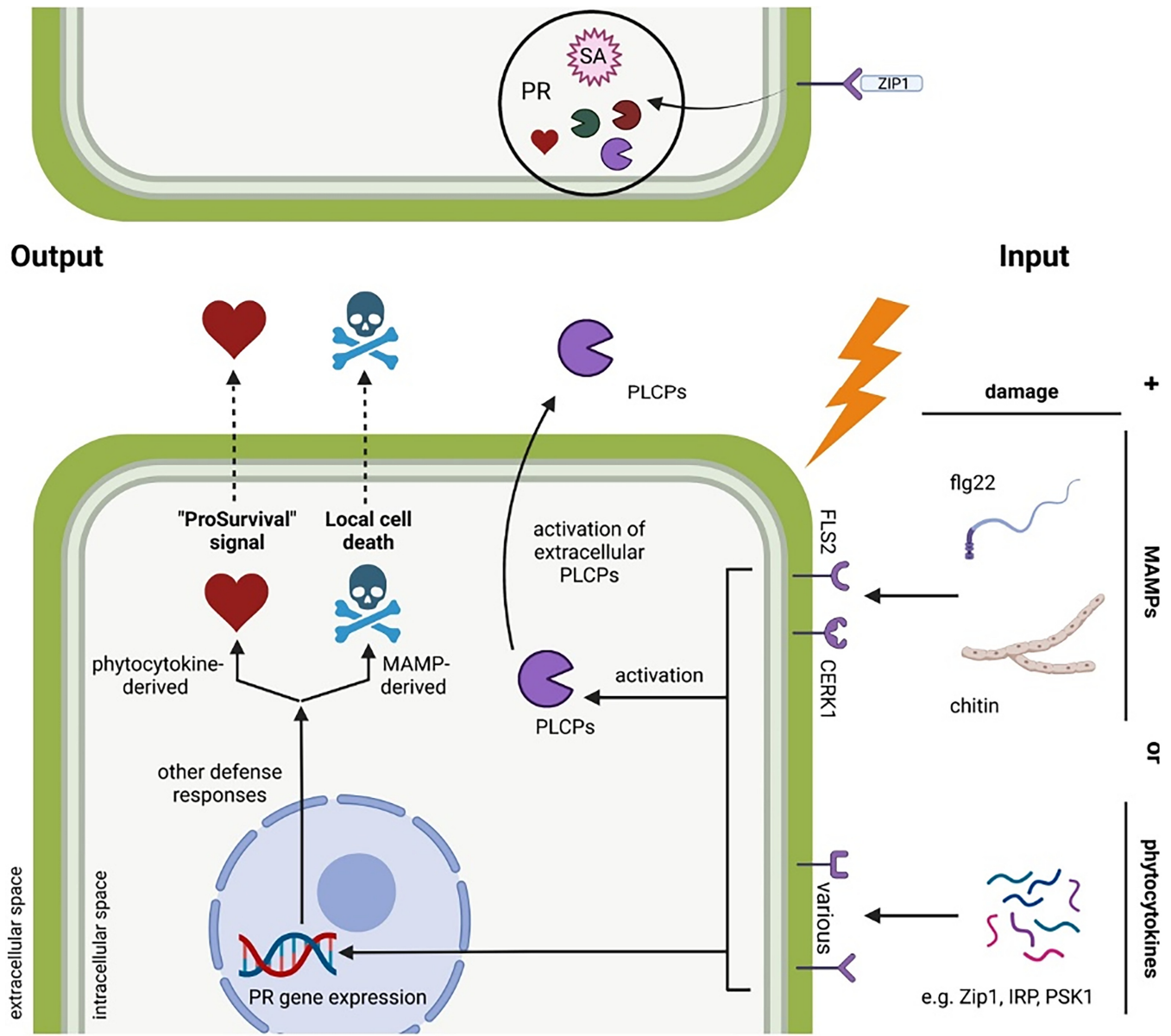


Fig. 5. Model of phytochemical immune activation. Microbe-associated molecular patterns (MAMPs) and phytochemicals are recognized by surface receptors triggering immune responses such as induction of pathogenesis-related (PR) gene expression and papain-like cysteine protease (PLCP) activation. In coincidence with wounding (input), recognition of MAMPs and phytochemicals activate differential pathways in- or outside the surrounding cells, leading to a pro-survival signal (output) triggered by the phytochemicals in contrast to a local cell death signal (output) induced by MAMPs.

17,000 × g for 20 min at 4°C, and the supernatant was transferred to new tubes and was kept on ice. Fifty-microliter labeling reactions were prepared and 48.5 µl of protein extract was used together with either 1 µl of dimethyl sulfoxide or E64 (PLCP inhibitor) (Hanada et al. 1978) and 0.5 µl of 1 M dithiothreitol. After a 30-min pre-incubation, 1 µl of 100 µM DCG04-Cy5 probe (Greenbaum et al. 2000), obtained from H. Overkleef (Leiden University), was added. The samples were labeled for 3 h at room temperature in the dark. Labeling was stopped by adding 15 µl of Laemmli buffer and heating for 10 min at 98°C. Fifteen microliters of the sample was loaded on 15% poly-amino acid gels and was run for 70 min at 200 V in the dark. The ABPP signals were analyzed immediately after the run, using a ChemiDoc (Bio-Rad) system with a Cy5-suitable setting. Afterward, the gels were incubated in SyproRuby fixation solution (50% MeOH, 7% acetic acid) for 30 min and were incubated overnight in SyproRuby staining solution (Thermo Fisher Scientific). The following day, the gels were washed, applying SyproRuby washing solution (10% MeOH, 7% acetic acid) for 20 min. The signals were detected afterward, using the SyproRuby setting from the ChemiDoc. ABPP and SyproRuby signals were quantified using the Image Lab software. A conserved protein band at 55 kDa was used to determine the relative protein concentration for each sample. The calculated correction factor was used to compare and analyze PLCP signals for A, B, and C between the mock sample and samples of treatments. Mock PLCP values have been set to 100% and, accordingly, the samples of the respective treatments are depicted in the percentage of PLCP activity.

Botrytis cultivation and infection assays

It has been previously shown that *B. cinerea* causes disease symptoms in maize leaves under control conditions (Leisen et al. 2022; Ziemann et al. 2018). *B. cinerea* strains were cultured on agar containing malt extract medium. Conidia were collected from 10-day-old plates with 10 ml of water, using a glass spatula, were filtered through Miracloth (VWR), and were counted using a hemocytometer. Infection tests were performed with detached second leaves of 9-day-old maize (*Z. mays* cv. Golden Bantam) seedlings. Prior to infection, the seedlings were treated with MAMPs or phytochemicals, as described previously, for 24 h. After 1 day, leaf inoculations were performed using 10-µl droplets with 2×10^5 conidia per milliliter in GB5 minimal medium (GB5: 3.05 g of GB5 per liter, 10 mM KH₂PO₄, pH 5.5). Multiple droplets were placed on individual leaves and were considered technical replicates. This experiment was performed with three biological replicates. For one biological replicate, at least three leaves were used for a single treatment. The lesion area was quantified 48 h after leaf infection, using ImageJ software.

Generation of *Ustilago*-phytochemical overexpression lines

Corresponding sequences of the peptides Zip1, ZmIRP, ZmPSK1e, and ZmPIP1 were cloned into the p123 vector system, using the Gibson assembly method (Gibson et al. 2009). The vector harbors a constitutive promoter (pro^{pit2}) for overexpression, a terminator (Tnos), and a resistance marker cassette (carboxin [cbx]). The assembled vectors were transformed into TOP10 *Escherichia coli* cells by heat shock for plasmid multiplication. Purified plasmids were digested by *Ssp*I restriction enzyme for linearization, to allow the homologous recombination into the *ip* locus. Protoplasts (50 µl) of *Ustilago maydis* (SG200; solo pathogenic mutant) were transfected by adding 5 µg of linearized plasmid, 1 µl of heparin, and 0.5 ml of STC (100 mM CaCl₂, 10 mM Tris-HCl, pH 7.5, 0.9 M sorbitol) to 40% polyethylene glycol (sterile) and incubating for 15 min on ice. The samples were plated on Regeneration agar, poured as a

two-layer system (without [top] and with cbx [bottom]). Plates were incubated at 28°C for 4 to 5 days. Colonies were picked and singled out onto potato dextrose agar plates for 2 days at 28°C. Two-milliliter overnight cultures of singled-out colonies were used for DNA extraction (Hoffman and Winston 1987). The extracted DNA was digested by *Hind*III, was separated on 0.9% agarose gel (100 V, 2 h), and was blotted on a nylon membrane for Southern blot analysis. The detection of cbx-containing DNA fragments was performed using a digoxigenin antibody targeting the *ip* locus via a cbx probe. Successfully confirmed strains were used for infections.

***Ustilago* cultivation and infection assays**

SG200, SG200_Zip1, SG200_ZmIRP, SG200_ZmPSK1e, and SG200_ZmPIP1 were grown to an optical density at 600 nm (OD₆₀₀) of 0.8 in 55 ml of YEPS_{light} (0.4% yeast extract, 0.4% peptone, and 2% saccharose). The cultures were pelleted at 2,850 × g for 7 min and the supernatant was discarded. The pellets were washed with 20 ml of ddH₂O. At last, the pellets were resuspended in the calculated volume of water to reach an OD₆₀₀ of 1.0. Ten-microliter droplets of each culture were placed on charcoal plates to check for filamentation (pathogenicity). Seven-day-old maize seedlings were infected, using a 1-ml syringe with needle, injecting *Ustilago* suspension into the stem of the seedlings. The plant phenotype was investigated 12 dpi, using a disease rating chart for *Ustilago maydis* comprising healthy plants, chlorosis, small tumors (<2 mm), normal tumors (2 to 10 mm diameter), heavy tumors (>10 mm or stunted growth), and dead plants. Infected plants were categorized based on phenotypical symptoms and were compared with SG200 for the analyses.

Cell death assays

MAMP- and phytochemical-treated leaf samples were harvested 24 hpi and were scanned for autofluorescence, using the ChemiDoc (Bio-Rad) autofluorescence settings (530/280 nm filter). The images were analyzed by Image Lab software. Non-infiltrated areas of leaves were selected as background signals and were compared with the overall signal intensity of the whole leaf surface. The signal intensity of mock (water-treated) leaves was plotted against MAMP- and phytochemical-treated leaf samples. Mock was set to 1 and was compared with signals of the remaining samples, depicting the fold changes relative to mock.

Acknowledgments

We thank H. Overkleef for providing the DCG04-Cy5 probe and J. Werner for helping with *Botrytis* infection assays. We are also grateful to U. Meyer for technical support. We are thankful for P. Saake for help with the bioinformatic analysis during her lab rotation. We also thank reviewers for great comments and suggestions improving our manuscript.

Literature Cited

- Altschul, S. F., Gish, W., Miller, W., Myers, E. W., and Lipman, D. J. 1990. Basic local alignment search tool. *J. Mol. Biol.* 215:403-410.
- Altschul, S. F., Madden, T. L., Schäffer, A. A., Zhang, J., Zhang, Z., Miller, W., and Lipman, D. J. 1997. Gapped BLAST and PSI-BLAST: A new generation of protein database search programs. *Nucleic Acids Res.* 25:3389-3402.
- Amano, Y., Tsubouchi, H., Shinohara, H., Ogawa, M., and Matsubayashi, Y. 2007. Tyrosine-sulfated glycopeptide involved in cellular proliferation and expansion in *Arabidopsis*. *Proc. Natl. Acad. Sci. U.S.A.* 104:18333-18338.
- Bartels, S., Lori, M., Mbengue, M., van Verk, M., Klauser, D., Hander, T., Böni, R., Robatzek, S., and Boller, T. 2013. The family of Peps and their precursors in *Arabidopsis*: Differential expression and localization but similar induction of pattern-triggered immune responses. *J. Exp. Bot.* 64:5309-5321.

- Blanvillain, R., Young, B., Cai, Y., Hecht, V., Varoquaux, F., Delorme, V., Lancelin, J.-M., Delseny, M., and Gallois, P. 2011. The *Arabidopsis* peptide kiss of death is an inducer of programmed cell death. *EMBO J.* 30:1173-1183.
- Boller, T., and Felix, G. 2009. A renaissance of elicitors: Perception of microbe-associated molecular patterns and danger signals by pattern-recognition receptors. *Annu. Rev. Plant Biol.* 60:379-406.
- Boller, T., and Flury, P. 2012. Peptides as Danger Signals: MAMPs and DAMPs. Pages 163-181 in: *Plant Signaling Peptides*, H. R. Irving and C. Gehring, eds. Springer Berlin.
- Borrego, E., and Kolomiets, M. 2016. Synthesis and functions of jasmonates in maize. *Plants* 5:41.
- Brutus, A., Sicilia, F., Macone, A., Cervone, F., and de Lorenzo, G. 2010. A domain swap approach reveals a role of the plant wall-associated kinase 1 (WAK1) as a receptor of oligogalacturonides. *Proc. Natl. Acad. Sci. U.S.A.* 107:9452-9457.
- Butenko, M. A., Patterson, S. E., Grini, P. E., Stenvik, G.-E., Amundsen, S. S., Mandal, A., and Aalen, R. B. 2003. *INFLORESCENCE DEFICIENT IN ABSCISSION* controls floral organ abscission in *Arabidopsis* and identifies a novel family of putative ligands in plants. *Plant Cell* 15:2296-2307.
- Camacho, C., Coulouris, G., Avagyan, V., Ma, N., Papadopoulos, J., Bealer, K., and Madden, T. L. 2009. BLAST+: Architecture and applications. *BMC Bioinf.* 10:421.
- Campbell, L., and Turner, S. R. 2017. A Comprehensive analysis of RALF proteins in green plants suggests there are two distinct functional groups. *Front. Plant Sci.* 8:37.
- Cessna, S. G., Sears, V. E., Dickman, M. B., and Low, P. S. 2000. Oxalic acid, a pathogenicity factor for *Sclerotinia sclerotiorum*, suppresses the oxidative burst of the host plant. *Plant Cell* 12:2191-2199.
- Chen, Y. C., Siems, W. F., Pearce, G., and Ryan, C. A. 2008. Six peptide wound signals derived from a single precursor protein in *Ipomoea batatas* leaves activate the expression of the defense gene sporamin. *J. Biol. Chem.* 283:11469-11476.
- Chien, P. S., Nam, H. G., and Chen, Y. R. 2015. A salt-regulated peptide derived from the CAP superfamily protein negatively regulates salt-stress tolerance in *Arabidopsis*. *J. Exp. Bot.* 66:5301-5313.
- Chinchilla, D., Bauer, Z., Regenass, M., Boller, T., and Felix, G. 2006. The *Arabidopsis* receptor kinase FLS2 binds flg22 and determines the specificity of flagellin perception. *Plant Cell* 18:465-476.
- Cock, P. J. A., Antao, T., Chang, J. T., Chapman, B. A., Cox, C. J., Dalke, A., Friedberg, I., Hamelryck, T., Kauff, F., Wilczynski, B., and de Hoon, M. J. L. 2009. Biopython: Freely available Python tools for computational molecular biology and bioinformatics. *Bioinformatics* 25:1422-1423.
- Decreux, A., and Messiaen, J. 2005. Wall-associated kinase WAK1 interacts with cell wall pectins in a calcium-induced conformation. *Plant Cell Physiol.* 46:268-278.
- DeFalco, T. A., and Zipfel, C. 2021. Molecular mechanisms of early plant pattern-triggered immune signaling. *Mol. Cell* 81:3449-3467.
- Denoux, C., Galletti, R., Mammarella, N., Gopalan, S., Werck, D., de Lorenzo, G., Ferrari, S., Ausubel, F. M., and Dewdney, J. 2008. Activation of defense response pathways by OGs and Flg22 elicitors in *Arabidopsis* seedlings. *Mol. Plant* 1:423-445.
- Depotter, J. R. L., Misa Villamil, J. C., and Doehlemann, G. 2022. Maize immune signalling peptide ZIP1 evolved de novo from a retrotransposon. *bioRxiv*.
- Dolezal, A. L., Shu, X., O'Brien, G. R., Nielsen, D. M., Woloshuk, C. P., Boston, R. S., and Payne, G. A. 2014. *Aspergillus flavus* infection induces transcriptional and physical changes in developing maize kernels. *Front Microbiol.* 5:1-10.
- Engelberth, J., Contreras, C. F., and Viswanathan, S. 2012. Transcriptional analysis of distant signaling induced by insect elicitors and mechanical wounding in *Zea mays*. *PLoS One* 7:e34855.
- Frey, M., Spittler, D., Boland, W., and Gierl, A. 2004. Transcriptional activation of *Igl*, the gene for indole formation in *Zea mays*: A structure-activity study with elicitor-active *N*-acyl glutamines from insects. *Phytochemistry* 65:1047-1055.
- Gibson, D. G., Young, L., Chuang, R.-Y., Venter, J. C., Hutchison, C. A., and Smith, H. O. 2009. Enzymatic assembly of DNA molecules up to several hundred kilobases. *Nat. Methods* 6:343-345.
- Glazebrook, J. 2005. Contrasting mechanisms of defense against biotrophic and necrotrophic pathogens. *Annu. Rev. Phytopathol.* 43:205-227.
- Goujon, M., McWilliam, H., Li, W., Valentin, F., Squizzato, S., Paern, J., and Lopez, R. 2010. A new bioinformatics analysis tools framework at EMBL-EBI. *Nucleic Acids Res.* 38:W695-W699.
- Greenbaum, D., Medzihradsky, K. F., Burlingame, A., and Bogoy, M. 2000. Epoxide electrophiles as activity-dependent cysteine protease profiling and discovery tools. *Chem. Biol.* 7:569-581.
- Gully, K., Pelletier, S., Guillou, M.-C., Ferrand, M., Aligon, S., Pokotylo, I., Perrin, A., Vergne, E., Fagard, M., Ruelland, E., Grappin, P., Bucher, E., Renou, J.-P., and Aubourg, S. 2019. The SCOP12 peptide regulates defense response and root elongation in *Arabidopsis thaliana*. *J. Exp. Bot.* 70:1349-1365.
- Gust, A. A., Pruitt, R., and Nürnberger, T. 2017. Sensing danger: Key to activating plant immunity. *Trends Plant Sci.* 22:779-791.
- Hanada, K., Tamai, M., Yamagishi, M., Ohmura, S., Sawada, L., and Tanaka, I. 1978. Isolation and characterization of e-64, a new thiol protease inhibitor. *Agric. Biol. Chem.* 42:523-528.
- Hander, T., Fernández-Fernández, Á. D., Kumpf, R. P., Willems, P., Schatowitz, H., Rombaut, D., Staes, A., Nolf, J., Pottier, R., Yao, P., Gonçalves, A., Pavie, B., Boller, T., Gevaert, K., van Breusegem, F., Bartels, S., and Stael, S. 2019. Damage on plants activates Ca²⁺-dependent metacaspases for release of immunomodulatory peptides. *Science* 363:eaar7486.
- Hemetsberger, C., Herrberger, C., Zechmann, B., Hillmer, M., and Doehlemann, G. 2012. The *Ustilago maydis* effector Pep1 suppresses plant immunity by inhibition of host peroxidase activity. *PLoS Pathog.* 8:e1002684.
- Henikoff, S., and Henikoff, J. G. 1992. Amino acid substitution matrices from protein blocks. *Proc. Natl. Acad. Sci. U.S.A.* 89:10915-10919.
- Hoffman, C. S., and Winston, F. 1987. A ten-minute DNA preparation from yeast efficiently releases autonomous plasmids for transformation of *Escherichia coli*. *Gene* 57:267-272.
- Hou, S., Liu, D., and He, P. 2021. Phytocytokines function as immunological modulators of plant immunity. *Stress Biol.* 1:8.
- Hou, S., Liu, Z., Shen, H., and Wu, D. 2019a. Damage-associated molecular pattern-triggered immunity in plants. *Front. Plant Sci.* 10:646.
- Hou, S., Shen, H., and Shao, H. 2019b. PAMP-induced peptide 1 cooperates with salicylic acid to regulate stomatal immunity in *Arabidopsis thaliana*. *Plant Signal. Behav.* 14:1666657.
- Hou, S., Wang, X., Chen, D., Yang, X., Wang, M., Turrà, D., di Pietro, A., and Zhang, W. 2014. The secreted peptide PIP1 amplifies immunity through receptor-like kinase 7. *PLoS Pathog.* 10:e1004331.
- Huffaker, A., Dafoe, N. J., and Schmelz, E. A. 2011. ZmPep1, an ortholog of *Arabidopsis* elicitor peptide 1, regulates maize innate immunity and enhances disease resistance. *Plant Physiol.* 155:1325-1338.
- Huffaker, A., Pearce, G., and Ryan, C. A. 2006. An endogenous peptide signal in *Arabidopsis* activates components of the innate immune response. *Proc. Natl. Acad. Sci. U.S.A.* 103:10098-10103.
- Hunter, J. D. 2007. Matplotlib: A 2D graphics environment. *Comput. Sci. Eng.* 9:90-95.
- Huo, T., Wang, C.-T., Yu, T.-F., Wang, D.-M., Li, M., Zhao, D., Li, X.-T., Fu, J.-D., Xu, Z.-S., and Song, X.-Y. 2021. Overexpression of *ZmWRKY65* transcription factor from maize confers stress resistances in transgenic *Arabidopsis*. *Sci. Rep.* 11:4024.
- Leisen, T., Werner, J., Pattar, P., Safari, N., Ymeri, E., Sommer, F., Schroda, M., Suárez, I., Collado, I. G., Scheuring, D., and Hahn, M. 2022. Multiple knockout mutants reveal a high redundancy of phytotoxic compounds contributing to necrotrophic pathogenesis of *Botrytis cinerea*. *PLoS Pathog.* 18:e1010367.
- Li, Q., Wang, C., and Mou, Z. 2020. Perception of damaged self in plants. *Plant Physiol.* 182:1545-1565.
- Lori, M., van Verk, M. C., Hander, T., Schatowitz, H., Klausner, D., Flury, P., Gehring, C. A., Boller, T., and Bartels, S. 2015. Evolutionary divergence of the plant elicitor peptides (PEPs) and their receptors: Interfamily incompatibility of perception but compatibility of downstream signalling. *J. Exp. Bot.* 66:5315-5325.
- Luo, L. 2012. Plant cytokine or phytocytokine. *Plant Signal. Behav.* 7: 1513-1514.
- Manni, M., Berkeley, M. R., Seppely, M., and Zdobnov, E. M. 2021. BUSCO: Assessing genomic data quality and beyond. *Curr. Protoc.* 1.
- McGurl, B., Pearce, G., Orozco-Cardenas, M., and Ryan, C. 1992. Structure, expression, and antisense inhibition of the systemin precursor gene. *Science* 255:1570-1573.
- Misa Villamil, J. C., van der Hoorn, R. A. L., and Doehlemann, G. 2016. Papain-like cysteine proteases as hubs in plant immunity. *New Phytol.* 212:902-907.
- Nakaminami, K., Okamoto, M., Higuchi-Takeuchi, M., Yoshizumi, T., Yamaguchi, Y., Fukao, Y., Shimizu, M., Ohashi, C., Tanaka, M., Matsui, M., Shinozaki, K., Seki, M., and Hanada, K. 2018. AtPep3 is a hormone-like peptide that plays a role in the salinity stress tolerance of plants. *Proc. Natl. Acad. Sci. U.S.A.* 115:5810-5815.
- Peng, Y., van Wersch, R., and Zhang, Y. 2018. Convergent and divergent signaling in PAMP-triggered immunity and effector-triggered immunity. *Mol. Plant-Microbe Interact.* 31:403-409.

- Pontiggia, D., Benedetti, M., Costantini, S., de Lorenzo, G., and Cervone, F. 2020. Dampening the DAMPs: How plants maintain the homeostasis of cell wall molecular patterns and avoid hyper-immunity. *Front. Plant Sci.* 11:613259.
- Poretsky, E., Dressano, K., Weckwerth, P., Ruiz, M., Char, S. N., Shi, D., Abagyan, R., Yang, B., and Huffaker, A. 2020. Differential activities of maize plant elicitor peptides as mediators of immune signaling and herbivore resistance. *Plant J.* 104:1582-1602.
- Ray, S., Alves, P. C. M. S., Ahmad, I., Gaffoor, I., Acevedo, F. E., Peiffer, M., Jin, S., Han, Y., Shakee, S., Felton, G. W., and Luthe, D. S. 2016. Turnabout is fair play: Herbivory-induced plant chitinases excreted in fall armyworm frass suppress herbivore defenses in maize. *Plant Physiol.* 171:694-706.
- Rhodes, J., Yang, H., Moussu, S., Boutrot, F., Santiago, J., and Zipfel, C. 2021. Perception of a divergent family of phytolectins by the Arabidopsis receptor kinase MIK2. *Nat. Commun.* 12:705.
- Ryan, C. A., and Pearce, G. 2003. Systemins: A functionally defined family of peptide signals that regulate defensive genes in Solanaceae species. *Proc. Natl. Acad. Sci.* 100:14577-14580.
- Rzemieniewski, J., and Stegmann, M. 2022. Regulation of pattern-triggered immunity and growth by phytolectins. *Curr. Opin. Plant Biol.* 68:102230.
- Saijo, Y., Loo, E. P., and Yasuda, S. 2018. Pattern recognition receptors and signaling in plant-microbe interactions. *Plant J.* 93:592-613.
- Schäffer, A. A., Aravind, L., Madden, T. L., Shavirin, S., Spouge, J. L., Wolf, Y. I., Koonin, E. V., and Altschul, S. F. 2001. Improving the accuracy of PSI-BLAST protein database searches with composition-based statistics and other refinements. *Nucleic Acids Res.* 29:2994-3005.
- Schilling, L., Matei, A., Redkar, A., Walbot, V., and Doehlemann, G. 2014. Virulence of the maize smut *Ustilago maydis* is shaped by organ-specific effectors. *Mol. Plant Pathol.* 15:780-789.
- Schulze, S., Yu, L., Hua, C., Zhang, L., Kolb, D., Weber, H., Ehinger, A., Saile, S. C., Stahl, M., Franz-Wachtel, M., Li, L., el Kasm, F., Nürnberger, T., Cevik, V., and Kemmerling, B. 2022. The *Arabidopsis* TIR-NBS-LRR protein CSA1 guards BAK1-BIR3 homeostasis and mediates convergence of pattern- and effector-induced immune responses. *Cell Host Microbe* 30:1717-1731.e6.
- Seppy, M., Manni, M., and Zdobnov, E. M. 2019. BUSCO: Assessing genome assembly and annotation completeness. Pages 227-245 in: *Gene Prediction*. M. Kollmar, ed. Springer New York.
- Skibbe, D. S., Doehlemann, G., Fernandes, J., and Walbot, V. 2010. Maize tumors caused by *Ustilago maydis* require organ-specific genes in host and pathogen. *Science* 328:89-92.
- Stamatakis, A. 2014. RAxML version 8: A tool for phylogenetic analysis and post-analysis of large phylogenies. *Bioinformatics* 30:1312-1313.
- Stegmann, M., Monaghan, J., Smakowska-Luzan, E., Rovenich, H., Lehner, A., Holton, N., Belkhadir, Y., and Zipfel, C. 2017. The receptor kinase FER is a RALF-regulated scaffold controlling plant immune signaling. *Science* 355:287-289.
- Stegmann, M., Zecua-Ramirez, P., Ludwig, C., Lee, H., Peterson, B., Nimchuk, Z. L., Belkhadir, Y., and Hüffelhoven, R. 2022. RGI-GOLVEN signaling promotes cell surface immune receptor abundance to regulate plant immunity. *EMBO Rep.* 23:1-15.
- Tareen, A., and Kinney, J. B. 2019. Logomaker: Beautiful sequence logos in python. *bioRxiv* 635029.
- van der Linde, K., Egger, R. L., Timofejeva, L., and Walbot, V. 2018. Application of the pathogen Trojan horse approach in maize (*Zea mays*). *Plant Signal. Behav.* 13:e1547575.
- van der Linde, K., Hemetsberger, C., Kastner, C., Kaschani, F., van der Hoorn, R. A. L., Kumlehn, J., and Doehlemann, G. 2012. A maize cystatin suppresses host immunity by inhibiting apoplastic cysteine proteases. *Plant Cell* 24:1285-1300.
- Vega-Muñoz, I., Duran-Flores, D., Fernández-Fernández, Á. D., Heyman, J., Ritter, A., and Stael, S. 2020. Breaking bad news: Dynamic molecular mechanisms of wound response in plants. *Front. Plant Sci.* 11:610445.
- Wang, P. P., Yao, S., Kosami, K. ichi, Guo, T., Li, J., Zhang, Y., Fukao, Y., Kaneko-Kawano, T., Zhang, H., She, Y. M., Wang, P. P., Xing, W., Hanada, K., Liu, R., and Kawano, Y. 2020. Identification of endogenous small peptides involved in rice immunity through transcriptomics- and proteomics-based screening. *Plant Biotechnol. J.* 18:415-428.
- Wrzaczek, M., Brosché, M., Kollist, H., and Kangasjärvi, J. 2009. *Arabidopsis* GRI is involved in the regulation of cell death induced by extracellular ROS. *Proc. Natl. Acad. Sci. U.S.A.* 106:5412-5417.
- Wrzaczek, M., Vainonen, J. P., Stael, S., Tsiatsiani, L., Help-Rinta-Rahko, H., Gauthier, A., Kaufholdt, D., Bollhöner, B., Lamminmäki, A., Staes, A., Gevaert, K., Tuominen, H., van Breusegem, F., Helariutta, Y., and Kangasjärvi, J. 2015. GRIM REAPER peptide binds to receptor kinase PRK 5 to trigger cell death in *Arabidopsis*. *EMBO J.* 34:55-66.
- Yamaguchi, Y., Barona, G., Ryan, C. A., and Pearce, G. 2011. GmPep914, an eight-amino acid peptide isolated from soybean leaves, activates defense-related genes. *Plant Physiol.* 156:932-942.
- Yamaguchi, Y., Pearce, G., and Ryan, C. A. 2006. The cell surface leucine-rich repeat receptor for AtPep1, an endogenous peptide elicitor in *Arabidopsis*, is functional in transgenic tobacco cells. *Proc. Natl. Acad. Sci. U.S.A.* 103:10104-10109.
- Zhang, Z., Guo, J., Zhao, Y., and Chen, J. 2019. Identification and characterization of maize *ACD6*-like gene reveal *ZmACD6* as the maize orthologue conferring resistance to *Ustilago maydis*. *Plant Signal. Behav.* 14:e1651604.
- Zhou, F., Emonet, A., Dénervaud Tendon, V., Marhavy, P., Wu, D., Lahaye, T., and Geldner, N. 2020. Co-occurrence of damage and microbial patterns controls localized immune responses in roots. *Cell* 180:440-453.e18.
- Ziemann, S., van der Linde, K., Lahrmann, U., Acar, B., Kaschani, F., Colby, T., Kaiser, M., Ding, Y., Schmelz, E., Huffaker, A., Holton, N., Zipfel, C., and Doehlemann, G. 2018. An apoplastic peptide activates salicylic acid signalling in maize. *Nat. Plants* 4:172-180.